

OFFICE BUILDING ENERGY SIMULATION FOR SEVEN CLIMATIC REGIONS OF BANGLADESH USING BIM

Mizanoor Rahman¹ and Habibur Rahman Sobuz²

¹Lecturer, Department of Building Engineering and Construction Management (BECM), Khulna University of Engineering & Technology (KUET), Bangladesh, email: mizanbecm@gmail.com

²Assistant Professor, Building Engineering and Construction Management (BECM), Khulna University of Engineering & Technology (KUET), Bangladesh, email: habibkuet@gmail.com

ABSTRACT

Building energy consumption depends on many factors such as climate, occupant's behavior, building size and orientation. Analysis of building energy performance at the early phase of the project is crucial for sustainable building design. The purpose of this paper is to determine the energy performance of an office building located in the various climatic region of Bangladesh. A ten story high and circular shape office building conceptual model was developed by incorporating BIM tools Autodesk Revit® 2015. The whole building conceptual energy simulation was performed by Autodesk Green Building Studio (GBS). From the energy simulated results by Autodesk Revit, it was observed that the analyzed office building located in Dhaka which is the main city of South central zone of Bangladesh consumed more energy than the others zones. On the contrary, the same office building located in Jessore which is the main city of the South Western region of Bangladesh consumed less energy than that from other zones.

Keywords: Energy, climatic zones, office building, simulation, performance

1. INTRODUCTION

Globalization, changing of living standard and lifestyle as well as increasing industrialization raise energy demand. Globally, around 40% of the total annual energy consumed by buildings (Barua & Billah). Bangladesh has the lowest per capita primary energy consumption within the Indian subcontinent. In 2011, per capita primary energy consumption in Bangladesh was about 205 kilogram oil equivalent (kgoe) whereas it was 614 kgoe in India, 482 kgoe in Pakistan, 383 kgoe in Nepal, and 499 kgoe in Sri Lanka. The primary energy utilization in Bangladesh was increased to 26.7 Mtoe in 2013 that is almost double from 14.8 Mtoe in 2002 (Halder, Paul, Joardder, & Sarker, 2015). Moreover, residential sector in Bangladesh is responsible for around 47% of total energy consumption in Bangladesh (Alam, Islam, & Biswas, 2014).

Nowadays, building, energy and environment are the fundamental issue for the building industry worldwide because there are possible environmental impacts on ambient air conditions and fresh water supply (Fong & Lee, 2017). It is very much important to consider carefully the energy and environmental performance of building (Alrashed & Asif, 2015). However, building energy demand varies with respect to the outdoor weather conditions of a country. Therefore, selection of appropriate passive concept for building design with respect to the local climatic condition is one of the important factor (Panchabikesan, Vellaisamy, & Ramalingam, 2017). Energy simulation at the conceptual stage of a building plays an important role to design energy efficient building because energy efficiency is a key factor for a high quality building.

A climatic zone may be defined as an area for which common outdoor conditions for calculating the energy demand are defined by using a few parameters (Carpio, Jódar, Rodríguez,

&Zamorano, 2015).Building design consultants and energy researchers could get a better idea about the possible impacts on the thermal performance of the office buildings in the different climates from energy analysis and its findings (Eskin & Türkmen, 2008).In order to examined the influences of diverse climate conditions on the thermal and energy performance of office buildings in China(H. J. Wu, Yuan, Zhang, & Bi, 2012),Thailand (Kunchornrat, Namprakai, & du Pont, 2009)and Europe (Tsikaloudaki, Laskos, & Bikas, 2011)were conducted through climatic data analysis to improve the thermal performance of buildings. Research have shown that total energy demand can be reduced more than 50% by identifying and implementing sensitive climatic design parameter(Zhao, Künzelt, & Antretter, 2015).Moreover, climatic zoning for building energy efficiency applications is an important parameter in many programs and policies (Walsh, Cóstola, & Labaki, 2017).

There are many types research has been conducted on the effect of the climatic zone on building energy performance; however, there is no research conducted in the context of Bangladeshi climatic zones. The main objective of this study is to analyze the effect of Climatic zones on the energy performance of building including life cycle cost, carbon emissions, and renewable energy potential.

2. GEOGRAPHICAL AND CLIMATIC CONDITION OF BANGLADESH

Bangladesh, a south-Asian low-income country is located between 20°40' and 26° 38' north latitude and 88° 01' and 92° 41' east longitude with an area of 147,570 km².The country is surrounded by India on the west, north, and northeast while by Myanmar on the south-east and the Bay of Bengal on the south. The density of population in the country has increased dramatically from 704.75 peoples /km² in 1990 to 1074.07 peoples /km² in 2014. The country has 32.1 million households distributed in over 59,229 mauzas (Halder et al., 2015).Bangladesh has a subtropical monsoon climate characterized by wide seasonal variations in rainfall, high temperatures, and humidity. There are three distinct seasons in Bangladesh: a hot, humid summer from March to June; a cool, rainy monsoon season from June to October; and a cool, dry winter from October to March. In general, maximum summer temperatures range between 30°C and 40°C. April is the warmest month in most parts of the country. January is the coldest month when the average temperature for most of the country is about 10°C(Alam et al., 2014).Bangladesh has been divided into seven climatic sub-regions that have indicated in figure1 and these seven climatic sub-regions are South-Eastern (Chittagong), North-Eastern (Sylhet), Northern part of the north region (Panchagarh), North- western region (Rajshahi), Western dry region (Bogra), South-western region (Jessore) and South-central region (Dhaka).



Figure 1: The climatic zones of Bangladesh

3. BUILDING INFORMATION MODELING (BIM)

The building information modeling is a digital representation of the physical and functional characteristics of a building project & its life cycle (D. Wu, 2013). BIM is currently the most common denomination for a new way of approaching the design, construction, and maintenance of buildings (Abanda & Byers, 2016). In order to conduct building energy simulation during design and construction phases, various types of information such as building materials, labor force, and facilities are needed and BIM able to provide that information. Various tools are needed in order to generate BIM models (Che, Gao, Chen, & Nguyen, 2010). Many software assists the designers to create a 3D digital model of a building while also providing 4D information, 5D information and other related performance analysis such as costing, scheduling, structural analysis, energy analysis, etc. The most popular and powerful BIM software is Autodesk Revit® that has been used in this study.

4. METHODOLOGY

4.1 Design Parameters

A ten-storied circular shape office building of 100 ft high and 50 ft radius with total floor area 78,529 ft² and net exterior wall area 31,416 ft² has been considered in this investigation. The

analyzed model is suitable for 292 peoples. Exterior window to wall ratio has been chosen about 40%. The circular shape of office building model has been chosen in order to avoid shape and orientation effect because different geometric shapes have different capacity to receive solar energy depending on its orientation. For instance, rectangular shape elongated East-West direction received highest amount solar insulation with compare to other orientation(Ling, Ahmad, & Ossen, 2007).Autodesk has provided the virtual code of weather stations for the climatic zones, outdoor maximum and minimum temperature. The key information for the seven climatic zones of Bangladesh was presented in Table 1.

Table 1: Key information for the climatic zones of Bangladesh

Climatic Zones	Regions	Major city	Coordinates	Code of weather station	Outdoor Temperature (°F)		
					Max	Min	Average
A	South Eastern	Chittagong	22°22'N91°48'E	756952	96	51	73.5
B	North-Eastern	Sylhet	24°54'N91°52'E	756334	101	49	75
C	Northern part of the northern region	Panchagarh	26.25°N 88.50°E	456719	100	45	72.5
D	North- western region	Rajshahi	24°51'N89°22'E	456026	102	44	73
E	Western zone	Bogra	24°22'N88°36'E	458057	101	47	74
F	South-western zone	Jessore	23.17°N 89.20°E	457028	101	43	72
G	South-central zone	Dhaka	23°42'N90°22'E	460412	101	46	73.5

4.2 Energy Simulation

Computerized building information modeling (BIM) tools such as Autodesk Revit[®]2015 has been used as a tool to create the mass model. Building categories have been chosen as the office building. The same model has been used for energy simulation at seven climatic zones where major influencing factors were weather data such as temperature, solar radiation, wind condition and humidity. The percentage of glazing was kept 0.4 for all the models. The office buildings operating schedule was 24/7 and HVAC system was central VAV, HW heat, chiller 5.96. Typical energy analyzed model and sun path diagram and the whole building energy simulation process is shown in figure 2,3 and 4 respectively.

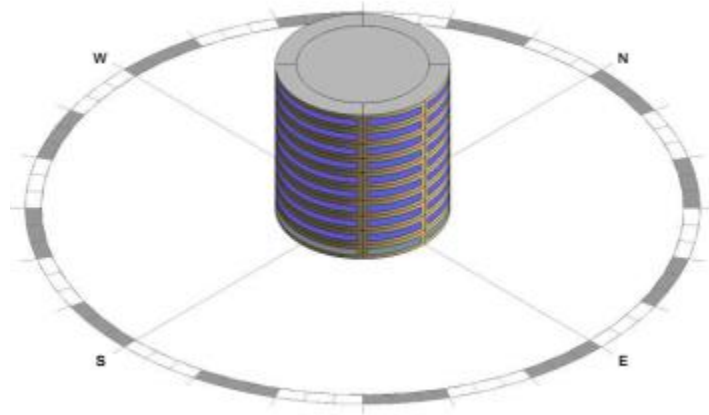


Figure 2: Energy analytical model for the analyzed building

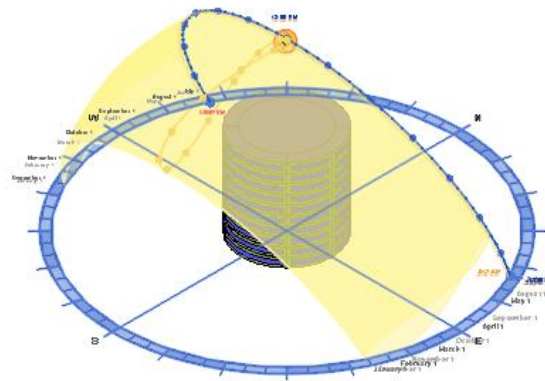


Figure3: Sun path diagram at Dhaka city for summer session

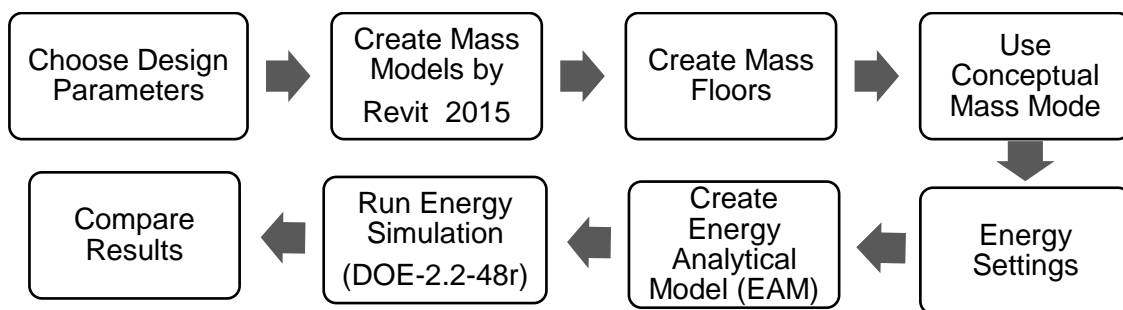


Figure 4: Conceptual energy simulation flow diagrams by BIM

5. RESULTS AND DISCUSSION

5.1. Life Cycle Energy Consumption

The simulation results in figure 5 showed that life cycle energy consumption varies from climatic zone to climatic zone of Bangladesh. Whole life energy consumption at Chittagong, Sylhet, Panchagarh, Rajshahi, Bogra & Jessore is almost identical but Dhaka city consumed around 20% higher than rest of the zone of Bangladesh. It was found from the simulated results that natural gas used in Dhaka city around 13% of total energy. Likewise, the rest of the city individually used around 6-7 % of total energy.

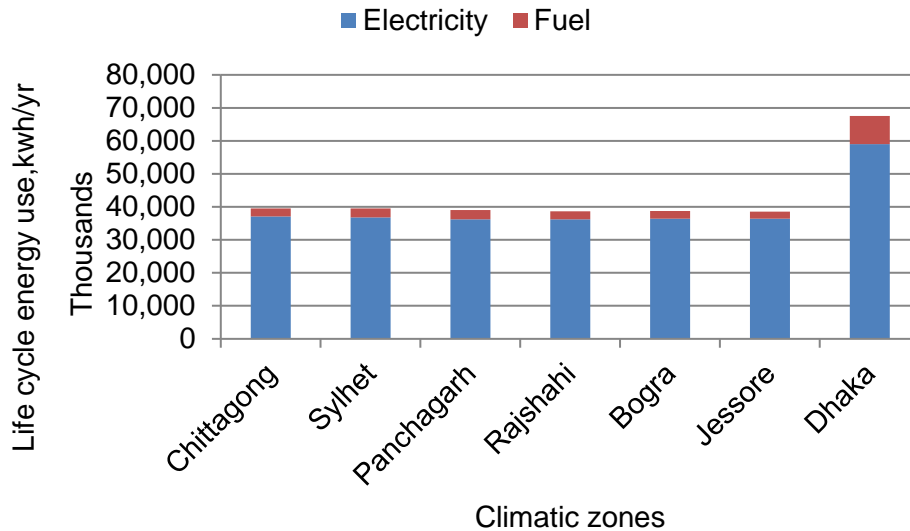


Figure 5: Life cycle energy consumption at various climatic zones

5.2. Monthly Electricity Consumption

Monthly electricity consumption for the analyzed building model at various climatic zones of Bangladesh is illustrated in figure 6. From the simulated results it has been found that except Dhaka city the energy consumption pattern for the rest of the city almost identical but Dhaka city consumed almost 33% higher than others zones. The energy requirement for all cities is low from November to February because of low temperature during the winter season. The principle influencing factors that were responsible for the variation of energy consumption were weather condition which is temperature, relative humidity, wind condition and solar radiation.

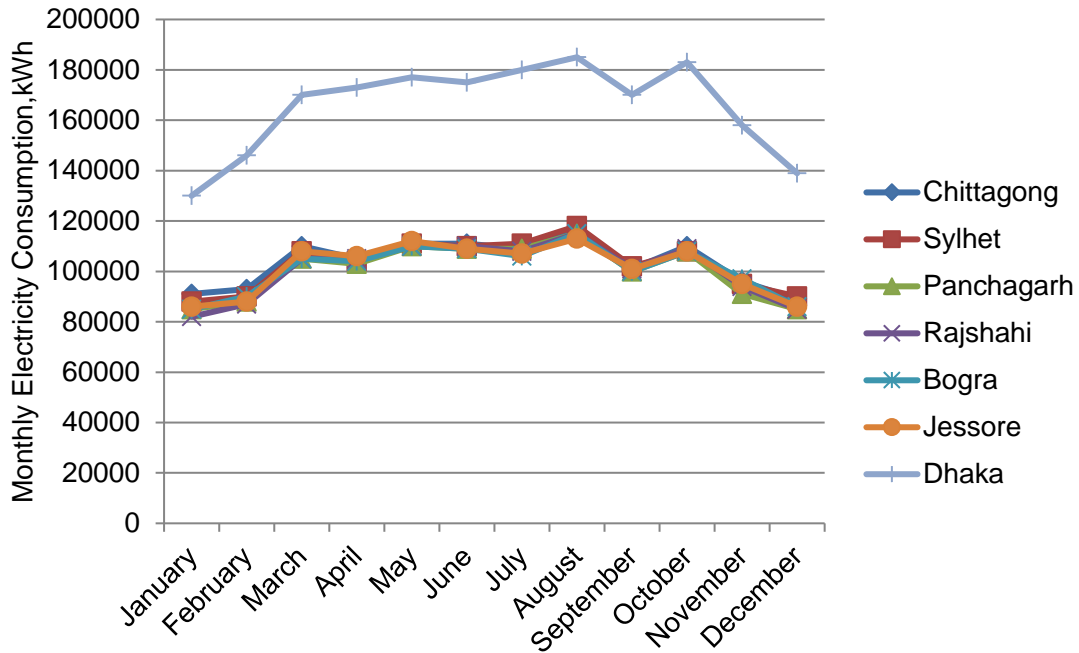


Figure 6: Monthly energy consumption at various climatic zones

5.3. Life Cycle Energy Cost

The estimated energy usage and cost over the life of the building assuming a 30-year lifespan. In order to estimate life-cycle cost, the unit rate of electricity is \$0.09/kWh and natural gas is \$0.78/ Therm has been considered. The rate has been chosen by Autodesk based on statewide, territory-wide or nationwide average utility rates. From the simulated result, it was noticed that the life cycle energy cost varies from climatic zone to zone that has been represented in figure 7. The life cycle cost for the selected building model is higher at Dhaka city and lower at Rajshahi city. Except for Dhaka city, the variation of life cycle cost for rest of the city is very little. Life cycle cost for the analyzed office building in Dhaka city is around 64 % higher than the average cost of the other climatic city.

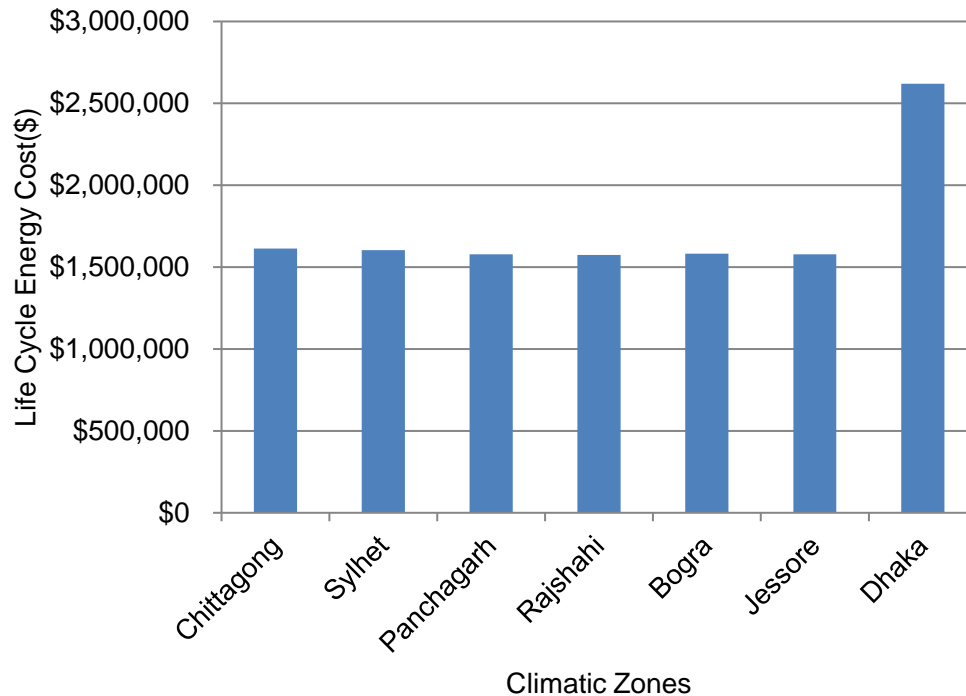


Figure 7: Life cycle energy cost at various climatic zones

6. CONCLUSION

Bangladesh is divided into seven climatic zones and the energy simulation of the analyzed building model conducted for each climatic zone. From this research, it has been concluded that climatic zone of Bangladesh plays a significant role in building energy performance. Building located in the South-central region of Bangladesh where Dhaka is the main city consumed around 20 % more life cycle energy than other zones of Bangladesh. Energy consumption for all climatic zones except South-central region is almost identical. The energy performance of the analyzed building model at Dhaka city is greatly affected by temperature, relative humidity, solar radiation & wind condition. However, it is very much important to classify the climatic zone precisely otherwise energy simulation results will not consistent with real climatic characteristics.

ACKNOWLEDGEMENT

The authors would like to thank the Department of Building Engineering and Construction Management (BECM) at Khulna University of Engineering & Technology (KUET), Khulna, Bangladesh for utmost support to conduct this research.

REFERENCES

- Abanda, F., & Byers, L. (2016). An investigation of the impact of building orientation on energy consumption in a domestic building using emerging BIM (Building Information Modelling). *Energy*, 97, 517-527.
- Alam, M. J., Islam, M. A., & Biswas, B. K. (2014). *Energy simulation to estimate building energy consumption using EnergyPlus*. Paper presented at the International Conference on Mechanical, Industrial and Energy Engineering.

- Alrashed, F., & Asif, M. (2015). Climatic classifications of Saudi Arabia for building energy modelling. *Energy Procedia*, 75, 1425-1430.
- Barua, S., & Billah, S. B. Promoting Sustainable Development: Solar Energy for the Urban Building Application.
- Carpio, M., Jódar, J., Rodríguez, M. L., & Zamorano, M. (2015). A proposed method based on approximation and interpolation for determining climatic zones and its effect on energy demand and CO₂ emissions from buildings. *Energy and Buildings*, 87, 253-264.
- Che, L., Gao, Z., Chen, D., & Nguyen, T. H. (2010). *Using building information modeling for measuring the efficiency of building energy performance*. Paper presented at the Proceedings of the International Conference on Computing in Civil and Building Engineering (ICCCBE).
- Eskin, N., & Türkmen, H. (2008). Analysis of annual heating and cooling energy requirements for office buildings in different climates in Turkey. *Energy and Buildings*, 40(5), 763-773.
- Fong, K., & Lee, C. (2017). Investigation of climatic effect on energy performance of trigeneration in building application. *Applied Thermal Engineering*.
- Halder, P., Paul, N., Joardder, M., & Sarker, M. (2015). Energy scarcity and potential of renewable energy in Bangladesh. *Renewable and Sustainable Energy Reviews*, 51, 1636-1649.
- Kunchornrat, A., Namprakai, P., & du Pont, P. T. (2009). The impacts of climate zones on the energy performance of existing Thai buildings. *Resources, Conservation and Recycling*, 53(10), 545-551.
- Ling, C. S., Ahmad, M. H., & Ossen, D. R. (2007). The effect of geometric shape and building orientation on minimising solar insolation on high-rise buildings in hot humid climate. *Journal of Construction in Developing Countries*, 12(1), 27-38.
- Panchabikesan, K., Vellaisamy, K., & Ramalingam, V. (2017). Passive cooling potential in buildings under various climatic conditions in India. *Renewable and Sustainable Energy Reviews*, 78, 1236-1252.
- Tsikaloudaki, K., Laskos, K., & Bikas, D. (2011). On the establishment of climatic zones in Europe with regard to the energy performance of buildings. *Energies*, 5(1), 32-44.
- Walsh, A., Cóstola, D., & Labaki, L. C. (2017). Comparison of three climatic zoning methodologies for building energy efficiency applications. *Energy and Buildings*, 146, 111-121.
- Wu, D. (2013). Building knowledge modeling: Integrating knowledge in BIM.
- Wu, H. J., Yuan, Z. W., Zhang, L., & Bi, J. (2012). Life cycle energy consumption and CO₂ emission of an office building in China. *The international journal of life cycle assessment*, 17(2), 105-118.
- Zhao, M., Künzle, H. M., & Antretter, F. (2015). Parameters influencing the energy performance of residential buildings in different Chinese climate zones. *Energy and Buildings*, 96, 64-75.

COMPARATIVE STUDY OF IPS & PPVC PRECAST SYSTEM- A CASE STUDY OF PUBLIC HOUSING BUILDINGS PROJECT IN SINGAPORE

Mizanoor Rahman¹ and Habibur Rahman Sobuz²

¹Lecturer, Department of Building Engineering and Construction Management (BECM), Khulna University of Engineering and Technology (KUET), Bangladesh, e-mail: mizanbecm@gmail.com

²Assistant Professor, Building Engineering and Construction Management (BECM), Khulna University of Engineering and Technology (KUET), Bangladesh, e-mail: habibkuet@gmail.com

ABSTRACT

A key means of upgrading the construction industry in Singapore is to improve the existing industry techniques and practices that affect construction productivity and cost efficiency, in addition to reviewing the management practices of the industry. Precast technology is not new to the industry, but its use in the local context is still limited for many reasons. The purpose of this paper is to study the construction techniques and compare the performances of the Individual Panel System (IPS) & Prefabricated Prefinished Volumetric Construction (PPVC) precast system through a case study that has been adopted in a high rise public building project in Singapore. From the drawings, specifications, method statements and site documents, it was observed that all the precast components except House Hold Shelter (HHS) were fabricated and installed as an IPS system. Only HHS was used as a PPVC system. The research result indicates that IPS is less productive than PPVC system. Therefore, it could be recommended to introduce PPVC system for the upcoming project that will reduce construction time, cost, waste, site safety hazard, noise, and dust. On the other hand, it will enhance the productivity with better quality of workmanship.

Keywords: Precast concrete, modular construction, productivity, PPVC, quality

1. INTRODUCTION

In Singapore, mandatory requirements for prefabrication are enforced indirectly through statutory compliance with “build ability” provisions in the building control system. Singapore is the first country to formulate guidelines for quantifying “build ability” and making the assessment mandatory for building developments under its Buildable Design Appraisal System (BDAS). With a scoring system, the Building Construction Authority requires building designs to achieve minimum build ability scores under building regulations (Chiang, Chan, & Lok, 2006). The mandatory requirements do pose new contractual and legal burdens on developers and consultants (Pheng & Chan, 2001). However, empirical studies have demonstrated a positive correlation between build ability, quality and productivity (Pheng Low, 2001). Precast construction method plays an important role in the modern construction industry; it refers to the making of parts in an offsite precast yard prior to the installation at the site. “The primary purpose of precast construction is to produce building components in an efficient work environment with accesses to specialized skills and equipment in order to reduce cost and time expenditures on the site while enhancing quality and consistency (Anderson & Anderson, 2007).

The precast concrete system is cost-effective than cast in place concrete system. But, the main limitation of use of precast concrete construction is the transportation of precast members from precast yard to the construction site because the cost of transportation is considerably high (Turai & Waghmare, 2015). Precast technologies are not only helping contractors and builders to get their buildings faster but also made easier to perform non-destructive testing

(NDT) if the need arises, In addition, Precast is a smart way to achieve the sustainability objectives of Green Building (Jain, Kumar, & Patterson, 2016).A review of the seismic performance and behavior of precast concrete structures indicates that the buildings designed and constructed by incorporating seismic design concepts performed remarkably well(Khare, Maniyar, Uma, & Bidwai, 2011).Despite a lot of advantages from the precast system, many countries do not want to implement this system because there is a major shortage of expert personnel capable of designing and organizing precast building projects(Arditi, Ergin, & Günhan, 2000).

In order to promote building and construction industries embarking towards sustainability and higher productivity, the Singapore Building and Construction Authority (BCA) had introduced an advanced, leading-edge modular construction technology to promote off-site manufacturing for onsite assembly, namely Prefabricated Prefinished Volumetric Construction (PPVC).The PPVC is defined as a construction method whereby free-standing volumetric modules complete with finishes for walls, floors, and ceilings are constructed and assembled outside the premises of the building works and installed at those premises for the purposes of those building works (Rui & Yahya).Design for Manufacturing and Assembly (DfMA) is a new concept in the construction sector. The principle of DfMA concept is planning more works offsite; manpower and time needed to construct buildings are reduced while ensuring work sites are safe, conducive and have minimal impact on the surrounding living environment. Therefore, PPVC system supports the DfMA concept. However, In Singapore until 2016 it was used only at bathroom and HHS. Most of the builders in Singapore are not keen to be first movers to PPVC due to lack of expert and experience.

Modular construction comprises prefabricated room-sized volumetric units that are normally fully fitted out in the manufacture and are installed on-site as load-bearing “building blocks(Lawson, Ogden, & Bergin, 2011).A module is characterized as a three-dimensional object, which, by its size, is able to provide utility space. Each module consists of a frame, floor, ceiling, walls, and other accessories(Kyjaková & Bašková, 2016).Modular construction is essentially a construction method where individual modules or volumes are constructed offsite, stand-alone, transported to the site and are then assembled together onsite to make up a larger structure(Velamati, 2012).Modular construction is saved about half the time with compared to conventional construction method, meaning the property can be leased faster and added revenue can be created that would not be possible using traditional construction system(i.e. cast-in-place). Modular construction also provides consistent and better quality increases workers skills and reduces errors in construction(Ganiron Jr & Almarwae, 2014).Precast concrete system becoming a very popular technique in order to fulfill the rapid demand of infrastructure. But, most of the country in Asia like Singapore, Malaysia, Thailand and HongKong practicing individual panel system (IPS).But IPS had some limitation such as less productive than PPVC, lots of onsite activity still needed for example Mechanical and Electrical services works, skim coat on precast elements. In order to overcome the limitations of IPS, a sophisticated Prefabricated Prefinished Volumetric Construction (PPVC) method has been recommended in this paper throughout the whole project.

2. ABOUT THE PROJECT

Housing is the basic need of every human being. Due to the faster-growing population, and to fulfill the tremendous housing demand, a more reliable, faster, sustainable method of construction is deemed necessary by the Singapore Housing Authority so-called Housing Development Board (HDB). The concept of “Built to Order (BTO)” in the most economical way has not changed since the beginning; however, new technologies have been developed to suit

the modern world construction. One such solution is precast concrete construction technology. The project comprises of 10 blocks of the 16-story residential building with 6 story height car-park. The project is located East part of Singapore namely Sengkang Neighborhood area. The developer of the project is Housing Development Board (HDB). The case study is based on drawing, the method of statement, specification and site installation. To avoid complicated details of a precast column/wall at level 1, conventional cast-in-situ construction was adopted at level 1. Except HHS, rest of the precast elements were used as an IPS system. Moreover, using the precast system started from level 2 to the roof. The location plan, site plan, and typical unit layout plan were shown in figure 1, 2& 3 respectively. In addition, some others basic information about the project shown in Table 1.

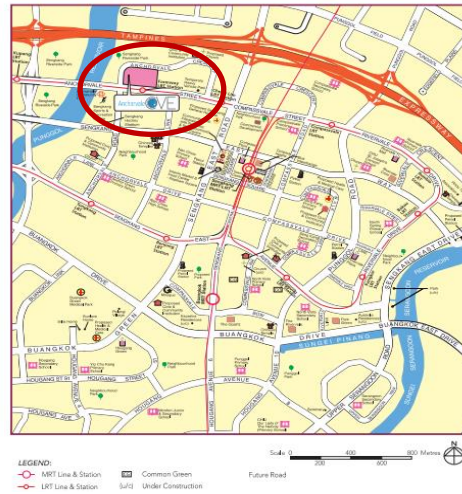


Figure 1: Location plan of the project

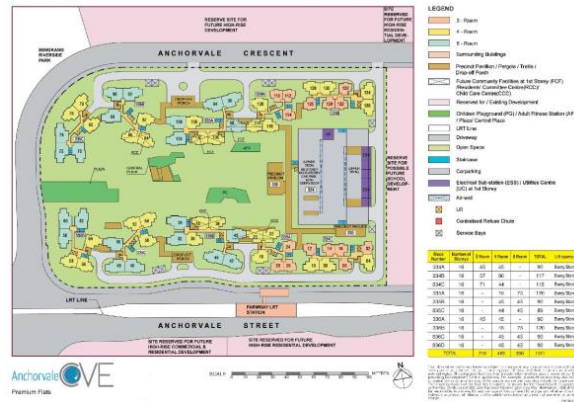


Figure 2: Site plan

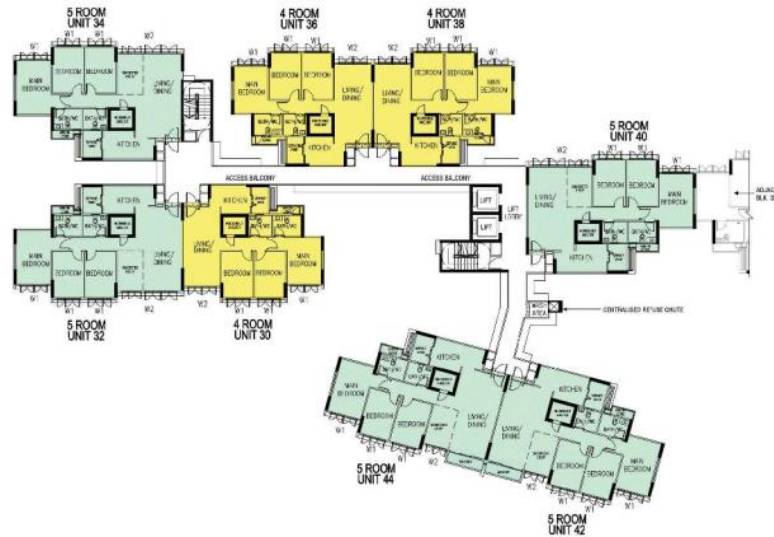


Figure 3: Typical floor plan

Table 1: Basic information of the project

Project Name	Anchor vale Cove
Total nos. of building blocks	10 nos. of 16 story residential building with one multi storey carpark.
Total nos. of residential units	1011
Amount precast used	90% of total build up area (10% cast in situ)
Structural system (sub-structure)	Bored pile
Structural system (super-structure)	Precast beam, column, wall and slab.
Basement	2 basement at multi storey car park
Residential unit type	3,4 & 5 bed room platinum flat

3. METHOD OF CONSTRUCTION

One of the biggest challenges in the precast system is connection details. Connections are needed not only to transfer loads but also to provide continuity and overall monolithic behavior of the entire structure. A complete system of precast units can be integrated to form a structure that behaves monolithically with sufficient strength, stiffness & durability to resist seismic & other dynamic loadings. The connections act as bridging links between the components (Bommi, Somaraju, Senou, & Barde). Structural precast elements can largely be classified into two categories based on their production methodology, namely vertical and horizontal. For a typical residential unit construction, the major elements are columns, wall, household shelter, beams, canopy, facade, balcony, staircase, slabs etc. Out of these columns, wall, facade, household shelter are vertical and slabs, beam, balcony, AC ledge are horizontal elements. The common area of a building has many other precast elements such as lift core, boundary walls, and curbstones. However, the installation techniques for some of the key precast elements that have been implemented in this project were discussed below:

3.1 Method of installation of column/Wall

The type of precast column/wall that had been used in this project was IPS. And the installation of precast column/wall started from level 2 to upward. Starter bars from bottom slab are protruding out with a specified length and another starter bar came down from the precast column. Both starter bars are connected by the spiral connector. After checking the verticality, the recess in the precast column is cast back by pressure grouting. Figure 4 to 7 shown precast wall/column connection details and installation procedure.

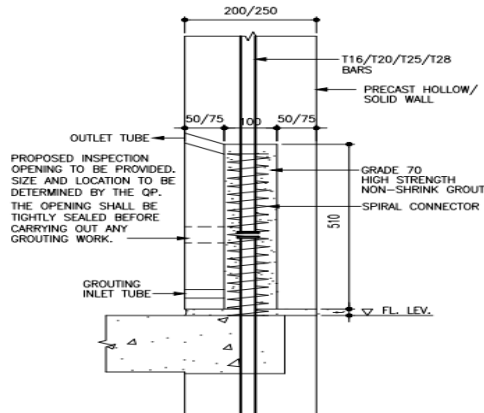


Figure 4: Typical column connection details



Figure 5: Spiral connector for column or wall connection



Figure 6: Bedding preparation for column or wall connection



Figure 7: Column after installation of column wall connection

3.2 Method of installation of facade

Precast façade panels are monolithically cast with the beam on top of facade. It was an IPS system as well. The thickness of façade panels were 100 and 120 mm. Before installing the façade panels on site, waterproofing strips are placed on the RC curb and then just placed the façade panel on the curb. Both ends of a façade panels had recess with the exposed link. Another exposed link came out from adjacent columns or walls. Both exposed links were connected with U shape link. Finally, the recess cast back with non-shrink grout. Figure 8 to 11 shown typical connection details and installation procedure of precast facade panels.

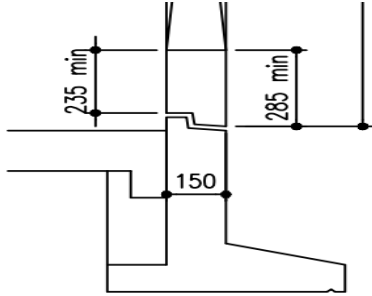


Figure 8: Typical bottom connection of façade panels



Figure 9: Bedding preparation for façade installation

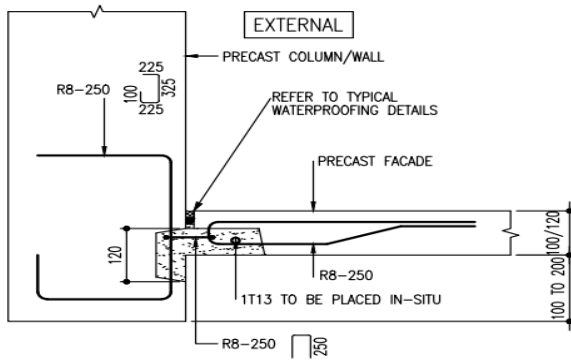


Figure 10: Typical Façade connection details



Figure 11: Façade panel being installed

3.3 Method of installation of slab

Precast slab system consists of precast pre-stressing planks and that is why it is possible to achieve larger unsupported span. Typical thickness of planks was 70, 90 and 110mm. These planks were cast offsite as per approved shop drawing and then delivered to the site. The planks were placed in position using tower cranes. The bottom layer of rebar placed in the precast planks and the top layer of rebar placed on site at top of planks. PVC conduit for M&E services placed just below of the top mesh and then top up with 80 to 90 mm in-situ concrete. Figure 12 to 15 shown the typical connection details of the precast slab as well as installation procedure.

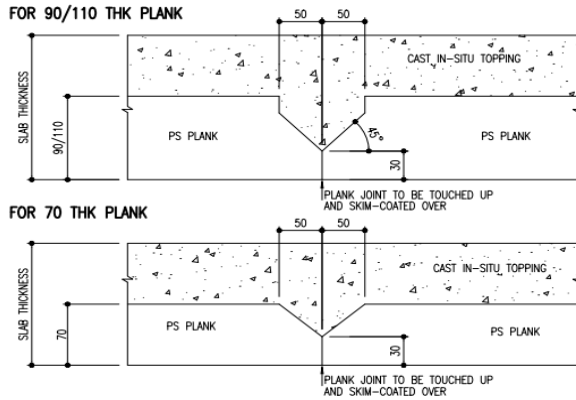


Figure 12: Typical precast slab system



Figure 13: Preparation for precast plank placement



Figure 14: Placing of precast plank



Figure 15: Top layer of rebar placed and slab is ready for casting

3.4 Method of Installation of Household Shelter (HHS)

The precast house hold shelter is a PPVC (modular compartment) module that was used in this project. But, the percentage was very little with compared to total precast elements. It has the hollow core at every side of the wall. The starter bar comes from below slab and passes through the hollow core. The core then cast back with cast-in-situ concrete. Figure 16 to 19 show the connection details and installation procedure of the precast house hold shelter. From this single PPVC element it was found that total installation time for HHS was reduced 75% with compared to IPS system.

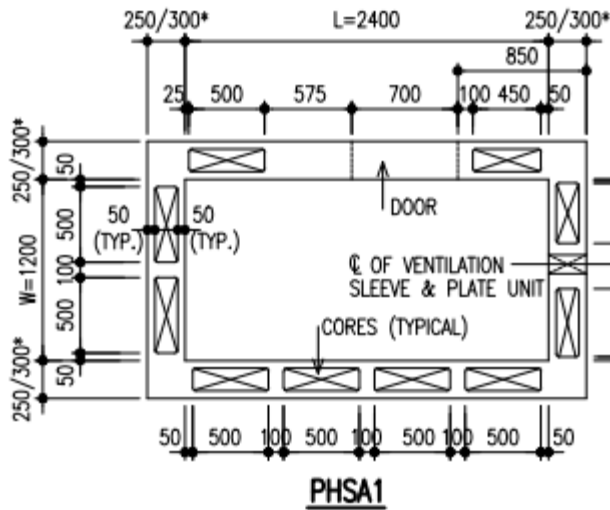


Figure 16: Typical shop drawing for house hold shelter

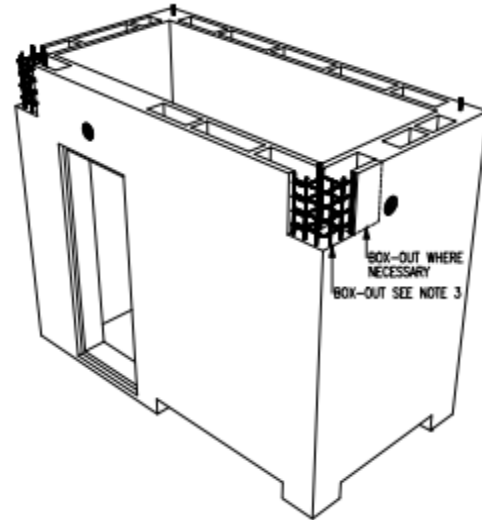


Figure 17: Typical 3D view of household shelter



Figure 18: Installation of household shelter in progress



Figure 19: After installation of household shelter

4. CHALLENGES EXPERIENCED

Initially, the main contractor appointed one precast supplier but they failed to deliver the precast components on time, as a result, the project was delayed and this experienced similar to previous research finding (Ali, Hammad, Sweis, & Samhuri, 2009). After that, the main contractor deployed two precast suppliers and they managed to catch the delay. Concrete supply was another challenge. Initially, the builder engaged one concrete supplier, but they could not cope with the site demand. As a result, later on, added one more supplier in order to avoid delay. Manpower was a serious issue because Singapore construction industry mainly depends on foreign manpower. The Ministry of Manpower continuously changes immigration policy that greatly affects the quota of firms. The main reason behind the above challenge was adoption of IPS system because lots of onsite activity was required in IPS system. That can be reduced significantly by adopting PPVC system within the whole project. But transportation and hoisting for PPVC system was a big challenge that has to be carefully considered during the

design phase. Nevertheless, the challenges that experienced from this particular project will be the learning curve for future projects.

5. BENEFITS OF PPVC SYSTEM OVER IPS SYSTEM

In IPS system still lots of onsite activity needed for example slab topping-up, Mechanical Electrical & Plumbing (MEP) services installation, skim coating. On the other hand in PPVC system, very minimum on-site works required like grouting at joint area only. Manpower saving with compare to in-situ construction for the IPS & PPVC system was presented in table 2.

Table 2: Comparison of manpower requirement

Trade	Precast system	Manpower saving
Structural (project level)	IPS	10%
	PPVC	40%
Architectural (Trade level)	IPS	30%
	PPVC	70%
MEP (Trade level)	IPS	30%
	PPVC	70%

6. RESULTS AND DISCUSSION

6.1 Total construction period

The as-built master program that has been followed in this project shown in figure 20. From the program it has been found that the whole project that means 10 building blocks of 16 stories comprise 1011 units and one 6 story car-park completed by 28 months. It was possible by adoption of the IPS precast system. As PPVC system was used only in HHS and it was very small percentage with respect to the whole project, the separate master program for the project was not prepared. However, the total construction period can be reduced to 19 months.

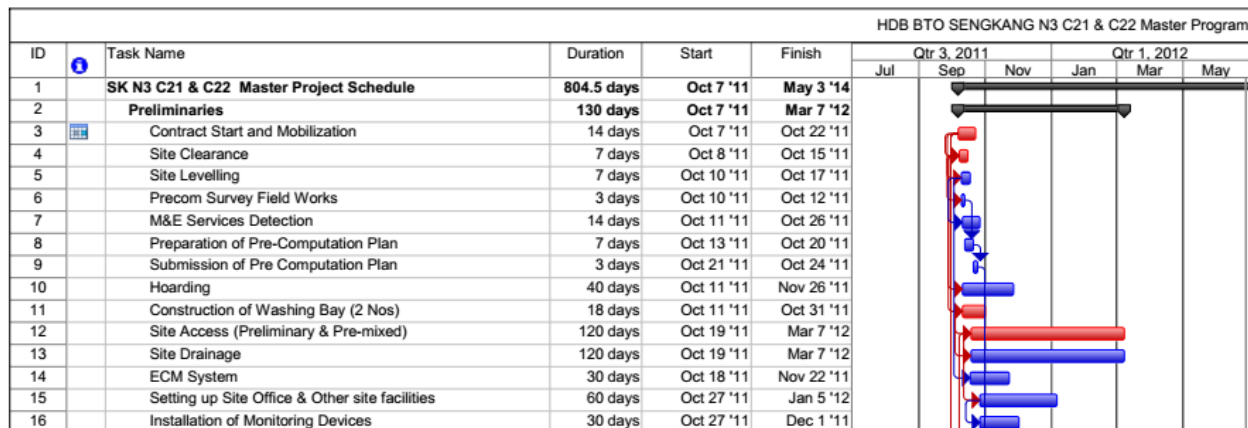


Figure 20: As built master program for the study project

6.2 Casting Cycle

The as built master program for super-structure has represented in figure 21. From the result it has been found that achieved slab casting cycle of 12-14 days. It can be reduced to 6 days cycle by adopting PPVC system.

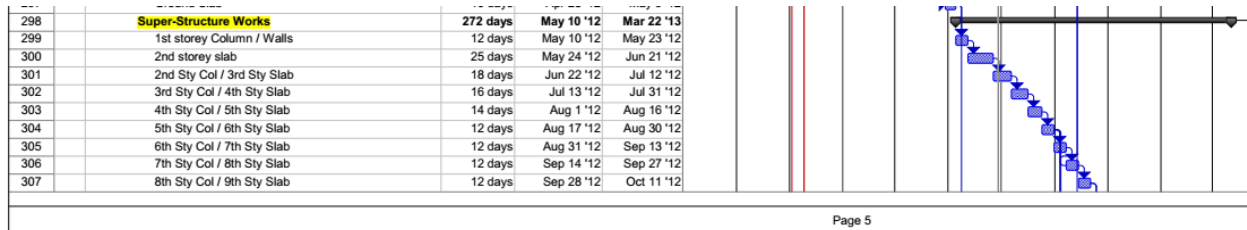


Figure 21: As built master program for super-structure

6.3 Quality of Workmanship

From the figure 22, it was found that by implementing IPS precast system high quality-finishing workmanship was achieved by doing only skim coat directly on the precast elements. No plaster works were needed for IPS system. On the other hand, no onsite plaster as well as skim coat required for PPVC system but achieved very high quality finishing compared to IPS system that has been shown in figure 23.



Figure 22: Quality of workmanship using IPS



Figure 23: High quality workmanship using PPVC

6.4 Other Achievements

Some others astonishing results along with learning experiences achieved through this landmark project which is noted as follows:

- Cost and time optimization.
- Eliminated brickworks and plasterwork on precast wall, column & facade.
- Overall cost required for constructing the building using IPS system is reduced by 20% when compared to conventional method. It can be possible to reduced 40% by adopting PPVC system.

- The IPS precast system saved form work requirement 75%, scaffolding requirement 75% to 90%, and wet concrete requirement 90%. On the other hand, it can be reduced to 95 % by adopting PPVC system.

7. CONCLUSIONS

The precast system represents an efficient method of building construction. Design for Manufacturing and Assembly (DfMA) concept was developed to enhance the construction speed significantly. Prefabricated Prefinished Volumetric Construction (PPVC) is one of the game-changing technologies that support the DfMA approach. By adopting IPS precast technique, the construction period was reduced by over 50%; construction waste was reduced by 70% relative to the site-intensive building. Precast wall panel system was lead to a more economical design as well. The productivity of IPS precast system is not sufficient enough to meet the industry demand because the client wanted to complete the project within 19 months that was not possible by IPS system. Therefore, to overcome the limitations of the IPS system that has been addressed in this study, the PPVC system (modular system) has proposed to implement in the upcoming whole project as a pilot project. A high-rise residential project that takes three years to complete can potentially save nine months if the PPVC is used. However, the transportation and hoisting factor for the PPVC system need to be carefully considered prior to the design of PPVC module.

ACKNOWLEDGEMENTS

The authors gratefully acknowledge the support of the below organizations

- Housing and Development Board (HDB), Singapore
- Axis Architects Planners Pte Ltd, Singapore.
- Mainhardt (Singapore) Pte Ltd., Singapore
- KayLim Construction and Trading Pte Ltd., Singapore

REFERENCES

- Ali, S. M. A., Hammad, A. A. A., Sweis, G. J., & Samhoury, M. S. (2009). Productivity Improvement of Pre-cast Concrete Installation. *Jordan Journal of Civil Engineering*, 3(2), 50-60.
- Anderson, M., & Anderson, P. (2007). *Prefab prototypes: site-specific design for offsite construction*: Princeton Architectural Press.
- Arditi, D., Ergin, U., & Günhan, S. (2000). Factors affecting the use of precast concrete systems. *Journal of architectural engineering*, 6(3), 79-86.
- Bommi, S., Somaraju, K., Senou, K., & Barde, A. D. Precast High-Rise Residential Projects in India: Design Implementation.
- Chiang, Y.-H., Chan, E. H.-W., & Lok, L. K.-L. (2006). Prefabrication and barriers to entry—a case study of public housing and institutional buildings in Hong Kong. *Habitat International*, 30(3), 482-499.
- Ganiron Jr, T. U., & Almarwae, M. (2014). Prefabricated Technology in a Modular House. *International Journal of Advanced Science and Technology*, 73, 51-74.
- Jain, S., Kumar, R., & Patterson, M. (2016). *A Case-study on use of Precast Technology for Construction of High-Rise Buildings*.

- Khare, R., Maniyar, M., Uma, S., & Bidwai, V. (2011). Seismic performance and design of precast concrete building structures: an overview. *Journal of Structural Engineering*, 38(3), 272-284.
- Kyjaková, L., & Bašková, R. (2016). Advantages and disadvantages of modern methods of construction used for modular schools in Slovakia. *Czasopismo Techniczne*, 2016(Budownictwo Zeszyt 1-B (6) 2016), 35-41.
- Lawson, R. M., Ogden, R. G., & Bergin, R. (2011). Application of modular construction in high-rise buildings. *Journal of architectural engineering*, 18(2), 148-154.
- Pheng, L., & Chan, P. (2001). Legal/contractual implications arising from the legislation of buildability requirements. *International Construction Law Review*, 18(3), 574-607.
- Pheng Low, S. (2001). Quantifying the relationships between buildability, structural quality and productivity in construction. *Structural Survey*, 19(2), 106-112.
- Rui, O. Y., & Yahya, K. The Productivity Rate of Prefabricated Pre-Finished Volumetric Construction (PPVC).
- Turai, V., & Waghmare, A. (2015). A Study of Cost comparison of precast concrete vs. Cast-in-Place. *International Journal on Recent and Innovation Trends in Computing and Communication*.
- Velamati, S. (2012). *Feasibility, benefits and challenges of modular construction in high rise development in the United States: a developer's perspective*. Massachusetts Institute of Technology.

BUILDING RESPONSE AND FRAGILITY CURVES FOR A HIGH-RISE BUILDING WITH AND WITHOUT SOFT STOREY WITH SOIL-STRUCTURE INTERACTION

Avik Samanta¹ and Ravi Kanth Sriwastav²

¹ Assistant Professor, Department of Civil and Environment Engineering, IIT Patna, Bihta, Patna, Bihar - 801103, India, e-mail: asamanta@iitp.ac.in

² Former post-graduate student, Department of Civil and Environment Engineering, IIT Patna, Bihta, Patna, Bihar – 801103, India, e-mail: ravi.mtce14@iitp.ac.in

ABSTRACT

Ground floors of high-rise buildings are often kept open in order to facilitate the social and functional needs of the people such as parking spaces, open halls, etc. This creates a major weak point in this part of the building, causing the lateral forces to concentrate more on this point leading to the sudden change in response parameters along its height, making the buildings more vulnerable to collapse during seismic events. In this study, two residential buildings are studied: a high-rise building with a soft storey and a high-rise building without a soft storey to see their performances during earthquake events. The candidate buildings are located in Patna, India which is a major earthquake prone zone as per the seismic code of India. Non-linear time history analysis is performed for the two candidate buildings using SAP2000. Seismic response of these buildings are obtained in terms of structural acceleration, inter-storey drift etc. Incremental dynamic analysis has been performed to obtain fragility curves for various damage states of the buildings in order to show the comparative performances of the two buildings.

Keywords: Building response, Fragility curves, High-rise building, Non-linear time history analysis, Soft-storey building

1. INTRODUCTION

In the urban areas throughout the world multi-storied buildings have been constructed abundantly keeping the ground storey open. Such opening has been often kept for using the ground floor as parking and social gathering. Performances of such building have been very poor in past earthquakes. The soft or open ground storied buildings are vulnerable to damage during seismic events due to the fact that their ground stories have major weak points which cause the lateral force to concentration more than in any other parts of the buildings. This issue is due to the sudden change of stiffness along the height of these buildings, leading to sudden alteration of transmission of force in the building. The bare frame resists the loads through frame action only while in case of a soft ground storey frame; its upper stories resist the applied lateral loads both through frame action as well as through infill walls while its ground storey resists the loads only through frame action. This sudden alteration of transmission of force in the structure leads to the creation of soft storey mechanism in the building.

Indian state of Bihar has faced a number of moderate to severe earthquakes in the past and it lies in seismic zones IV and V with possible maximum intensity up to 8.4 on the Richter scale. Patna is the capital and most important city of Bihar. The city is located in seismic source zones which in reality are active faults. Patna has huge number of important public and private buildings with many of them are having soft or open ground stories. The main aim of this work is to obtain seismic response of a high-rise building and carry out incremental dynamic analysis to obtain IDA curve and fragility curve for the building with and without soft-storied in Patna. These curves can be used for emergency response and disaster planning, designing retrofitting schemes, risk mitigation, calibration of seismic codes

etc. Soil-structure interaction (SSI) is considered in this study which may be the case for buildings situated on deep soft-soil deposits.

2. BUILDING MODELLING

Reinforced concrete ordinary moment resisting frame buildings are the most common type of building with varied number of storey, shape etc. in this region. These buildings are designed as per the conventional method of IS 456 (BIS, 2000) and ductile detailing is generally absent for these buildings in Patna. A representative nine-storied high-rise building is considered in this study the plan view of which is shown in Figure 1. M25 grade concrete is taken for all structural members while M35 grade concrete is taken for piles. HYSD415 grade steel is taken as all kind of reinforcement bar. slab of 150 mm thick is taken. Design is checked as per IS 456 (BIS, 2000) and IS 1893 (BIS, 2002). The building is designed as ordinary moment resisting framed residential building located at soil type II in Patna, which is in seismic zone IV as per IS 1893 (BIS, 2002). Infill walls are modelled in the form of equivalent struts as “double braced multi-linear plastic link” elements followed by hysteretic Pivot model. According to Cavaleri and Di Trapani (2014) and Cavaleri and Di Trapani (2015), infill wall is mechanically characterized by the parameters the Elastic Young Modulus, Shear Modulus and Poisson Ratio. Plastic hinges are assigned to the numerical model for the sample building. Moment hinges (M3) as per Table 6-7 of FEMA 356 (Concrete Beams) (2000) are assigned at the ends of the beams. P-M2-M3 hinges as per Table 6-8 of FEMA 356 (Concrete Columns) are assigned at the ends of the columns to consider the interaction of axial force and bi-axial bending moments.

2.1 Modelling of Soil-structure Interaction

The soil is modelled as eight-nodded hexahedral solid brick element. The most prominent nature of soil in this region is soft soil. In this study, the boundaries which can fully absorb body waves propagating normal to the boundary proposed by Lysmer and Kuhlemeyer (1969) is used to model damping in the soil. The bottom surface of the soil is fixed. The depth and width of the absorbing boundary are taken as four (4B) and three (3B) times the width of the structure (B) from the centre of the structure in both sides. Pile soil interface is modelled using gap element (Cook et al., 2002). Side views of the building with soil-structure model and infill walls without and with soft storey are shown in Figure 1 and 2, respectively. The modelling is implemented using SAP2000 (CSI, 2013).

3. INPUT SEISMIC GROUND MOTIONS

3.1 Site Specific Design Spectrum

The time history data are required to be compatible with the target response spectrum representing the design seismic action at a site. Anbazhagan et al. (2015) developed the seismic hazard maps of Patna district considering the region specific maximum magnitude and Ground Motion Prediction Equations (GMPEs) by worst-case deterministic and classical probabilistic approaches. Normalized design spectrum at various zones for Patna for 5% damping from four zones for 2% and 10% probability of exceedance in 50 years is obtained from at rock site (Anbazhagan et al., 2015). In this study, the spectrum corresponding to the PSHA for 2% probability of exceedance in 50 years is selected as site specific design spectrum.

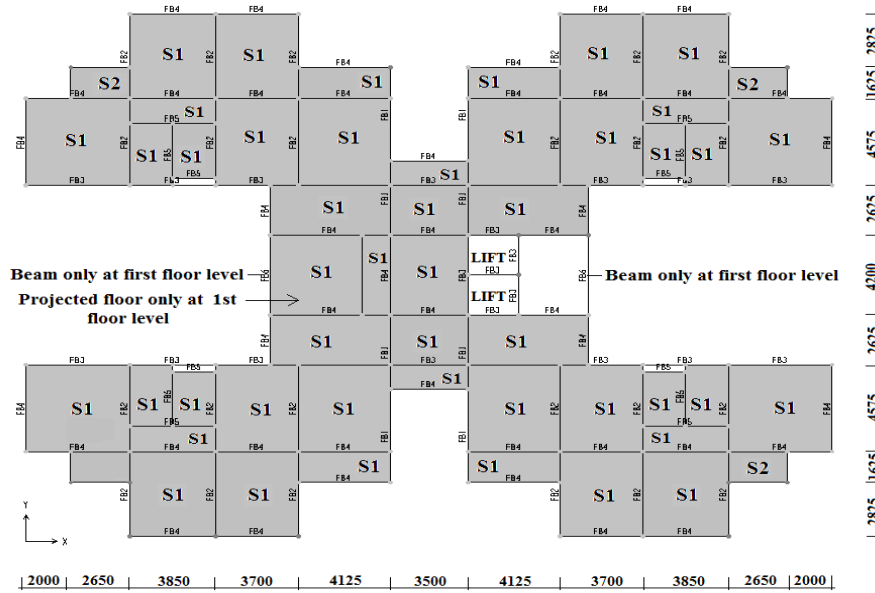


Figure 1: 1st floor plan of slab and floor beams of the building

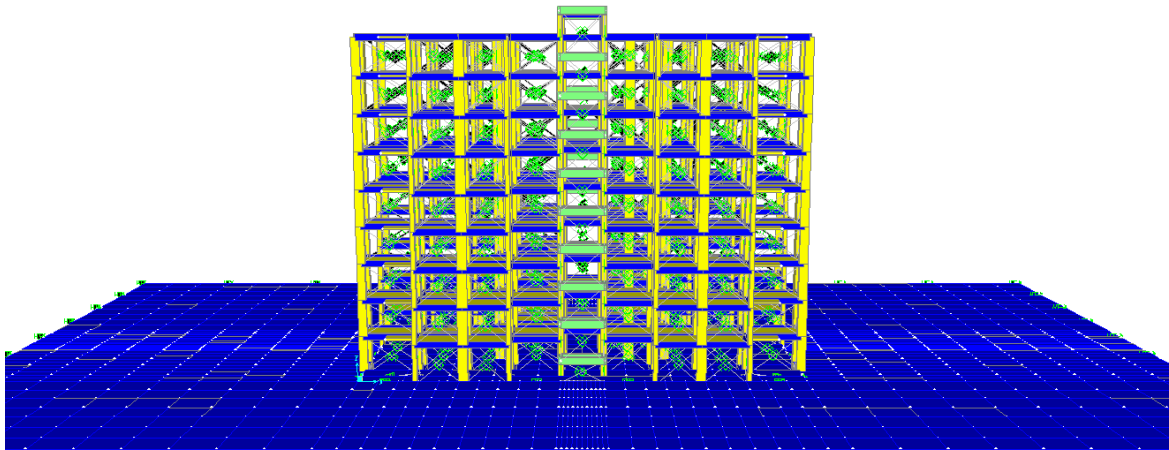


Figure 2: Side view of the building (without soft storey) with infill walls

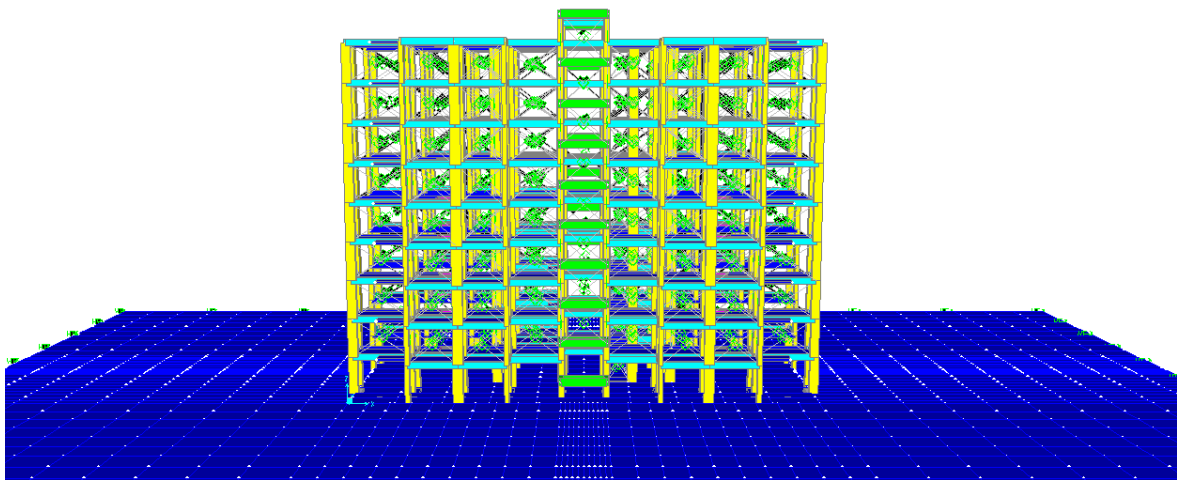


Figure 3: Side view of the building with ground floor as soft storey with infill walls

In this study, 30 pairs of raw ground motions as shown in Table 1 are selected from PEER Ground Motion Database (2015) based on the following parameters: Min and Max Magnitude (M_w) - 6 to 7.5; Min and Max Epicentral Distance (R_{rup}) : 10 to 500 km; Fault Mechanism Type : Reverse, Strike Slip; Min and Max Shear Wave Velocity (V_{S30}): 73 m/s to 385 m/s. The ground motions are selected also depending on the unscaled pseudo acceleration spectra falling in a particular range.

In this study, spectral matching is conducted using spectral matching program RSPMATCH developed by Abrahamson (1998) to all the 30 pairs of selected raw ground motions. Acceleration spectra of all scaled ground motions are compared with the target spectra of Patna as shown in Figure 4.

3.2 Soil Amplification

Shear wave velocity relations with SPT N value correlation equations for Patna are not available in literature. The correlations available in literature for IGB (Indo Gangetic Basin) as well as for regions for different soil conditions in the vicinity of Patna are studied. The equations used in this study are obtained from studies for Kolkata and Kanpur as the soil profile of these areas are similar to Patna. The amplification study is done using EERA (Bardet et al., 2000) for which the variation of shear wave velocity with depth is shown in Figure 5. The amplified ground motions are used as input for the buildings with SSI as some earlier studies have used the same ground motions for the analyses of the both models.

Table 1: Selected ground motions from PEER NGA database

RSN No.	Earthquake name	Year	Station Name	Magnitude	Mechanism	Vs30 (m/s)	Rrup (km)
12	Kern county	1952	"LA - Hollywood Stor FF"	7.36	Reverse	316.46	117.75
13	Kern county	1952	"Pasadena - CIT Athenaeum"	7.36	Reverse	315.13	125.59
15	Kern county	1952	"Taft Lincoln School"	7.36	Reverse	385.43	38.89
22	El Alamo	1956	"El Centro Array #9"	6.8	strike slip	213.44	121.7
36	Borrego Mtn	1968	"El Centro Array #9"	6.5	strike slip	213.44	222.42
37	Borrego Mtn	1968	"LA - Hollywood Stor FF"	6.63	strike slip	316.46	199.84
38	Borrego Mtn	1968	"LB - Terminal Island"	6.63	strike slip	217.92	207.14
39	Borrego Mtn	1968	"Pasadena - CIT Athenaeum"	6.63	strike slip	315.13	129.11
51	San Fernando	1971	"2516 Via Tejon PV"	6.61	Reverse	280.56	173.16
52	San Fernando	1971	"Anza Post Office"	6.61	Reverse	360.45	113.02
53	San Fernando	1971	"Bakersfield - Harvey Aud"	6.61	Reverse	241.41	214.32
54	San	1971	"Borrego	6.61	Reverse	338.54	112.52

	Fernando		Springs Fire Sta"					
1	Helena Montana	1935	"Carroll College"	6		strike slip	286.00	2.86
3	Humboly bay	1937	"Ferndale Hall"	City 6.8		strike slip	219.31	71.57
6	Imperial Valley-02	1938	"El Centro Array #9"	6		strike slip	213.44	6.09
7	Northwest Calif-02	1941	"Ferndale Hall"	City 6.6		strike slip	219.31	91.22
17	Southern Calif	1952	"San Luis Obispo"	6		strike slip	293.50	73.41
19	Central Calif-01	1954	"Hollister Hall"	City 6.3		strike slip	198.77	25.81
24	Central Calif-02	1960	"Hollister Hall"	City 6		strike slip	198.77	9.02
31	Parkfield	1966	"Cholame Shandon Array #5"	- 6.19		strike slip	289.56	63.34
42	Lytle Creek	1970	"Cedar Springs Pumphouse"	6.53		Reverse Oblique	277.22	19.35
47	Lytle Creek	1971	"Lake Hughes #1"	6.53		Reverse Oblique	225.34	30.02
95	Managua Nicaragua	1972	"Managua ESSO"	6.95		strike slip	288.77	4.33
96	Point Mugu	1973	Hueneme "Gilroy Array #1"	6.59		strike slip	213.44	17.71
97	Hollister-03	1974	Gilroy "Hollister Hall"	City 7.14		strike slip	128.14	10.46
98	Hollister-03	1974	Hollister "San Juan Bautista"	7.14		strike slip	198.77	9.39
99	Hollister-03	1974	"San Juan Polk St"	24 7.2		strike slip	335.50	9.11
101	Northern California	1975	"Cape Mendocino"	7.36		Reverse	267.78	34.73
15	Kern county	1952	"Taft School"	Lincoln 6.4		strike slip	385.00	38.89
10	Imperial Valley-03	1951	"El Centro Array #9"	6		strike slip	213.44	25.24

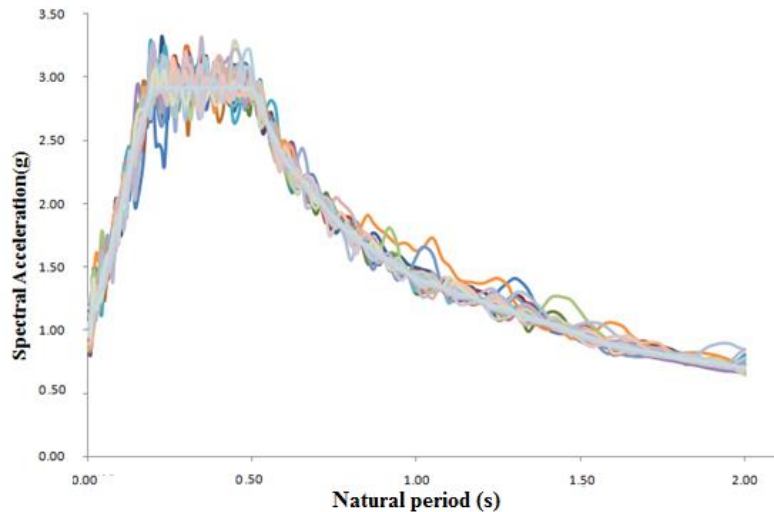


Figure 4: Comparison of spectra of 30 spectrally matched ground motions with the target spectrum

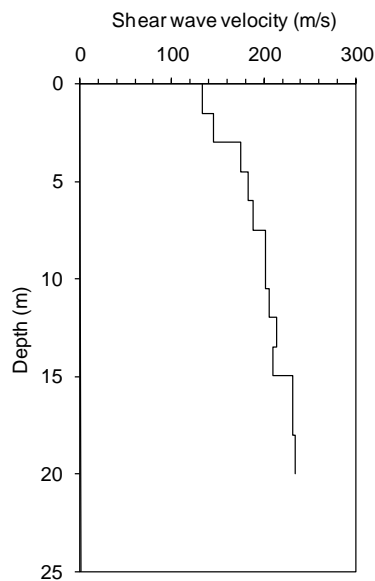


Figure 5: Borehole data used for present analysis

4. RESULTS OF NONLINEAR TIME HISTORY ANALYSIS

The results are shown in the form of median and dispersion of inter-storey drift, floor acceleration and average floor spectral accelerations between 0.0303s to 0.2s period (5-33 Hz) range for all stories through Figures 6-11. The responses are plotted with minimum, 16th percentile, median, 84th percentile, maximum values. The responses are plot shown for buildings without and with soft storey effect including SSI.

For the building with SSI fundamental period is found as 1.02 sec and for the same building with open ground storey (OGS) SSI structural system it is 1.38sec. This is due to decrease in stiffness of the system.

There is huge difference in dispersion pattern of the floor displacement for different storey when the model of building with and without OGS is compared. For the model without OGS floor displacement is increasing with the increasing storey level whereas for the model with OGS it is almost same with increasing storey level. The pattern of inter-storey drift ratio is also completely different for these two cases. For the model without OGS inter-storey drift ratio is increasing till 4th floor above which it is decreasing (Figure 6). In building model with OGS inter-storey drift ratio is maximum at the first floor and the value is decreasing with increasing floor levels (Figure 7). Maximum inter-storey drift ratio is at 4th floor for building without OGS and for the building with OGS it is at 1st floor.

The floor acceleration in case of building without OGS is higher (Figure 8) compared to the building with OGS (Figure 9). Trend of mean spectral acceleration values are similar in both cases except it is slightly higher for the building without OGS (Figures 9 and 10).

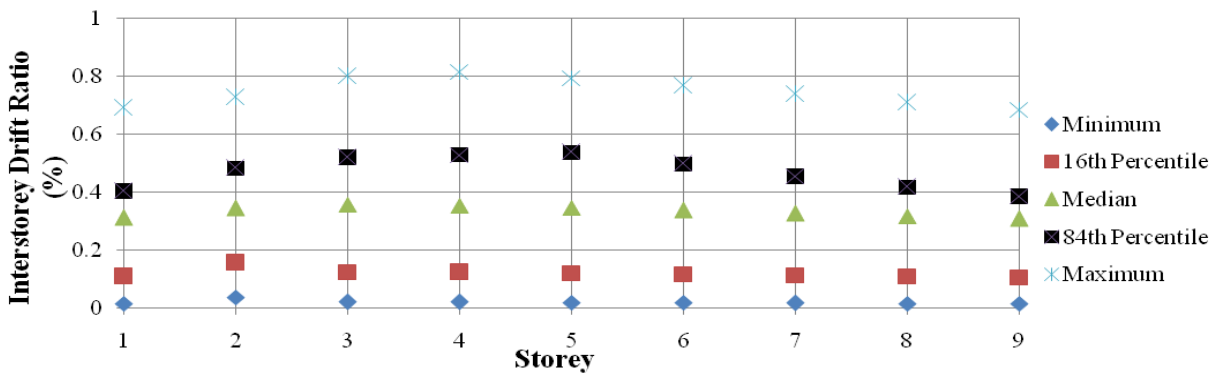


Figure 6: Inter-storey drift ratio for different floors for building without soft storey in x-axis

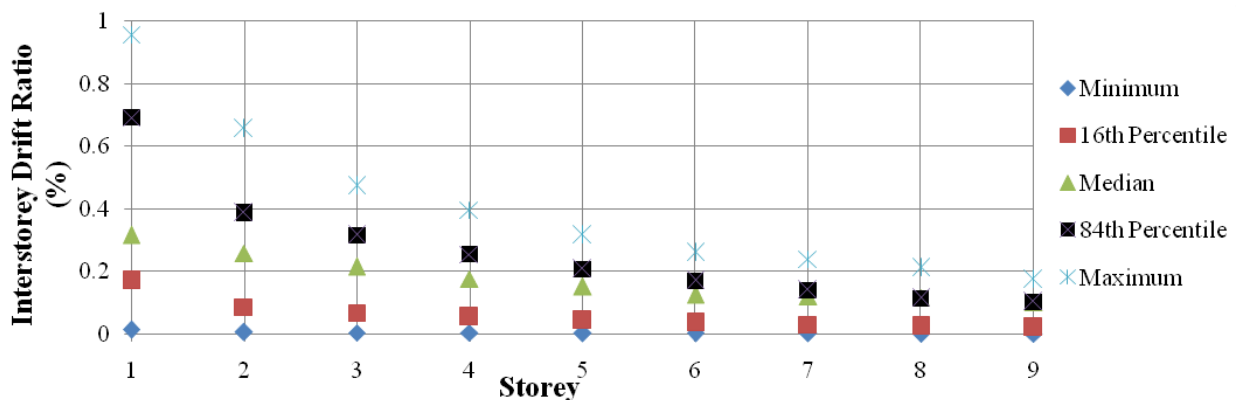


Figure 7: Inter-storey drift ratio for different floors for building with soft storey in x-axis

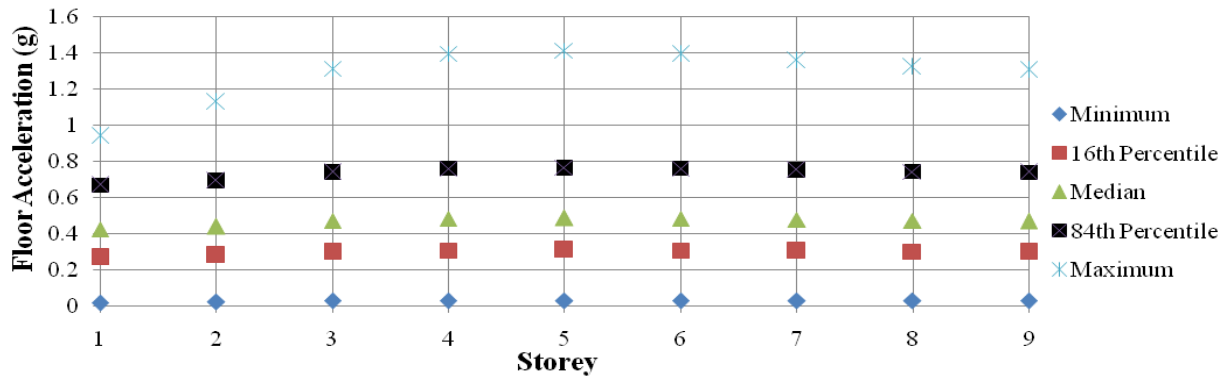


Figure 8: Floor acceleration for different floors for building without soft storey in x-axis

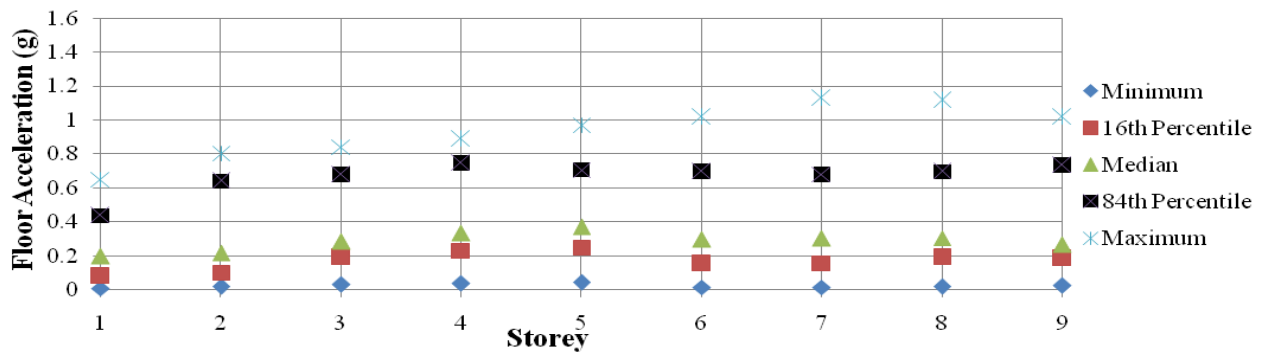


Figure 9: Floor acceleration for different floors for building with soft story in x-axis

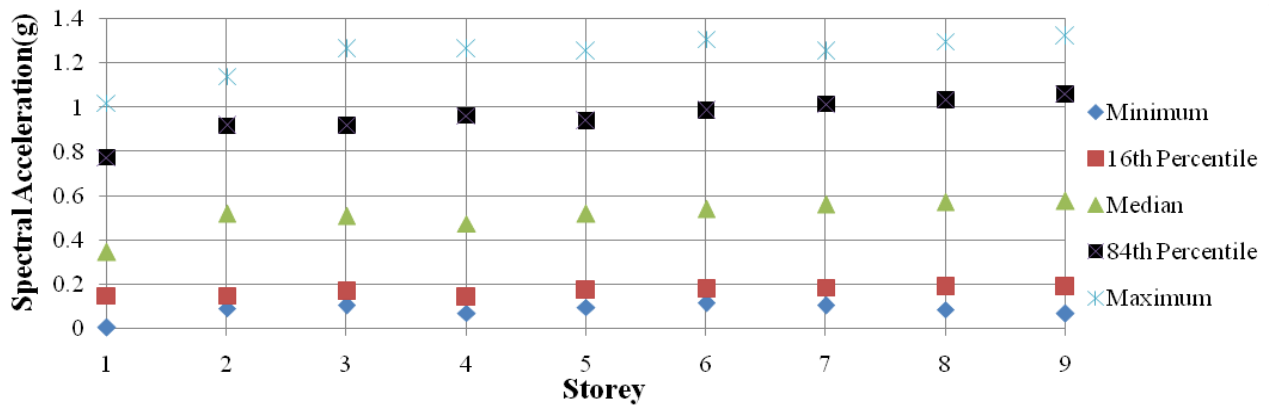


Figure 10: Average Floor Spectral Acceleration between 0.0303s to 0.2s for different floor for building without soft storey

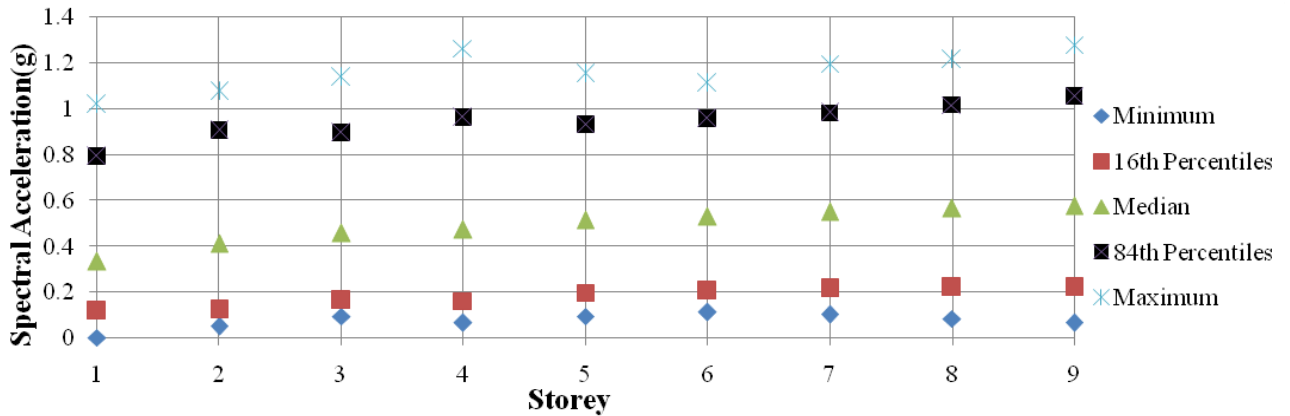


Figure 11: Average Floor Spectral Acceleration between 0.0303s to 0.2s for different floor for building with soft storey

5. DEVELOPMENT OF FRAGILITY CURVES

IDA curve is the plot of peak ground acceleration in ordinate and the inter storey drift ratio in abscissa. The curve is obtained by carrying out incremental dynamic analysis in which time history analysis is conducted a number of times for 30 pairs of acceleration time histories for various level of scaling. For each scaling level PGA as well as maximum inter-storey drift ratio is taken and the curve is plotted for each ground motion. IDA curve is the key requirement for plotting fragility curve by incremental dynamic analysis. Here a set of 30 ground motion is taken and 30 IDA curves are plotted in Figures 12 and 13. IDA curve is less scattered for low inter-story drift ratio values in case of building without OGS. The values are more scattered for low inter-story drift ratio for the building with OGS.

From the IDA curves of each ground motion, PGA values are calculated for IDR values corresponding to 0.63%, 1%, 2% and 4% which represent slight, moderate, extensive and complete damage states, respectively. Median and lognormal standard deviation values of PGA for each damage state are calculated and corresponding fragility curve for the same damage state is obtained by using cumulative normal distribution function. The comparison of fragility curves are shown in Figure 14 to Figure 15. Table 2 obtained from the fragility curves of buildings (Figures 14 and 15) clearly indicates that OGS in a building has increased the level of risk for all damage states. There is not much change in probability of exceedance in slight damage states. For moderate, extensive and complete damage states the risk increases with the application of OGS.

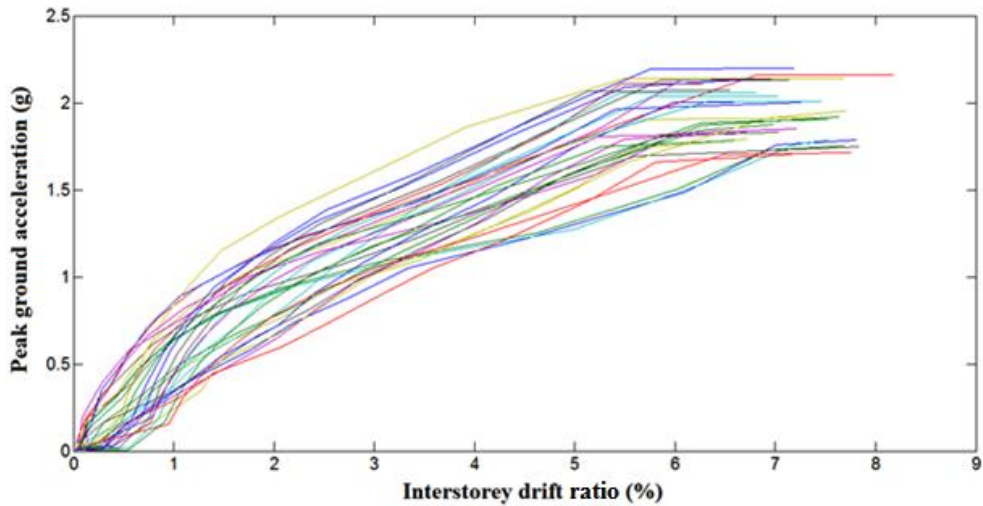


Figure 12: IDA curve of building without soft storey for 30 ground motions

Table 2: Result table

Max PGA	SHA	Damage state	Probability of exceedance	
			Building with SSI	Building with SSI & OGS
1.22g	PSHA, 2% probability of exceedance in 50 years	Slight	98%	100%
		Moderate	80%	97%
		Extensive	61%	78%
		Complete	37%	35%
0.456g	PSHA, 10% probability of exceedance in 50 yrs	Slight	48%	56%
		Moderate	19%	11%
		Extensive	10%	1%
		Complete	3%	0%

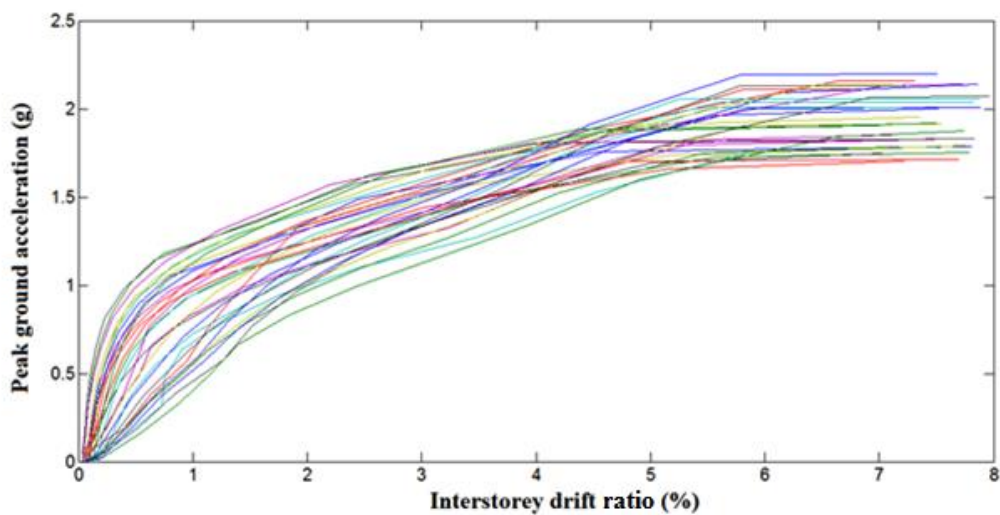


Figure 13: IDA curve of building with soft storey for 30 ground motions

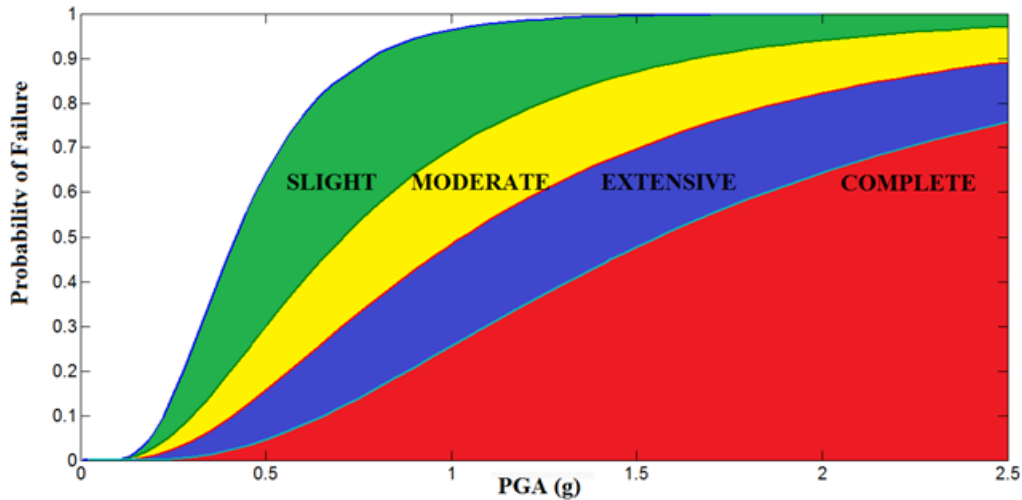


Figure 14: Fragility curve of building without soft storey

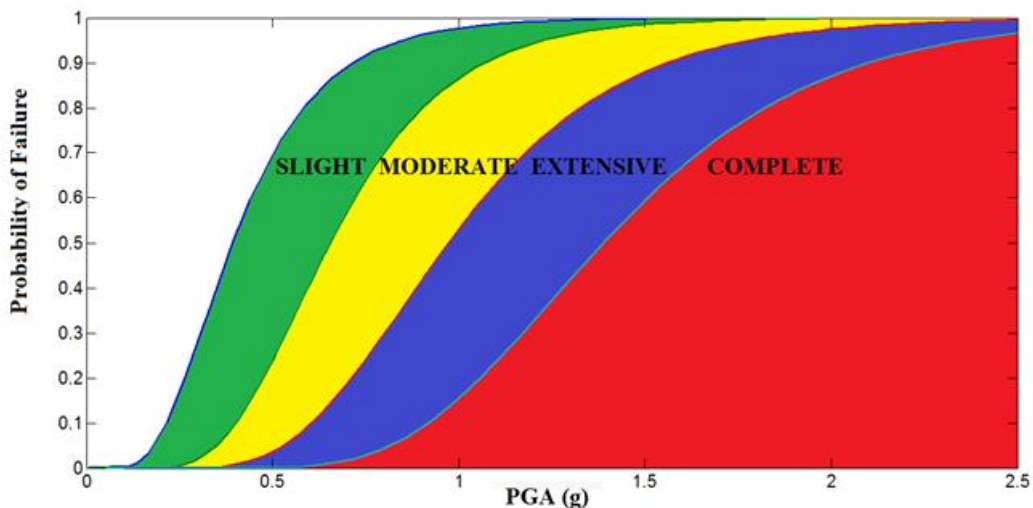


Figure 15: Fragility curve of building with soft storey

6. SUMMARY AND CONCLUSIONS

In this study a set of 30 raw acceleration time histories are used which are selected based on regional earthquake characteristics of Patna, to obtain spectrally matched and amplified ground motions and they are used to obtain fragility curves for a nine-storied building with and without open ground storey. For amplification of the ground motion, suitable shear wave velocity - 'N' value correlations available in literature for different type of soil is selected. The knowledge of the buildings already present in Patna and the construction practices is also necessary to determine its importance and to model the building. The high-rise building is modeled in SAP2000 with SSI by gap/link element method, and dynamic non-linear analysis is carried out for obtaining the response of the building in terms of maximum inter-storey drift ratio, floor acceleration and mean spectral acceleration of all the floors. The study includes soil-structure interaction, which may be a case for buildings resting on soft-soil to derive the seismic fragility curves. It is shown through fragility curve that building with soft storey or open ground storey show increased probability of damage during earthquake.

REFERENCES

- Abrahamson, N.A. (1998). Non-stationary spectral matching program RSPMATCH. Pacific Gas and Electric Company Internal Report.
- Anbazhagan, P., Bajaj, K., & Patel, S. (2015). Seismic hazard maps and spectrum for Patna considering region-specific seismotectonic parameters. *Natural Hazards*, 78(2), 1163–1195.
- Bardet, J.P., Ichii, K., & Lin, C.H. (2000). EERA: A Computer program for Equivalent-linear Earthquake site Response Analysis of Layered soil deposits. Department of Civil Engineering, University of Southern California.
- Bureau of Indian Standards (BIS). (2000). IS 456: 2000 Indian Standard Plain and Reinforced Concrete - Code of Practice.
- Bureau of Indian Standards (BIS). (2002). IS 1893 (Part 1): Indian Standard Criteria for Earthquake Resistant Design of Structures, General Provisions and Buildings (Fifth Revision).
- Cavaleri, L., & Di Trapani, F. (2014). Cyclic response of masonry infilled RC frames: Experimental results and simplified modeling. *Soil Dynamics and Earthquake Engineering*, 65, 224–242.
- Cavaleri, L., & Di Trapani, F. (2015). Prediction of the additional shear action on frame members due to infills. *Bulletin of Earthquake Engineering*, 13, 1425–1454.
- Computers and Structures, Inc. (2013). CSI Analysis Reference Manual.
- Cook, R.D., Malkus, D.S., Plesha, M.E., & Witt, R.J. (2002). *Concepts and Applications of Finite Element Analysis*. John Wiley & Sons.
- FEMA - Federal Emergency Management Agency, (2000). *Prestandard and commentary for the seismic rehabilitation of buildings*, FEMA 356. Washington, D.C.
- Lysmer, J., & Kuhlemeyer, R.L. (1969). Finite Dynamic Model for Infinite Media. *Journal of Engineering Mechanics Division*, 95, 859–878.
- Pacific Earthquake Engineering Research Center (PEER) (2015). PEER NGA database flatfile. <http://peer.berkeley.edu/nga/flatfile.html>.

FABRICATED STEEL BOX COMPOSITE COLUMN AND ITS ADVANTAGES - BANGLADESH PERSPECTIVE

A.K.M. Ruhul Amin¹, Md. Khasro Miah² and Md. Nazrul Islam³

¹Ph.D Student, Department of Civil Engineering, DUET, Gazipur, Bangladesh,
e-mail: ruhul69@yahoo.com

² Professor, Department of Civil Engineering, DUET, Gazipur, Bangladesh,
e-mail: mkhasro@duet.ac.bd

³ Professor, Department of Civil Engineering, DUET, Gazipur, Bangladesh,
e-mail: nazrul2100@duet.ac.bd

ABSTRACT

Tall buildings are now widely constructed in all over the world. The construction materials strength is the key factor to build the high rise structures. Concrete has compressive strength, stiffness and stability whereas steel has tensile strength, ductile behavior but both of those behaviors are not found in one material. As a result the composite materials are required to build tall buildings. The combined behavior of steel and concrete is reduced the member size and provide more strength for constructing tall buildings. Steel is widely used as reinforcement in reinforced concrete structure. On the other hand, in steel building construction system, steel is used to build the main frame work to resist the structural forces. Steel construction is rapid and speedy work in respect to reinforce concrete construction work. So, considering all the behavior of steel and concrete, a new type of member with different shape and geometry of steel plate with concrete called composite members is developed. The composite column is one of them. There are three type of composite column according to their construction, geometry and placement of steel and concrete. The behavior of concrete is changing with it placement in column. The concrete confinement is a factor to implement the total concrete strength of a member. The strength of confined concrete is more than unconfined concrete. As a result the concrete filled box composite column is contributing better strength than other composite columns. The steel box composite column can be constructed in hot rolled tube or box section. But for the shape and size of the hot rolled box is fixed in its construction process. In cold rolled process, the steel box is fabricated with steel plate of different thickness like the built up members. As a result because of different type and shape, different combination of plate can be made to fabricate the steel box. So the fabricated box is now popular for the box column construction all over the world. Also the box can be fabricated manually or automatically. There is some automated machine is available to fabricate the steel box.

Keywords: steel box, fabrication, concrete properties, finite element, composite, ANSYS,

1. INTRODUCTION

Tall buildings would be impossible without advances in technology. The composite steel frame skeleton was nothing, but a structural revolution when it was developed in Chicago in the late nineteenth century, and it has been evolving ever since. Early tall buildings constructed with cast iron framing were susceptible to fire and it was discovered that encasing the iron with concrete increased the material's resistance to fire. United State of America introduced composite construction system in 1894. After that it used in many tall building structures all over the world. Experimental researches were carried out on the composite column for different shape and size, different materials strength, different ratio of steel and concrete proportion. The experimental and theoretical research were conducted on concrete filled steel tubular column from 1960 to 2000 by many researchers. Furlong (1967) conducted tests on the ultimate loads of concrete-filled steel box columns. Knowles and Park (1969), Tomii et al. (1977), Shakir-Khalil and Mouli (1990) and Schneider (1998) have conducted tests on concrete-filled steel tubular column. Ge and Usami (1992), Uy and Bradford (1995) and Uy (2000) studied on local buckling of concrete-filled steel box columns.

Liang and Uy (1998) proposed effective width models for the analysis and design of steel plates in concrete-filled thin-walled steel box columns. Structural steel and its use in Bangladesh can be traced back from the British period with its use in bridges and railway projects. After Bangladesh established and from the early nineties structural steel is starting use in steel buildings mainly gable frame structures. At that time, those steel section are imported from abroad. After ninety, local fabrication factories develop and started the fabrication of built up section. Using hot rolled plates those members are fabricated. The source of plate materials was available in local market, and ship breaking, and some are imported plates from abroad. Hot rolled sections were also used as per project requirement. Bangladesh has no hot rolled steel section production factory, so all hot rolled steel sections were imported from abroad. Now-a-days Bangladesh construction industries developed the steel construction system, many multistoried steel building is constructed and start using the composite members in the structural system. For the fire rating requirements concrete encasing steel column is introduced first. Again the same type of column introduce for retrofitting of the weak structures. Now the designer start using the composite column in the design of new structures. Recently Concrete filled fabricated steel box composite column (FSBCC) is introduced in buildings and a renowned prefabricated steel company Bultrade Engineering Limited is started fabrication of FSBCC. Composite columns can have high strength for a relatively small cross-sectional area, meaning that usable floor space can be maximized. There are several different types of composite column, the most common being a hollow section steel tube which is filled with concrete shown in Figure 1 or and open steel section encased in concrete. The concrete infill increase the compression resistance of the steel section and preventing the steel from buckling.

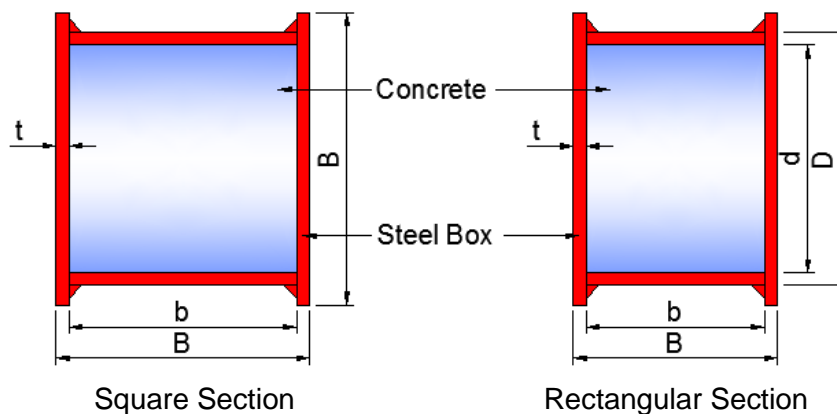


Figure 1: Concrete-filled steel box columns

2. TYPE OF COMPOSITE COLUMN

Two basic types of composite columns are mostly used in buildings: those with the steel section encased in concrete and those with the steel section filled with concrete. One of the common and popular columns is the encased steel profile as shown in Figure 2, where a steel H-section is encased in concrete. Sometimes, structural pipe, tube, or built up section is placed instead of the H-section. In addition to upholding a proportion of the load acting on the column, the concrete encasement enhances the behavior of the structural steel core and horizontal bar reinforcement, and so making it more effective against both local and overall buckling. The load-bearing concrete encasement performs the additional function of fireproofing the steel core. The cross sections, which normally are square or rectangular, must have one or extra longitudinal bars placed in every single corner and these have to be tied by lateral ties at regular vertical intervals in the manner of a reinforced concrete column. Ties are effective in rising column strength, confinement and ductility. Furthermore, Ties stop the longitudinal bars from being displaced during construction and they resist the tendency

of these same bars to buckle outward under load, which would cause spalling of the outer concrete cover even at low load levels, remarkably in the case of eccentrically loaded columns. It will be noted that these ties will be open and U-shaped. Otherwise, they might not be installed, because the steel column shapes will have always been erected at an earlier time.

2.1 Concrete Filled Composite Columns

In this type of composite columns, a steel pipe, steel tubing, or built up section is filled with concrete showed in Figure3. The most common steel sections used are the hollow rectangular and circular tubes. Filled composite columns may be the most efficient application of materials for column cross sections. It provides forms for the inexpensive concrete core and increases the strength and stiffness of the column. In addition, because of its relatively high stiffness and tensile resistance, the steel shell provides transverse confinement to the concrete, making the filled composite column very ductile with remarkable toughness to resist the loads. Fabricated Steel box composite column is a built up hollow box section, assemble with four steel plate and bearing stiffeners in both ends of column. Some intermediate stiffeners also given in the column to transfer the concrete load to steel box and reduce the plate buckling. FSBCC has the flexibility to make any size with different combination of steel plate with the different width thickness ratio.

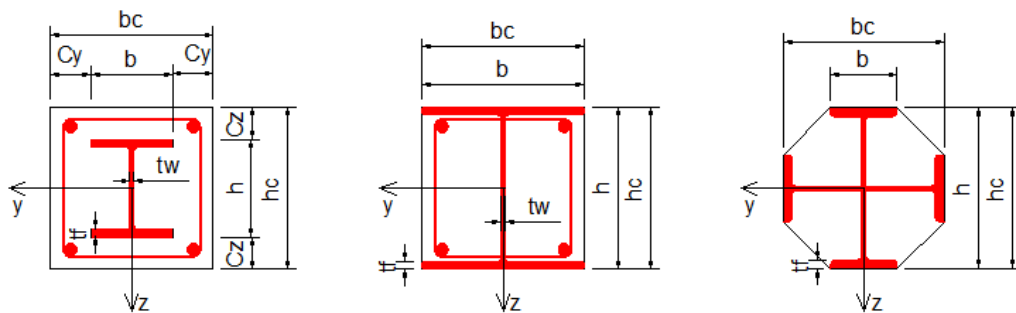


Figure 2: Typical Section of Fully and partially encase composite column

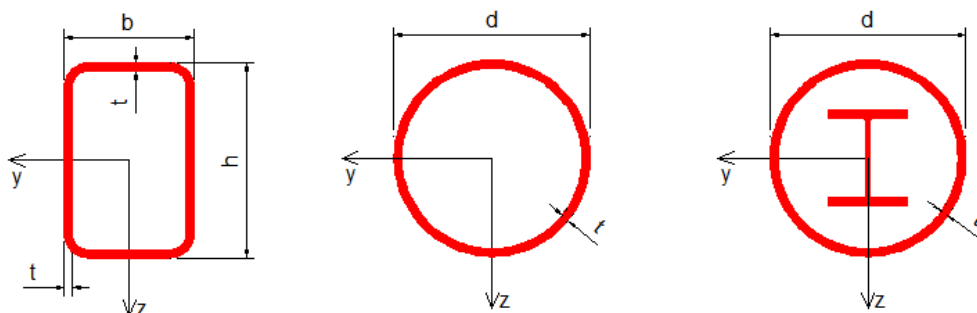


Figure3: Typical Section of Concrete fill composite column

3. FABRICATED STEEL BOX COMPOSITE COLUMN IN BANGLADESH

In 2016 the first FSBCC has been constructed in dormitory Building at BSRM Bilade Casting Plant, Chittagong. After that, in 2017 Bachelor quarter of Jessore Air Force Base, started and the construction work is running Figure 4. Special type box fabrication machine is invented, using those machine, four steel plates assemble the box and welded

automatically. So the quality of welding is found error free. The columns can be fabricated with all require connectivity and after site erection, concrete is filled by pumping. Steel-concrete composite column are widely use in high rise building and bridges. Tall building construction is increased all over the world and the structural member size became larger in the structures according to its height and loading. Reinforced concrete structure and steel structures are commonly used for construction of high rise buildings. High strength material is introduced in construction industries to build the high rise structures. From the continuous research on material and its behavior the composite material is found as hybrid materials for construction work



Figure4: Concrete-Filled Fabricated Steel Box Composite Column (FSBCC) Bachelor Quarter, Air Force Base, Joshore Bangladesh 2017

4. DESIGN AND CODE FOR FSBCC

Rectangular and circular hollow sections are most commonly used, although rectangular sections are beneficial for being having flat faces suitable for end plate beam to column connections. However, fin plates can be used for rectangular and circular shape. Composite structure design procedure are describe in AISC LRFD(2010), ACI 318(2014), Euro code-4(2005), Canadian Standard Association CSA (2009), Architectural Institute of Japan(AIJ 2005) and Egyptian code(2012).The AISC-LRFD (2010) defines a composite column as a steel column fabricated from rolled or built up steel shapes and encased in structural concrete or fabricated from steel pipe or tubing and filled with structural concrete. In this specification, the design method for composite columns is based on the ultimate strength of the materials of the cross section and takes into account the inelastic material properties with the required design loads as factored service loads. It contains the latest design approach of structural steel based on the ultimate strength concept.

The nominal strength of a composite cross section is calculated from the ultimate resistance to load, and reduction capacity factors related to material properties and characteristics of member failure are applied to the nominal strength of the cross section. The strength provisions for concrete-encased composite columns as recommended in Chapter I of the AISC-LRFD (2010). In order for dissimilar materials to act in a composite manner, forces must be transferred between the materials so that they achieve a state of internal equilibrium with one another. Previous editions of the AISC-LRFD specification briefly address load transfer; however, these provisions are quite limited in scope and clarity. The AISC-LRFD (2010) specification significantly expands load transfer requirements in a new section. Clear guidance is now provided for the allocation of forces between steel and concrete sections as well as for force transfer mechanisms used for composite members.

The design of composite column is based on the design equation for steel columns AISC-LRFD (2010). The slenderness and area parameters are modified for the presence of concrete. Load transfer should be provided by direct bearing at the connections. Compressive strength for non-compact filled members is determined in accordance with AISC Specification Section 2.2b(b). The capacity calculation of FSBCC is calculated by the equations as;

$P_p = f_y A_s + C_2 f'_c \left(A_c + A_{sr} \frac{E_s}{E_c} \right)$ where, P_p is the column capacity at $C_2 = 0.85$ for rectangular section.

$P_y = f_y A_s + 0.7 f'_c \left(A_c + A_{sr} \frac{E_s}{E_c} \right)$ P_y is the column capacity at $C_2 = 0.7$

$P_{no} = P_p - \frac{P_p - P_y}{(\lambda_r - \lambda_p)} (\lambda - \lambda_p)^2$ where $\lambda = \frac{bi}{t}$, $\lambda_r = 3 \sqrt{\frac{E}{f_y}}$, $\lambda_p = 2.26 \sqrt{\frac{E}{f_y}}$

$C_3 = 0.6 + 2 \left(\frac{A_s}{A_c + A_s} \right)$ where $C_3 \leq 0.9$

$EI_{eff} = E_s I_s + E_s I_{sr} + C_3 E_c I_c$

$P_e = \pi^2 (EI_{eff}) / (KL)^2$ where P_e is the buckling load of column

$P_n = P_{no} [0.658^{P_{no}/P_e}]$ where P_n is maximum load capacity of column

Where

A_c = area of concrete mm²

A_{sr} = area of continuous reinforcing bars, mm²

A_s = area of steel section, mm²

E_c = modulus of elasticity of concrete, MPa

E_s = modulus of elasticity of steel, MPa

EI_{eff} = effective moment of inertia rigidity of composite section, Kip-mm²

f_{cu} = specified minimum concrete compressive strength, MPa

f_y = yield stress of steel section, MPa

f_{ysr} = specific minimum yield stress of reinforcing bars, MPa

I_c = moment of inertia of the concrete section, mm⁴

I_s = moment of inertia of the steel section, mm⁴

I_{sr} = moment of inertia of the reinforcing bars, mm⁴

K = effective length factor

L = laterally unbraced length of the member, mm.

5. NUMERICAL MODEL OF COMPOSITE COLUMN

Finite element (FE) technique is becoming more and more popular in modeling of composite columns. There are some commercially available software for this work, such as ANSYS and ABAQUS. Three dimensional solid model analysis allows the direct modeling of the composite action between the steel and concrete components with different factors. The same allows for detailed simulation of composite members. In this type of analysis, the concrete core is commonly modeled with solid elements, while the steel tube is modeled with shell elements. The interface between the two materials is assembled together by some connector or interface elements to simulate the interaction between the steel and concrete components. Many researchers adopted solid model for simulating the static performance of composite columns. For example, Schneider(1998) presented an experimental and analytical study on the behavior of short, concrete filled steel tube columns concentrically

loaded in compression to failure. 20-noded brick element and 8-noded shell element are adopted for simulating concrete and steel tube.

5.1 Element consider in numerical model

In this Numerical study ANSYS (APDL) and ANSYS Work Bench Version 15 is use to analysis all the models to verify and check the validity and accuracy of the finite elements results. The results are compared with the experimental result to predict the accuracy of the numerical analysis. The 3D model is used Solid elements for modeling the concrete and steel materials Figure 5. The solid is capable of cracking in tension and crushing in compression. The element is defined by eight nodes and has three degrees of freedom at each node. The concrete element SOLID 65 is simulate the behavior of concrete and SOLID 45 element is use to simulate the steel materials. The elements have plasticity, creep, swelling, stress stiffening, large deflection, and large strain capabilities. The parameters of the concrete and steel use in this study is, modulus of elasticity $E_c=4700\sqrt{f'_c}$ in SI unit and $E_s = 2 \times 10^5 \text{Mpa}$.

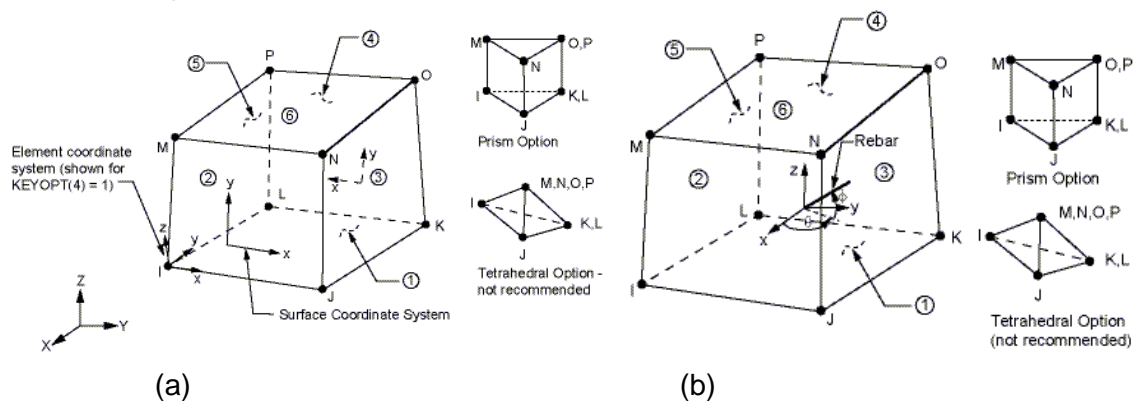


Figure 5: Elements Geometry (a) SOLID 65 and (b) SOLID45

5.2 Material models for structural steel

Modeling of the steel box has been carried out as an elastic-perfectly plastic material in both tension and compression. Mainly steel plate materials with different yield strength are used for fabricating the box. Steel is a ductile material which experience large inelastic strain beyond the yield point. So the true stress and logarithmic strain graph which is also called hardening curve is considering for the material behavior of steel. In ANSYS Parametric Design Language (APDL) bilinear and multi-linear stress strain curve can be used to analysis the steel materials. The stress-strain curve used for the steel box is shown in Figure 6(a). The yield stress, modulus of elasticity, and Poisson's ratio of the steel box have been respectively taken as 252MPa, $2 \times 10^6 \text{MPa}$, and 0.3 that are identical to those in the corresponding experiment. VonMises yield criterion, an associated flow rule, and isotropic hardening have been also utilized in the nonlinear material model.

5.3 Material model for concrete

Material models for concrete are assumed that the confinement effect increases only the ductility of the concrete in concrete-filled steel box columns but not its strength (Tomii and Sakino, 1979). The multi linear stress-strain curve for concrete in concrete-filled steel box columns is shown in Figure 4. The stress-strain curve is modeled using the equation suggested by Mander et al. (1988). The compressive strength and modulus of elasticity of concrete have been respectively adopted as 25MPa and $23.5 \times 10^3 \text{MPa}$ which are the same as those in the corresponding experiment. 6(b) shows the equivalent uniaxial stress-strain curves for concrete, which have been used in this study to model concrete.

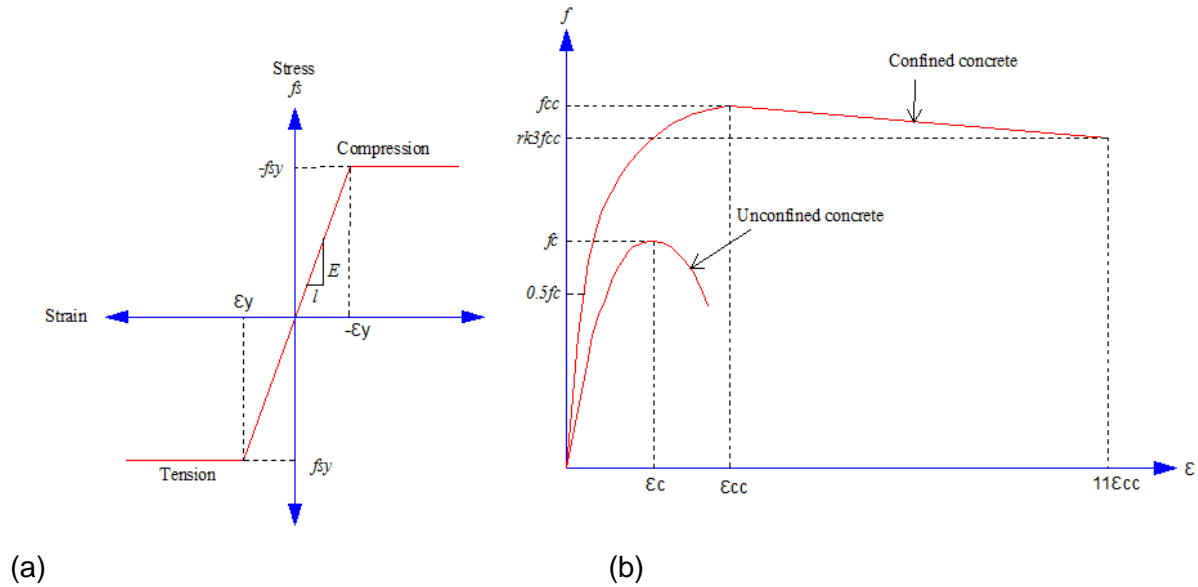


Figure 6: stress-strain curve (a) steel, (b) concrete

The confined concrete compressive strength, f_{cc} and the corresponding confined strain ϵ_{cc} is obtained from equations as shown below;

$$f_{cc} = f_c + K_1 f_1 \quad \text{where, } K_1 \text{ is a factor}$$

$$\epsilon_{cc} = \epsilon_c \left(1 + K_2 \frac{f_1}{f_c} \right) \text{ where, } K_2 \text{ is a factor}$$

The empirical equation has been used to determine the initial Young's modulus of confined concrete E_{cc} . The Poisson's ratio ν_{cc} of confined concrete has been considered as 0.2.

$$E_{cc} = 4700 \sqrt{f_{cc}}$$

6. EXPERIMENTAL DATA

A set of experimental data is taken from the paper of Hasan Abdulhadi (2015), published in the Journal (International Journal of Innovative Research in Science, Engineering and Technology) February 2015. The test specimen details are given in Table 1. The experimental and analytical data are shown in Table 2.

Table 1: Specimen detail of Hasan Abdulhadi(2015)

Square Sample	Width (mm)	Thickness (mm)	Length (mm)	Type of Concrete	f_c Mpa	f_y Mpa
SH-1	150	3	300	Hollow	-	252
SF-1-A	150	3	300	Normal concrete (A)	25	252
SF-1-B	150	3	300	High Strength concrete (B)	60	252
SH-2	150	4	300	Hollow	-	306
SF-2-A	150	4	300	Normal concrete (A)	25	306
SF-2-B	150	4	300	High Strength concrete (B)	60	306
SH-3	150	5	300	Hollow	-	285
SF-3-A	150	5	300	Normal concrete (A)	25	285
SF-3-B	150	5	300	High Strength concrete (B)	60	285

Table 2: Axial Load at failure and attendant deflection carried by the specimen of Hasan Abdulhadi (2015)

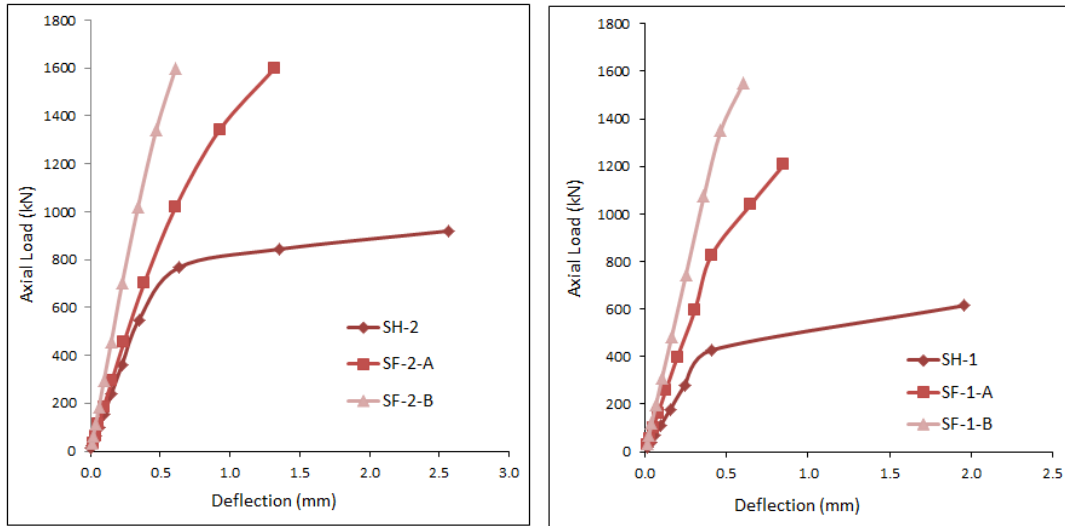
Samples	Axial load at failure (kN)			Deflection attendant at maximum load(mm)		
	P_{exp}	P_{ana}	P_{ana}/P_{exp}	Δ_{exp}	Δ_{ana}	$\Delta_{ana}/\Delta_{exp}$
SH-1	579	611	1.05	2.00	1.86	0.93
SF-1-A	1125	1296	1.15	3.31	3.40	1.02
SF-1-B	1361	1486	1.09	2.81	2.96	1.05
SH-2	620	662	1.06	2.11	2.24	1.06
SF-2-A	1215	1326	1.09	3.00	3.48	1.16
SF-2-B	1543	1724	1.11	2.91	3.23	1.10
SH-3	675	737	1.09	1.70	1.94	1.14
SF-3-A	1300	1450	1.11	2.61	2.90	1.11
SF-3-B	1615	1816	1.12	3.10	3.35	1.08

7. NUMEICAL RESULTS AND DISCUSSION

Using same geometry and material properties shown in Table 1, Table 2 and ANSYS APDL having version of 15 numerical analysis of a number of specimens are carried out. From the numerical analysis, a set of result found and shown in Table 3. Load carried capacity and deflection characteristic of each of the specimen are recorded and compared with experimental data of Hasan Abdulhadi (2015). The comparison is found well agreed and the variation is insignificant in respect of load carrying capacity. The data received are plotted in the form of load versus deflection curves as shown in Figure 7, in which the ordinate indicates applied load and the abscissa indicates deflection attendant at different ranges of load.

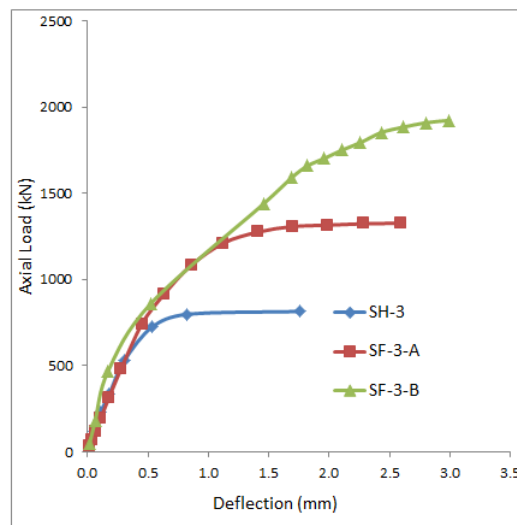
Table3: Axial Load at failure and attendant deflection data found from this analytical study

Samples	Axial load at failure (kN)			Deflection attendant at maximum load(mm)		
	P_{exp}	P_{ana}	P_{ana}/P_{exp}	Δ_{exp}	Δ_{ana}	$\Delta_{ana}/\Delta_{exp}$
SH-1	579	614	1.06	2.00	1.95	0.97
SF-1-A	1125	1206	1.07	3.31	0.88	0.26
SF-1-B	1361	1553	1.14	2.81	0.60	0.21
SH-2	620	627	1.01	2.11	2.12	1.00
SF-2-A	1215	1342	1.10	3.00	0.92	0.30
SF-2-B	1543	1599	1.03	2.91	0.61	0.20
SH-3	675	750	1.11	1.70	1.89	1.11
SF-3-A	1300	1326	1.02	2.61	2.59	0.99
SF-3-B	1615	1883	1.16	3.10	2.61	0.84



(a) Specimens SH-2, SF-2-A and SF-2-B

(b) Specimens SH-1, SF-1-A and SF-1-B



(c) Specimens SH-3, SF-3-A and SF-3-B

Figure 7: Load deflection curves for different type of specimens

8. CONCLUSIONS

On the basis of this study the following conclusions may be drawn for FSBCC:

- The ultimate strength of FSBCC depends on the plate thickness of fabricated steel box;
- Ultimate load capacity of FSBCC is also depends on the compressive strength of the concrete;
- The width thickness ratio of plate effect the strength of the FSBCC;
- The finite element method is an effective way to predict the behavior of FSBCC;
- In Bangladesh, Tall building or High rise buildings and factory buildings can be constructed with Fabricated SteelBox Composite Column.

ACKNOWLEDGEMENTS

This paper is a part of ongoing research funded and supported by the Department of Civil Engineering, Dhaka University of Engineering & Technology (DUET), Gazipur. The authors acknowledge all the supports provided.

REFERENCES

- Furlong RW (1967), strength of steel-encased concrete beam-columns. Journal of structural Division, ASCE, 3(5): 113-124.
- Knowles RB and Park R (1969), Strength of concrete-filled steel tubular columns. Journal of Structural Division, ASCE, 93(5): 113-124.
- Tomii M, Yoshimura K and Morishita Y (1977), Experimental studies on concrete filled steel Tubular stub columns under concentric loading. Proceedings of the International Colloquium on Stability of Structures under Static and Dynamic Loads, 718-741.
- Shakir-Khalil H and Mouli M (1990), Further tests on concrete-filled rectangular hollow-section Column. The Structural Engineer, 68(20):405-413.
- Schneider SP (1998), Axially loaded concrete-filled steel tubes. Journal of Structural Engineering, ASCE, 124(10):1125-1138.
- Ge HB and Usami T (1992), Strength of concrete-filled steel thin-walled steel box columns Experiment. Journal of Structural Engineering, ASCE, 118(11): 3036-3054.
- Uy B. Bradford and MA (1995), Local buckling of thin steel plates in composite construction; Experimental and theoretical study. Proc. Instn Civ. Engrs. Structures and Buildings, 110: 426-440.
- Uy B (2000), Strength of concrete filled steel box columns incorporating local buckling. Journal of Structural Engineering, ASCE, 126(3): 341-352.
- Liang QQ and Uy B (1998), Parametric study on the structural behavior of steel plates in concrete - filled fabricated Thin-walled box columns. Advances in Structural Engineering, 2(1): 57-71
- American Institute of Steel Construction. (2010). "Specification for structural steel buildings." *An American National Standard, ANSI/AISC 360-10*, Chicago.
- American Concrete Institute. (2014), "Building code requirements for structural concrete (ACI 318-14) and commentary." *ACI 318-14*, Farmington Hills, MI.
- Eurocode 4, BS EN 1994-1-1, Design of composite steel and concrete structures- Part 1-1: General rules and rules for buildings. London: British Standard Institution, 2004.
- Tomii M, Sakino K (1979), Elastic-plastic behavior of concrete filled square steel tubular beam-column. Trans. Arch. Inst. Japan, 280: 111-120.
- Mander JB, Priestly MNJ and Park R (1998), Theoretical stress-strain model for confined concrete. Journal of structural Engineering, ASCE, 114(8): 1804-1826.
- Hasan Abdulhadi (2015), Experimental and Analytical Investigations of Composite Stub Columns. International Journal of Innovative Research in Science, Engineering and Technology, 185-200.

BEHAVIOUR OF RC BEAMS STRENGTHENED WITH WOVEN JUTE FIBERS

Tanvir Ahmed Khan¹ and Md. Mahfuzur Rahman²

¹ Undergraduate Student, Department of Civil Engineering, Khulna University of Engineering & Technology, Bangladesh, e-mail: tanvir.khan@live.com

² Assistant Professor, Department of Civil Engineering, Khulna University of Engineering & Technology, Bangladesh, e-mail: m_mahfuz11@yahoo.com

³ Undergraduate Student, Khulna University of Engineering & Technology, Khulna-9203, Bangladesh, e-mail: solaimankuet117@gmail.com

ABSTRACT

Bangladesh is one of the largest Jute producing country in the world. Considering efficiency, cost and availability, potential application of jute in various engineering purposes should be searched. For experiments associated with this paper, three beams were cast and strengthened by heat treated woven jute fiber and tested under three-point bending load. Main objective of this study was to observe the effectiveness of natural bio-based woven jute fibers for strengthening of RC beams. Load carrying capacity, first cracking load and load-deflection behaviors were also observed experimentally. Sample beams were cast and retrofitted with bio-based woven jute in different wrapping configurations. It was found that the woven jute fiber can be a very effective retrofitting material for strengthening of RC beams.

Keywords: RC beams, Flexural Strength, Strengthening, Woven Jute Fiber.

1. INTRODUCTION

In developing countries like Bangladesh, buildings are mostly low-rise structures. Due to lack of awareness, regulation and law enforcement, in most of the cases buildings are not built according to national or international codes. Moreover, rapid and unplanned development of construction creates scare of land which forces people to extend building vertically, most of the cases, which are not designed to carry this increased loading. This increased loading, inadequate design and lack of detailing for seismic and other severe natural events may result in considerable structural damage and loss of life, particularly in reinforced concrete buildings. Since, construction of new buildings or rebuilding is not a very good option because of their costing, strengthening is the best solution to preventing collapse of the damaged RCC structures and ensuring safety.

If design and construction of these elements are not proper and adequate, some problems such as excessive deflection, flexural and shear failure as well as materials degradation i.e. spalling of concrete and corrosion of steel may occur. To prevent fatal collapse, the elements require flexural strengthening (Reddy, 2013). Flexural strengthening may also be required if there is a change in the use of a structure, and this change results in an increase in the applied loadings. Generally, strengthening is a means of enhancing the structural performance of an existing structure beyond its current level. When the strength of a damaged concrete structure is enhanced and its design life extended, several economic and environmental problems can be avoided since concrete is bulky and rarely recycled. On the other hand, Bangladesh is the second largest Jute producing country in this planet. So, jute is readily available and price is very low cost per unit volume basis comparing to artificial fibers. Jute is also very eco-friendly as it is completely bio-degradable.

Many experiments have been carried out to assess the flexural response of RC members externally strengthened with FRP fabrics both natural and artificial. Dundu (2011), Olga

Oronthalyova & Olga Koron (2005), T. Munikenche Gowda (1999) and many others conducted experiments on carbon fiber reinforced polymer (CFRP), Glass fiber reinforced polymer and other artificial polymer wrapping strengthening, and found them very impressive. On the other hand, Andressa Cecília Milanese (2011) did their research on mechanical behavior of natural fiber composites. Experimental results showed a higher tensile strength for these natural fibers. Parthraj R. Puranik (2014) did research on use of Woven Fabrics for strengthening of RC beams. Finding of the experiment was that double wrapping does increase ultimate load bearing capacity as expected, because of increase in fabric stiffness around the beam limits deflection of beam. Jochen Gassan (1999) investigated on improving the mechanical properties of jute/epoxy composites by alkali treatment. A comparison with comparable glass-fiber/epoxy composites showed that the Young's moduli of composites with NaOH-treated and untreated jute fibers were respectively, approximately 30% and 50% lower. T. Munikenche Gowda (1999) conducted experiment for evaluation of the mechanical properties- modulus, Poisson's ratio and strength of woven jute fabric-reinforced composites. From this experiment, it was found that the mechanical properties of jute composites do not have strengths like those of artificial composites but they do have better strengths than wood and some plastics composites. Therefore, these composites could be considered for future materials use. Since the reinforcing material is eco-friendly, non-toxic, non-health hazardous, low in cost. Tara Sen (2013) researched on pretreatment of woven jute FRP Composites as well as their use in strengthening of reinforced concrete beams in flexure. The study concludes that woven jute FRP is a suitable material which can be used for flexural upgradation of reinforced concrete beams. John Summerscales (2010) reviewed on bast fibers and their composites. S.V. Joshi (2004) conducted their experiment on the environmental impact of natural fibers on environment and compared it with other artificial fibers like glass fiber composites. The future of natural fiber composites predicted to be better as they are more affordable, lightweight and eco-friendly to glass and carbon fiber composites. Alva Peled (2000) experimented on geometrical characteristics and efficiency of textile fabrics for reinforcing cement composites. The improved bonding in low modulus yarn was found to be mainly the result of the special shape of the yarn induced by the fabric. When the strength of a concrete structure is enhanced and its design life extended, several economic and environmental problems can be avoided since concrete is bulky and rarely recycled (Dundu, 2011).

Carbon Fiber Reinforced polymer (CFRP) and Glass fibre Reinforced Polymer(GFRP) are two popular artificial materials used for strengthening beams by wrapping. A comparison of cost and relative strengthening among GFRP and CFRP (Reddy, 2013) and woven jute fiber, is presented in Table 1.

Table 1: Comparison of Woven Jute Fiber with CFRP and GFRP (Reddy, 2013)

Materials	Woven Jute Fiber	GFRP	CFRP
Relative Cost (considering woven jute fiber as 1/ft ²)	1	25	45
Increment of Strength (%)	40	125	150

So, Fiber Reinforced Polymer composite materials offers an attractive method to any other strengthening and retrofitting technique in the field of repair and strengthening of concrete elements. Most used fibers, which are used for the strengthening of concrete structures are artificial fibers which are carbon, glass, and aramid, etc. However, the cost of those synthetic fibers is very high. Natural fibers like jute has several mechanical properties, such as, it have high specific stiffness and strength, a good fiber aspect ratio and they are readily available from natural sources. By some treatment properties like flexural strength and tensile strength of jute fiber caul be enhanced. It is realistic to expect that there will be existing cracks in the reinforced concrete element prior to the application of any strengthening method. In this

context, the influence of the presence as well as the orientation of woven jute on cracked RC beams is investigated in this paper.

2. METHODOLOGY

2.1 Geometry of specimens

Three identical reinforced concrete beams were cast from same batch of concrete at the same time. The first one was considered as reference beam (RB) and other two were strengthened by wrapping partially and fully with woven jute fiber and denoted as SW and FW, respectively. The cross-section of beams was 4"×6" and the length was 5' as summarized in Table 2.

Table 2 : Geometry of reinforced concrete beams

Beam	Specification	Cross-Section (in×in)	Length (ft)	Effective Length (ft)	Thickness of Wrap (mm)	Wrap Configuration
RB	Reference Beam	4×6	5	4.5	0	Unwrapped
SW	Strip Wrapped	4×6	5	4.5	7	Strips of 6 inch
FW	Fully Wrapped	4×6	5	4.5	7	Fully wrapped

2 nos. 10 mm diameter mild steel deformed bar was used as tensile and compression reinforcement and 8 mm diameter stirrup was used @ 12inch c/c with 0.5 inch clear cover, as shown in Figure 1.

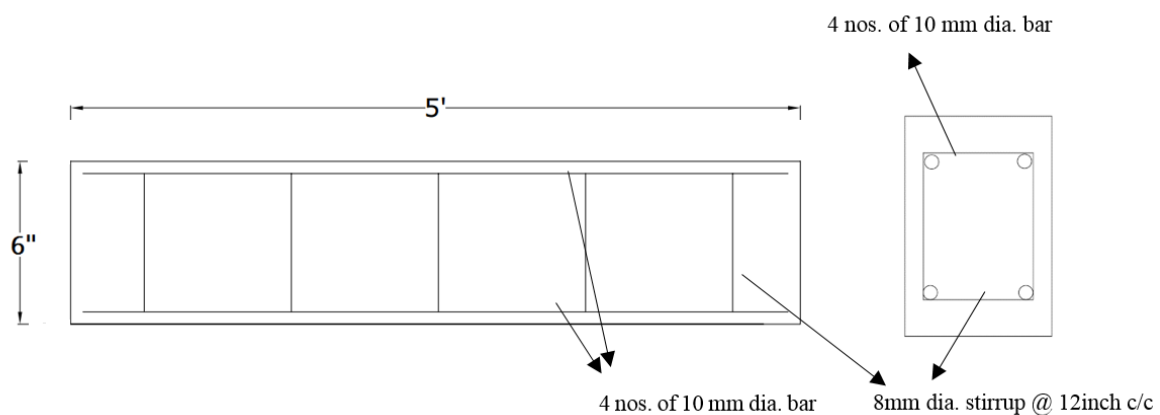


Figure 1 : Detailing of beams

2.2 Properties of Jute Fiber

The jute fabric was collected locally and all other chemicals used for the fabrication of the natural jute fiber textile composite such epoxy adhesive which consists of Part A epoxy resin, and Part B hardener were obtained from local market of Khulna, Bangladesh.

2.2.1 Pre-treatment of Jute Fiber

The mechanical treatment in the form of heat treatment was carried out. Jute fabric mats were cut into the size as required for tensile strength test as per ASTM D 638- 03, for the natural fiber woven mats. These woven fiber mats were then placed into the oven at 50°C for 48 hours. After that the samples were kept in an air tight chamber so that atmospheric moisture could not be absorbed by these samples.

Basically, when the fibers are exposed to atmosphere, it results in the absorption of moisture. This moisture which gets accumulated in the fiber which is required to be eliminated. This elimination of the moisture from the fibers was attained by the process of heat treatment. Heat treated composites of natural fabrics or mats have shown a higher strength than untreated composites of natural fiber fabrics or mats. The effect of elevated temperature conditioning can be described as a threefold effect on the cellulosic fibers of jute. Firstly, the modification of cellulosic structure by enhanced cross-linking. Secondly, increased amount of crystallinity in the fibers and thirdly, by de-moisturization, which improves adhesion between fibers and natural rubber backing. (Tara Sen, 2013)

Thermal treatment also results in moisture loss of the fabric thereby enhancing the extent of bonding between fabric and the natural rubber backing. As we know that de-moisturization plays a vital role in enhancing mechanical properties, the overall properties of composites prepared with high temperature conditioned woven jute are better than the composites prepared with untreated ones of the same woven fibers of jute. (T. Munikenche Gowda, 1999)

Another important aspect for thermal conditioning is that the fibers are exposed to atmosphere during manufacturing, processing, transporting, etc. which results in the absorption of moisture by the fibers from the environment. This moisture which gets accumulated in the fibers also requires to be eliminated, and can be attained by the process of thermal conditioning. (Jochen Gassan, 1999)

2.2.2 Tensile Test of Jute Fiber

In order to conduct the tensile tests, it was necessary to prepare the coupon samples. The samples were cut to proper size according to ASTM D 638-03. All the specimens were cut to standard length 165 mm and gauge length 50 mm as shown in figure 2(a). The thickness of the jute fiber composite was 7mm.

For tensile strength test a Universal Testing Machine (UTM) was used. This machine is able to apply tensile loads as shown in Figure 2(b). Specimens were placed in Universal Testing Machine and pulled out until its failure.

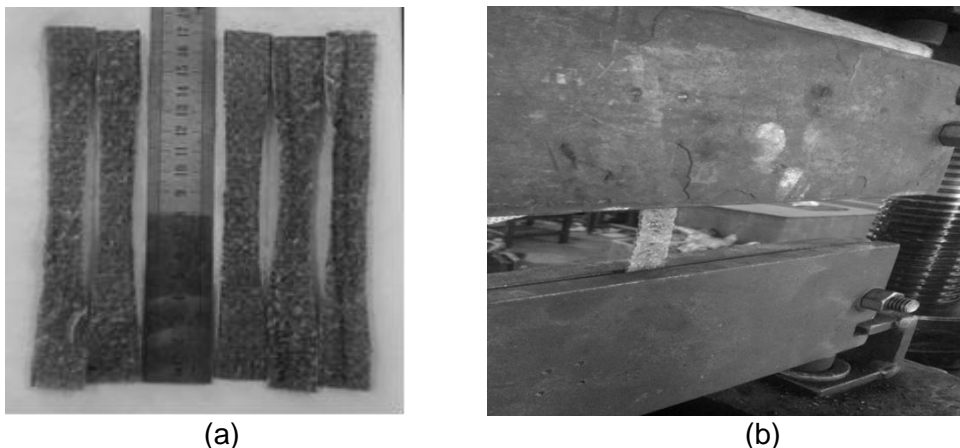


Figure 2 : (a) Samples of Jute fiber composites & (b) Test setup of Jute fiber coupons

2.2.3 Tensile Test Result of Jute Fiber

Table 3 shows the tensile test results of jute fiber composite and Figure 3 illustrates their stress-strain curves. Table 3 show the values of strength, elongation percentage and maximum deformation of jute fiber composites and their average values respectively.

Table 3 : Tensile Test results of Jute Fiber Composite

Tensile Parameters	Sample 1	Sample 2	Sample 3	Average
Maximum Deformation (mm)	1	0.96	0.97	0.98
Ultimate Strength (MPa)	88.25	83.5	86.8	88.18
Modulus of Elasticity (Mpa)	4062.5	4348.96	4474.23	4295

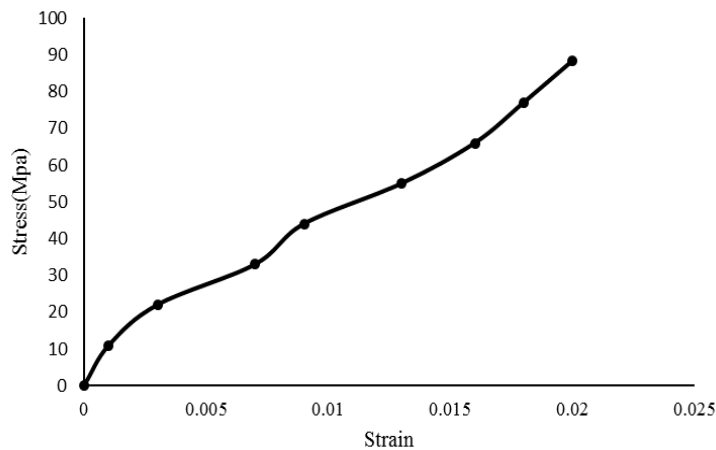


Figure 3 : Average Stress-strain curve of jute fiber composite

2.3 Other materials

Mechanical properties of materials used for the experiment was evaluated before casting of beams and are given in the Table 4 below.

Table 4 : Material properties

Material	Test Name	Results	Test Method
coarse aggregate	Specific gravity	1.86	ASTM C127
	Absorption	11.26%	ASTM C127
	unit weight	1148 kg/m ³	ASTM C29
Fine Aggregate	Specific gravity	1.81	ASTM C128
	Absorption	10.85%	ASTM C128
	Fineness modulus (FM)	1.92	ASTM C136
	Unit weight	1021 kg/m ³	ASTM C29
Binder	normal consistency	28.5%	ASTM C187
	initial setting time	145 minutes	ASTM C191
	final setting time	270 minutes	ASTM C191
Concrete	Compressive Strength of Concrete	17.48 MPa	ASTM C39
Main Steel 10(mm)	Tensile Strength	68273 psi	ASTM A370
Stirrup Steel 8(mm)	Tensile Strength	66455 psi	ASTM A370

3. EXPERIMENTAL PROGRAM

All sample beams were cast on same day from same batch of concrete. The concrete mixing ratio was 1 (cement): 2 (fine aggregate): 4 (coarse aggregate) by weight with a water to cement ratio of 0.46 by weight. After casting, all beams were immersed into water and allowed for curing for 7 days.

All three beams, the reference beam (RB), fully wrapped beam (FW) and strip wrapped beam (SW) were tested in a loading frame under single point loading. Beam was simply supported and a dial gauge was placed exactly under the midpoint of the beam as shown in Figure 4. Load was applied by a hydraulic jack which has a self-weight of 25kg.

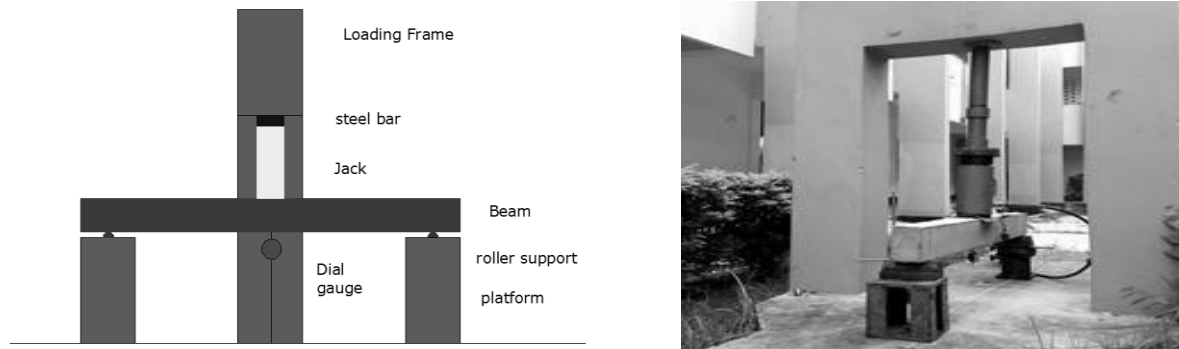





Figure 4 : Schematic Diagram and image of Experimental Setup.

The value of load noted in KN and corresponding readings from dial gauge were recorded at 2KN load increment. Load was applied until the crack initiated in tension zone and the corresponding cracking load was recorded. Beams were cracked to replicate a damaged beam.

Similarly, load equal to the cracking load of the beam RB was also applied to the other two beams, namely FW and SW. Summary of woven jute fiber wrapping configuration of beams are presented in Table 5.

Table 5 : Summary of woven jute fiber wrapping configuration on beams

Beam Name	Wrapping configuration	Strengthening material	Model beam designation	Type of strengthening	Strengthening scheme
Reference Beam	Nil 	Nil	RB	No strengthening	Nil
Beam 1	Full length wrapping, single layer Jute FRP 	JFRP	FW	Flexural strengthening using jute FRP	U – Wrap, three sided wrap
Beam 2	Strip wrapping, single layer 6" strips at 8" C/C 	JFRP	SW	Flexural strengthening using jute FRP	U – Wrap, three sided wrap

Finally, the beams were removed from loading frame and were kept in a simply supported condition. Beam FW and SW were then ready for strengthening with woven jute fibers. Surface of Beam FW & Beam SW was being roughen by scraping weir brush and dust was removed. Heat treated Woven Jute Fiber fabric was cut in necessary dimension. Standard adhesive resin and hardener were mixed thoroughly to prepare the epoxy resin. A layer of Epoxy Resin was applied on the surface of Beams by paint brush. One ply of woven jute fiber fabric was applied as U wrapping in two different orientations, as shown in Figure 5.

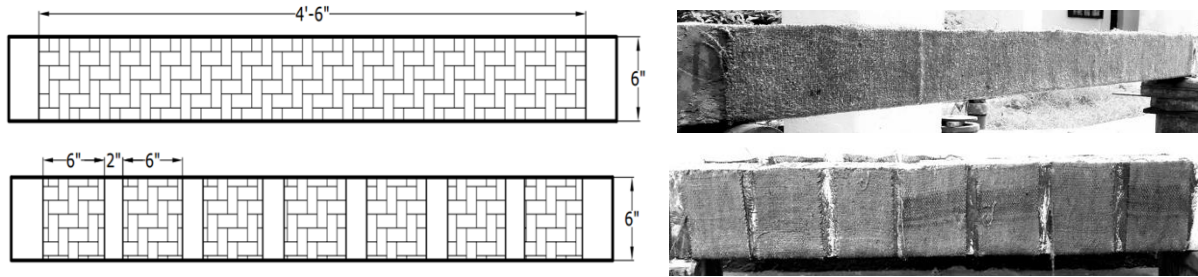


Figure 5 : Beams after wrapping with woven jute fiber

Single piece of Woven Jute Fiber was applied on three surfaces of beam FW. 6inch strips of woven jute fiber were applied on surface of Beam SW maintaining 2-inch gap between each strip to keep the 25% of total surface area of beam uncovered. Then another layer of resin was applied again on the woven jute fiber. Beams were kept 24 hours in simply supported condition to attain full bond strength between beams and woven jute fiber composites.

Next all beams were taken to loading frame and load was applied as previous experimental setup till ultimate failure. Beams after ultimate failure are shown in figure 6. The values of load were recorded in KN and corresponding readings from dial gauge were recorded at 2KN load increment.

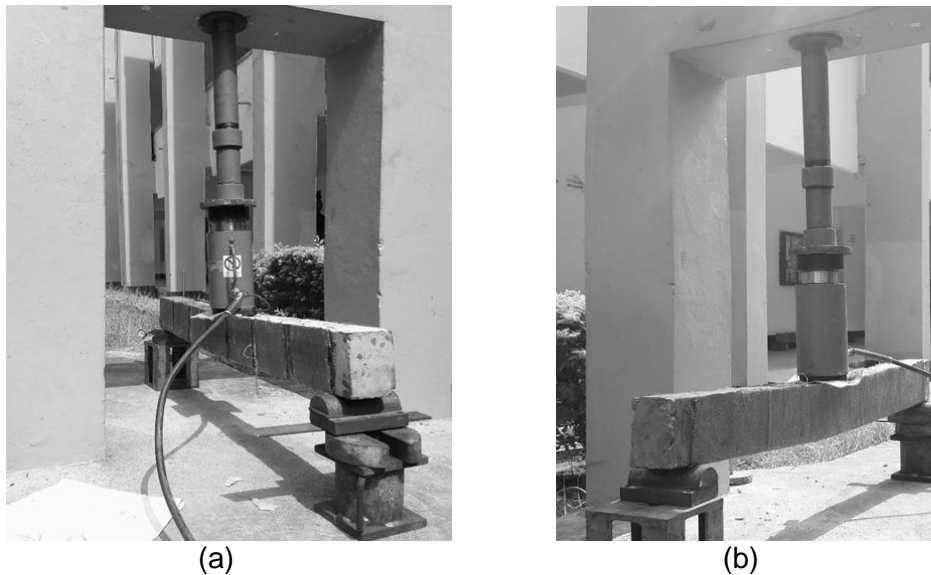


Figure 6 : (a) Beam FW and (b) SW after Failure

4. RESULTS AND DISCUSSIONS

All beams were tested in loading frame in the premises of Department of Civil Engineering, KUET. Loads were applied precisely in mid-span by hydraulic jack. Following Table 6 shows the ultimate capacity of all three beams in MPa and maximum deflection in mm.

Table 6 : Test Results of Reference Beam

Sample	Ultimate Capacity (MPa)	Maximum Deflection (mm)
Reference beam	17.51	9.94
Full Wrapped (FR)	22.65	13.8
Strip Wrapped (SR)	24.40	14.79

The load vs. deflection curves for the beams are shown in the Figure 7(a). The graph illustrates the variation of deflection with load at 2kN load interval. From the graph, the ultimate load carrying capacity of the reference beam is found to be 20kN and maximum deflection is 9.94mm. For the beams FR and SR strengthened with woven jute fiber composites, the graph illustrates the variation of deflection with load at 2kN load interval. From the graph, the ultimate load carrying capacity of two beams are found to be 28kN and 26kN and maximum deflections are 13.8mm and 14.79mm, respectively.

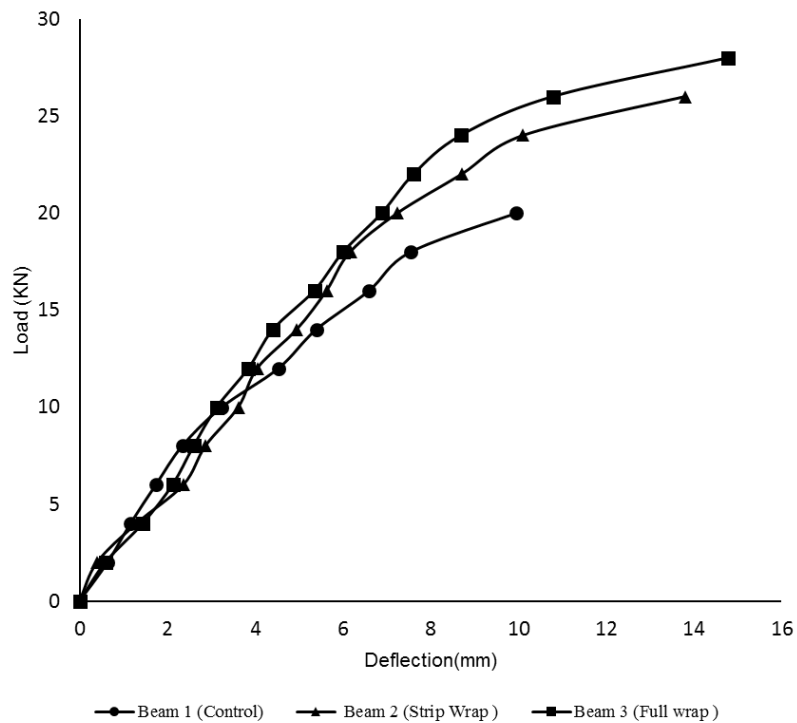


Figure 7 : Load deflection diagram for all beams

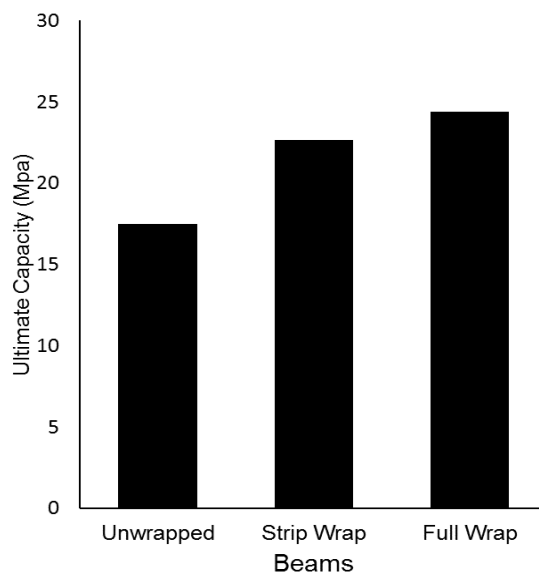


Figure 8 : Comparison of Ultimate Capacity(Mpa)

Figure 7 shows that deflection of beams decreases due to woven jute fiber wrap and bar diagram (Figure 8)) shows a comparison among the ultimate capacity of all three beams. The ultimate strength increases about 40% for full wrap configuration beam (FW) than that of the unwrapped control beam (RB) where the ultimate strength increases about 30% for strip wrap configuration beam (SW) than that of the unwrapped beam which was taken as control.

5. CONCLUSIONS

The experimental work was aimed to find out the efficiency of woven jute fiber composites for strengthening cracked reinforced concrete beam. The ultimate load carrying capacity of RCC beams is greatly influenced by the use of woven jute fiber composites. Full wrap configuration of woven jute fiber increased 40% of the unwrapped ultimate capacity of reference beam where only 25% ultimate capacity was increased due to Strip Wrap configuration. Considering the relative cost of woven jute fiber, CFRP and GFRP woven jute fiber is much more cost effective than the other available strengthen material. Considering the percentage increase in strength for other strengthening technique like CFRP or GFRP, woven jute fiber fabric is not as much effective. However, considering price and availability of Jute fiber, it could be used very efficiently instead of artificial polymer fiber composites like CFRP or GFRP for strengthening of damaged reinforced beams. A full wrapping technique is recommended as it increases strength considerably higher than strip wrapping technique and costing is not high at all.

REFERENCES

- Alva Peled, A. B. (2000). Geometrical characteristics and efficiency of textile fabrics for reinforcing cement composites. *Cement and Concrete Research*, 781-790.
- Andressa Cecilia Milanese, M. O. (2011). Mechanical behavior of natural fiber composites. *Procedia Engineering*, 2022-2027.
- Dundu, M. (2011). Strengthening of concrete slabs using bonded steel plates. *International Conference on Steel and Composite Structures*, 78-92.
- Jochen Gassan, A. K. (1999). Possibilities for improving the mechanical properties of jute/epoxy composites by alkali treatment of rebres. *Composites Science and Technology*, 1303-1309.
- John Summerscales, N. P. (2010). A review of bast fibres and their composites. Part 2 – Composites. *Composites: Part A*, 1336-1344.
- olga koronhalyova, & olga koron, I. m. (2005). Effect of presence of salt on hygric performance of ceramic bricks. 52-60.
- Parthraj R. Puranik, D. A. (2014). Use of Woven Fabrics for Strengthening of Reinforced Concrete Beams. *Journal of Engineering Research and Applications*, 52-58.
- Reddy, T. S. (2013). Strengthening of RC beams in flexure using natural jute fibre textile reinforced composite system and its comparative study with CFRP and GFRP strengthening systems. *International Journal of Sustainable Built Environment*, 41-55.
- S.V. Joshi, L. D. (2004). Are natural fiber composites environmentally superior to glass fiber reinforced composites? *Composites: Part A*, 371-376.
- T. Munikenche Gowda, A. N. (1999). Some mechanical properties of untreated jute fabric-reinforced polyester composites. *Composites: Part A*, 277-284.
- Tara Sen, H. N. (2013). Pretreatment of Woven Jute FRP Composite and Its Use in Strengthening of Reinforced Concrete Beams in Flexure. *Advances in Materials Science and Engineering*, 15-30.
- ASTM D638-03, Standard Test Method for Tensile Properties of Plastics, ASTM International, West Conshohocken, PA, 2003, www.astm.org
- ASTM C127-15, Standard Test Method for Relative Density (Specific Gravity) and Absorption of Coarse Aggregate, ASTM International, West Conshohocken, PA, 2015, www.astm.org

- ASTM C29, Standard Test Method for Bulk Density (“Unit Weight”) and Voids in Aggregate, ASTM International, West Conshohocken, PA, 2017, www.astm.org
- ASTM C128-15, Standard Test Method for Relative Density (Specific Gravity) and Absorption of Fine Aggregate, ASTM International, West Conshohocken, PA, 2015, www.astm.org
- ASTM C187-16, Standard Test Method for Amount of Water Required for Normal Consistency of Hydraulic Cement Paste, ASTM International, West Conshohocken, PA, 2016, www.astm.org
- ASTM C191-13, Standard Test Methods for Time of Setting of Hydraulic Cement by Vicat Needle, ASTM International, West Conshohocken, PA, 2013, www.astm.org

THERMAL CHARACTERIZATION OF POLYMER CONCRETE FROM UNSATURATED POLYESTER RESIN REINFORCED WITH WHITE SAND

Muhtasim Kader Mukit¹, Md. Abdul Gafur², Dos Mohammad³ and Md. Arif Mokammel⁴

¹Applied Chemistry and Chemical Engineering Department, Noakhali Science and Technology University, Bangladesh, e-mail: muhtasimmukit@yahoo.com

²Pilot Plant and Process Development Centre (PP and PDC), Bangladesh Council of Scientific and Industrial Research (BCSIR), Bangladesh, e-mail: d_r_magafur@yahoo.com

³Applied Chemistry and Chemical Engineering Department, Noakhali Science and Technology University, Bangladesh, e-mail: Dos.mohammad70@gmail.com

⁴Applied Chemistry and Chemical Engineering Department, Noakhali Science and Technology University, Bangladesh, e-mail: Sirius.abcd@gmail.com

ABSTRACT

Polymer concrete as a building material can benefit construction industry in maintaining its economy. Thermal properties are important material properties for engineering applications. Analysis of prepared polymer concrete is an important issue for a composite of unsaturated polyester resin and white sand. The main purpose of this research is to prepare polymer concrete having high performance and standard thermal properties. Thermal properties such as thermal conductivity, thermo-mechanical properties and thermo-gravimetric properties have been studied of prepared polymer concrete at various compositions. Collection of raw materials, washing of white sand, purchasing of unsaturated polyester resin and methyl ethyl ketone peroxide, weighing, mixing and molding have been done. Prepared polymer concrete has been sectioned around 10mmx10mm cross-sectional area and cleaning has been done after sectioning. After cleaning; prepared polymer concretes have been set to TMA and TGA respectively for obtaining graph in the computer. Thermal conductivity of prepared polymer concrete has been measured by Lee's and Charlton's method. Thermal conductivity of prepared polymer concrete decreases with increasing of white sand. Linear average co-efficient of thermal expansion is the outcome of thermo-mechanical analysis. Linear average co-efficient of thermal expansion of prepared polymer concrete decreases with increasing of white sand. The maximum degradation rate is 1.574 mg/min that has been found for prepared polymer concrete without white sand. The maximum degradation rate of prepared polymer concrete containing 50% and 60% white sand have been increased slowly.

Keywords: Thermal conductivity, TMA, TGA, The Rate of Degradation

1. INTRODUCTION

Polymer concrete is a composite material which results from polymerization of a monomer/aggregate mixture. The polymerized monomer acts as binder for the aggregates and the resulting composite is called "Concrete". Polymer concrete in which the binder is an organic polymer; a construction and structural material that is a solidified mixture of a macro molecular substance with a mineral aggregate.^[1-2] Polymer and polymer-cement concretes are used for floors in industrial plants, garages, and hospitals. They are used in the production of high-quality road and air field paving, sand for repairing damaged concrete surfaces and patching cracks. The overall goal of this research work has to investigate some thermal properties of prepared polymer concrete from unsaturated polyester resin reinforced with white sand. In order to study the possibility of superior performance, preventing the composite from extreme heat; polymer

concrete has been prepared with different compositions. In view of the above consideration, the following work- plans have been undertaken: collection of raw materials, preparation of polymer concrete with different compositions from unsaturated polyester resin and white sand, determination of thermal properties such as thermal conductivity, thermo-mechanical analysis (TMA) and thermo-gravimetric analysis (TGA) of prepared polymer concrete. The main objectives of this research work are:

- i) Preparation of high- performance polymer concrete for construction purposes.
- ii) Preparation of polymer concrete with standard thermal properties.

The thermal behaviors of prepared polymer concrete have been analyzed to correlate the structure- property relation. This research work gives the ideas to find a suitable composite for the application in the field of construction.

2. MATERIALS AND METHODS

2.1 Materials

Polymer concrete formulation has been prepared by mixing white sand and unsaturated polyester resin. White sand content in polymer concrete has been varied from 20% to 60% in the polymer concrete formulation. Methyl ethyl ketone peroxide (MEKP) is an organic, colorless and oily liquid which has been used as hardener in the polymer formulation. Methyl ethyl ketone peroxide (MEKP) has been used as 1% of unsaturated polyester resin in the polymer concrete formulation.

2.2 Equipments

The equipments have been used here, such as Slide-calipers, Screw gauge, Huber-thermal conductivity analyzer, Thermo-gravimetric analyzer and Thermo-mechanical analyzer.

2.3 Methods

2.3.1 Collection of Raw Materials

Firstly, for the preparation of polymer concrete, the basic raw materials are white sand; unsaturated polyester resin and methyl ethyl ketone peroxide have been purchased. To prepare polymer concrete from these raw materials following steps are involved:-

- ✓ Washing of white sand and purchasing of unsaturated polyester resin and methyl ethyl ketone peroxide from the market.
- ✓ Weighing
- ✓ Mixing
- ✓ Molding

2.3.2 Method of Thermo-Gravimetric Analysis (TGA) Measurement

Thermo-gravimetric analysis or thermal gravimetric analysis (TGA) is a method of thermal analysis in which changes in physical and chemical properties of materials are measured as a function of increasing temperature (with constant heating rate), or as a function of time (with constant temperature and/or constant mass loss). TGA can provide information about physical phenomena, such as second-order phase transitions, including vaporization, sublimation,

absorption, adsorption, and desorption.^[3-4] The prepared polymer concrete has been sectioned and around 10mmx10mm cross-sectional area has been prepared. Cleaning of prepared polymer concretes have been done after sectioning prepared polymer concrete. After then polymer concretes have been set to TGA for obtaining graph in the computer. The obtaining graph has been analyzed in that computer of the TGA.

2.3.3 Method of Thermo-Mechanical Analysis (TMA) Measurement

Thermo-mechanical analysis (TMA) is a technique used in thermal analysis, a branch of materials science which studies the properties of materials as they change with temperature. Thermo-mechanometry is the measurement of a change of a dimension or a mechanical property of the sample while it is subjected to a temperature regime. The prepared polymer concrete has been sectioned and around 10mmx10mm cross-sectional area has been prepared. Cleaning of prepared polymer concretes has been done after sectioning. After then polymer concretes have been set to TMA for obtaining graph in the computer. The obtaining graph has been analyzed in that computer of the TMA (Wellisch E. et. al., 1961 & Farahany et.al., 2012).

2.3.4 Method of Thermal Conductivity Measurement

According to the ASTM method C 201 the thermal conductivity can be measured. But an alternative method for the test of thermal conductivity is Lee's and Charlton's method. The method is described as follows: The thermal conductivity of a bad conductor or sample like rubber, ebonite, glass, refractory, concrete etc. can be measured by this method. In measuring the conductivity of such poor conductors or samples, a thin layer or slab of the material or sample is used. The difficulty arises in maintaining the face at uniform temperature and in measuring that temperature. Lee's and Charlton's method has overcome this difficulty by placing a good conductor such as brass or copper, of exactly the same diameter as the experimental slab on each side of the poor conductor or sample. In this method two metal discs are used and a poor conductor or sample is placed between two that metal discs. ^[7-8] there is an oil chamber from where heat is produced. Heat passes to the upper metal disc and then flows through poor conductor or sample to the bottom metal disc. When heat is passed through the upper disc, the poor conductor or sample is warmed. When the rate of flow of heat through the sample equals the heat loss from the upper disc by radiation and convection then steady state will be reached (Rao V. V. L. K. et. al., 1993 & Chmielewska B. et. al., 2006). If

T_1 =temperature of the upper disc in the steady state

T_2 = temperature of the bottom disc in the steady state

A = Cross-sectional area of the sample

K = thermal conductivity of the sample

d = thickness of the sample

Then the quantity of heat conducted per second through the sample is

$$Q=KA (T_1-T_2)/d$$

In the steady state this heat Q is radiated per second from A . if m and S be the mass and specific heat of A and dT/dt be its cooling rate at temperature T_2 , the heat loss (radiated per second) from A is,

$$Q= ms (dT/dt)$$

dT/dt is determined by performing s subsidiary experiment. From the above equations the thermal conductivity of the sample is

$$K = ms \left(\frac{dT}{dt} \right) \frac{d}{A} (T_1 - T_2)$$

The weight, diameter and thickness of the sample have been measured with a balance and a slide calipers respectively. Then the sample has been polished by polishing paper for good contact. The oil chamber generates heat. The temperature T_1 and T_2 has been noted at an interval of one minute until they remain steady, for at few consecutive readings for several minutes. Then heat supply has been stopped and the upper disc has been removed. ^[9-10] with the slab, the sample is still on the top, the bottom disc has been heated to a temperature of $(T_2 + 20^\circ\text{C})$. Then the bottom disc has been allowed to cool. By keeping the sample on the bottom disc, it has been ensured that the heat lost to the surrounding is the same as in the first part the experiment when it has gained heat. The cooling time has been measured for decreasing temperature in every minute.

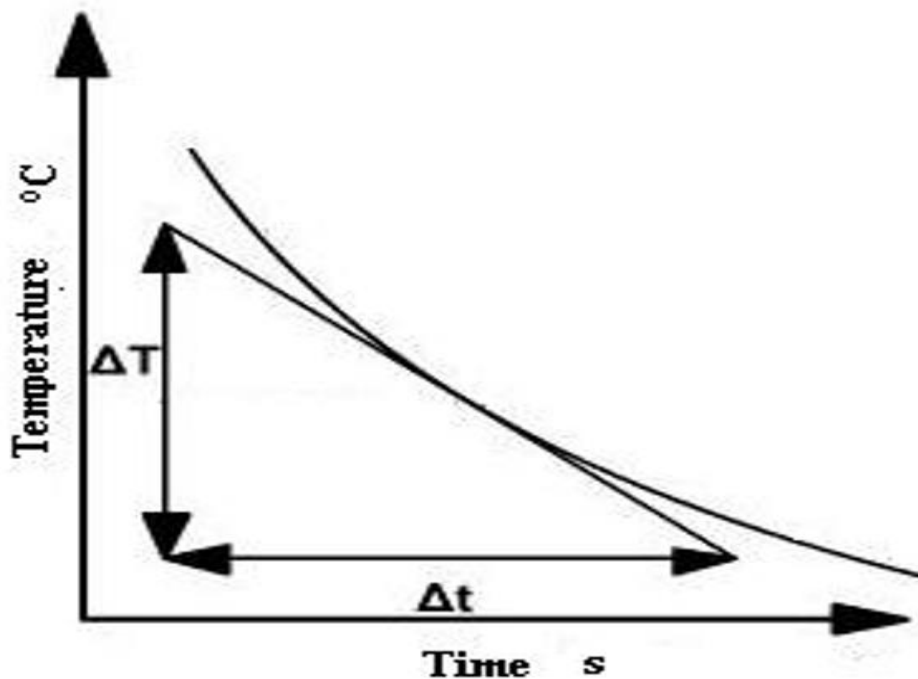


Figure 1: Cooling curve of thermal conductivity analysis of prepared polymer concrete

3. RESULTS AND DISCUSSION

3.1 Thermal conductivity of Prepared Polymer Concrete

Table 1: Thermal conductivity observation of prepared polymer concrete containing unsaturated polyester resin and white sand at various compositions

Prepared polymer concrete composition	Thermal conductivity, $Wm^{-1}C^{-1}$
0% sand and 100%unsaturated polyester resin	94.39
20% white sand and 80%unsaturated polyester resin	59.89
40% white sand and 60%unsaturated polyester resin	53.30
50% white sand and 50%unsaturated polyester resin	52.48
60% white sand and 40%unsaturated polyester resin	46.70

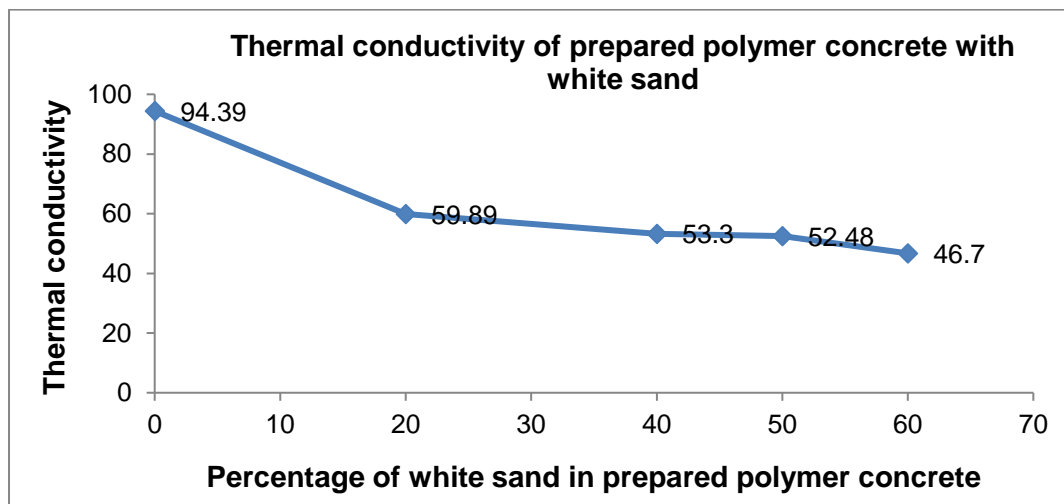


Figure 2: Thermal conductivity of prepared polymer concrete with white sand

From figure 2, it shows that thermal conductivity of prepared polymer concrete has been decreased with increasing of white sand amount in prepared polymer concrete. So it can say that prepared polymer concrete containing high percentage of white sand behaves low thermal conductive properties, on the contrary, prepared polymer concrete containing low percentage of white sand behaves high thermal conductive properties. Porosity of prepared polymer concrete has been increased with increasing white sand amount in prepared polymer concrete. The free path has been decreased resulting in lower thermal conductivity.

3.2 Thermo-Mechanical Analysis of Prepared Polymer Concrete

Prepared polymer concrete of unsaturated polyester resin and white sand has been analyzed by heating the temperature range of 30-90°C in the thermo-mechanical analyzer for observing the linear average co-efficient of thermal expansion. The Linear average co-efficient of thermal expansion (CTE) of prepared polymer concrete has been obtained from thermo- mechanical analysis.

Table 2: CTE at 30-90°C of prepared polymer concrete with white sand

Prepared polymer concrete composition	CTE at 30-90°C
Polymer concrete with 0% sand and 100% unsaturated polyester resin	1.16E-4
Polymer concrete with 20% white sand and 80% unsaturated polyester resin	1.29E-4
Polymer concrete with 40% white sand and 60% unsaturated polyester resin	1.35E-4
Polymer concrete with 50% white sand and 50% unsaturated polyester resin	1.39E-4
Polymer concrete with 60% white sand and 40% unsaturated polyester resin	4.69E-5

It has been observed that linear average co-efficient of thermal expansion of prepared polymer concrete of white sand is decreasing with increasing the sand amount in prepared polymer concrete. And decreasing level of linear average co-efficient of thermal expansion of prepared polymer concrete is very small margin.

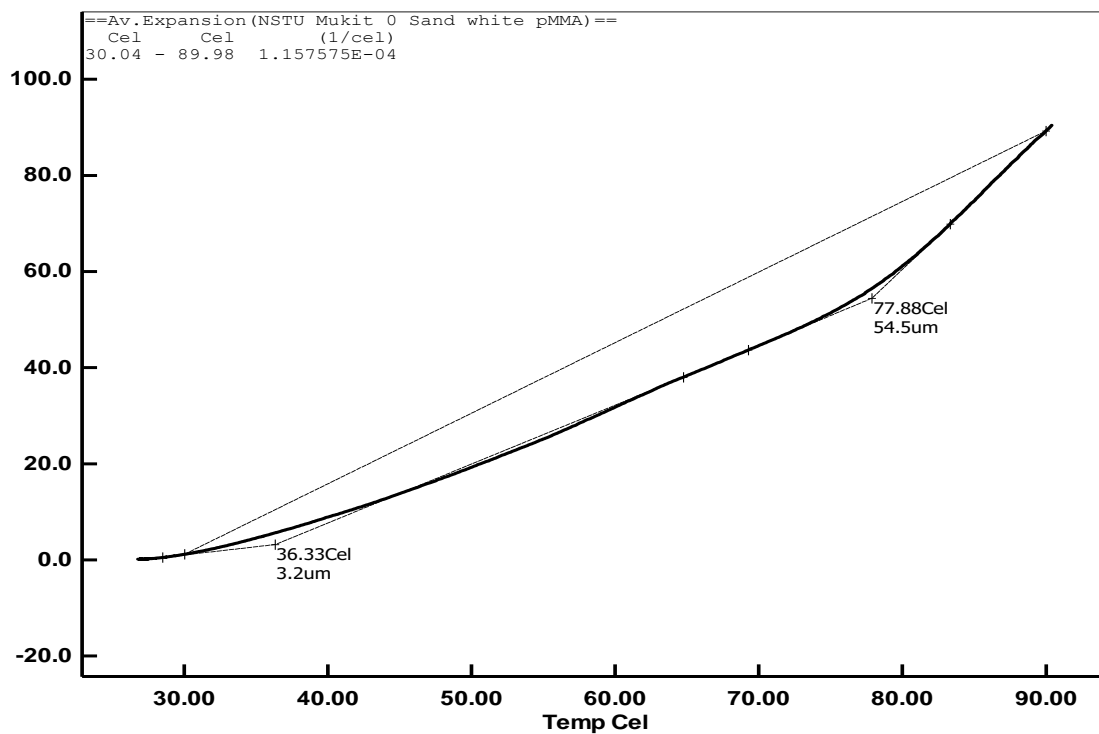


Figure 3: TMA plot of 0% white sand containing prepared polymer concrete

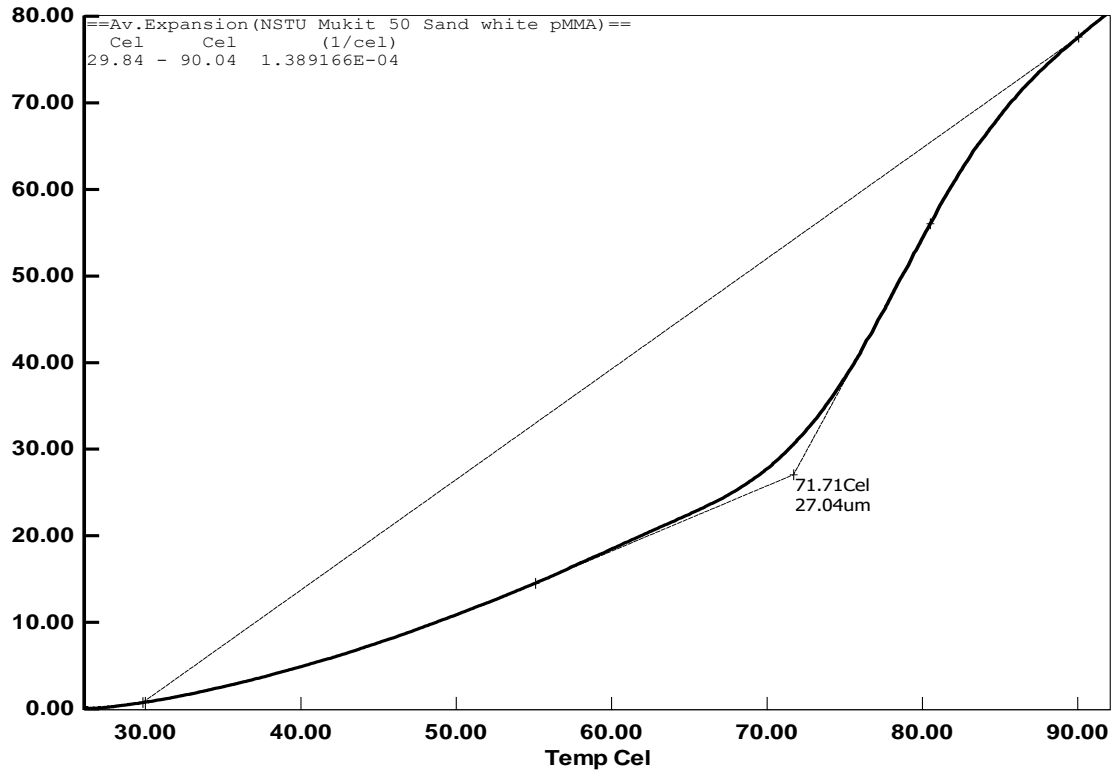


Figure 4: TMA plot of 50% white sand containing prepared polymer concrete

3.3 Thermo-Gravimetric Analysis of Prepared Polymer Concrete

Table 3: Thermal degradation of prepared polymer concrete with white sand

Composition	Onset degradation(°C)	50%degradation	Max. Slope	Max. degradation rate
0% white sand containing sample,	342.8		382249.51	1.574 mg/min
50% white sand containing sample,	336.6		387.0249	41.502 mg/min
60% white sand containing sample,	338.0		369.0251	81.601 mg/min

Thermo-gravimetric is one of the methods of thermal analysis. The maximum degradation rate is 1.574 mg/min that has been found for polymer concrete without sand. The maximum degradation rate of polymer concrete containing 50% and 60% white sand have been increased slowly.

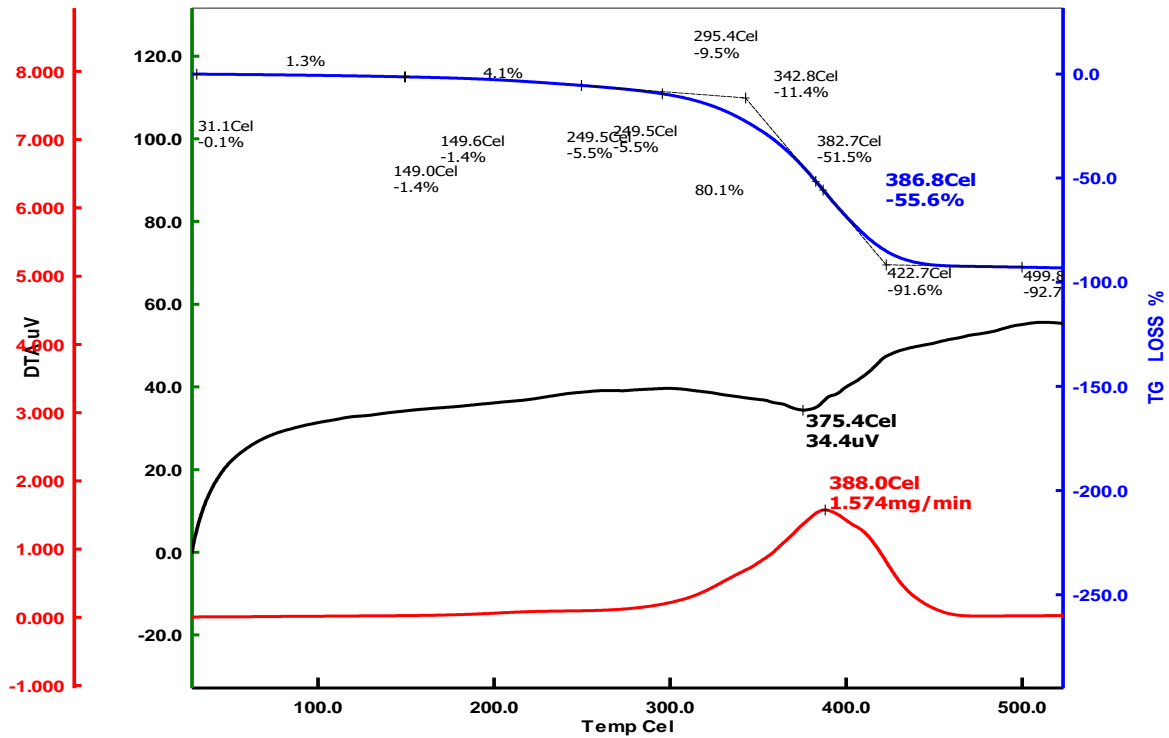


Figure 5: TGA plot of 0% white sand containing prepared polymer concrete

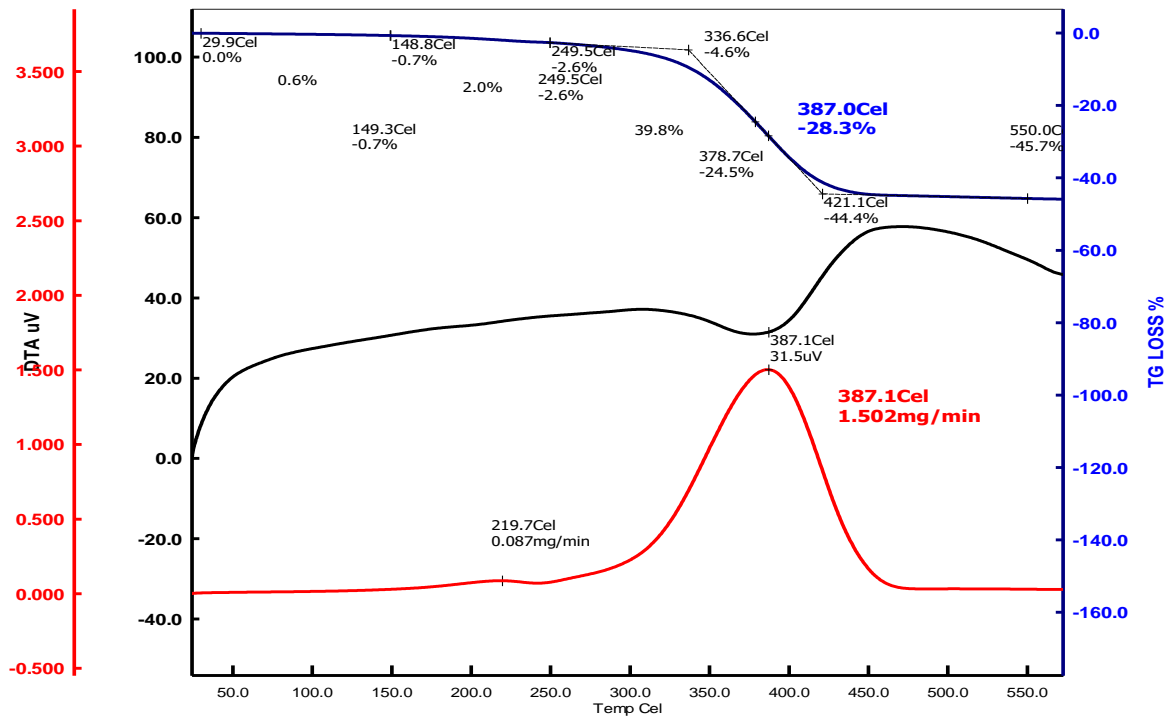


Figure 6: TGA plot of 50% white sand containing prepared polymer concrete

4. CONCLUSIONS

Polymer concrete has been introduced in the late 1950s and became well known in the 1970s for its use in repair, thin overlays and floors, and precast components. In this research work, the features of prepared polymer concrete from unsaturated polyester resin reinforced with white sand have been analyzed. The thermal conductivity, thermo-mechanical properties and thermo-gravimetric properties have been calculated and quantified. The thermal properties of the polymer concrete play important role in the behavior of concrete at elevated temperature. These properties have been studied and the prepared polymer concrete can be considered for using as an acceptable construction material. It is well known that polymer concrete exhibits far better thermal properties than ordinary Portland cement concrete. Polymer concrete has proven itself to be a material which holds much promise due to its better thermal properties. So, at the end of research, it can say that polymer concrete from unsaturated polyester resin and white sand will be found application in very specialized domains in the field of construction.

ACKNOWLEDGEMENTS

First and foremost, all praise is upon to the omnipotent and omniscient Allah. I am extremely thankful to Dr. Abdul Gafur, Principal Scientific Officer, Pilot Plant and Process Development Centre (PP and PDC), Bangladesh Council of Scientific and Industrial Research (BCSIR), Dhaka, Bangladesh and Dr. Muhammed Yusuf Miah, Associate Professor, Department of Applied Chemistry and Chemical Engineering, Noakhali Science and Technology University, Sonapur, Noakhali. I would also like to express my heart warming thanks to the head of the following institutions for helping me a lot in doing my entire thesis work.

1. Pilot Plant and Process Development Centre (PP and PDC), Bangladesh Council of Scientific and Industrial Research (BCSIR), Dhanmondi, Dhaka, Bangladesh.
2. Applied Chemistry and Chemical Engineering Department, Noakhali Science and Technology University, Sonapur, Noakhali, Bangladesh.

I am heartedly grateful to Ministry Science and Technology for financial support by enlisting me of the National Science and Technology Fellowship.

REFERENCES

- ASTM Standard D5334-08 – Standard Test Method for Determination of Thermal Conductivity of Soil and Soft Rock by Thermal Needle Probe Procedure, Doi:10.1520/D5334-08.
- B. Chmielewska, L. Czarnecki, J. Sustersic, and A. Zajc, "The influence of silane coupling agents on the polymer mortar," *Cement and Concrete Composites*, vol. 28, no. 9, pp. 803–810, 2006.
- Farahany, Saeed, Ali Ourdjini and Mohd Hasbullah Idris, "The usage of computer-aided cooling curve thermal analysis to optimize eutectic refiner and modifier in Al–Si alloys". *Journal of Thermal Analysis and Calorimetry* 109 (1): 105–111. Doi: 10.1007/s10973-011-1708-1, 2012.
- V. V. L. K. Rao and S. Krishnamoorthy, "Aggregate mixtures for least-void content for use in polymer concrete," *Cement, Concrete and Aggregates*, vol. 15, no. 2, pp. 97–107, 1993.
- Wellisch E., Marker L., Sweeting O. J., *Viscoelastic properties of regenerated cellulose*, *J. Appl. Polym. Sci.*, 5, 647-654, 1961.

PROJECT PLANNING USING SCHEDULING TECHNIQUES: TIME & COST ASPECTS

Jhumana Akter¹, Akramul Hoq Hriday² and Tareq Rahman³

¹ Assistant Professor, Department of Building Engineering and Construction Management, KUET, Bangladesh, e-mail: jhumana@becm.kuet.ac.bd

² Undergraduate Student, Department of Building Engineering and Construction Management, KUET, Bangladesh, e-mail: hridayhoq97@gmail.com

³ Undergraduate Student, Department of Building Engineering and Construction Management, KUET, Bangladesh, e-mail: Tareq2626@gmail.com

ABSTRACT

Completing a project on time and within budget depend on dead line or completion date of the project. Cost generally increases if we want to complete the project shorter than its completion time. This process reminds as crashing. Which involve additional cost of project. However, we need to find minimum project cost that makes the project successful. Proper Project planning and scheduling plays a central role in predicting both the time and cost aspects of a project. This study is aimed at finding trade-off the cost within expected time that will be required to complete the project foundation [TSC-block-A] in 60 days due to weather impact in rainy season. The calculation data was obtained from KUET Engineering section. Both (CPM) and (PERT) method were used for the analysis. Project duration for foundation work was 106 days. Using PERT techniques, we get 78 days completion time, which is 27 days shorter than schedule time. Due to this, shorten time cost also increase. This amount was tk.950000. Because of unfriendly climate, state project delay 6 month, instead of 12-month completion time. For this work budget was approximately tk.10076000. But our completion baseline was 60 days. there is need to 18 days crash than critical time 78 days .so that additional cost is required.so in this study our objective is to find minimum additional cost associated with the reduction in timing is tk.800000 which increases the total expected cost required to complete the substructure from tk. 10076000 to tk. 11826000.

Keywords: Construction planning, Critical Path Method, Project Evaluation and Review Technique, crashing.

1. INTRODUCTION

Completing a project on time and within budget is not an easy task. In spite of advances in the field of project management today, most projects in Bangladesh today face cost and time over-runs which increases with the increase in complexity of the project. A various number of factors influence to delays that comprise primarily of contractor delays, client delays, consultant delays, labor related delays and Various other external delays. These delays causes time overrun, cost overrun, dispute, negotiation, total rejection and litigation. This is because small amount of project activities are critical in the common sense that delay in their beginning will delay the overall project completion time. Hence good planning and scheduling of project is important to overcome this problem. For many years, two approaches that have been proven to be useful for planning, scheduling and controlling construction projects have been the Critical Path Method (CPM) and the Project Evaluation and Review Technique (PERT). (Adebowale & Oluboyede, 2011) These techniques enables project managers to evaluate the early and late times at which activities can start and finish, calculate activity float (slack), define critical activities, and evaluate the impact of variations in duration, logical relations and cost on the overall project duration. Both CPM and PERT are network based techniques and therefore help in programming and monitoring the progress of the stages involved so that the project is completed within the deadline. (Sharma, 2006) In doing this, it specifies the part of

the project that are crucial which if delayed beyond the normal time would increase the completion time of the project as a whole. It help to assists in allocating resources, such as labour and equipment and thus helps to make the total cost of the building project a minimum by finding the optimal trade-off between various costs and time involved .Hence CPM assumes preceding experience with similar projects from which the relationships between resources and job times are obtainable. On the other hand, PERT includes uncertainties in activity times in its analysis.(Adebowale & Oluboyede, 2011) It determines the possibilities of completing various stages of the project by specified deadlines. It also calculates the expectedtime to complete the project. In further words, it detects the activities that have high potential for causing delays in completing the project on schedule. Thus, even earlier the project has started, the project manager knows where he or she can guess delays. Then manager can take the necessary preventive measures to decrease possible delays so that the project schedule is on track. Actually, both techniques, PERT and CPM,(Grant, 1983) were developed almost simultaneously. Project managers (PM) often meet the problem of having to shorten the scheduled completion time in order to accelerate the execution of a project. Reducing the project duration can achieved by adding more resources to the, resources or by assigning additional labor. This managerial decision of supplementary resources, overtime and labor will however rises the overall cost of the project thus trimming down the project duration of activities on critical path. This idea of project management which involves investment of extra budget in order to minimize the duration to meet the targeted date is known as crashing.(Adebowale & Oluboyede, 2011) The objective of accelerating project by crashing total project duration is helpful so that delays can be recovered and liquidated damages can be avoided.

2. STUDY AREA & METHODOLOGY

2.1 Study location and data description

“TSC-building-KUET” (Figure 1&2) which is situated in besides KUET auditorium in Teligati, PhulBari Gate was selected as our study area. This building consists of 4-block. Block –A was selected for analysis. It is two storied building. Specifically we work with foundation portion (Figure 2) illustrate this.



Figure 1: Location of TSC from google earth



Figure 2: Site construction image of TSC-KUET

The project plan of the TSC building foundation work has the various activities that would be carried out, as well as the duration (days) and cost of each activity in KUET area. The activities included planning, procurement of materials, excavation, plumbing and so on. The data contains the level of precedence among various activities, as well as the cost of each activity. To prevent clumsy analysis, activities were grouped.

2.2 Methods

This study focused on the cost and on the available duration (days) of the activities of carrying out the project. The duration is in multiple time estimates, that is, the optimistic time, the most likely time and the pessimistic time estimate. The network analysis procedures were used in analyzing the data; this involves the critical path method (CPM), project evaluation and review technique (PERT) and probability estimation. The aim of estimating probability is to find out the possibility that a node j in the network will occur by a pre-specified scheduled time, S_j , assuming that all the activities in the network are statistically independent. This probability was estimated in this study using

In CPM networking, all the activities time estimates are single values with the assumption that activity time are known with certainty by using a single activity time estimate. In reality however, it is rare to have activity time estimate to be certain. This is because projects longest time is the activity required to be completed assuming everything went on normally. Therefore, the three time estimates were subsequently used to estimate the expected time (mean) and variance of the distribution. Expected time is the weight average of the three time estimates (optimistic (a), pessimistic (b) and most likely time (M)).(Adebowale & Oluboyede, 2011)

Average of the three time estimates (optimistic (a), pessimistic (b) and most likely time (M)):

$$\text{Expected time (mean)} = \frac{a+b+4M}{6} \quad (1)$$

$$\text{Variance} = \frac{(b-a)^2}{6} \quad (2)$$

Project crashing was done using:

$$\text{Cost slope} = \frac{\text{Crash Cost}(CC) - \text{Normal Cost}(NC)}{\text{Crash Time}(CT) - \text{Normal Time}(NT)} \quad (3)$$

The data were collected from KUET Engineering section scheduling & costing tender document & site engineer. The floor plan of the building is the first phase of the building project after clearing of the bush on the site.

PERT analysis was used to obtain the cheapest cost by crashing as many activities as possible on the critical path.

3. ANALYSIS & RESULT

3.1 Data presentation & Activity selection

Table 1 shows the description of activities involved for the construction process of TSC-block [A] construction project in Teligati, PhulBari Gate, at KUET. The construction activities begin with activity A and ends with activity k. Table 2 shows the distribution of the project activities relative to the actual number of days to complete individual activity and their respective cost implication in terms of Bangladeshi tk. of the project. The costs are basically labour costs based on the assumption that materials are already available for use. If, once the materials are available, the reduction in number of days to complete a particular activity will only be affected by the cost of hiring additional labour. Table 3 shows the project activity according to activities that must be performed before the next activity can begin, this is called the predecessor. The optimistic estimate (a), most likely estimate (m) and pessimistic estimate

(b) of the building were determined to see the variations in the estimates as they affect the construction activities, were computed as shown in Table 4. The critical path calculations (Kelley Jr & Walker, 1959) involve two passes: The forward pass determines the earliest occurrence times of the events, and backward pass calculates their latest occurrence times (Oberlender & D, 1993). The earliest time is calculated as follows:

Table 1: Description of activities in a research process to completion the project foundation

Activity	Activity description	Predecessors
A	Site clearing & removal of trees	—
B	Earthwork Excavation	A
C	Grading General area	A
D	Earth filling & brick flat soling	B,C
E	Footing formwork & concrete placing	B
F	Rever binding for column & GB	D,E
G	Installing utility lines	B,D
H	Formwork for column & GB	F,G
I	Pouring concrete	H
J	Removal of formwork	I
K	Filing with sand up to plinth	880

3.2 Critical path method (CPM) & PERT analysis

Using activity relationship from (table-1) critical path was drawn. Where i is the starting node number for a particular activity; j is the ending node number for a particular activity; tij is the expected time to complete activity.

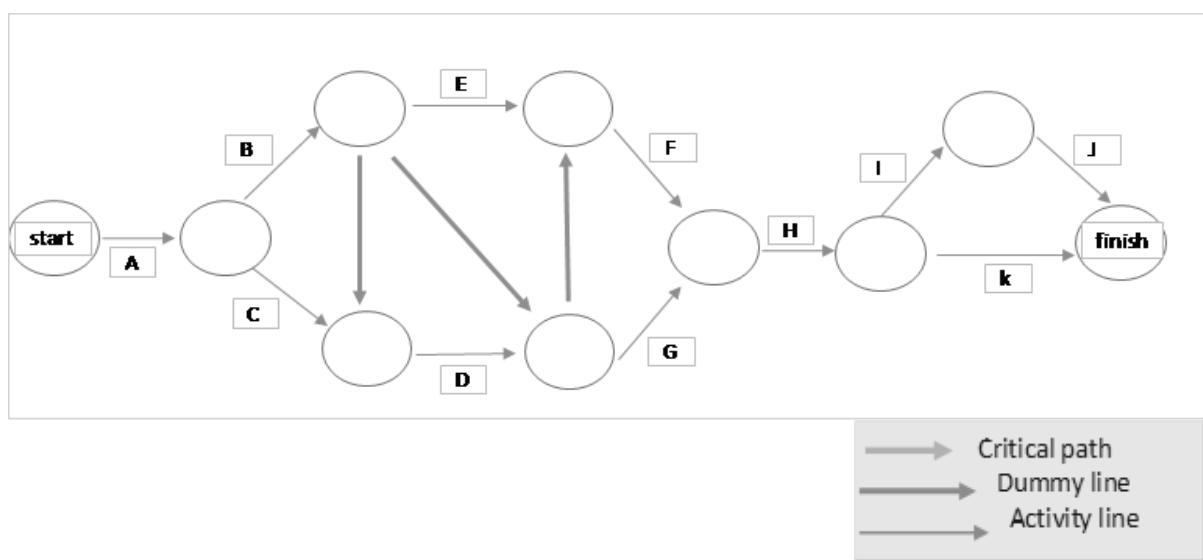


Figure 3: Network diagram of --TSC-block [A]

Table 2: Project Activity, Predecessor, optimistic estimate (a), most likely estimate (m) and pessimistic estimate (b) of a construction project TSC-block [A]-foundation work

Activity	Predecessors	Optimistic estimate (a)	Most likely estimate (m)	Pessimistic Estimate (b)
A	—	17	19	27
B	A	12	14	22
C	A	5	7	14
D	B,C	5	8	10
E	B	7	10	15
F	D,E	5	7	13
G	B,D	4	6	10
H	F,G	4	6	8
I	H	9	11	19
J	I	4	6	14
K	H	4	5	9

Table 3. Mean and variances of activities of a building construction project at KUET area, in PhulBari-Gate

Activity	Predecessors	Expected duration- (a+4m+b/6)	Standard Deviation (sigma)-(b-a/6)	Variance (b-a/6) ²
A	—	20.00	1.67	2.78
B	A	15.00	1.67	2.78
C	A	7.83	1.50	2.25
D	B,C	7.83	0.83	0.69
E	B	10.33	1.33	1.78
F	D,E	7.67	1.33	1.78
G	B,D	6.33	1.00	1.00
H	F,G	6.00	0.67	0.44
I	H	12.00	1.67	2.78
J	I	7.00	1.67	2.78
K	H	5.50	0.83	0.69

The analyses of the paths are shown as:

Various path:

1. PATH-1: A-B-E-F-H-I-J (time= 78 days)
2. PATH-2: A-B-E-F-H--K (time= 64.5 days)
3. PATH-3 : A-C-D-G-H-I-J (time = 67 days)
4. PATH-4: A-C-D-G-H-K (time = 54 days)
5. PATH -5 : A-G-I-DUMMY-K-L-M (time = 26.08)
6. Path-6 : A-G-I-J-L-M (time =24.75)

Table 3 shows the Means and Variances of Activities along the Identified Critical Path. In actual fact, many project work are full of uncertainties, in this project however, the longest path is ABEFHJ (critical activity), which means the completion time is approximately 78 days. Then, it becomes necessary to know how realistic this will be by estimating the probability of achieving this scheduled date. Therefore, in order to know whether this project time can be completed at this time, we assumed a completion number of days say 85. Thereafter, we computed the concept of crashing.

3.3 Project variance & probability analysis

Project variance on critical path = 2.78+2.78+1.78+1.78+0.44+2.78+2.78= 15.12

Therefore, in order to know whether this project time can be completed at this time, we assumed a completion number of days say 85. Thereafter, we computed the probability that the project will be completed in less than 85 days as:

$$Z = \frac{x-\mu}{\sigma} = \frac{\text{DUE DATE} - \text{EXPECTED DATE OF COMPLETION}}{\sqrt{\text{PROJECT VARIANCE}}} \quad (4)$$

$$= \frac{90-78}{\sqrt{15.12}} = 1.80$$

p(z ≤ 1.80) from Z distribution table = 0.961 = 96% (approximate.).Therefore, the probability that project will be completed in less than 85 days

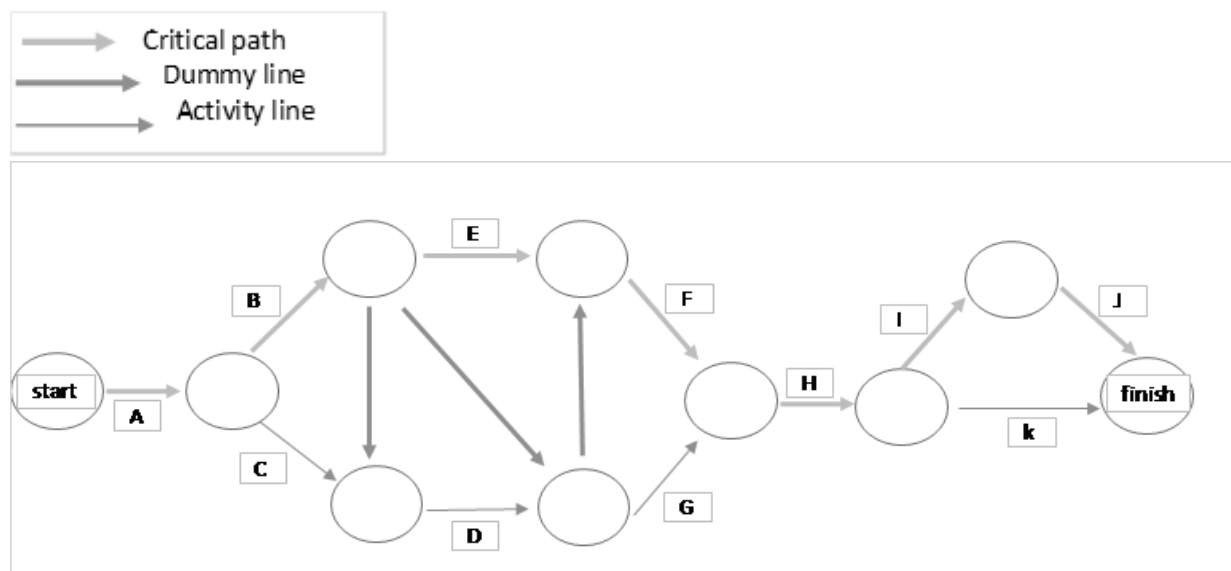


Figure 4: Network diagram with critical path--TSC-block [A]

Table 4: The earliest time, latest time and slack activities of a building construction project at KUET, in Teligati, PhulBari Gate

	Duration	ES	EF	LS	LF	Slack(TF)
A	20	0	20	3	20	0
B	15	20	35	0	35	0
C	7.83	20	27.83	5	37.5	9.67
D	7.83	35	42.83	7	45.33	2.5
E	10.33	35	45.33	9	45.33	0
F	7.67	45.33	53	21.33	53	0
G	6.33	42.83	49.16	10.33	53	3.84
H	6	53	59	11.33	59	0
I	12	59	71	16.33	71	0
J	7	71	78	23.66	78	0
K	5.50	59	64.5	22.33	78	13.5

3.4 Cost analysis using crashing

This building project analyses will be incomplete if the cost associated with its monetary terms is not worked out. The essence of cost analyses is to determine the optimum cost of the project using the method of least cost scheduling. (Wiest & Levy) This was done by reducing the time of activities on the critical path with the lowest cost slope. (Adebowale & Oluboyede, 2011) If the time is reduced this will in turn increase the cost. This could result to extending the hours of work per day or hiring more labour:

$$\text{Cost slope} = \frac{\text{Crash Cost (CC)} - \text{Normal Cost (NC)}}{\text{Crash Time (CT)} - \text{Normal Time (NT)}} \quad (5)$$

Table 5: Project Activity, Days (actual and crash) and cost (actual and crash) of TSC-block [A] foundation construction project at KUET in Teligati, PhulBari Gate

Activity	Duration (days)		Cost (tk* 10 ³)		Cost slope
	Actual	crash	Actual	Crash	
A	20	15	338	423	17
B	15	10	468	608	28
C	7.83	5.83	250	310	30
D	7.83	5.83	2060	2310	125
E	10.33	7.33	2260	2560	100
F	7.67	5.67	1450	1630	90
G	6.33	4.33	550	620	35
H	6	4	800	950	75
I	12	8	650	760	27.5
J	7	5	450	525	37.5
K	5.50	4.50	800	880	80
Total			10076	11576	

Table 6: Activities crash cost/day calculation of TSC-block [A] foundation construction project at KUET in Teligati, PhulBari Gate

Activity	Actual time	crash time	maximum crash time	Actual cost 1000 tk	Crash cost	crash cost /day
A	20	15	5	338	423	17
B	15	10	5	468	608	28
C	7.83	5.83	2	250	310	30
D	7.83	5.83	2	2060	2310	125
E	10.33	7.33	3	2260	2560	100
F	7.67	5.67	2	1450	1630	90
G	6.33	4.33	2	550	620	35
H	6	4	2	800	950	75
I	12	8	4	650	760	27.5
J	7	5	2	450	525	37.5
K	5.50	4.50	1	800	880	80

Table 7: Crashing analysis of TSC-block [A] foundation construction project at KUET ,for 18 days reduction from critical path duration.

A-B-E-F-H-I-J =73 DAYS (AFTER 5 DAY CRASHING)	this is critical path & A crash due to lowest cost slope
A-B-E-F-H-I-J =71 DAYS (AFTER 2 DAY CRASHING)	this is critical path & H crash due to lowest cost slope
A-B-E-F-H-I-J = 67 DAYS (AFTER 4 DAY CRASHING)	this is critical path & I crash due to lowest cost slope
But now we get two critical path of same time 67 days path -1 & path-3	
A-B-E-F-H-I-J = 64.5 DAYS (AFTER 2.5 DAY CRASHING)	this is critical path & B crash due to lowest cost slope
A-C-D-G-H-I-J= 65 DAYS(AFTER 2 DAY CRASHING)	this is not critical path & C crash due to lowest cost slope
But now we get two critical path of same time 64.5 days path -1 & path-2	
A-B-E-F-H-I-J = 62 DAYS (AFTER 2.5 DAY CRASHING)	this is critical path & B crash due to lowest cost slope
A-B-E-F-H-K= 62 DAYS (AFTER 2.5 DAY CRASHING)	this is critical path & B crash due to lowest cost slope
But now we get two critical path of same time 62 days path -1 & path-2	
A-B-E-F-H-I-J = 60 DAYS (AFTER 2 DAY CRASHING)	this is critical path & J crash due to lowest cost slope
A-B-E-F-H-K= 61 DAYS (AFTER 1 DAY CRASHING)	this is not critical path & K crash due to lowest cost slope

Table 8: Crashing cost of TSC-block [A] foundation construction project in Teligati, PhulBari Gate at KUET after 18 days reduction from critical path duration

Activity	calculation	cost(TK*10 ³)
A	338+(5*17)	423
B	250+(2*30)	608
C	468+(5*28)	310
D	2060	2060
E	2260	2260
F	1450	1450
G	550	550
H	800+(2*75)	950
I	650+(4*27.5)	760
J	450+(2*37.5)	525
K	800+(1*80)	880
	Total	10876

4. CONCLUSIONS

The problem of poor project execution, non-completion And behind schedule, which are rampant in our society. A various number of factors influence to delays. Due to cost and time over-runs can increases complexity of the project. so that this require proper analysis to control. Our main objectives to find minimum cost in project completion time. For this actually use PERT & CPM to find optimum time which is less than schedule time 105 days in foundation work of TSC-block[A]. That we find that was the longest path in network (critical path). Where we get time 78 days less than 105 days .in this path slack was zero. Our completion time was 60 days .which is less than 18 days of 78 days. So that crashing was required to reach completion time & find cost minimum. so for his finally we get total project cost TK.10876000. If network analysis tools are employed and incorporated into the project plan at the onset of work activities. Also, the task of building project management can be improved if network analysis technique is adopted, this will identify minimum time a building project can take before completion. It will eliminate any sort of redundancy or dangling of activities, so that the developer can meet the needs of other clients who need its services at

other building sites. So that we can complete in due time the project TSC-block [A] KUET, where it was delay 6 months than its schedule time 12 months.

ACKNOWLEDGEMENTS

Actually this work is very difficult to do because management system is not popular in Bangladesh, so that proper data collection was difficult. Thanks to Assistant professor (Mrs.) Jumna Akhter, Eng. Ikramul Hoque (BECM, KUET) for guideline & Eng. Saidul Islam (Engineering Section KUET) for tender document providing.

REFERENCES

- Adebowale, S., & Oluboyede, E. (2011). Network analysis and building construction: Implications for timing and costing of activities. *Journal of Civil Engineering and Construction Technology*, 2(5), 90-100.
- Grant, D. P. (1983). *PERT and CPM: Network Methods for Project Planning, Scheduling and Control; Publ. by the Small-Scale Master Builder.*
- Kelley Jr, J. E., & Walker, M. R. (1959). *Critical-path planning and scheduling.* Paper presented at the Papers presented at the December 1-3, 1959, eastern joint IRE-AIEE-ACM computer conference.
- Oberlender, & D, G. (1993). *Project management for engineering and construction* (Vol. 2): McGraw-Hill New York.
- Sharma, S. (2006). *Operation research: Pert, Cpm & cost analysis:* Discovery Publishing House.
- Wiest, J., & Levy, F. A Management Guide to PERT/CPM: With GERT/PDM/DCPM and Other Networks, 1977: Prentice-Hall: Englewood Cliffs, NJ.

USE OF SUPPLEMENTARY CEMENTITIOUS MATERIALS IN RECYCLED BRICK AGGREGATE CONCRETE

Md. Omar Ali Mondal¹, Md. All Mokadim², Abu Zakir Morshed³

¹Student, Department of Civil Engineering, Khulna University of Engineering & Technology, Bangladesh, e-mail: moamondal@gmail.com

²Student, Department of Civil Engineering, Khulna University of Engineering & Technology, Bangladesh, e-mail: shazibkuet@gmail.com

³Professor, Department of Civil Engineering, Khulna University of Engineering & Technology, Bangladesh, e-mail: azmorshed@ce.kuet.ac.bd

ABSTRACT

Recycling of construction and demolition waste could be a great source of concrete aggregates. The use of waste concrete as recycled concrete aggregate conserves natural aggregate, reduces the impact on landfills, save energy and can provide a cost benefit. The scope of this project was to compare the concrete properties between recycled brick aggregate concrete and natural brick aggregate concrete by using a different percentage of fly ash, blast furnace slag, and super plasticizers to enhance the durability of the recycled concrete. Residual strength of structural members was determined by core cutting and the residual strength was around 15 MPa. The properties of recycled brick aggregate slightly varied from the natural brick aggregate. The specific gravity and unit weight of recycled brick aggregate was less than that of natural brick aggregate. The absorption capacity of recycled brick aggregate (12.84%) was higher than the absorption capacity of natural brick aggregate (11.26%). Total 18 batches of cylindrical specimens were cast for compressive strength, water permeability, and rapid chloride permeability test. The compressive strength was 20.09 and 24.27 MPa, respectively for the concrete made by recycled brick aggregate and natural brick aggregate at 28 days. By using 10%, 15%, and 20% blast furnace slag with recycled brick aggregate, the compressive strength at 28 days was found to be 21.81, 24.52 and 25.30 MPa, respectively. By increasing the percentage of fly ash to 10%, 15%, 20%, 25%, 30% and 35% with recycled brick aggregate, the compressive strength was decreased at 28 days but at 60 days the compressive strength was increased gradually up to 30% of fly ash. Water permeability and rapid chloride permeability was decreased with the increase of the compressive strength at 28 days. Properties like compressive strength, permeability, and rapid chloride permeability were comparable to that of the natural aggregate concrete.

Keywords: Recycle Aggregate, Fly Ash, Blast Furnace Slag, Permeability, RCPT

1. INTRODUCTION

In recent years, the escalating urbanization has led to excessive demolition work and construction activities, which consequently resulted in the production of large quantities of construction and demolition (C&D) waste, especially concrete waste. A huge amount of C&D waste has become available a seriously significant impact on the environment and society. The great recycling of concrete waste was identified as the most feasible way to minimize the growing problem of waste disposal through landfills. The application of recycled aggregates is important in providing alternative material sources to reduce the dependence of the construction industry on natural aggregates. A critical curtailment in the sources of natural aggregates is becoming a worldwide problem, especially in the face of the development of major urban centers. Demolition and construction waste produce a large amount of crushed concrete which increasing day by day. The annual rate of generation of construction waste is 1,183 million ton worldwide (Khaitan, 2013). In the year of 2011 to 2016, about 82,646,051 m³ of C&D waste (average 16,529,210 m³ per year) were generated in Tehran which only about 26% of them have been recycled (Asgari, A et al., 2017). Huge

land area required for accompanied this huge amount of waste. Therefore, recycling construction waste is vital, to reduce land filling and to preserve the environment. Also, from the viewpoint of sustainable and green building technologies, the use of recycled aggregate (RA) in new concrete production has enlarged globally.

On the other hand, production and utilization of concrete are rapidly increasing, which results in increased consumption of natural aggregate as the largest concrete component. For example, two billion tons of aggregate are produced each year in the United States. Production is expected to increase to more than 2.5 billion tons per year by the year 2020 (Gonzalez & Young, 2004). This situation leads to a question about the preservation of natural aggregates sources. A possible solution to these problems is to recycle demolished concrete and produce an alternative aggregate for structural concrete in this way.

Moreover, Bangladesh is a developing country and her population is increasing day by day. Consequently, it is facing an alarming population explosion which is overshadowing all other fundamental problems. At the initial period of this century has to meet the increased demand for shelter for an increasing population, there will be a lot of demand for building materials. However, as the cost of building materials is becoming higher and higher, it has become necessary to search for low-cost available materials. So, increase in demand and decrease in supply of conventional aggregate for the production of concrete result in the need to identify new source of aggregate. At the same time, increasing quantities of demolished concrete from deteriorated and absolute structure are generated as waste materials in the same areas. Utilization of recycled concrete as an aggregate will contribute to the solution of the problem.

Almost every year Bangladesh is affected seriously by the conventional calamity. Flood is an annual affair in Bangladesh. A large portion of roads is damaged by this conventional calamity. It is to be noted that some old buildings, bridges, and culverts are also damaged by conventional calamity. In some areas, heavy urban expansion has depleted. So, as a developing country, the proper utilization of waste concrete as a coarse aggregate is an important national aspect. For this reason, in developing countries, restrictions and regulations on disposal sites will require greater recycling of this industrial waste.

2. METHODOLOGY

This study was divided into two parts, determination of Residual Strength before demolition the existing building and determination of the property of concrete after made with recycled aggregate with supplementary cementations materials & admixture.

2.1 Determination of Residual Strength

Cores were cut by a rotary cutting tool according to ASTM C-42. Three specimens were cut from 3 different columns before the demolition of the building behind the Civil Building of Khulna University of Engineering & Technology. Then the specimens were cut such as H/D ratio was 2. Then takes the dimension of the sample and weight. After 5 days the samples we recapped with lime and tested for compressive strength.



Figure 1: Core Sample

2.2 Determination of Recovered Strength

Recovered strength means the strength developed in the concrete made with recycled aggregate with supplementary cementations materials & admixture. This was including collection of materials, concrete casting and curing finally testing of strength.

2.2.1 Collection of Materials

Demolished concrete was collected from the demolished building behind the Civil Building of Khulna University of Engineering & Technology. This concrete was crushed as coarse aggregate by using hand tools. This aggregate denoted as Recycled Coarse Aggregate (RCA). New bricks were collected & crushed into natural coarse aggregate (NCA) Sylhet sand is used as natural fine aggregate. Blast Furnace Slag (BFS) and Fly Ash (FA) were collected from Seven Rings Cement, Khulna. Figure 2 shows Natural and Recycled coarse aggregate and Figure 3 shows Fly Ash and Blast Furnace Slag.



Figure 2: Natural Aggregate & Recycled Aggregate



Figure 3: Fly Ash and Blast Furnace Slag

2.2.2 Concrete Mixture Proportioning

A mix proportion (1:2:3.5) was selected for the concrete mixing with a water-cement ratio of 0.45. Concrete was mixed according to ASTM C192 (ASTM 2007) using a standard concrete mixture. (100mm×200mm) concrete cylinders were cast and compacted according to ASTM C39 (ASTM 2001). In this study total, eighteen batches of concrete were cast. Among the one batch were cast with Natural Coarse Aggregates (NCA), Natural Fine Aggregate (Sand) and Ordinary Portland Cement (OPC) another other seventeen batches were cast with Recycled Coarse Aggregate (RCA), Natural Fine (NFA) Aggregate and OPC. Three of them were cast by replacing natural fine aggregate with 10% to 20% blast furnace slag (BFS), six of them were cast by replacing 10% to 35% of cement with Fly Ash.

Table 1: Proportion of different materials

Specimen ID	Coarse Aggregate (%)		Fine Aggregate (%)		Binder (%)		Admixture (%)
	NCA	RCA	Sand	BFS	OPC	FA	
TSN-1	-	100	100	-	100	-	-
TSN-2	-	100	90	10	100	-	-
TSN-3	-	100	85	15	100	-	-
TSN-4	-	100	80	20	100	-	-
TSN-5	-	100	100	-	90	10	-
TSN-6	-	100	100	-	85	15	-
TSN-7	-	100	100	-	80	20	-
TSN-8	-	100	100	-	75	25	-
TSN-9	-	100	100	-	70	30	-
TSN-10	-	100	100	-	65	35	-
TSN-11	-	100	90	10	90	10	-
TSN-12	-	100	85	15	85	15	-
TSN-13	-	100	80	20	80	20	-
TSN-14	-	100	100	-	75	25	0.3
TSN-15	-	100	100	-	70	30	0.3
TSN-16	-	100	100	-	65	35	0.3
TSN-17	-	100	100	-	100	-	0.3
TSN-18	100	-	100	-	100	-	-

Three of them were cast by replacing natural fine aggregate with blast furnace slag and cement with fly ash other three batches was cast by replacing 25% to 35% cement with fly ash & 0.3% plasticizing admixture. Rest one batch was cast with recycled coarse aggregate,

natural fine aggregate cement & 0.3% plasticizing admixture. The details mix design are shown in Table 1.

2.2.3 Determination of Compressive Strength

The compressive strength of concrete is one of the most important and useful properties of concrete. The compressive strength of concrete determined by testing cylinder made in the laboratory according to ASTM C39 (ASTM 2001). The details of compressive strength test are shown in Figure 4.



Figure 4: Illustration of prepared sample for compressive strength test

2.3 Determination of Permeability

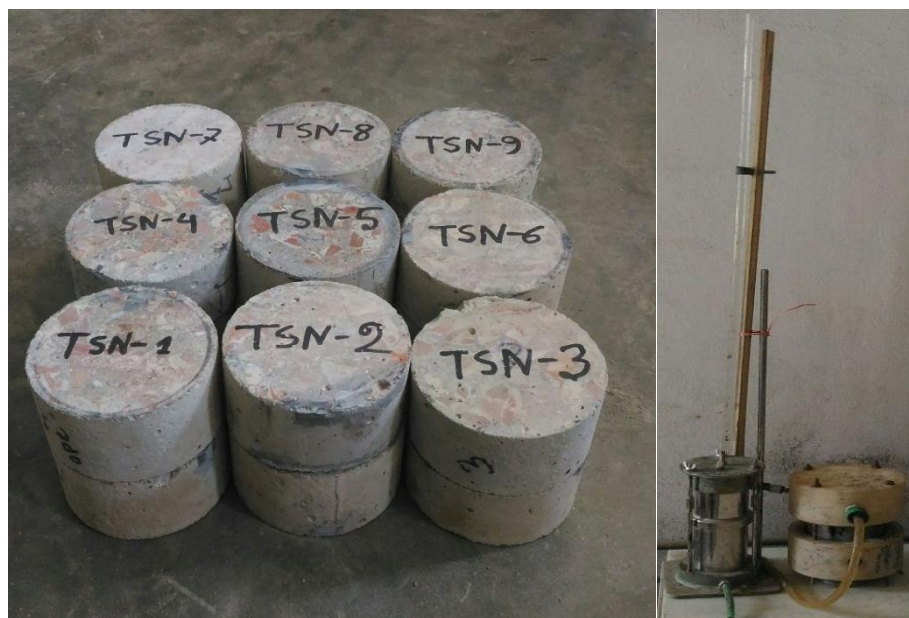


Figure 5: Specimen for permeability test & experimental setup

Eighteen group of consisting of 10 cm diameter and 5 cm height cylindrical sample were tested. The sample was saturated and the standpipes were filled with de-aired water to a given level. The test then starts by allowing water to flow through the sample until the water in the standpipe reaches a given lower limit. The time required for the water in the standpipe to drop from the upper to the lower level was recorded. Often, the standpipe was refilled and

the test was repeated for a couple of times. Each group contained one specimen. Figure 5 shows the specimen & experimental setup for permeability test. The test was performed at 28 days curing and the test was run for 16 hours. The recorded time should be the same for each test within an allowable variation of about 10%.

2.4 Rapid Chloride Permeability Test (RCPT)

The ability of concrete to resist permeability from aggressive elements (i.e., chloride ions) is key to the durability of reinforcing steel in concrete. To evaluate the resistance of concrete against chloride penetration, this test was performed according to ASTM C1202-5 one specimen per mixture at the age of 28 days. Concrete cylinders 100x200mm in size were prepared and cut into 50mm thick disks from the center of the specimen. Subsequently, the specimens were loaded into two Plexiglas half cells and sealed using silicone rubber. Each half cell had a reservoir filled with a solution of 3.0% NaCl at negative side and 0.3N NaOH at positive side. The cells were subjected to a 60-volt DC voltage across the specimen's cross section. The voltage was applied for 6h, and average charge passed (Coulombs) was recorded every 30 min. These values were adjusted by converting the charge passed through the diameter of the test specimens (100 mm) to the equivalent charge passed through a standardized diameter (95 mm). The schematic diagram of RCPT test is given in Figure 6. The rating of chloride ion penetrability Based on charged passed as per ASTM C1202 is given in Table 2:

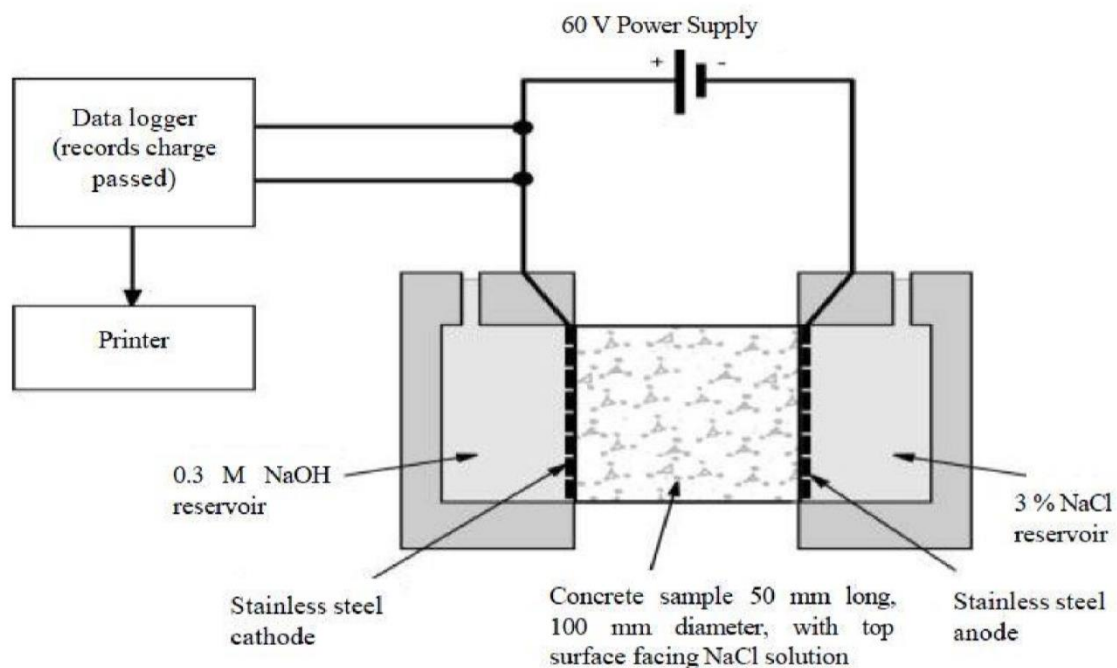


Figure 6: Schematic diagram of RCPT test

Table 2: Rating of chloride ion penetrability Based on charged passed (ASTMC1202)

Chloride Ion penetrability	Charge Passed (coulomb)
High	>4000
Moderate	2000-4000
Low	1000-2000
Very low	100-1000
Negligible	<100

3. RESULTS AND DISCUSSION

3.1 Core Cutting Test

The result of core cutting test is shown in Table 3. The residual strength of existing column was 15MPa.

Table 3: Result of Core Cutting

Column	C1	C2	C3
Length of Cylinder (cm)	13.7	13.2	13.8
Diameter of Cylinder (cm)	6.9	6.9	7.0
Area of Cylinder (cm ²)	37.39	37.39	38.48
Volume of Cylinder (cm ³)	512.28	493.59	531.09
Weight of Cylinder (gm.)	1001.3	983.6	1039.8
Unit Weight of Cylinder (gm./cc)	1.95	1.99	1.96
Applied Load (KN)	57.8	55.4	53.0
Compressive Strength (MPa)	15.46	14.84	13.78
Compressive Strength (psi)	2240	2150	2000

3.2 Materials Properties

3.2.1 Grain Size Distribution

The result of the grain size distributions of the recycled coarse aggregate and natural coarse aggregate are shown in Figure 7 and the grain size distributions of fine aggregate (Sand) and Blast Furnace Slag (BFS) are shown in Figure 8. The natural coarse aggregate used for casting was same graded as the recycled coarse aggregate.

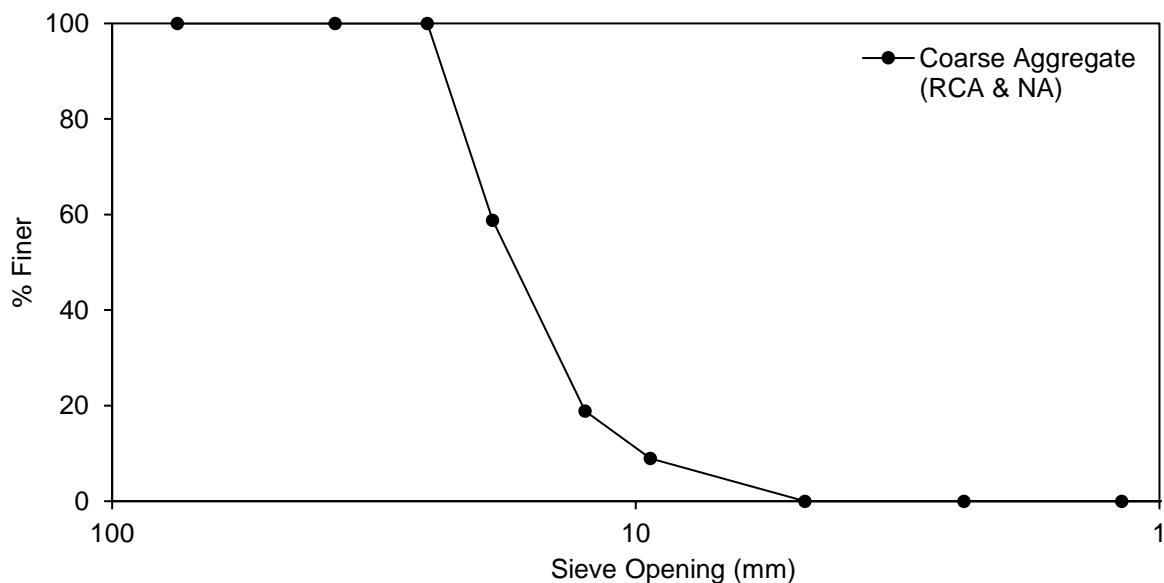


Figure 7: Grain size distribution curve of Coarse Aggregate

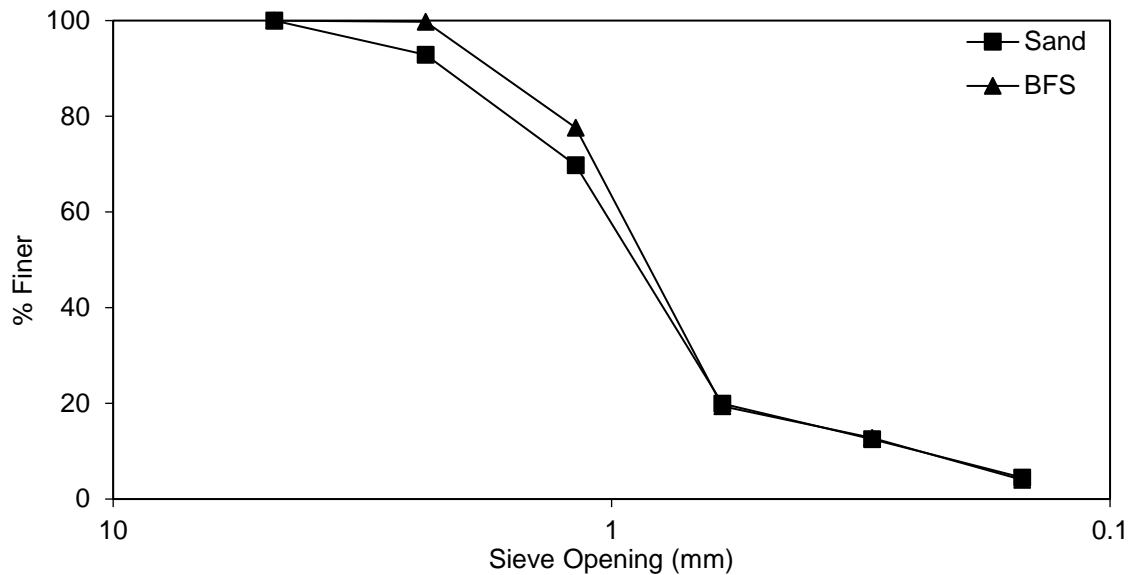


Figure 8: Grain size distribution curve of sand and Blast Furnace Slag (BFS)

3.2.2 Physical Properties

The specific gravity, unit weight, moisture content, absorption capacity & fineness modulus of coarse and fine aggregate was determined and the results are shown in Table 4. The specific gravity & unit weight of recycled coarse aggregate is lower than of the specific gravity of the natural coarse aggregate. The specific gravity, unit weight, moisture content & absorption capacity of blast furnace slag is lower than that of the natural fine aggregate.

Table 4. Properties of Aggregate

Types of Aggregate	RCA	NCA	Sand	BFS
Specific Gravity	1.79	1.86	2.36	2.31
Unit Weight (kg/m ³)	1070	1148	1589	1339
Moisture Content (%)	3.46	1.40	2.40	1.25
Absorption Capacity (%)	12.84	11.26	5.82	4.17
Fineness Modulus	8.13	8.13	3.0	3.1

3.3 Properties of Concrete

3.3.1 Recovered Strength

Figure 9 shows the effects of Blast Furnace Slag (BFS) on the compressive strength of concrete. It shows that by increasing the amount of BFS replacing the natural fine aggregate (Sand) was increasing the compressive strength of concrete at 7 days, 28 days & 60 days. TSN-1 (RCA + sand + OPC) was a 28-day's compressive strength of 20.09MPa which was 17% lower than TSN-18 (NCA + sand + OPC) was a compressive strength of 24.27MPa but TSN-4 (RCA + 80% sand + 20% BFS+ OPC) was a compressive strength of 25.21MPa which comparable with TSN-18.

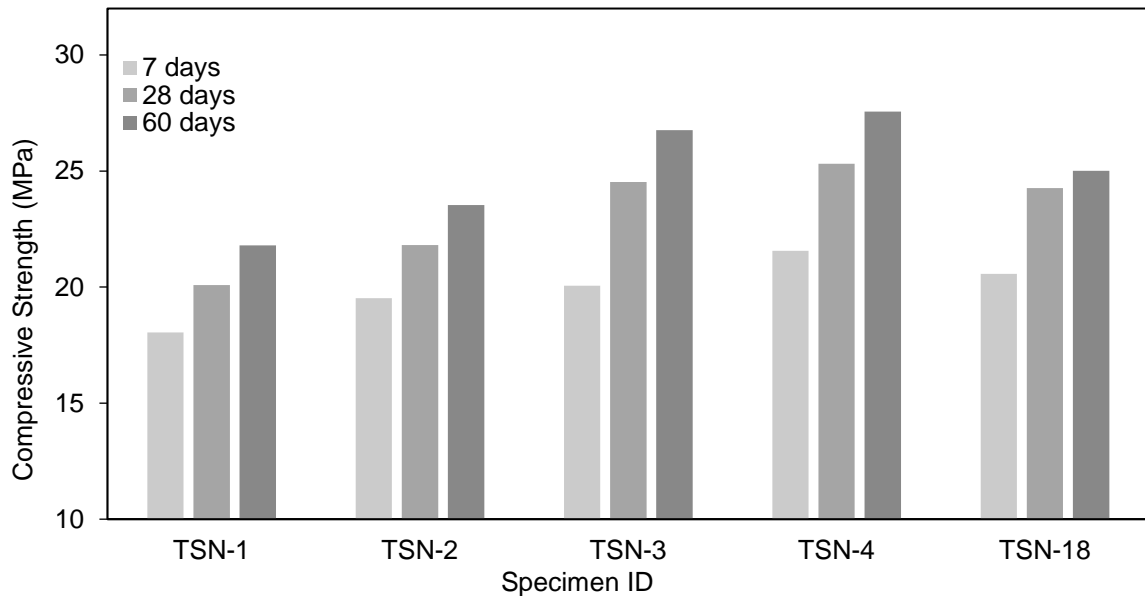


Figure 9: Effect of Blast Furnace Slag (BFS) on compressive strength of concrete

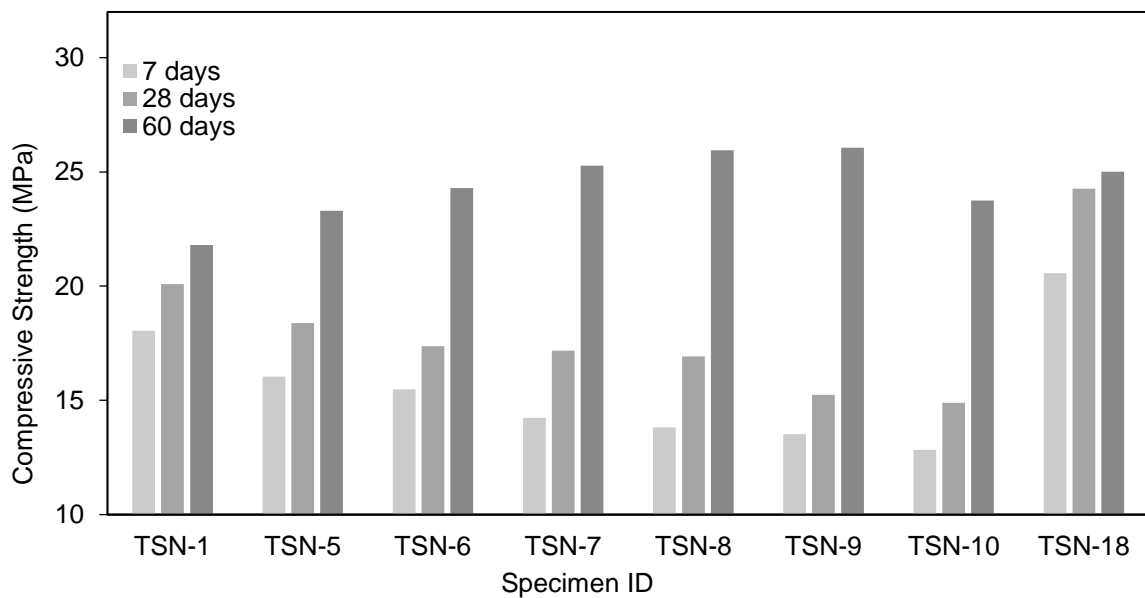


Figure 10: Effect of Fly Ash (FA) on compressive strength of concrete

Figure 10 shows the effect of fly ash on the compressive strength of concrete. It shows that by increasing the amount of fly ash replacing Ordinary Portland Cement (OPC) the compressive strength of concrete was decreasing at 7 days & 28 Days but increasing the compressive strength at 60 days up to replacing 30 % OPC by fly ash. Further increasing the amount of fly ash was reducing the compressive strength of concrete at 60 days also. From this figure of TSN-1 (RCA + sand + OPC) was a 28 days' compressive strength of 20.09MPa which was less than the compressive strength of TSN-18 (NCA + sand + OPC) was 25.27MPa but by increasing the amount of fly ash TSN-5, TSN-6, TSN-7, TSN-8, TSN-9 and TSN-10 decreasing compressive strength at 28 days but TSN-9 (30% FA) was a compressive strength of 26.06MPa at 60 days which was comparable with the compressive strength of TSN-18 at 60 days.

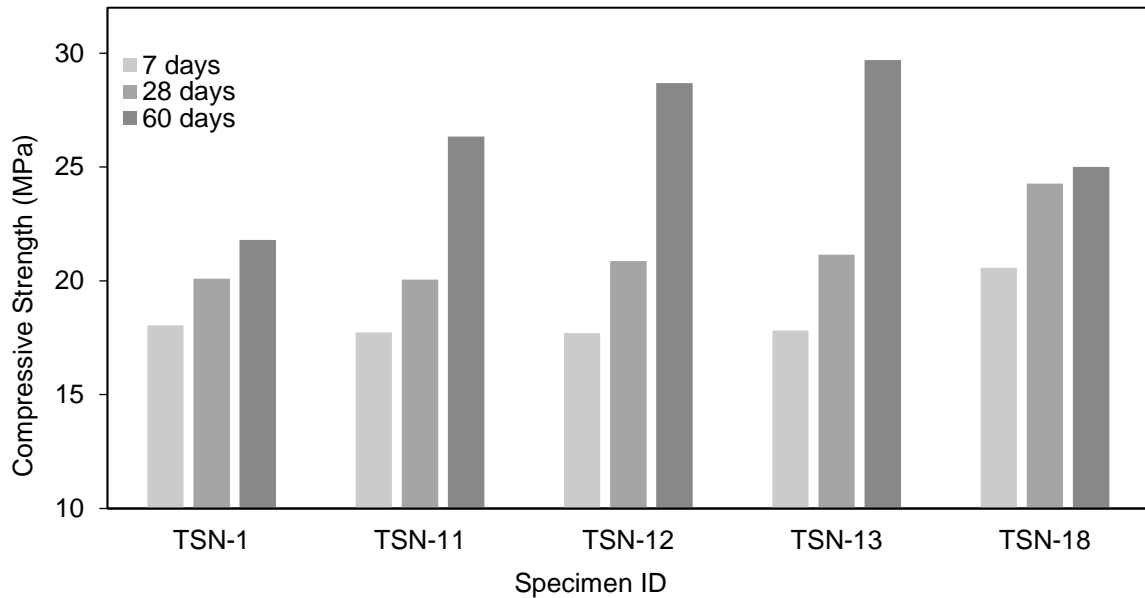


Figure 11: Effect of Fly Ash and Blast Furnace Slag on compressive strength of concrete

Figure 11: shows the combined effect of FA and BFS on the compressive strength of concrete. It shows that by increasing the amount of BFS replacing fine aggregate and FA replacing OPC was fewer effects on 7days & 28 days' compressive strength but increasing 60 days' compressive strength. TSN-11 (RCA + 90% sand + 10% BFS + 90% OPC + 10% FA) has a 28 days' compressive strength of 20.06MPa which is almost same of TSN-1 (RCA + sand + OPC) but TSN-12 (RCA + 85% sand +15% BFS + 85% OPC + 15% FA) & TSN-13 (RCA + 80% sand +20% BFS + 80% OPC + 20% FA) was slightly higher compressive strength than TSN-1, in 28 days' but at 60 days the compressive strength was higher than the compressive strength of TSN-18 (RCA + sand + OPC).

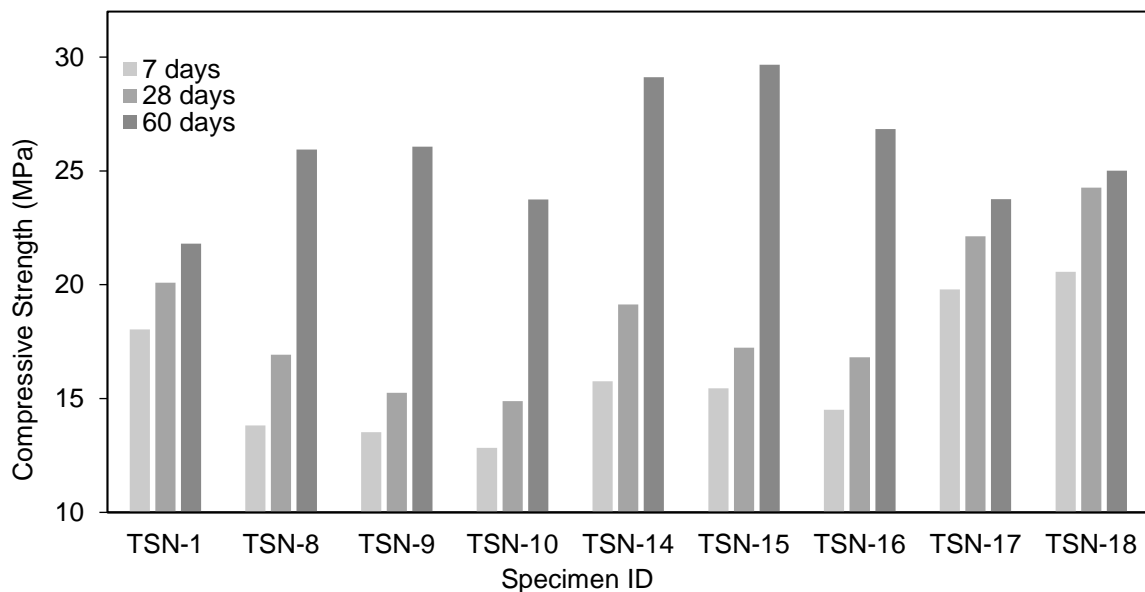


Figure 12: Effect of Fly Ash (FA) and Admixture on compressive strength of concrete

The effect of fly ash and plasticizer admixture on compressive strength is shown in Figure 12. It shows that by using of admixture the compressive strength was increased (8%-14%) Comparing TSN-1 (RCA+ sand + OPC) and TSN-17 (RCA + sand + OPC + 0.3% admixture) the compressive strength of TSN-17 was 10% higher than TSN-1 which comparable with

TSN-18. From this result, the compressive strength of the test samples was higher than the residual strength which was determined by core cutting.

3.4 Water Permeability

Figure 13 shows the results of permeability test. The permeability of concrete was decreased with the increase of 28 days compressive strength. The value of permeability was higher for TSN-10 (RCA + sand + 65% OPC + 35% FA) which was lowest compressive strength in 28 days, and lowest value for TSN-18 (RCA + sand + OPC). With the increasing of fly ash, the compressive strength in 28 days was decreased as a result permeability was increased, again with increasing of blast furnace slag the compressive strength was increased as a result the value of permeability was decreased.

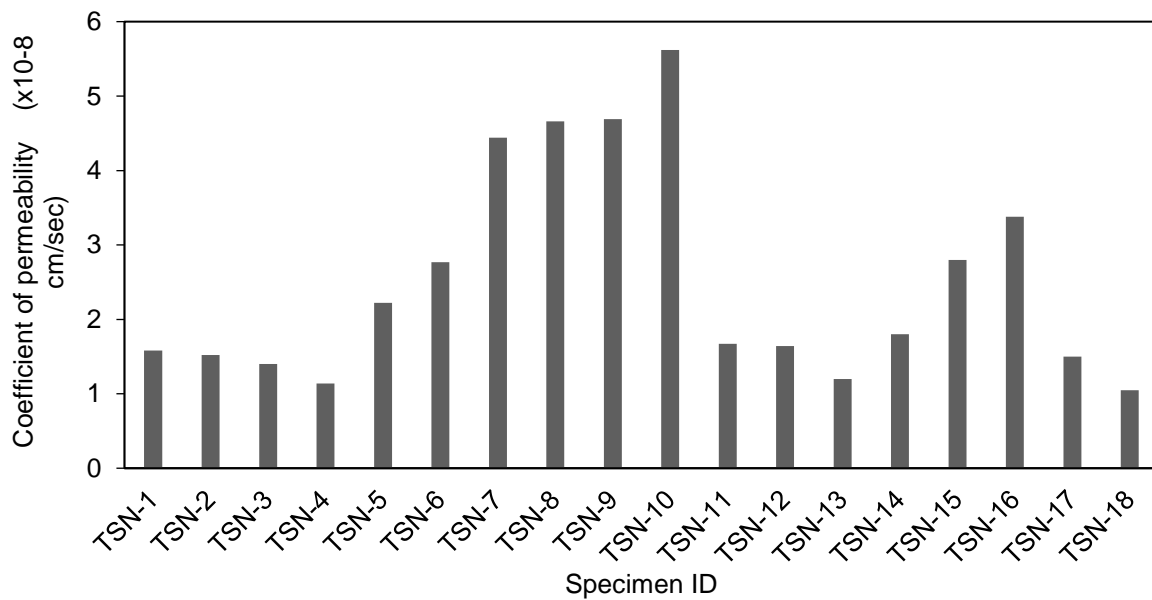


Figure 13: Water permeability of different specimen

3.5 Rapid Chloride Permeability

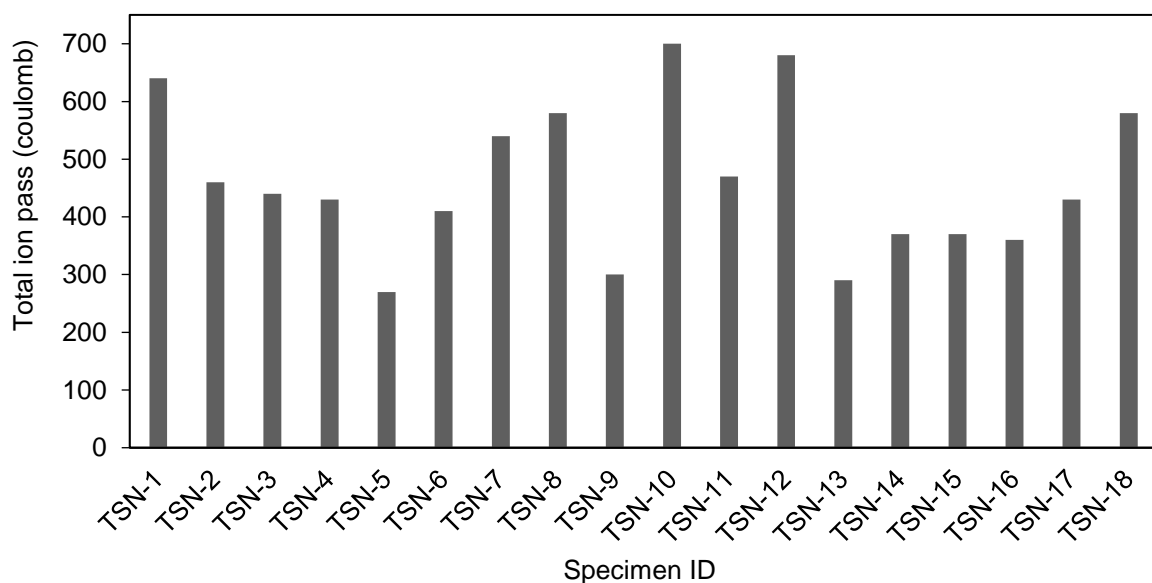


Figure 14: Rapid chloride permeability of different specimen

Figure 14 shows the result of rapid chloride permeability test. The result shows that total ion passes form TSN-1 (RCA + sand + OPC) 640 coulomb was higher than TSN-18 (RCA + sand + OPC) 580 coulomb total ion pass in TSN-17 (RCA + sand + OPC + 0.30% admixture). Figure 14 shows that by increasing the amount of blast furnace slag in TSN-2 to TSN-4 the value of passing ion was decreased. By increasing the amount of Fly Ash, the strength of concrete was decreased in 28 days and the value of passing ion was increased in TSN-5 to TSN-10. With the increased of compressive strength the value of total ion pass was decreased.

4. CONCLUSIONS

The recycled aggregate used in the present study fulfilled the requirements for RCA with respect to the physical and mechanical properties, however, the same were lower than those for natural aggregates. The natural aggregate concrete (TSN-18) and the RCA mix TSN-2, TSN-3, TSN-4, and TSN-17 exhibited similar behavior in compression. Chemical admixtures in the recycled concrete will modify significantly the properties of the fresh or hardened natural concrete. High concentration of water-soluble chloride ion in the recycled concrete may contribute to accelerated corrosion of steel embedment's in the natural concrete. It may be suggested that the properties of RCA are satisfactory for use in concrete; however, a detailed investigation on the long-term performance of RCA is needed before their actual use in structural infrastructure.

REFERENCES

- Asgari, A., Ghorbanian, T., Yousefi, N., Dadashzadeh, D., Khalili, F., Bagheri, A., ... & Mahvi, A. H. (2017). Quality and quantity of construction and demolition waste in Tehran. *Journal of Environmental Health Science and Engineering*, 15(1), 14.
- ASTM, C. (1992). C 42-90. Standard Test Method for Obtaining and Testing Drilled Cores and Sawed Beams of Concrete. *1991 Annual Book of ASTM Standards, Concrete, and Aggregates*, 4.
- ASTM, C. (2001). 39, Standard test method for compressive strength of cylindrical concrete specimens. *ASTM International*.
- ASTM, C. (2005). 1202, "Standard Test Method for Electrical Indication of Concrete's Ability to Resist Chloride Ion Penetration," Annual Book of ASTM Standards, Vol. 4.02. *Amer Soc for Test and Mater*.
- ASTM, C. (2007). 192. *Standard Practice for Making and Curing Concrete Test Specimens in the Laboratory (ASTM C192-07)*. West Conshohocken, PA: ASTM International.
- Gonzalez, G., & Moo-Young, H. (2004). Transportation Applications of Recycled Concrete Aggregate, FHWA State of the Practice National Review. *Washington DC: Federal Highway Administration*.
- Khaitan, C. K. (2013). "Construction and demolition waste; Regulatory issues and initiatives of MoUD." Proc., *Workshop on C&D Waste Recycling, Organized by Indian Concrete Institute-Central Public Works Dept., New Delhi, India*, 20–23.

INVESTIGATION OF SCREW FASTENED PROFILE STEEL SHEET SUBJECTED TO SIMULATED UPLIFT LOAD

S. M. Zahurul Islam¹, Habibur Rahman² and Mohd. Waliul Alam³.

¹ Professor, Department of Civil Engineering, Rajshahi University of Engineering and Technology, Bangladesh, e-mail: zahurul90@gmail.com

² Student, Department of Civil Engineering, Rajshahi University of Engineering and Technology, Bangladesh e-mail: dedar007@gmail.com

³ Student, Department of Civil Engineering, Rajshahi University of Engineering and Technology, Bangladesh e-mail: waliulalamnayan12@gmail.com

ABSTRACT

Profiled steel sheets play an important role in light gauge metal building construction, particularly as roof claddings in houses, low-rise commercial and industrial buildings. Thin profiled steel sheets are commonly connected to the underlying purlins of steel trusses and frames by drilling or tapping of screws. Screw fastened light gauge steel profiled roofing sheets are mostly subjected to wind suction or wind uplift forces. Strong and fluctuating wind uplift force may fail locally in the vicinity of screw. The objective of this study is to investigate the structural strength and behaviour of profiled steel sheet roofing elements under simulated wind uplift forces. A series of tests was performed on profiled steel sheet roofing subjected to wind uplift simulated pressure. Different diameter of screw and different span length of sheeting were considered in this research. The failure loads, failure modes and the load- deformation behaviour of screwed fastened profile steel sheet under simulated wind load were presented. It was observed that during the increase of loading, the upward deflection of the unscrewed crest became larger than that of the screwed crest. It was found that the local diamond-shaped deformations progressively developed around the screw fasteners at the support due to uplift load. The use of cyclone washers with screw fasteners reduced local plastic deformations and, in general, increased initial failure loads of the roofing sheets. It was found that, the structural behaviour of the roofing sheets under uplift loads was greatly dependent on the diameter of the screw and span length of profiled steel sheet.

Keywords: Test, roofing, profiled sheet, screw fastener, uplift load, local failure

1. INTRODUCTION

Profile steel shell structures are used in roofing elements popularly due to aesthetic and economical use of materials. Profiled steel sheets are increasingly used in structural application in recent years as shown in Fig. 1. The light gauge steel profiled roofing sheets are usually screwed and bolted fastened to cold-formed steel purlins or high-quality timber battens. Screwed and bolted are conventional connection type which are widely used in light gauge and thin steel structures as shown in Fig. 2. When used in high wind areas, structural performance of such roof systems under wind loads became a main concern for the structural design engineers. Wind loads acting on the roofs and walls of a low building are determined by the interaction of wind flow with the surface of the building. A large quantity of wind tunnel tests and field measurements has shown that roof claddings are predominantly subjected to wind suction, i.e., wind uplift (Holmes et al. 1990). Cyclone-induced sustained fluctuating wind uplift may cause fatigue damage to roofing sheets whilst short-term strong wind uplift could damage roofing sheet collapses (Beck and Stevens, 1979). Parsons (1976) conducted an extensive test of steel roofing sheets under static and cyclic loads for commercial purposes. Only the maximum allowable load which the sheeting can sustain without permanent deformations was involved in the static load test. Beck and Stevens were probably the first to perform fatigue tests of the arc-tangent type roofing sheet. Before the fatigue tests, some static tests simulating wind uplift were carried out on the roofing sheets

with different crest fastening arrangements. They found that a local diamond-shape deformation progressively developed on the crest of the corrugation under the head of the central screw fastener, which was followed by an elastic buckle at a nominal fastener tensile reaction force of 700 newtons per fastener. Mahendran (1990) investigated the effects of cyclone washers, roofing spans and fastener spacing on the structural behaviour of the arc-tangent type roofing sheets. He found that for a roofing assembly with an alternate crest fastening system, the local plastic buckling 'load', in terms of reaction force per fastener at the central support, was independent of the roofing spans and could be significantly increased by using cyclone washers. Xu and Reardon (1992,1993) conducted research on screw fastened profiled roofing sheets subject to simulated wind uplift. However, very little information on the structural behaviour of roofing sheets under wind suction is available in the public domain. Therefore, a research is needed to investigate the structural strength and behaviour of profiled steel sheet roofing elements under simulated wind uplift forces. It is a novel approach for light gauge profile steel sheet for housing construction.

In this paper, the structural strength and behaviour of profiled steel sheet roofing elements are investigated under simulated wind uplift forces. A series of tests was performed on profiled steel sheet roofing subjected to wind uplift simulated pressure. Different diameter of screw and different span length of sheeting are considered in this research. The failure loads, failure modes and the load- deformation behaviour of screwed fastened profile steel sheet under simulated wind load were investigated. The interaction between the overall and local structural behaviour of the roofing sheets was examined, to some extent, in terms of measured sheeting deflections, uplift loads and fastener reaction forces at the central support. The effects of cyclone washers and roofing spans on the structural behaviour of all three types of roofing assemblies were studied in terms of sheeting deflections and initial or ultimate failure loads. The structural behaviour of the roofing sheets under uplift loads was greatly dependent on the diameter of the screw and span length of profiled steel sheet is investigated.





Figure 1: Field application of profiled steel sheet for roofing system



Figure 2: Field application of profiled steel sheet using screwed and bolted connections

2. METHODOLOGY

2.1 Material Properties

Profile steel sheets are being used on an increasing scale for roofing. Profile steel sheet element is suitable for roofing because of its efficiency as load carrying member with a high degree of reserved strength and structural integrity, high strength to weight ratio, very small thickness ratio to other dimensions, very high stiffness and containment of space. The main advantages of using profile steel sheet as a roofing material are speedy installation, no shuttering required, less installation errors, lower dead load on the walls, light weight and easy handling, high strength to weight ratio, corrosion-resistant, economical considering mean service life. Profile steel sheets are available in an extensive range of models that are used as an excellent material for wide variety of architectural styles. Profiled steel sheet is extremely durable against corrosion because of the usage of seven layers of coating as shown in Fig. 3(b). Profile steel sheet and composition layer of profiled steel sheet are shown in Fig. 3. Moreover, profiled steel sheet can be used in relief center after disaster for short-term construction. The material properties of the profiled steel sheet were determined by tensile coupon tests. The tensile coupons were prepared and tested according to the American Society for Testing and Materials Standard, ASTM (1997) and the Australian Standard AS 1391 (1991) for the tensile testing of metals using 12.5 mm wide coupons as shown in Fig. 4. (Zahurul-Islam et al 2006). The coupons were tested in a Universal Testing Machine and the load was applied gradually. Deformation was measured by using deformation gauge. The test set-up and tested specimen after tensile test is shown in Fig. 5(a) and 5(b) respectively. Measured material properties obtained from tensile coupon tests are given in Table 1 and Fig 6.

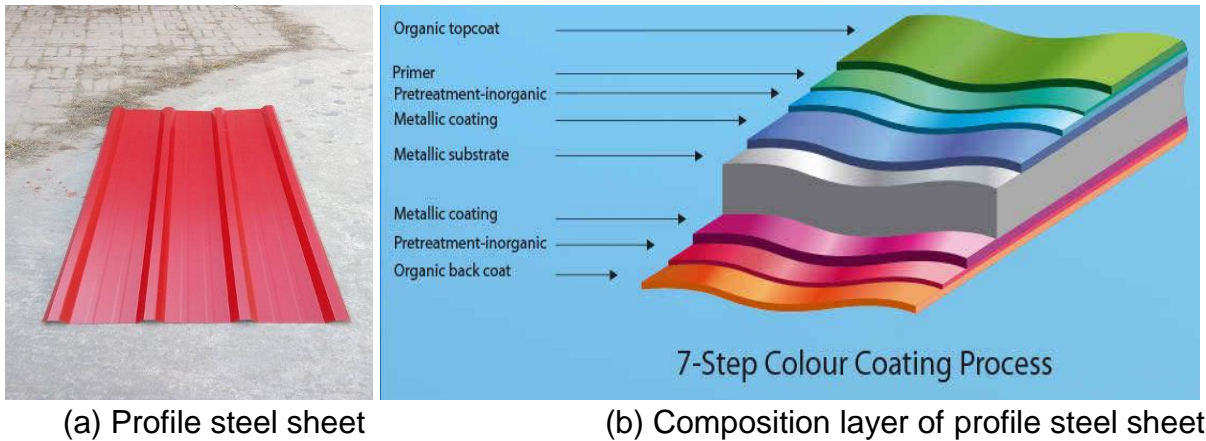


Figure 3: Profile steel sheet and its composition

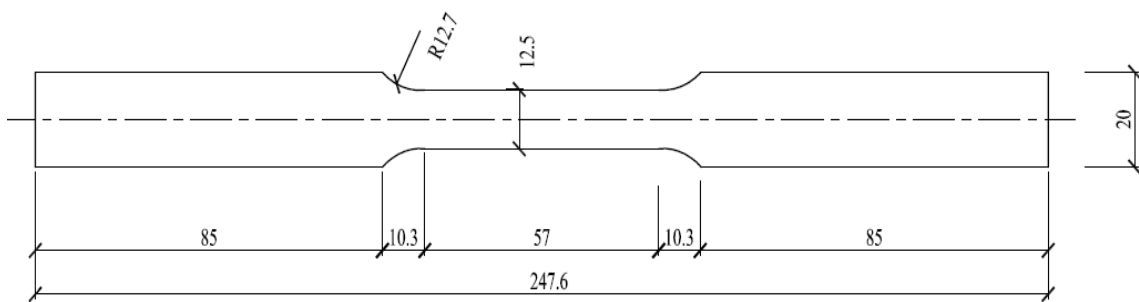


Figure 4: Dimension (mm) of coupon test specimen



(a) Coupon test



(b) Failure mode

Figure 5: Tensile coupon test and failure mode of profiled steel sheet

Table 1: Measured material properties obtained from tensile coupon tests

Specimen No.	Width b_c (mm)	Thickness t_c (mm)	Yield Stress σ_y (N/mm ²)	Ultimate Stress σ_u (N/mm ²)
1.	12.5	0.46	245.50	260.07
2.	12.6	0.46	237.54	262.51
3.	12.5	0.46	239.7	260.73

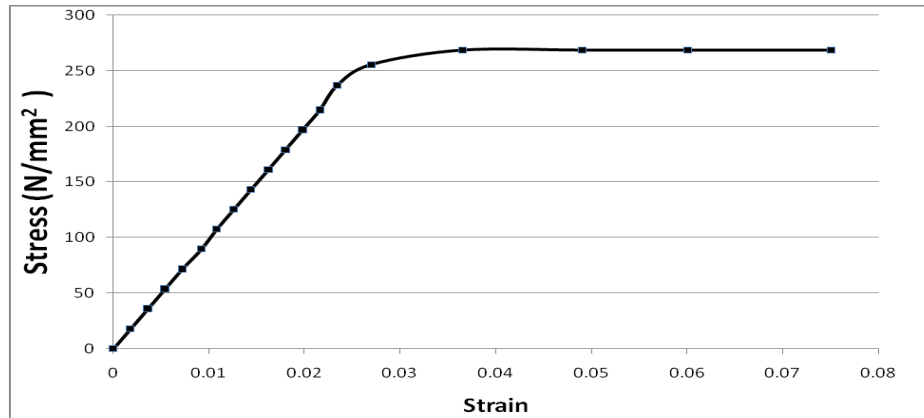


Figure 6: Stress- strain curve of coupon test results of profiled steel sheet

2.2 Screwed Connection Tests

A series of screwed connection tests were conducted in this study. The screwed connection tests were conducted by a servo-controlled hydraulic Universal Testing Machine which is mainly used for the coupon tests. Drilling and conneting of tensile test specimen are shown in Fig 7. The connection specimens were set into the grip of the machine as shown in Fig. 8. A pair of grip apparatus was specially fabricated in order to provide pin assembly at both ends of the test specimen. Two special gaskets were inserted in the grips, so that the shear surface of the single and doubly lapped specimen was purely vertical in-line to the loading direction. Clips linked with iron wire were used to prevent the extent of out-of-plane curling at the end of the profile steel sheet. After that, tensile load was applied gradually and the tensile stresses obtained from the machine were recorded at the room temperature.



Figure 7: Drilling and conneting of tensile test specimen



Figure 8: Test setup of tensile test specimen

A series of test was conducted on screws connection of 3 different diameter of 5.90 mm, 4.70 mm and 4.30 mm for single shear and double shear conditions to find out suitable connection specimen and optimum screw dia. Failure mode of screw and bolt connection are show in Fig. 9. The optimum diameters of 4.7 and 4.3 mm for screw connections were found for single shear and double shear respectively. Based on test results, two screwed parallel connections provided better performance than vertical arrangement.



Figure 9: Tested failure mode of screw and bolt connection

3. WIND LOAD CALCULATION

Wind loads are of important, particularly in the design of large structures tall buildings, radio towers, and long span bridges and for structure such as mill building and hangers having large open interiors and walls in which large opening may occur. Profile steel sheets are being used efficiently for roofing element which is frequently experienced wind load (Lysaght, 1990). Roofing element should satisfy wind load which is prescribed in Code. Roofing element should fulfill the code of practice or wind load for different areas as described in BNBC. The minimum design wind load on buildings and components there of shall be determined based on the velocity of the wind, the shape and size of the building and the terrain exposure condition of the site. For building specification, AISI state that the frame of a building must be designed to carry a pressure not less than 20 psf, on the vertical projection of the exposed surface of the finished structure. Wind load can be calculated based on Datchman wind effect, ASCE recommendation and BNBC code.

Dutchmen wind effect:

$$\text{Load, } P = KV^2 = 29.65 \text{ lb/ft}^2 \quad (1)$$

Where, $K=0.003$, $V= 99.42$ mph

$$P_n = P \times \frac{2\text{Sin}\theta}{1 + \text{Sin}^2\theta} = 29.65 \times \frac{2\text{Sin}26.56^\circ}{1 + \text{Sin}^2 26.56^\circ} = 22.1 \text{ lb/ft}^2 \quad (2)$$

BNBC code wind effect:

$$\text{For average condition} = 0.002558 v^2 = 23.73 \text{ psf} \quad (3)$$

Here, V = wind velocity in mile/h, P = wind pressure in psf,

For Rajshahi city, $v = 155$ km/h, = 96.31 mile/h,

Wind load as recomendated in ASCE, final report is shown in figure 10. According to ASCE final report, the maximum wind force and suction pressure is 16.128 and 21 psf wind word and lee word directions respectively.

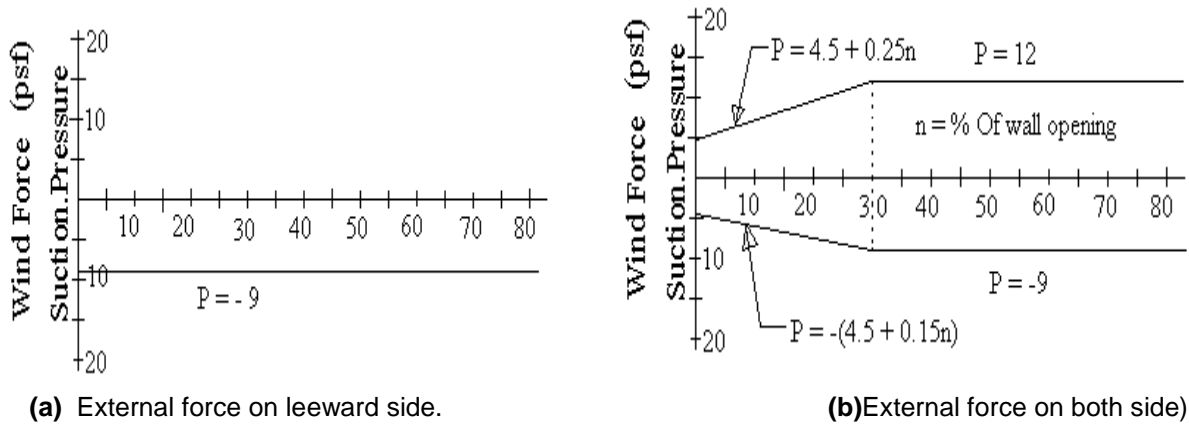


Figure 10: Wind load calculation according to ASCE final report (ASCE, 2005)

4. TEST ARRANGEMENT

Recently, there are three methods used to test roofing sheets namely the air bag method, the mid span load method, and the chamber method. It is believed that the mid span load method is the least expensive and easy to perform in a common structural laboratory. In the mid span load method, the limited band pressure at the mid span across the full width of the sheeting is used to replace the uniformly distributed pressure over the entire sheeting surface. Correspondingly, an equivalent sheeting span should be used in the test to replace the sheeting span in the prototype such that the fastener reaction force and bending moment of the test sheet at the central support are the same as those of the sheet prototype (as a two-span continuous beam). A force relationship between the mid span load on a test sheet and the average wind pressure on the sheet prototype is also established from the above modeling requirements. In this investigation, the mid span load method was chosen partly due to the practical considerations associated with the use of a commercial hydraulic jack. The basic sheeting span in the test was 1'6", 2'0", 2'6". A total of 24 roofing sheets were tested with and without cyclone washers. The experimental set-up is shown schematically in Fig. 11, with a hydraulic testing machine of 100kN capacity being the major apparatus. Flexible rubber loading pads were used to apply a narrow band of pressure to the bottom surface of the test sheet to simulate wind uplift.

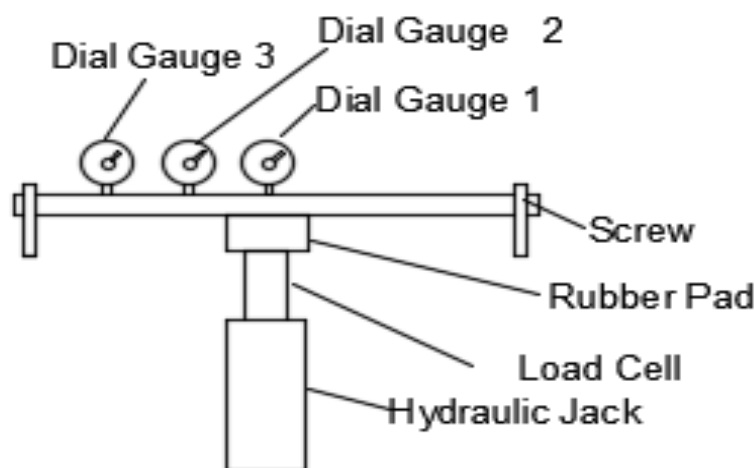


Figure 11: Schematic view of experimental set-up

Test arrangement of wind uplift load is shown in Fig 12. The upper face of the loading pads was formed to coincide with the shape of the sheeting profiles. The total fastener reaction force at the central support was measured by a load cell. The average reaction force on

each fastener was obtained by dividing the total reaction force by the number of fasteners at the central support. A load cell of a capacity of 30 kN was employed to measure the total uplift load on the roofing sheet, which was then used to calculate the average wind pressure on the sheet prototype. Dial gauges, graduated to 0.01 mm, were arranged at screwed crests (or centre lines of the pans) of the test sheets to measure the upward deflections.



Figure: 12 Test arrangement of wind uplift load

5. TEST RESULTS AND DISCUSSIONS

The results were obtained by experimentally using hydraulic jack, load cell and dial gauges. The failure loads, failure modes and behaviour of profiled steel sheeting subjected to wind uplift load are shown in Fig 13. The typical upward deflections of mid-point located on the screwed crest or rib at the mid span are plotted against the prototype average pressure for the roofing sheets which is shown in Fig. 14. When the prototype average pressure was below 10 psf, the overall structural behaviour of the roofing sheet was predominantly linear and elastic. With the increase of loading, the upward deflection of the unscrewed crest became larger than that of the screwed crest. The sheeting profile was distorted. Therefore, the non-linear characteristic of the sheeting was mainly attributed to the geometrical deformation. As the load increased further, local diamond-shaped deformations progressively developed around the screw fasteners at the central support. The deformations were plastic and significantly affected the overall sheeting deflection behaviour. When the average pressure was increased to about 25 psf, a local buckle with a clear sound occurred around the screw fasteners at the central support and caused a sudden drop of the loading. The local plastic buckling was followed by an overall cross-sectional distortion along the central support without any load increase. Correspondingly, the load-deflection curve exhibited an abrupt flattening.



Figure 13: Failure mode of uplift pressure

After the screwed crests at the central support totally flattened and the upward deflections of the unscrewed crests at the central support sufficiently increased, a different roof sheeting profile developed along the central support and caused a change in the deflection behavior. The structural stiffness of the roofing sheet suddenly increased from a nearly zero value and an approximate linear relationship between the load and the deflection was resumed. It was not occurred in the prototype roofing sheet results.

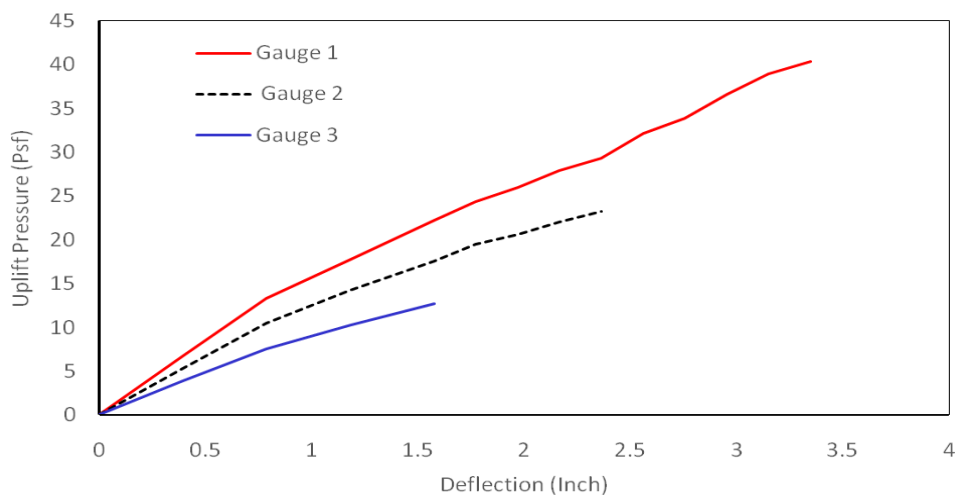


Figure 14: Comparison of uplift pressure vs. deflection at different point

According to BNBC code, the uplift pressure due to wind effect is 23.73 psf. Again according to ASCE code, the maximum wind force and suction pressure is 16.128 and 21 psf in wind ward and lee ward directions respectively. Based on the experimental results, it was found that the load carrying capacity of the proposed profiled steel sheet roofing system subjected to wind uplift load is 39.88 psf which is greater than BNBC and ASCE recommended wind uplift load. This roofing system satisfies BNBC code, ASCE code prescribed wind uplift load. Hence, this roofing system is suitable for housing construction in coastal areas also. Therefore, the proposed roofing system has a great potential to be exploited for the housing construction as well as disaster relief shelter.

5.1 Effect of Cyclone Washer

The local plastic failure of screw fastened profiled roofing sheets can be improved if the fastener is properly designed. The effectiveness of additional cyclone washers to the fastener was examined here. Although the cyclone washers are usually used in cyclone prone areas to resist sustained fluctuating wind and prevent roofing sheets from fatigue damage, the tests of the roofing sheets with the washers under static uplift load are useful for further understanding of the local plastic failure characteristic and for future work on cyclone-induced fatigue of the same profiled roofing sheets. Fig. 15 shows the comparison of the force-deflection curves of roofing sheet with and without the washers.

It is seen that the initial slope of the reaction force-deflection curve of the sheeting with the washers was steeper than that without the washers. As the uplift load was increased further, however, the steel washers of only 1 mm thick were distorted and were unable to prevent large local plastic deformations and large cross-sectional distortions. The yielding stage and the deflection hardening stage still remained. The final failure loads were also attributed to the overall buckling across the entire width of the sheeting at the mid span. For the roofing sheet with the washers, the upper limit value of reaction force per fastener at the central support for the initial failure was 1.12 times that for the sheeting without the washers. The lower limit value was approximately the same as the lower limit value for the sheeting without the washers. The limit value of reaction force per fastener was approximately increased by a factor of 1.26. The roofing sheet with the washers, the uplift load carrying capacity was increased 12% to 26% than without washers.

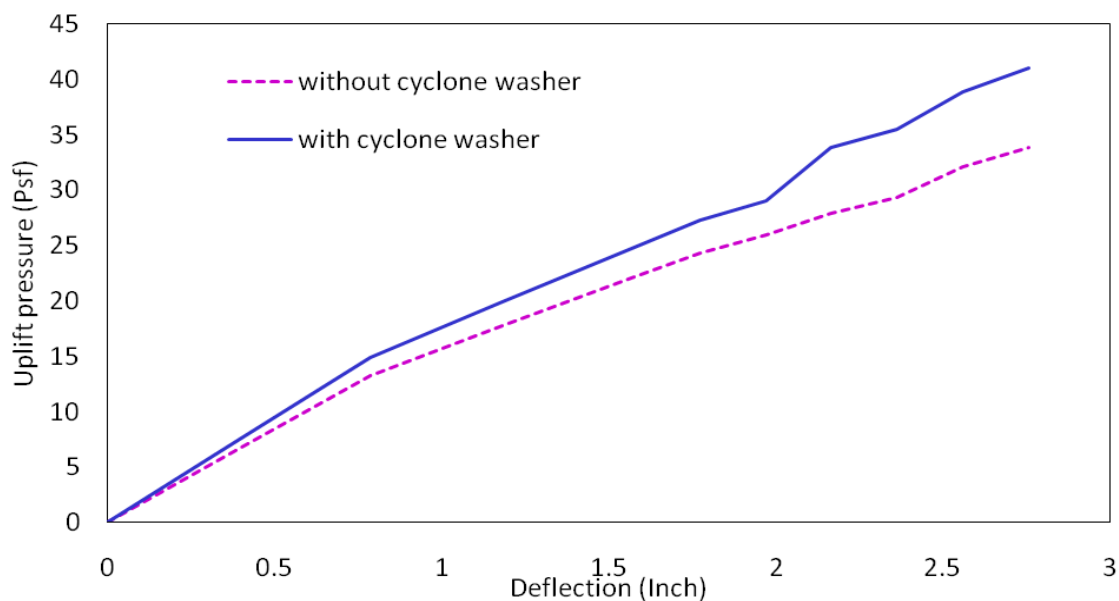


Figure 15: Comparison the effect of cyclone washer at mid point of the specimen

6. CONCLUSIONS

The paper presents an experimental investigation on the structural strength and behaviour of profiled steel sheet roofing elements under simulated wind uplift forces. A series of tests was performed on profiled steel sheet roofing subjected to wind uplift simulated pressure. The optimum diameters of 4.7 and 4.3 mm for screw connections were found for single shear and double shear respectively. Based on test results, two screwed parallel connections provided better performance than vertical arrangement. The failure loads, failure modes and the load-deformation behaviour of screwed fastened profile steel sheet under simulated wind load were presented. It was observed that during the increase of loading, the upward deflection of the unscrewed crest became larger than that of the screwed crest. It was found that the local diamond-shaped deformations progressively developed around the screw fasteners at the support due to uplift load. The use of cyclone washers with screw fasteners reduced local plastic deformations and, in general, increased initial failure loads of the roofing sheets. The roofing sheet with the washers, the uplift load carrying capacity was increased 12% to 26% than without washers. Based on the experimental results, it was found that the load carrying capacity of the proposed profiled steel sheet roofing system subjected to wind uplift load is 39.88 psf which is greater than BNBC and ASCE recommended wind uplift load. It was found that, the structural behaviour of the roofing sheets under uplift loads was greatly dependent on the diameter of the screw and span length of profiled steel sheet.

ACKNOWLEDGEMENTS

The authors gratefully acknowledge the Abul Khair (AKS) Steel Mills Dhaka, Bangladesh for supplying the test specimens.

REFERENCES

- AS. (1991) 'Methods for tensile testing of metals' Australian standard AS 1391. Sydney, Australia: Standards Association of Australia.
- ASCE. (2005). *Minimum design loads for buildings and other structures*, ASCE Standard 7-05. New York: American Society of Civil Engineers Standard.
- ASTM. (1997) 'Standard test methods for tension testing of metallic materials' E 8M-97. West Conshohocken: American Society for Testing and Materials.
- Beck, V. R. and Stevens, L. K. 1979. 'Wind loading failures of corrugated roof cladding', *Civ. Eng. Trans.*, CE21 (1), 45-56
- Gerhardt, H. J. and Kramer, C. (1986). 'Wind induced loading cycle and fatigue testing of lightweight roofing fixations', *J. Wind Eng. Ind. Aerodyn.*, 23, 237-247
- Holmes, J. D., Melbourne, W. H. and Walker, G. R. (1990). 'A commentary on the Australian standard for wind loads', Colour Graphics Pty Ltd, Vic., Australia.
- Lysaght Building Industries, (1990). *Design Manual: Steel Roofing and Walling*, Lysaght Building Industries, Sydney, Australia,
- Mahendran, M. (1990). 'Static behaviour of corrugated roofing under simulated wind loading', *Civ. Eng. Trans.* CE32 (4), 212-218
- Parsons, A. A. (1976). 'Practical development from static and cyclic load testing of steel claddings', *Proc. Metal Struct. Conf.*, The Institution of Engineers, Australia, 51-56
- Xu, Y. L. and Reardon, G. F. (1992). 'Behaviour of different profiled Roofing sheets subject to wind uplift', *Tech. Rep. 37*, Cyclone Testing Station, James Cook University, Australia,
- Xu, Y. L. and Reardon, G. F. (1993). Test of screw fastened profiled roofing sheets subject to simulated wind uplift, *Engineering Structure*, 15 (6) 423-430.
- Zahurul-Islam S. M., Abang-Abdullah A.A and Jafar M. S. (2006), 'An Investigation on Structural Performance of Profiled Steel Sheet to Develop Self-supporting Roofing System', *The International Journal of Advanced Steel Construction*, 2 (1), 87-108.

EFFECTIVENESS OF RICE HUSK ASH (RHA) AS A PARTIAL REPLACEMENT OF CEMENT IN CONCRETE

D Barua¹, M M Rahman², M W R Chowdhury³, M M Arif⁴ and M A Hasan⁵

¹ Graduate, Southern University Bangladesh, Bangladesh, e-mail: dipakbarua.ctg@gmail.com

² Graduate, Southern University Bangladesh, Bangladesh, e-mail: mohibur.pwd@gmail.com

³ Graduate, Southern University Bangladesh, Bangladesh, e-mail: wahidchowdhury88@gmail.com

⁴ Faculty, Southern University Bangladesh, Bangladesh, e-mail: engrareef@gmail.com

⁵ Faculty, Southern University Bangladesh, Bangladesh, e-mail: hasancuet90@gmail.com

ABSTRACT

An experimental investigation has been carried out to observe the efficacy of Rice Husk Ash (RHA) as a partial replacement of binding materials in concrete construction. Bangladesh, being an agro-based country, has plenty of RHA production as an agricultural by-product. Previous studies reported that about 400 pounds of rice husk can be obtained after milling approximately 2000 pounds of paddy. In this study, compressive strength of 4-inch concrete cubes has been determined to see the variation in strength of concrete with the partial replacement of cement by RHA. After a rigorous review on related available research articles, RHA to Cement ratios are selected as 10:90, 15:85, 20:80, 25:75, 30:70, 40:60, 50:50 and then, compared with the controlled concrete sample. Curing periods of 7, 14, 28, 60, 90 days are considered for all the combinations and a constant mixing ratio of 1:1.5:3 for binder, fine aggregate & coarse aggregate, respectively, and a w/c ratio of 0.45, are chosen. RHA is collected from a rice mill in Bogra district, where a temperature of about 300-350 degree Celsius is maintained usually. Results depict that with the inclusion of RHA as partial binders, the strength of concrete expectedly decreases. It is observed that addition of 10% and 15% RHA to cement by weight (curing period 60 days) yields nearly the same compressive strength of controlled concrete sample (curing period 28 days). Besides, it is found that addition of RHA by 40% and 50% to cement by weight, on an average, reduces more than 50% of the concrete compressive strength. Based upon the results, usefulness of different fusions for different types of permanent and interim constructions are recommended.

Keywords: RHA, concrete, compressive strength, curing periods, mixing ratio

1. INTRODUCTION

Buildings and any other similar constructions in Bangladesh chiefly depend on reinforced cement concrete (RCC) that requires a large amount of cement along with other construction materials. Ample amount of brick manufacturing, large amount of readily available stones and sands made the civil engineering building works economic and most popular in this country. But, cement, which needs proper and relatively expensive manufacturing cost, remains a matter of concern. Hence, it is a topic of interest to find out how the construction cost of concrete, cost of cement to be specific, can be optimized keeping the quality of construction almost unhampered. In general, Ordinary Portland Cement (OPC) remains the popular choice despite its high production cost. In search of an alternate material, Rice Husk Ash (RHA) which is richly available in Bangladesh, becoming the choice of cement replacement, partially though. RHA, which is an agricultural by-product, is a woody sheath surrounding the kernel or grain and consists of two interlocking halves. According to Food and Agricultural Organization (FAO), world rice production in the year of 2009 is about 678 million tons and according to Bangladesh Bureau of Statistics (BBS), annual production of all kind of rice in Bangladesh in year 2009-2010 is about 31 million metric tons. That means a large amount of RHA is available, which was previously considered just a waste material. According to Hossain (2011), yearly RHA production in Bangladesh is nearly 1.15 million metric tons. Besides, RHA has some good quality ingredients to be considered as binder

material in concrete construction. Typical chemical composition of RHA found in Bangladesh is given in Table 1. It can be seen that the silica is predominant in RHA. Materials those are rich in siliceous or siliceous and aluminous contents are known as pozzolans. Pozzolans, itself possesses little or no cementitious value, however, if divided into very fine powder and in the presence of water, chemically react with calcium hydroxide at ordinary temperatures to form compounds possessing cementitious properties. Therefore, RHA is becoming one of the best replacement materials to reduce the dependency on cement in many countries of the world where paddy production is substantial. RHA possesses adequate bonding quality and imparts additional strength if added to concrete as partial replacement of cement, under proper justification (Chindaprasirt et al., 2007; Ganesan et al., 2008; Givi et al., 2010; Ikpong & Okpala, 1992; Ismail & Waliuddin, 1996; Rodriguez, 2006; Van Tuan et al., 2011). Although RHA has been reported as good material to be used in concrete construction, yet, it is not in international best practice. In Bangladesh, large amount of paddy construction is available and we need to reduce the construction cost and need to recycle this agricultural by-product (RHA). So, many more solid evidences are required to make people aware of the use of RHA in all kinds of civil engineering constructions.

Table 1: Chemical composition of RHA found in Bangladesh (Givi et al., 2010)

Contituent	Percentage Composition
Fe ₂ O ₃	1.38
SiO ₂	90.20
Al ₂ O ₃	0.85
CaO	1.18
MgO	1.21
Loss on Ignition	3.95

This study is carried out to see the performance of RHA blended concrete. To look into the behaviour of concrete, particularly the compressive strength of concrete prepared with various ratios of RHA to cement, this study is undertaken, so that huge amount of RHA produced all over Bangladesh, can be utilized at its best and optimum level of RHA to be used as partial replacement of cement in concrete can be determined.

2. METHODOLOGY

2.1 Materials

Type-1 (CEM-1) Ordinary Portland Cement (OPC) collected from one of the famous cement factories in Chittagong, is used in casting the concrete. According to the company provided guidelines, the 52.5 N strength class cement has 95-100% clinker and 0-5% gypsum. RHA is collected from an Auto Rice Mill in Bogra district, Bangladesh. It was out of the scope of this study to personally burn the RHA within laboratory facilities. Rather, RHA are burnt in the above mentioned rice mill under a controlled temperature of 300°C to 350°C. Sylhet sand with FM (fineness modulus) value of 2.5-2.7 and ¾" down size stone chips (Sylhet boulder) are used as fine aggregate and coarse aggregate, respectively. The water used is plain water collected from the supply line of Chittagong WASA.

2.2 Casting and Testing

This study considers 7 different percentages of RHA to be partially used with cement. These are 10%, 15%, 20%, 25%, 30%, 40% and 50%. Previous studies considered a RHA replacement of up to 35% in investigating various aspects of RHA blended concrete (Saraswathy & Song, 2006; Ganesan et al., 2007; Obilade, 2014). In this study it was targeted to see the effectiveness of RHA to be replaced in regular civil engineering works as well as temporary civil engineering works, hence, a large range of RHA replacement is

considered. Considering the time constraint, concrete mix design was not carried out rather a commonly used mix ratio of 1:1.5:3 is adopted. Because this study considered all the usual construction materials commonly used in Bangladesh for construction works e.g. Sylhet sand, OPC cement, Stone chips and RHA, it is technically good to go with the above mentioned mix ratio. Having said that a water-cement ratio of 0.45 is used and cubic specimens of 100×100×100 mm are prepared. For each combination, 3 samples are cast and tested. Concrete compressive strength for curing periods of 7 days, 14 days, 28 days, 60 days and 90 days are obtained using the UTM (capacity of 1000kN) owned by the Strength of Materials Laboratory of department of Civil Engineering, Southern University Bangladesh, Chittagong. Alongside the concrete cast and tested for several RHA combinations, separate controlled samples (with 0% RHA replacement) are also cast with the same mixing ratio and water content and tested to compare the results.

3. RESULTS AND DISCUSSION

Compressive strengths of concrete for all the blending combinations are reported in this section. Figure 1, Figure 2, Figure 3, Figure 4 and Figure 5 depict the outcomes from this study for the curing periods of 7 days, 14 days, 28 days, 60 days and 90 days, correspondingly. From the results presented, it is evident that for any of the curing periods employed in this study, compressive strength of concrete in general decreased with the increase in percentages of RHA replacement. In a similar type of study, Obilade (2014) have reported the identical behaviour of concrete.

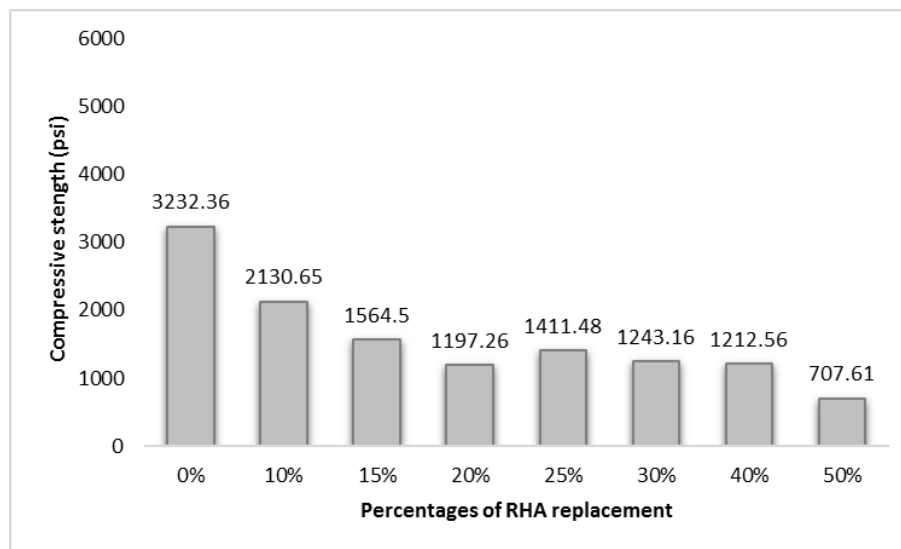


Figure 1: Compressive strength of RHA blended concrete for 7 days curing period

In reference to 28 days' compressive strengths (Figure 3), nearly 96% of controlled sample's (0% RHA) strength is gained for a RHA replacement of 5% and, 94% of controlled sample's (0% RHA) strength is gained for a RHA replacement of 10%. Even for a 15% of RHA replacement, around 88% of controlled sample's compressive strength is attained. Compressive strength is significantly reduced when the amount of RHA replacement is beyond 20%.

For a 10 % and 15% RHA replacement in cement, reasonable compressive strength is attained. Although, results of 10% RHA replacement is not uniform for all the curing periods but yielded satisfactory compressive strength for 28 and 90 days curing. Results of 15% RHA replacement showed somewhat uniform and adequate compressive strengths for all the curing periods considered for the problem in hand (Figure 1 to Figure 5).

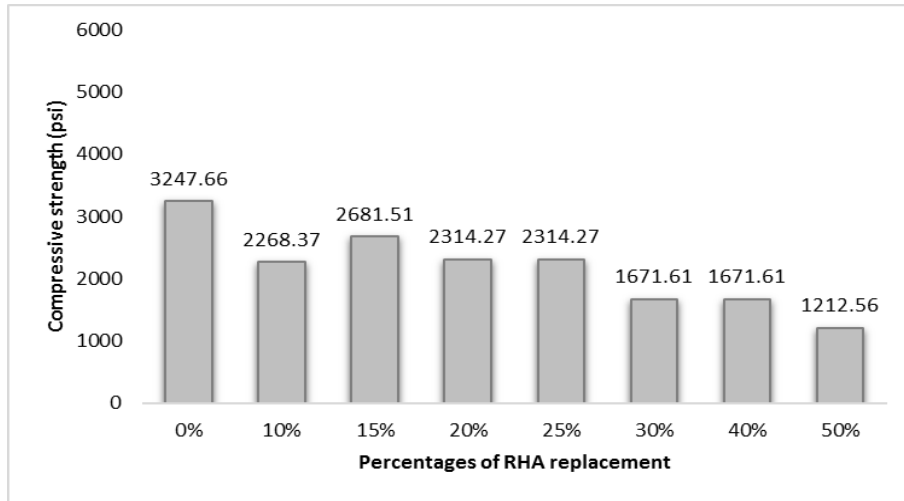


Figure 2: Compressive strength of RHA blended concrete for 14 days curing

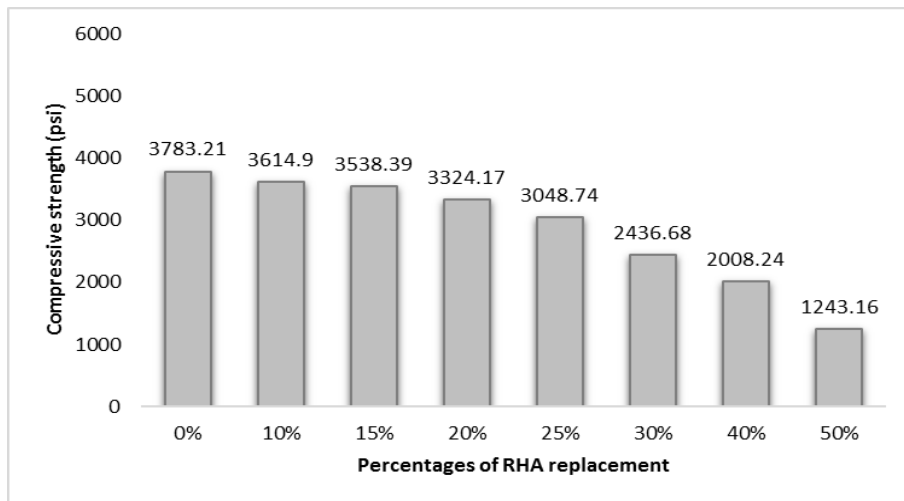


Figure 3: Compressive strength of RHA blended concrete for 28 days curing

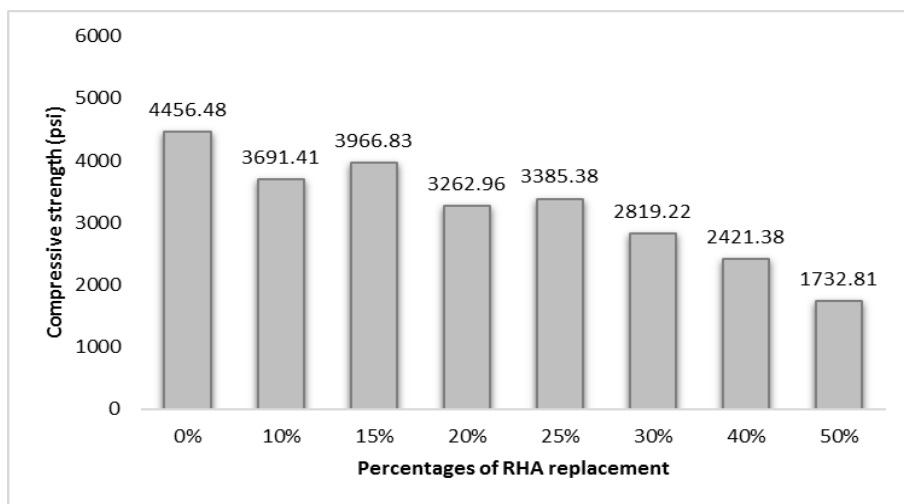


Figure 4: Compressive strength of RHA blended concrete for 60 days curing

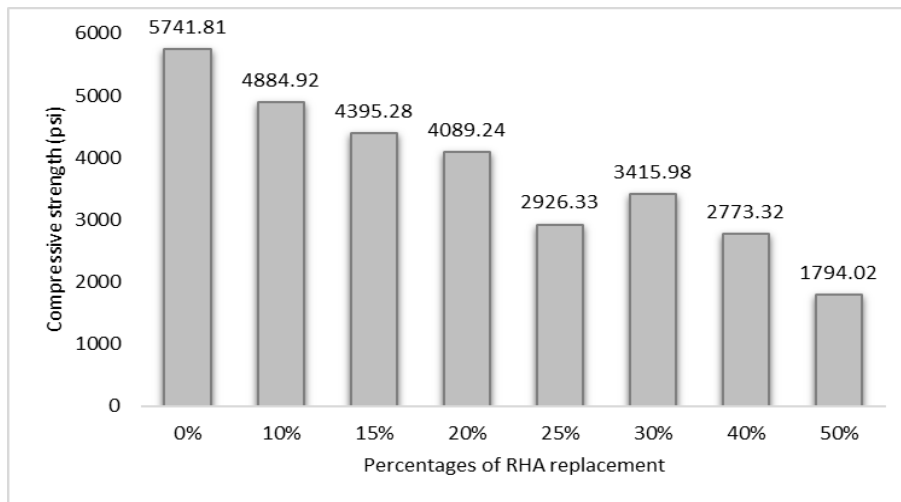


Figure 5: Compressive strength of RHA blended concrete for 90 days curing

A summary of the compressive strength of concrete studied, is illustrated in Figure 6. The general decreasing trend of compressive strength with the addition of RHA for a particular curing period is precisely understood. The typical strength gaining with curing periods 7 days, 14 days, 28 days, 60 days and 90 days is also obvious. Based upon the results of this study, it is clearly understood that for the regular civil engineering construction practice, partial replacement of RHA up to 15% can be undoubtedly considered, provided that RHA is properly burnt and suitably mixed in concrete. In a study carried out by Chik et al. (2011) somewhat similar conclusion is made.

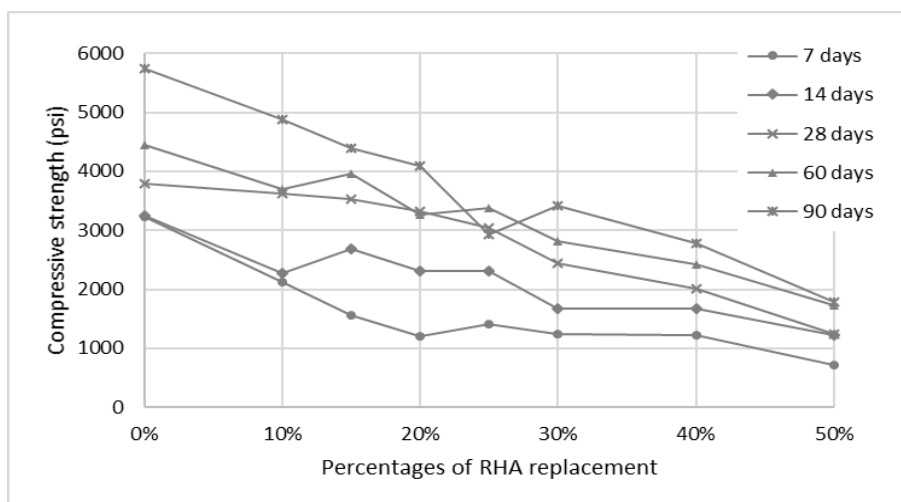


Figure 6: Compressive strength of concrete for varying percentages of RHA replacement to cement and different curing periods

Civil engineering construction types vary widely based upon the purposes of the construction and requires rich to lean concrete depending on the construction purpose. For example, a very good quality concrete is essential for normal residential building or bridges or other hydraulic structures whereas a lean concrete can be used for less durable or temporary constructions. As can be seen from the results presented in Figure 6, for 50% RHA replacement, compressive strengths of concrete for 28 days and 60 days are 1243.16 psi and 1732.81 psi, respectively, which necessarily state that a great amount of RHA can be consumed in concrete for casting lean concrete. Such lean concrete can be used for less important civil engineering works which in turn will substantially reduce the problem

associated with rice husk ash because typically it is a waste material that needed to be disappeared from the environment.

4. CONCLUSIONS

Current study considered replacement of locally available RHA in cement to be used in casting concrete. Seven different replacement ratios of RHA to cement are considered e.g., 10:90, 15:85, 20:80, 25:75, 30:70, 40:60, 50:50 and then, compared with the controlled concrete sample (with no addition of RHA in concrete). Curing periods of 7, 14, 28, 60 and 90 days are considered for all the blending combinations. The following conclusions are addressed based on the experimental results of this study:

- Compressive strength of concrete with 10% and 15% RHA replacement for a curing period of 60 days is similar to the result of control sample for 28 days' curing.
- Reasonable compressive strength of RHA blended concrete is attained. For few particular cases, compressive strength very near to the controlled concrete sample is available. For example, the 28 days' optimum concrete compressive strength for 10% RHA replacement is 3614.90 psi, which is 0.96 times the value for control sample. And, 60 days' optimum concrete compressive strength for 15% RHA replacement is 3966.83 psi, which is 0.89 times the value for control sample.
- In general, compressive strengths of concrete get reduced with the increase in replacement percentages of RHA.
- Overall, based upon the results it can be said that optimum RHA replacement of cement falls within a range of 0 to 15%, where, above 75% of controlled sample's compressive strength is available in RHA blended concrete, almost for all the curing periods, which can still be considered for good quality construction works
- A maximum of 50% RHA replacement yields a compressive strength of 1732.81 psi (60 days). Such a low strength is not recommendable for primary construction works but can be effective in temporary construction works.

ACKNOWLEDGEMENTS

The concrete compressive strength for this study is tested in the Strength of Materials Laboratory, Department of Civil Engineering, Southern University Bangladesh, Chittagong. The authors would like to express their gratitude to the lab in-charge and technician for their kind help during the laboratory works for current study.

REFERENCES

- Chik, F. A. W., Bakar, B. H. A., Johari, M. A. M., & Jaya, R. P. (2011). Properties of concrete block containing rice husk ash subjected to Girha. *International Journal of Recent Research and Applied Studies*, Vol. 8, No. 1 (2011) 08.
- Chindaprasirt, P., Jaturapitakkul, C., & Sinsiri, T. (2007). Effect of fly ash fineness on microstructure of blended cement paste. *Construction and Building Materials*, 21(7), 1534–1541. <https://doi.org/10.1016/j.conbuildmat.2005.12.024>
- Ganesan, K., Rajagopal, K., & Thangavel, K. (2008). Rice husk ash blended cement: Assessment of optimal level of replacement for strength and permeability properties of concrete. *Construction and Building Materials*, 22(8), 1675–1683. <https://doi.org/10.1016/j.conbuildmat.2007.06.011>
- Givi, A. N., Abdul Rashid, S., Abdul Aziz, F. N. & Mohd Salleh, M. a. (2010). Contribution of Rice Husk Ash to the Properties of Mortar and Concrete: A Review. *Journal of American Science*, 6(3), 157–165.
- Hossain, T., Sarker, S. K., & Basak, B. C. (2011). Utilization potential of rice husk ash as a construction material in rural areas. *Journal of Civil Engineering (IEB)*, 39(2), 175-188.
- Ikpong, A. A., & Okpala, D. C. (1992). Strength characteristics of medium workability ordinary Portland cement-rice husk ash concrete. *Building and Environment*, 27(1), 105–111. [https://doi.org/10.1016/0360-1323\(92\)90014-G](https://doi.org/10.1016/0360-1323(92)90014-G)

- Ismail, M. S., & Waliuddin, A. M. (1996). Effect of rice husk ash on high strength concrete. *Construction and Building Materials*, 10(7), 521–526. [https://doi.org/10.1016/0950-0618\(96\)00010-4](https://doi.org/10.1016/0950-0618(96)00010-4)
- Obilade, I. O. (2014). Use of rice husk ash as partial replacement for cement in concrete. *International Journal of Engineering and Applied Sciences*, Vol. 5, No. 4, (2014)
- Rodríguez De Sensale, G. (2006). Strength development of concrete with rice-husk ash. *Cement and Concrete Composites*, 28(2), 158–160. <https://doi.org/10.1016/j.cemconcomp.2005.09.005>
- Saraswathy, V., & Song, H. W. (2007). Corrosion performance of rice husk ash blended concrete. *Construction and Building Materials*, 21(8), 1779–1784. <https://doi.org/10.1016/j.conbuildmat.2006.05.037>
- Van Tuan, N., Ye, G., Van Breugel, K., & Copuroglu, O. (2011). Hydration and microstructure of ultra-high performance concrete incorporating rice husk ash. *Cement and Concrete Research*, 41(11), 1104–1111. <https://doi.org/10.1016/j.cemconres.2011.06.009>

COMPARISON OF WIND LOAD AMONG BNBC – 1993 AND PROPOSED BNBC - 2015

Md. Mehedi Hassan Masum¹, Anika Akter², Suraiya Akter³ and Md. Jobayath Hossen⁴

¹ Undergraduate student, Department of Civil Engineering, Chittagong University of Engineering & Technology, Bangladesh, e-mail: mehedi.ce.cuet@gmail.com

² Undergraduate student, Department of Civil Engineering, Chittagong University of Engineering & Technology, Bangladesh, e-mail: ankr2506@gmail.com

³ Undergraduate student, Department of Civil Engineering, Chittagong University of Engineering & Technology, Bangladesh, e-mail: suraiyasranoni01@gmail.com

⁴ Undergraduate Student, Chittagong University of Engineering & Technology, Bangladesh, e-mail: jobayathfd@gmail.com

ABSTRACT

Before BNBC 1993 a simple empirical formula is used to determine wind load which do not consider the effect of surrounding objects and height of structure in wind pressure. This shortcoming has overcome in BNBC 1993 by introducing the concept of exposure category and gust factor. The effect of surrounding objects and height of structures is further upgraded in proposed BNBC 2015. This paper aims at the comparison of provisions of wind load analysis given in existing BNBC 1993 to that in proposed BNBC 2015. Both are studied and compared in terms of wind load using parameters termed as Basic wind speed, Height and exposure coefficient, Gust factor, Sustained wind pressure, External pressure coefficient and Design wind pressure. This study reveals that wind load in urban areas according to BNBC 2015 found considerably higher than BNBC 1993. But wind load in obstructed and unobstructed open terrain type area according to BNBC 2015 is found significant lower than BNBC 1993.

Keywords:BNBC, Gust factor, Building code, exposure coefficient, wind pressure etc.

1. INTRODUCTION

Wind is a suddenly varying dynamic incident & a function of time & velocity. This is caused by the air flowing when air is moving from high pressure to low pressure. Bangladesh National Building Code (BNBC) was first introduced in the year of 1993. The code is further updated in proposed BNBC 2015 wind provision. The design of wind loads on a building is substantially more complex as a result a comparative study has been made to see the basic difference between BNBC 1993 and proposed BNBC 2015. This comparative study on design wind load will provide a relation showing percent increase or decrease of design wind load in the new code with respect to the old one.

2. METHODOLOGY

In this study, basic wind speed is compared between BNBC 1993 and BNBC 2015 for 8 divisions of Bangladesh to have an idea about variation of wind speed. By which we can get the overall idea of wind speed throughout the country. For comparison of wind load between BNBC 1993 and BNBC 2015, different parameters i.e. design wind load, basic wind speed, height and exposure coefficient, gust factor, sustained wind pressure, external pressure coefficient etc. are considered. Finally, three exposure conditions (i.e. Exposure A, Exposure B & Exposure C) have been studied for a typical multi-storeyed residential building to identify the changes in analysis and design with BNBC 2015 as compared to BNBC 1993.

3. COMPARISON OF WIND SPEED

3.1 Wind Speed of Dhaka Division

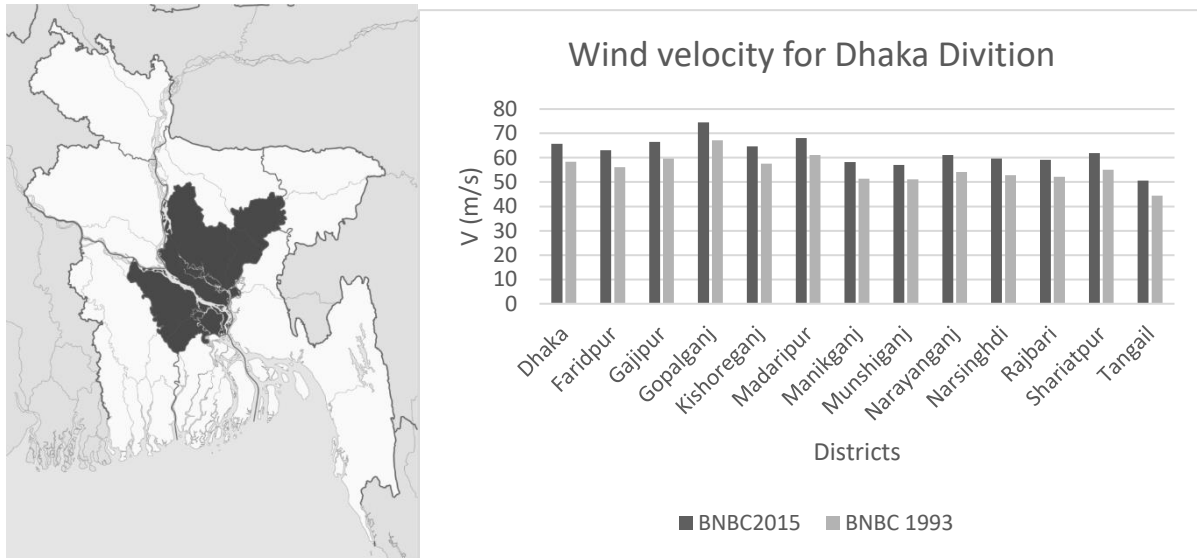


Figure 1: Comparison of wind speed in Dhaka Division.

Dhaka division is one of the most important divisions in Bangladesh. The location of this division is 24°10' N 90°25' E and its elevation is about 13.12 ft. with area 20,508.8 km² (7,918 sq mi). Total population is 36,433,505 & density is 1,800 /km² (4,600 / sq mi) . There are total 18 rivers. The average wind speed for this division was 55.46923 m/s according to BNBC 1993. The wind speed is increased about 12.38389 % by 2015. The maximum velocity was found in Gopalganj district & minimum was found in Tangail district.

3.2 Wind Speed of Mymensingh Division

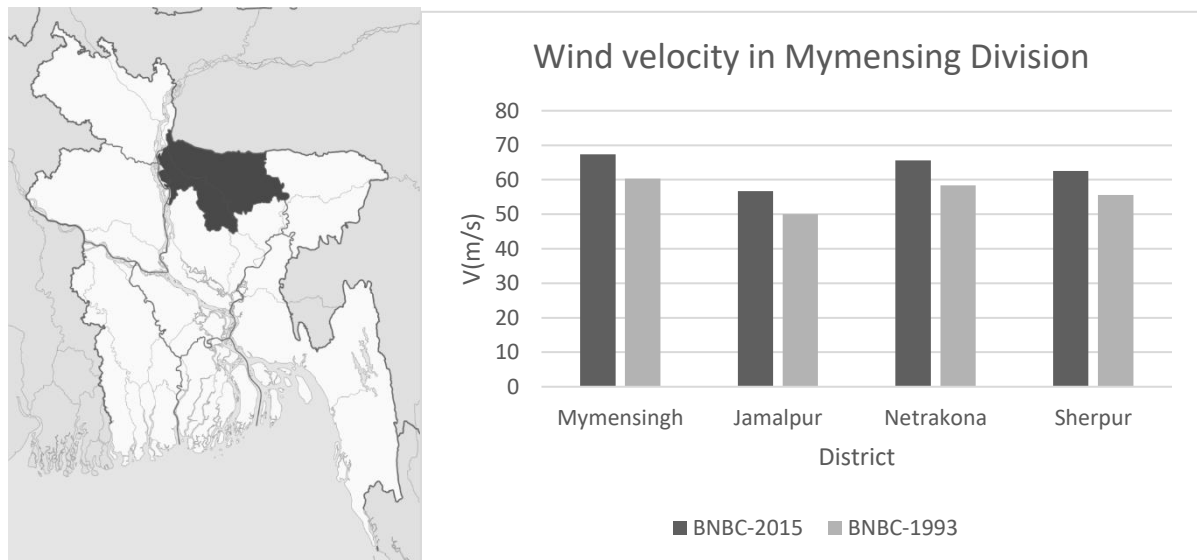


Figure 2: Comparison of wind speed in Mymensingh Division.

Coordinate of Mymensingh division is 24°10' N 90°25' E with an elevation of about 62 ft. Its area is about 10,584 km² (4,087 sq mi). Population, by 2011 census is total 11,370,000 & density is 1,100 / km² (2,800 / sqmi) .The average wind speed is 56.0425 m/s according to BNBC 1993 .The wind velocity increases 12.5034 % by 2015 . The maximum & minimum

velocities were in Mymensingh & Jamalpur districts respectively. There are 37 rivers in this division.

3.3 Wind Speed of Barisal Division

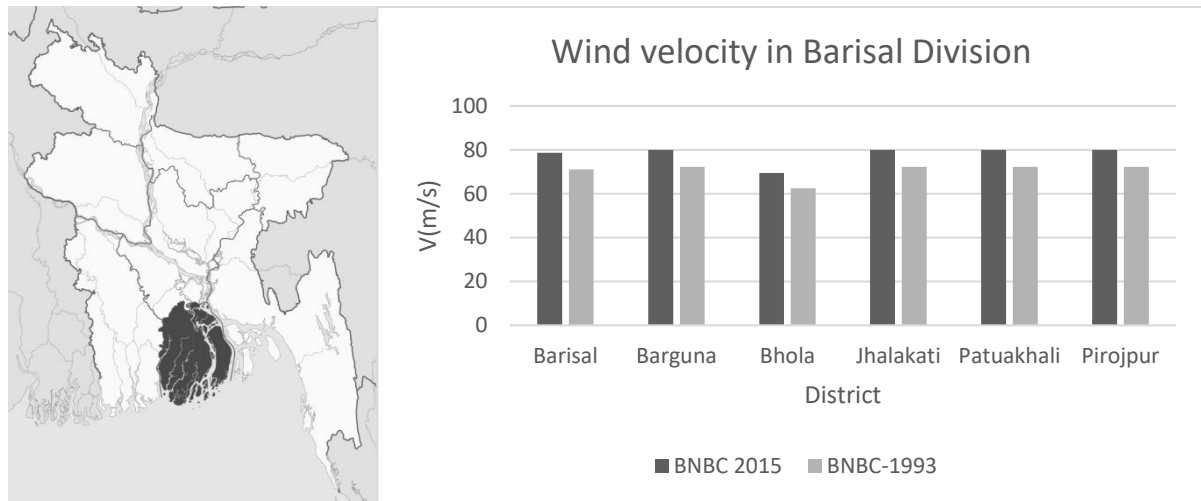


Figure 3: Comparison of wind speed in Barisal Division.

Position of this division is 22°30' N 90°20' E. Total area is 13,225.20 km² (5,106.28 sq mile). It is situated 3.9 ft above the sea level. This division consists of 6 districts. By census 2011, it is known that the total population is about 8,325,666 & lives about 630 people per km² or 1,600 per sqmi. Total 58 rivers flow through this division. The average wind speed is 70.415 m/s according to BNBC 1993. Maximum velocity was found in Borguna, Jhalokathi, Patuakhali & Pirojpur districts & minimum velocity is in Bholadistrict. Wind speed increases 10.819 % by 2015.

3.4 Wind Speed of Rajshahi Division

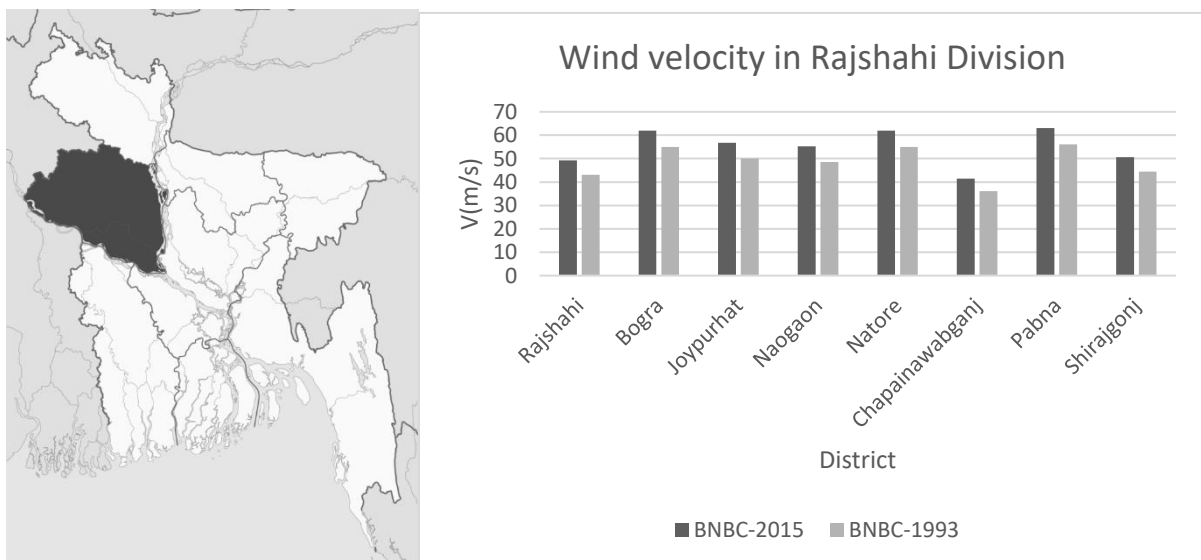


Figure 4: Comparison of wind speed in Rajshahi Division.

Rajshahi division is located at 25°00' N & 89°00' E with 18,174.4 km² (7,017.2 sq mi) area in total. The population is 18,484,858 with density of about 1,000 / km² (2,600sqmi). Average wind speed for this division is 48.54125 m/s according to BNBC 1993 & it is increased 13.3057 % by 2015. The maximum wind speed was found in Pabna, Natore & Bogra districts & minimum was in Chapainawabgonj district.

3.5 Wind Speed of Sylhet Division

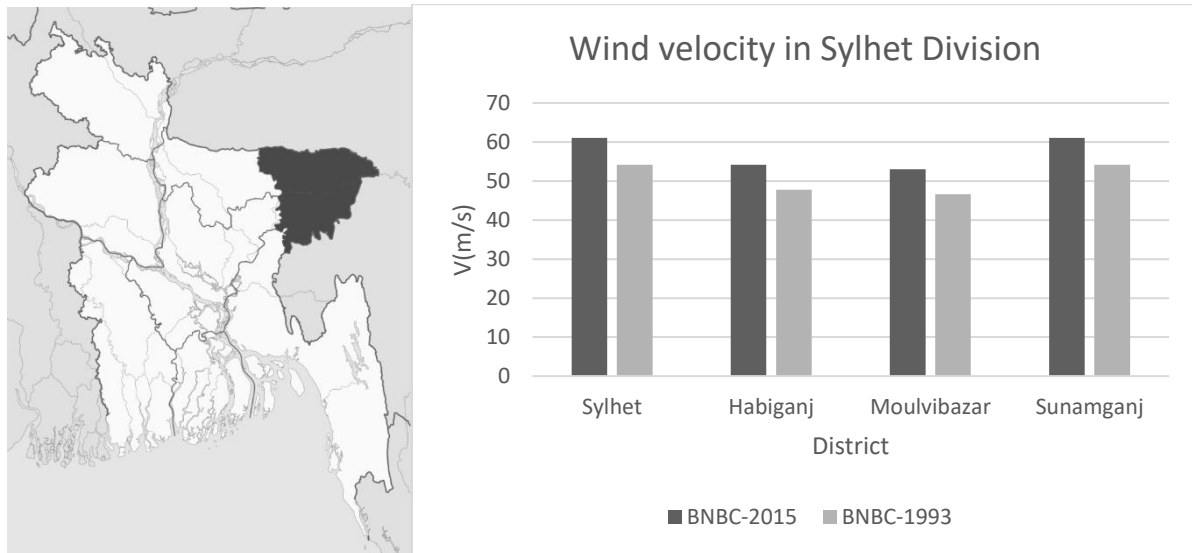


Figure 5: Comparison of wind speed in Sylhet Division.

Sylhet division is located in 24°30' N & 91°40' E. Its elevation is 15 ft with an area of 12,298.4 km² (4,748.4 sq mi). It has a population of 9,910,219 & is populated with 810 / km² (2,100 sq mi) according to census 2011. It comprises 4 huge districts. The average wind speed for this division was 50.6975 m/s according to BNBC 1993 & it increases 13.1219 % by 2015. Maximum velocity was found in Sylhet & Sunamganj districts & the minimum was found in Moulvibazar district.

3.6 Wind Speed of Khulna Division

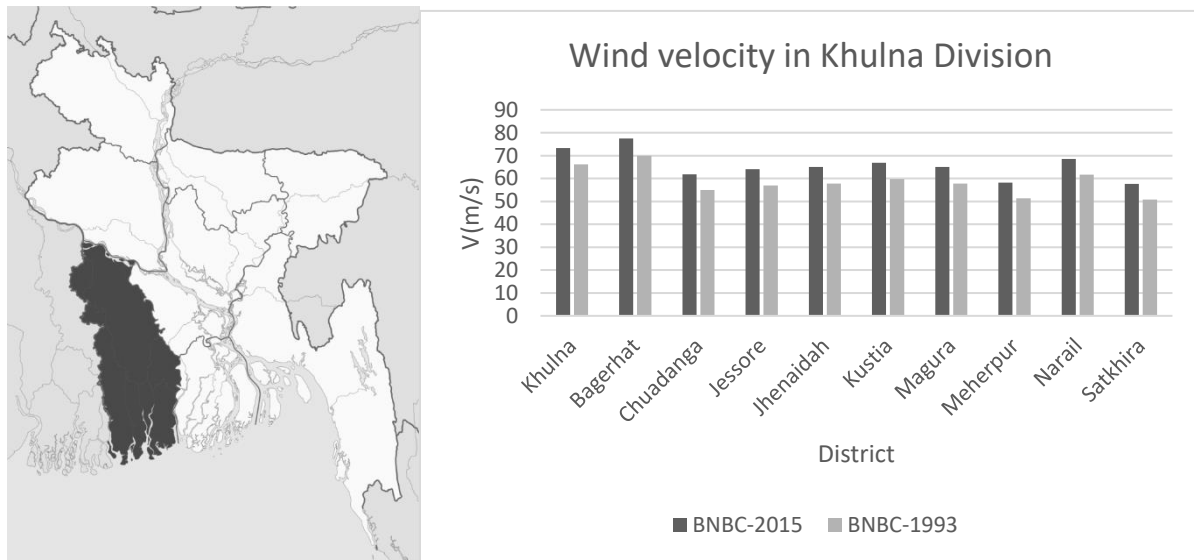


Figure 6: Comparison of wind speed in Khulna Division.

The next division is Khulna which is located at 22°55' N & 89°15' E. Total area is 22,284.22 km² (8,603.99 sq mi), where lives 700 people per km² (1,800 / sq mi) area with a population of 15,687,759 found by 2011 census. It is situated with an elevation of 30 ft. There are total 10 districts in this division. The average wind speed was 58.722 m/s according to BNBC 1993. Wind velocity was maximum in Bagerhat & Khulna districts & minimum in Chuadanga district. It increases 12.0704 % by 2015.

3.7 Wind Speed of Rangpur Division

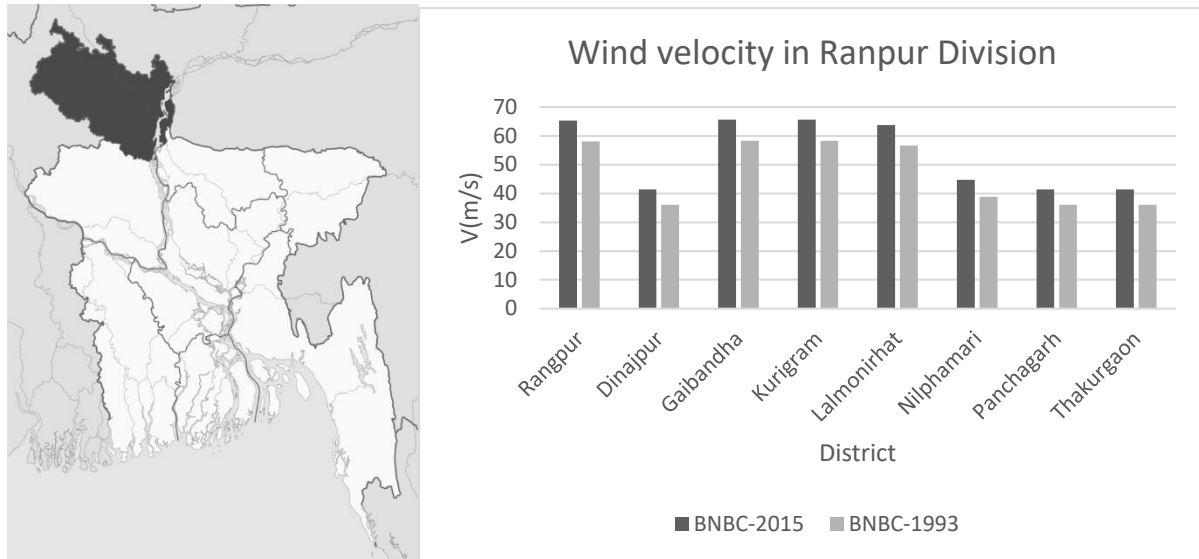


Figure 7: Comparison of wind speed in Rangpur Division.

The position of this division is 25°50' N 89°50' E. It comprises 16,184.99 km² (6,249.06 sq. mi) area with a population of 15,787,758 whose density is 980 / km² (2,500 / sq. mi) according to 2011 census. Average wind velocity was 47.32625 m/s which was found through BNBC 1993; maximum was found in Rangpur, Gaibandha, Kurigram, Lalmonirhat districts & minimum was found in Dinajpur, Panchagarh, Thakurgaon districts. The wind speed increases 13.3356 % by 2015.

3.8 Wind Speed of Chittagong Division

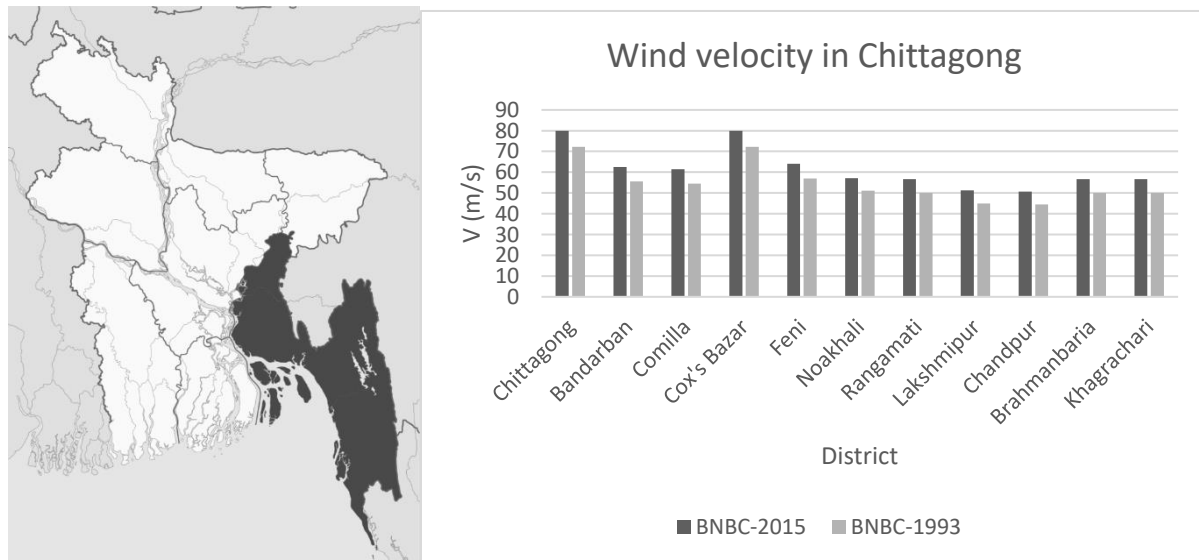


Figure 8: Comparison of wind speed in Chittagong Division.

Chittagong division is located at 22°55' N 91°30' E with an elevation of 1,152 ft. Total area of this division is 33,771.18 km² (13,039.13 sq. mi). Average wind speed for this division was 54.72091 m/s according to BNBC 1993 & maximum velocity was found in Chittagong & Cox's Bazaar districts; minimum velocity was found in Lakshmipur & Chandpur districts. The velocity increases 12.49812% by 2015. This is a hilly track region & it comprises many rivers.

4. COMPARISON OF WIND LOAD BETWEEN BNBC CODE 1993 AND PROPOSED CODE OF 2015

4.1. Comparison of Exposure Category

4.1.1 According to BNBC 1993

The terrain exposure in which a building or structure is to be sited shall be assessed as being one of the following categories:

Exposure A: Urban and sub-urban areas, industrial areas, wooded areas, hilly and other terrain covering.

Exposure B: Open terrain with scattered obstructions. This category includes air fields, open park lands, and sparsely built-up outskirts of towns, flat open country and grasslands.

Exposure C: Flat and unobstructed open terrain, coastal areas and riversides facing large bodies of water.

4.1.2 According to BNBC 2015

As exposure categories depends on wind directions and sectors and also surface roughness, so some of their categories are mentioned here-

Wind directions and sectors: For each selected wind direction at which the wind loads are to be evaluated, the exposure of the building or structure shall be determined for the two upwind sectors extending 45° either side of the selected wind direction.

Surface roughness categories:

Surface Roughness A: Urban and suburban areas, wooded areas, or other terrain with numerous closely spaced obstructions.

Surface Roughness B: Open terrain with scattered obstructions having heights generally less than 9.1 m.

Surface Roughness C: Flat, unobstructed areas and water surface outside cyclone prone regions.

Exposure Categories:

Exposure A: Exposure A shall apply where the ground surface roughness condition is as defined by surface roughness A. Exception is also there.

Exposure B: Exposure B shall apply for all cases where Exposure A or C do not apply.

Exposure C: Exposure C shall apply where the ground surface roughness is as defined by Surface Roughness C.

There are also some of the Exposure categories for:

Main wind-force resisting system

Buildings and other structures

Low-Rise Buildings

Components and cladding.

Velocity pressure exposure coefficient

4.2 Comparison of Topographic Effects

According to BNBC 1993

If a structure or any portion is thereof is located within a local topographic zone, such as regions around hills and ridges, the sustained wind pressure obtained from sec 2:4:6:2 shall be modified by multiplying by a local topographic coefficient, c_t .

According to BNBC 2015:

Topographic Effects:

Wind speed-up over hills, ridges and escarpments:

The wind speed-up effects shall be included in the design when buildings and other site conditions and locations of structures meet all the following conditions:

The hill, ridges, or escarpment is isolated and unobstructed upwind by other similar topographic features of comparable height for 100 times the height of the topographic feature or 3.22 km, whichever is less.

The hill, ridges, or escarpment protrudes above the height of upward terrain features within a 3.22 km radius in any quadrant by a factor of two more.

The structure is located as shown in Figure 6.2.4 in the upper one-half of a hill or ridge or near the crest of an escarpment.

$$H/L_h \geq 0.2$$

H is greater than or equal to 4.5 m for Exposure B and C and 18.3 m for Exposure A.

Topographic factor:

The wind speed-up effect shall be included in the calculation of design wind loads by using the factor

$$K_{zt}:K_{zt} = (1 + K_1 K_2 K_3)^2$$

4.3 Comparison of Gust Effect Factor:

According to BNBC 1993:

Wind Gust Effects:

Wind gusts causes additional loading effects due to turbulence over the sustained wind speed. A slender or wind-sensitive building shall be one having -

A height exceeding five times the least horizontal dimension, or

A fundamental natural frequency less than 1.0 Hz.

Gust coefficient, C_G shall account for such additional gust loading effects on non-slender and slender buildings and shall be set equal to Gust Response Factors G_h , G_z , or G as set forth below:

Gust Response Factor, G_h for Non-slender Buildings and Structures: Value of gust response factor, G_h shall be determined from Table 6.2.11.

Gust Response Factor, G_z for Building Components: Gust response factor, G_z shall be determined from Table 6.2.11.

Gust Response Factor, G for Slender Buildings and Structures: Gust response factor, G shall be calculated by the following relations.

$$G = 0.65 + \sqrt{\left(\frac{P}{\beta} + \frac{11.0T_1^2 S}{1 + KC}\right)}$$

$$\text{Where, } P = fJ; f = \frac{55.44fh}{sv_b}; T_1 = \frac{2.35\sqrt{D_0}}{\left(\frac{h}{13.72}\right)^\alpha}$$

According to BNBC 2015:

Gust Effect Factor:

Rigid Structures:

For rigid structures as defined in Sec 2.1.3, the gust-effect factor shall be taken as 0.85 or calculated by the formula:

$$G = 0.925 \frac{1 + 1.7g_{Q1z}Q}{1 + 1.7g_{v1z}}; I_z = c\left(\frac{10}{z}\right)^{\frac{1}{6}}$$

The background response Q is given by,

$$Q = \sqrt{\frac{1}{1 + 0.63\left(\frac{B+h}{L_z}\right)^{0.63}}}$$

Where B, h are defined in Sec 2.1.4; and L_z =the integral length scale of the turbulence at the equivalent height given by,

$$L_z = l \left(\frac{z}{10} \right)^\epsilon$$

Flexible or dynamically sensitive structures:

For flexible or dynamically sensitive structures as defined in Sec 2.1.3, the gust-effect factor shall be calculated by,

$$G_f = 0.925 \left(\frac{1 + 1.7 I_z \sqrt{g_Q^2 Q^2 + g_R^2 R^2}}{1 + 1.7 g_v I_z} \right)$$

The value of both g_0 and g_v shall be taken as 3.4 and g_R is given by,

$$g_R = \sqrt{2 \ln(3600 n_1)} + \frac{0.577}{\sqrt{2 \ln(3600 n_1)}}$$

R, the resonant response factor, is given by,

$$R = \sqrt{\frac{1}{\beta} R_n R_h R_g (0.53 + 0.47 R_L)}$$

Rational analysis and limitations of gust-factors are also mentioned there.

4.4 Comparison of Sustained Wind Pressure and Velocity Pressure

According to BNBC CODE 1993

Sustained Wind Pressure:

The sustained wind pressure, q_z on a building surface at any height z above ground shall be calculated from the following relation:

$$q_z = C_c C_I C_z V_b^2$$

According to BNBC CODE 2015:

Velocity pressure:

Velocity pressure, q_z evaluated at height z shall be calculated by the following equation:

$$q_z = 0.000613 K_z K_{zt} K_d V^2 I; (\text{KN/m}^2), V \text{ in m/s}$$

4.5 Comparison of Design Wind Pressure

According to BNBC CODE 1993

Design Wind Pressure:

The design wind pressure, p_z for a structure or an element of a structure at any height, z above mean ground level shall be determined from the relation: $P_z = C_G C_P q_z$

According to BNBC CODE 2015:

Design wind pressures for the MWFRS of buildings of all heights shall be determined by the following equation:

$$P = q G C_{P-q_i} (G C_{p_i})$$

4.6 Comparison of Pressure and Force Coefficient

According to BNBC CODE 1993

Pressure Coefficient for Buildings, Structures and Components:

The pressure coefficient C_p to be used in Eq (2.4.2) for the determination of design wind pressure shall be equal to the values described below:

C_{pe} : External pressure coefficient as given in Fig 6.2.5 and Fig 6.2.6 and in Table 6.2.13 for external surfaces of buildings or structures.

C'_{pi} : Internal peak pressure coefficient as given in Table 6.2.14 for internal surfaces of building. The coefficient shall be used along with the coefficients C'_{pi} for design wind load on components, or with C_{pe} for design wind load on buildings as per provisions of Sec 2.4.6.4 a(ii)

C'_{pe} : External peak pressure coefficient as given in Fig 6.2.7 and Fig 6.2.8 to be applied on external surfaces of buildings to obtain wind load on individual components and cladding in accordance with Sec 2.4.6.5.

\bar{c}_p : Overall pressure coefficient as given in Tables 6.2.15 through 6.2.21 for various cross-sectional shapes to be used with the projected area of the buildings or structures when Method 2 in Sec 2.4.6.4(b) is used.

If pressure coefficient C_{pe}, C'_{pi}, C'_{pe} or \bar{c}_p are not provided herein for certain buildings, structures or components, reliable references shall be followed or specialist advice shall be sought.

According to BNBC CODE 2015

Pressure and Force Coefficient:

Internal Pressure Coefficient:

Internal pressure coefficient, $G C_{pi}$ shall be determined from Figure 6.2.5 based on building enclosure classifications determined from Sec 2.4.9.

Reduction factor for Large Volume Buildings, R_i ; For a partially enclosed building containing a single, unpartitioned large volume, the internal pressure coefficient, $G C_{pi}$ shall be multiplied by the following reduction factor, R_i :

$$R_i = 1.0 \quad \text{or} \quad R_i = 0.5 \left(1 + \frac{1}{\sqrt{1 + \frac{v_i}{6951 A_0 g}}} \right) \leq 1.0$$

External Pressure Coefficient:

There are two kind of system in external pressure coefficient:

Main Wind-Force Resisting Systems

Components and Cladding.

4.7 Comparison of Design of Wind load

According to BNBC CODE 1993

For Buildings and Structures:

Design wind load on the main wind force resisting systems of buildings and structures shall be determined by using one of the following two methods:

Method 1 (Surface Area Method):

For all framing systems: $F_1 = \sum p A_z$

For gabled frames and single-storey rigid frames: $F_1 = \sum (p - P_i) A_z$

Method 2 (Projected Area Method): $F_2 = \sum p_z A_z$

For Components and Cladding:

Design wind load on individual structural components shall be determined in accordance with the following relation:

$$F' = \sum (C'_{pe} q - C'_{pi} q_i) A_z$$

There are also definite conditions for determination of the pressure q and q_i .

According to BNBC CODE 2015:

On Enclosed and Partially Enclosed Buildings:

Rigid Buildings of All Heights:

Design wind pressures for the MWFRS of buildings of all heights shall be determined by the following equation:

$$P = qG C_p - q_i(G C_{pi}) \text{ (KN/m}^2\text{)}$$

Low-Rise Building:

Design wind pressures in this case can be determined by the following equation:

$$P = q_h [(G C_{pf}) - (G C_{pi})] \text{ (KN/m}^2\text{)}$$

Flexible Buildings:

Design wind pressure shall be determined from the following equation:

$$p = q G_f C_p - q_i (G C_{pi}) \text{ (KN/m}^2\text{)}$$

5. RESULT AND DISCUSSION

For comparison purpose a typical multi-storeyed residential building is analysed for three exposure conditions (i.e. Exposure A, Exposure B & Exposure C). Two alternative methods are used in BNBC 1993 whereas single method is used in BNBC 2015. All pressures are multiplied with respective wind load factor to calculate factored total wind pressure. Corresponding parameters used in the respective two codes are presented below. The comparison results are presented graphically in Figure 9, Figure 10 and Figure 11.

Height of the building : 100 m

Length and width : 20 m

Basic Wind speed : 180 km/hr for BNBC 1993 and 56.70 m/s for BNBC 2015

Building type : Enclosed

Multiplying factor : 1.3 for BNBC 1993 and 1.6 for BNBC 2015

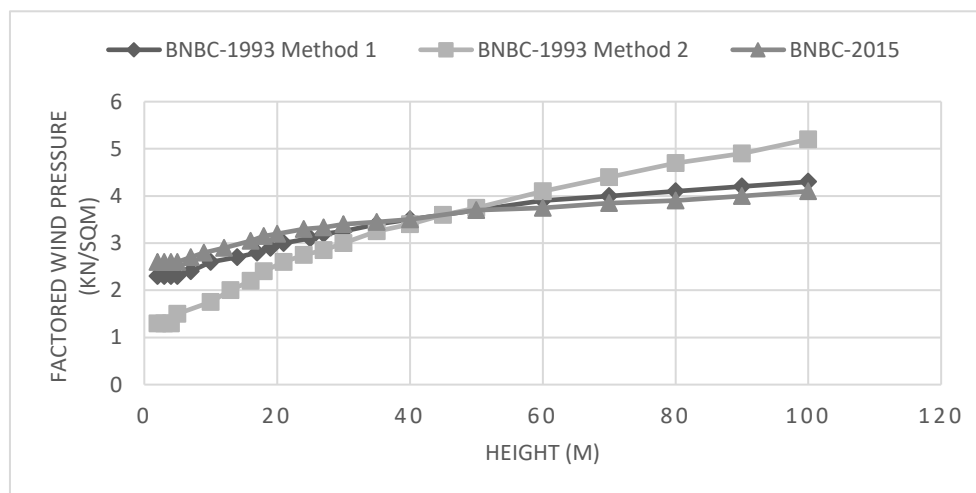


Figure 9: Factored total Wind Pressure for Exposure A condition

Findings are given below:

The change in factored total wind pressure with height in BNBC 2015 is more uniform than BNBC 1993.

Factored wind pressure in BNBC 2015 is 7-12% higher than BNBC 1993 up to 50 m. Then it gradually decreases with the increase of height.

At the height of 50 m, both BNBC 2015 & BNBC 1993 shows same factored total wind pressure.

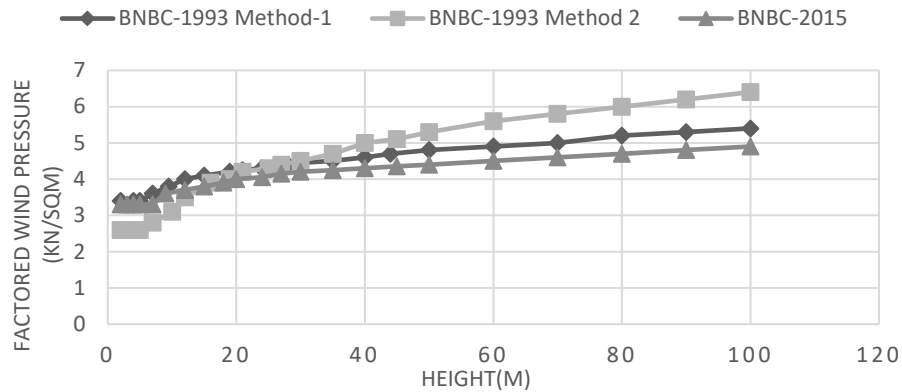


Figure 10: Factored total Wind Pressure for Exposure B condition

Findings are given below:

Factored total wind pressure with height in BNBC 2015 is lower than BNBC 1993.

Method 2 in BNBC 1993 shows a significant change in factored total wind pressure from height 10 m to 30 m.

The change in factored total wind pressure with height in BNBC 2015 is more uniform than BNBC 1993.

At the height of 20 m, both BNBC 2015 & BNBC 1993 shows almost same factored total wind pressure.

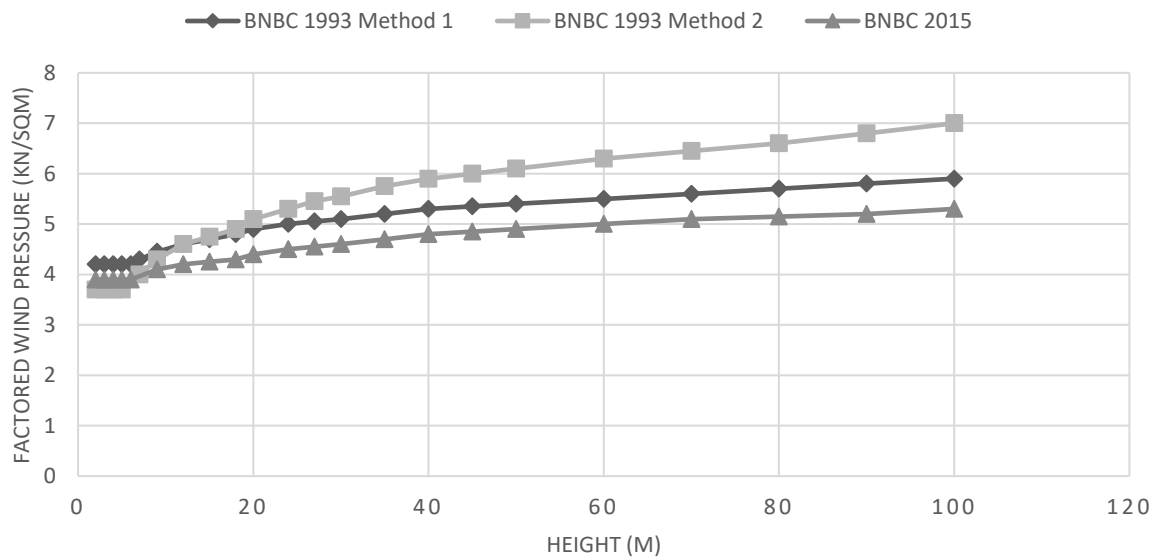


Figure 11: Factored total Wind Pressure for Exposure C condition

Findings are given below:

Factored total wind pressure with height in BNBC 2015 is lower than BNBC 1993.

The change in factored total wind pressure with height in BNBC 2015 is more uniform than BNBC 1993.

6. CONCLUSION

Following are the findings from the study for which BNBC 2015 seems to be more suitable for structural design purposes than BNBC 1993:

The effect of surrounding objects and height of structures are considered in proposed BNBC 2015. BNBC 1993 mentions basic wind speed in terms of fastest-mile wind speed whereas BNBC 2015 provides basic wind speed in terms of 3-second gust wind speed. Again the rate of increase in wind load with respect to numbers of stories is more uniform in BNBC 2015 in comparison with BNBC 1993. Both BNBC 1993 and BNBC 2015 provide basic wind speed associated with an annual probability of occurrences of 0.02 (50 year recurrence interval) measured at a point 3 ft (10m) above the mean ground level in a flat and open terrain. The calculation procedure for design wind pressure in BNBC 2015 is totally different than that of BNBC 1993. Two new terms topographic factor & directionality factor has been introduced in BNBC 2015. BNBC 2015 uses single method for the calculation of factored wind pressure whereas BNBC 1993 used two alternative methods. In Method 1, the windward and the leeward pressure are separately considered than combined but in Method 2, the overall pressure coefficient is used to determine the design wind pressure directly. All the factors related to wind speed has changed from BNBC 1993 to BNBC 2015. The wind load in Exposure A according to BNBC 2015 is found considerably higher by 7-12% than that of BNBC 1993. But for Exposure B & C according to BNBC 2015 is found significantly lower by 2-10% than BNBC 1993.

REFERENCES

- Atique, F. & Wadud, J. 2001. "A comparison of BNBC-93 with other building codes with respect to earthquake and wind analysis." The Eighth East Asia-Pacific Conference on Structural Engineering and Construction, Nanyang Technological University, Singapore
- BNBC 1993, "Bangladesh National Building Code (BNBC)", Bangladesh House Building Research Institute, Dhaka
- BNBC 2015, "Bangladesh National Building Code (Proposed)", Bangladesh House Building Research Institute, Dhaka
- Faysal, R. M., 2014, "Comparison of Wind Load among BNBC and other codes in different types of areas", International Journal of Advanced Structure and Geotechnical Engineering.
- Hasan, M. R. and Hoque, M. T., 2007, "Comparative studies of Different Building Codes in Context of Bangladesh National Building Code"
- Imam, F. S., Tahsin, S. and Hassan, A., 2014 "Comparative Study on Lateral Load Analysis By BNBC – 1993 And Proposed BNBC-2012", International Journal of Scientific & Technology Research.

EFFECTS OF CONTINUOUS MIXING ON MECHANICAL PROPERTIES OF CONCRETE

Maruf Hossain¹, Harunur Rashid² and Firoz Mahmud³

¹ Department of Civil Engineering, Khulna University of Engineering & Technology, Bangladesh, e-mail: marufhossain1205@gmail.com

² Professor, Khulna University of Engineering & Technology, Bangladesh, e-mail: hafin02@yahoo.com

³ Department of Civil Engineering, Khulna University of Engineering and Technology, Bangladesh, - email: 2k13firoz@gmail.com

ABSTRACT

Mixing time and Temperature have adversely influenced on the mechanical properties of concrete. The traveling time of the transit mixture from the plant to the work site is critical, especially where the forecast of travelling time is difficult due to a traffic jam or other uncertainties. At the same time, the ambient temperature at concrete casting time is another factor. A laboratory study was conducted to investigate the impact of different mixing time on the performance of concrete and find out its effect on concrete. To achieve the study goal, the concrete mixtures drum was continuously rotated for up to 5, 60, 120 and 180 min maintaining a constant rotation of 15 per minute under a controlled temperature of 25°C and 40°C. The effects of prolonged mixing scheme under various temperatures on critical properties such as the slump loss, compressive strength, splitting tensile strength and permeability of concrete were done at 3, 7, 28 and 90 & 120 days age of concrete. The results showed that concrete can undergo substantial slump loss when subjected to prolonged mixing at 40°C temperature. At 25°C temperature, compressive strength decreased with the increase of mixing time; but at 40°C temperature, reverse result was observed. At 25°C temperature, splitting tensile strength decreased, however, at 40°C temperature splitting tensile strength was increased with mixing time and the Permeability of concrete was increased with increasing of mixing time and temperature.

Keywords: *Mixing time, Temperature, Strength, Permeability*

1. INTRODUCTION

Concrete is a structural material widely used in the construction industry. The physical properties of aggregates, chemical composition of binding materials as well as water cement ratio influence on the properties of concrete. Since the long-term properties of concrete are seriously affected by its degree of compaction, it is vital that the consistency or workability of the fresh concrete be such that the concrete can be properly compacted, transported, placed and finished easily without segregation. The mixing time of the concrete production have a profound effect on the working performance and the strength property (Dong, et. Al. 2011). For mixing over a long period, workability decreases with time due to loss of moisture from the mix. To restore the workability, water is to be added and finally gives a lower strength of concrete (Neville, 2000). However, according to Shetty (1982), Long time mixing of concrete will generally result in increase of compressive strength of concrete within limits. Due to mixing over long periods, the effective water cement ratio gets reduced, owing to the absorption of water by aggregate and evaporation. It is also possible that the increase in strength may be due to the improvement in workability on account of excess of fines, resulting from the abrasion and attrition of coarse aggregate in the mix, and from the coarse aggregates themselves becoming rounded. The length of mixing time required for sufficient uniformity of the mix depends on the quality of blending of materials during charging of the mixer: simultaneous feed is beneficial. To ensure the uniform workable of concrete and good strength properties, an appropriate and economic mixing time should not be ignored (Dong, F., MingKai, Z. and HuaGang W. 2011). The

performance of concrete are also affected by temperature because of the loss of workability. On a hot weather it becomes necessary to increase the water content of the concrete mix in order to maintain desired workability. The amount of mixing water required to bring about a certain change in workability also increases with temperature (Gambhir, 2009). Although a higher temperature during placing and setting increases the very early strength, it may adversely affect the strength from about 7 days onwards. The explanation is that the rapid initial hydration appears to form products of a poorer physical structure, probably more porous, so that a proportion of the pores will always remain unfilled (Neville, 2000). In connection with the influence of temperature during the early life of concrete on the overall structure of the hydrated cement paste, it is useful to recall that a low early gain of strength has a beneficial effect on strength also when the hydration is slowed down by the use of retarders. Water reducing and reduction in the long-term strength of admixture free concrete placed at a high temperature. It should be realized, however, that their effect arises from water reduction and therefore a lower water cement ratio. It has been found that high early temperature has negative impacts on later strength of concrete. Some researchers investigated the adverse effect on long term strength of concrete due to high initial temperature. High initial rate of hydration due to increased temperature retards the subsequent hydration and produces a non-uniform distribution of the products of hydration. Its reason is that at high initial rate of hydration, there is insufficient time available for the diffusion of the products of hydration away from the cement particle and for a uniform precipitation in the interstitial space. Some field tests have confirmed the influence of temperature at the time of concrete placement. Typically, for an increase of 5°C (9°F) there is a decrease in strength of 1.9 MPa (270 psi) (Donson, C. J. and Rajagopalan, K. S. 1979). The coupled effects of ambient temperature and mixing time on the slump loss of fresh concrete are critical for hot weather concreting. The quality of concrete can be adversely affected during mixing, placing, and curing at elevated temperatures (Abbasi FA and Al-Tayyib AJ. 1983). So mixing time and temperature are an important factor which effect on the properties of concrete such as workability, strength, durability, stiffness, ductility, hardness, elasticity etc. Among them, in this study attention is given on workability, strength, permeability and absorption of concrete.

2. METHODOLOGY

2.1 Preparation of specimen

The concrete was prepared with 1:2.3:3.4 proportion of cement: C. Aggregate: Fine Aggregate and target slump value 80±3mm. In mixing concrete, a tilting concrete mixer was used. Coarse aggregate was weighted by water sprayed over it before 24 hours of casting to achieve SSD condition. The concrete mixer drum was moistened and then the weighted aggregate was poured in the mixer machine and rotated for 1 minute and thereafter 2 minutes with addition of cement. Finally tap water was added in two stages, at first 70% of water had been added and rotated the mixing hopper for 1 minute and additional 2 minutes rotation was performed after mixing the rest amount of water without stopping the mixer machine and finally adjusted initial slump value 80mm shown in Figure 1. After this the mixer machine had been continuously rotated for 5 minutes, 60 minutes, 120 minutes and 180 minutes for the test. In every 20 minutes initial slump were adjusted by adding extra water. Concrete slump value of 5 minutes mixing time was considered as reference one. The additional water was added at regular interval throughout the mixing time. The concrete was poured in cylindrical molds of 100mm diameter and 200mm height after completion of target time. Casting of mixed concrete was made in traditional way, filling from above and manual compaction confirmed with tamping rod in three layers and finally finished the top surface shown in Figure 2. A closed chamber was prepared to maintain the temperature shown in Figure 3. After 24 hours, they were submerged in water for curing about 3 days, 7 days, 28 days, 90 days and

120 days as required for the test. This process was performed at 25°C and 40°C. Curing was performed according to ASTM C192.



Figure 1: Mixing of Concrete

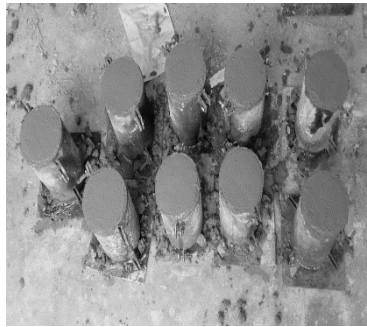


Figure 2: Concrete specimen



Figure 3: Control chamber

2.2 Testing

In this study, uniaxial compressive strength test on cylinder specimens (4 in x 8 in) at the age of 3, 7, 28, 90 and 120 days were performed according to ASTM C39. Splitting tensile strength test was also performed. Permeability test on concrete samples were performed according to ASTM C1202. In this test, 50 mm thick slices of 100 mm nominal diameter concrete cylinders were collected from cylindrical samples of 100 mm diameter and 200 mm height. The sides of the cylinder specimen were coated with epoxy and left to be dried. Then it had been put in vacuum chamber for 3 hours. The specimen had been kept for vacuum saturation for 1 hour and allowed to soak for 18 hours. It was then assembled with the test device. The left hand side (-) of the cell was filled with a 3% NaCl solution. The right-hand side (+) of the test cell was filled 0.3N NaOH solution. Figure-3.7 illustrates rapid chloride permeability test setup. After that the system was connected with a 60-volt DC current for 6 hours. Readings were taken at regular interval of 30 minutes. At the end of 6 hours the sample was removed from the cell and amount of coulombs passed through the specimen was calculated. Test setup is shown in Figure-4.

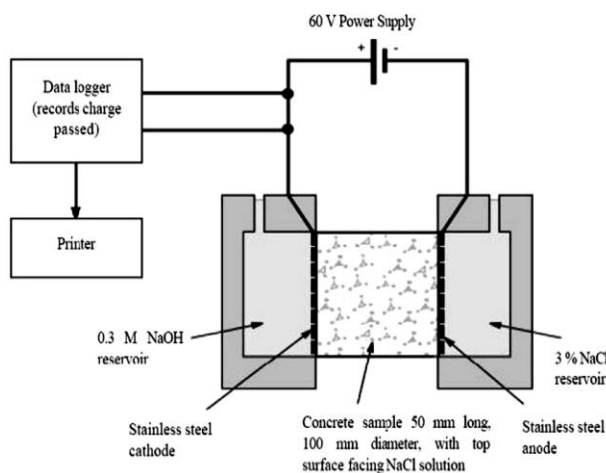


Figure 4: Rapid chloride permeability test setup

3. RESULTS AND DISCUSSIONS

3.1 Compressive strength

In this research work, the compressive strength is gradually decreased with increasing of mixing time showed in Figure 5. Due to adding extra water in the mixer the w/c ratio was increased and that's why the strength of concrete gets reduced at 25°C temperature. The graph shows that when the mixing time was 5min then the strength was high compared to the mixing time at 60, 120 and 180 minutes.

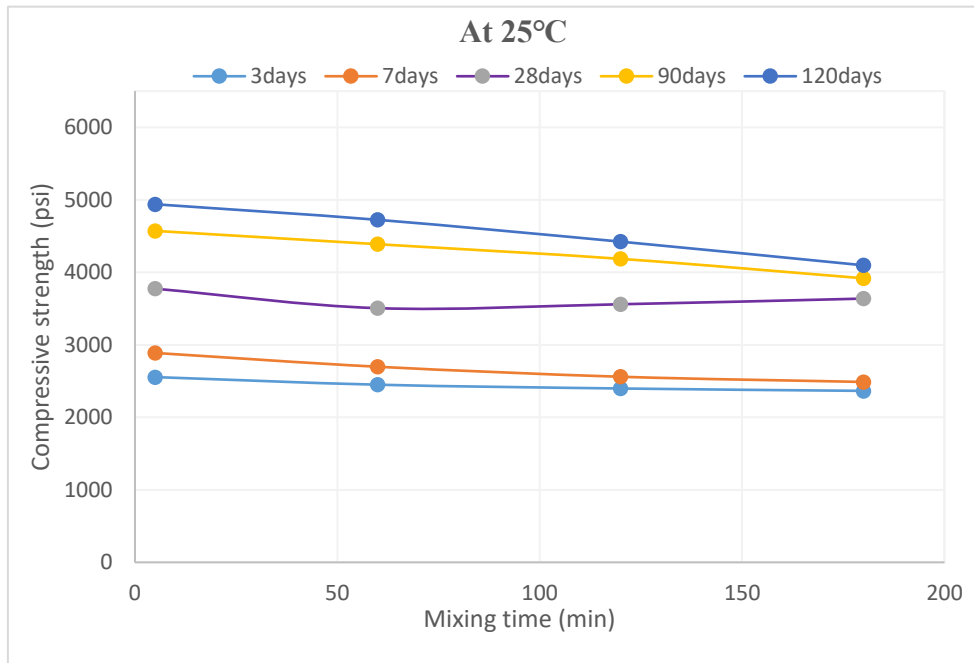


Figure 5: Compressive strength at different mixing time (25°C Temperature)

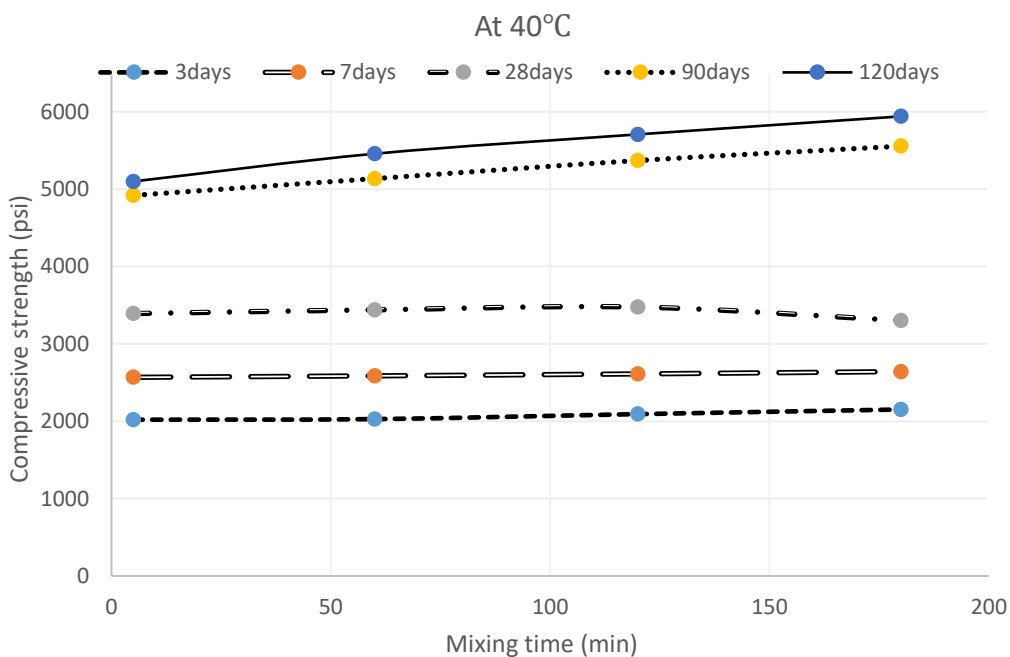


Figure 6: Compressive strength at different mixing time (40°C Temperature)

On the other hand, at 40°C temperature, the strength increased with the increasing of mixing time. It shows the opposite result compared to 25°C temperature. It is observed From Figure 6 that, the variation of compressive strength at different mixing time. Initially, the strength is low and after increasing of mixing time the strength is increased. At mixing time 180 minutes the result of compressive strength is higher than other mixing time of 5, 60 and 120minute.

Table 1 shows the Compressive strength test results. It is obtained from research work. The above graphs are based on this table.

Table 1: Compressive strength test results

Mixing Time (minute)	Temperature (°C) (±3)	Compressive strength (psi)				
		3days	7days	28days	90days	120days
5	25	2555	2888	3774	4572	4939
	40	2020	2568	3392	4920	5100
60	25	2450	2698	3506	4388	4724
	40	2028	2587	3440	5136	5458
120	25	2398	2560	3560	4186	4423
	40	2092	2612	3476	5370	5708
180	25	2365	2488	3638	3918	4097
	40	2152	2642	3303	5556	5941

3.2 Splitting tensile strength

It is seen from Figure 7, that splitting tensile strength increases with the increasing of mixing time for 40°C temperature. On the other hand, at 25°C temperature strength decreases with the increasing of mixing time.

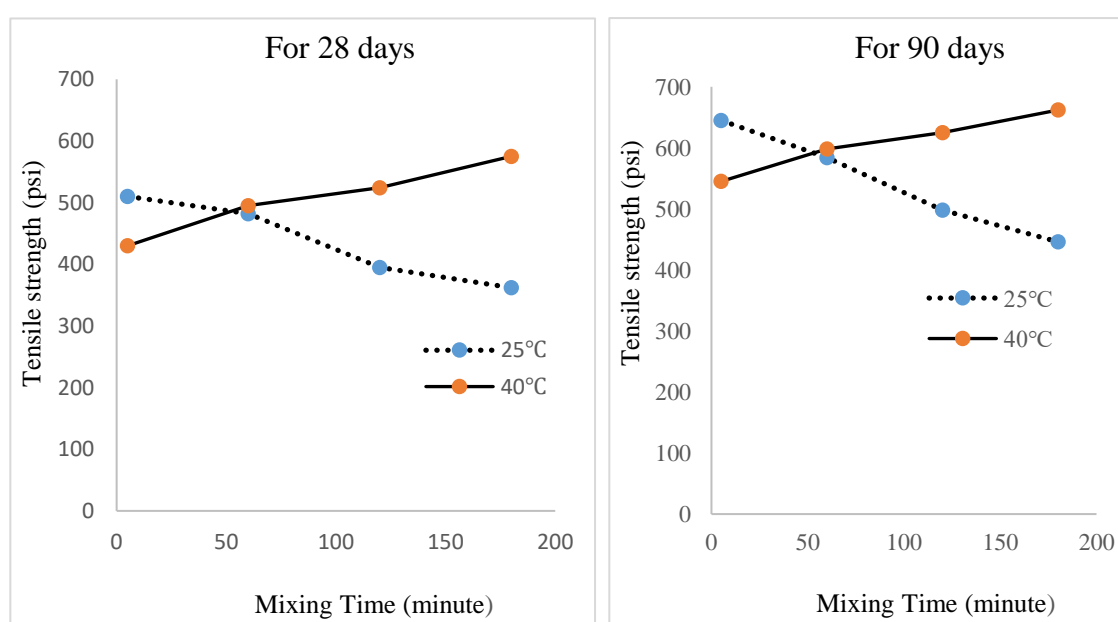


Figure 7: Tensile Strength at different mixing times and temperature

Table 2 shows the result of Tensile strength of concrete at different time and temperatures.

Table 2: Tensile strength test result

Mixing Time (minute)	Temperature (°C) (±3)	Splitting Tensile Strength (psi)	
		28days	90days
5	25	510	645
	40	430	545
60	25	482	584
	40	495	598
120	25	395	498
	40	524	625
180	25	362	446
	40	575	662

3.3 Permeability test result

From research, it is observed that At 25°C temperature, the permeability result is in between the range of 1000-2000C, which shows low permeability. On the other hand, initially for the 40°C temperature at mixing time 5-100 minute, the result is in between 1000-2000C, which means at this mixing time the permeability is low, but after that, the permeability result becomes moderate according to ASTM C1202. When the temperature is high then the hydration process becomes very fast and for that reason, the permeability of concrete increased with the increase of mixing time and temperature.

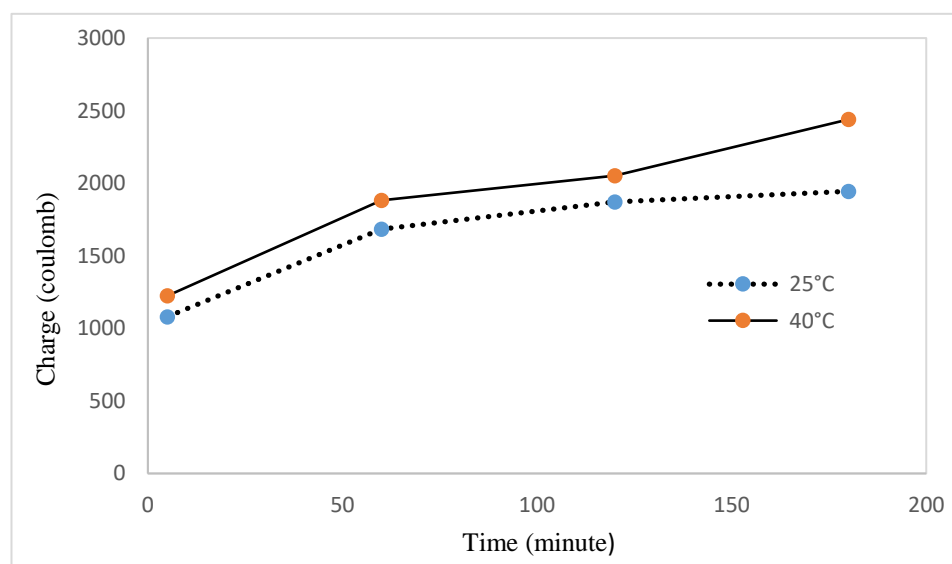


Figure 8: Effects of mixing time at different temperature on Permeability

Table 3 shows the result of Charge Passed at different mixing time & temperatures

Table 3: Charge Passed at different mixing time & Temperature

Mixing Time (minute)	Temperature (°C) (±3)	Charge Passed, Q (Coulombs)
5	25	1080
	40	1224
60	25	1683
	40	1881
120	25	1872
	40	2052
180	25	1944
	40	2439

4. CONCLUSIONS

Based on the findings of this work, the following conclusions are summarized.

Water demand for Concrete of constant workability at 40°C temperature was high compared to 25°C temperature. At 25°C casting temperature, the Compressive strength was decreased with the increasing of mixing time, however, reverse result was found at 40°C temperature.

At 25°C temperature splitting tensile strength decreases but at 40°C temperature splitting tensile strength increases with mixing time. The permeability of concrete was increased with increasing of mixing time and temperature.

ACKNOWLEDGEMENTS

I am thankful to all of my teachers, friends and other members who helped me in the whole works and also thankful to my Institution for giving me the chance to work there.

REFERENCES

- Abbasi FA and Al-Tayyib AJ. 1983. Effect of hot climate on shear strength of concrete. Transportation Research Record, No. 924, 27–32. Transportation Research Board, Washington DC, USA.
- Aguwa, J. I. 2011. Effect of mixing time on the compressive strength of concrete. Journal of Science, Technology, Mathematics and Education (JOSTMED).
- ASTM. 2004. Standard Test Method for Splitting Tensile Strength of Cylindrical Concrete Specimens. ASTM C496, Annual Book of American Society for Testing Materials Standards, Vol. C 04.02.
- ASTM. 2006. Standard Test Method for Density, Absorption, and Voids in Hardened Concrete. ASTM C642, Annual Book of American Society for Testing Materials Standards. Vol. C 04.02.
- ASTM. 2006. Standard Test Method for Sieve Analysis of Fine and Coarse Aggregates. ASTM C136, Annual Book of American Society for Testing Materials Standards. Vol. C 04.02.
- ASTM. 2007. Standard Practice for Making and Curing Concrete Test Specimens in the Laboratory. ASTM C192, Annual Book of American Society for Testing Materials Standards. Vol. C 04.02.
- ASTM. 2010. Standard Test Method for Electrical Indication of Concrete's Ability to Resist Chloride Ion Penetration. ASTM C1202, Annual Book of American Society for Testing Materials Standards. Vol. C 04.02.

- Dong, F., MingKai, Z. and HuaGang W. 2011. Influence of mixing time on workability and strength properties of concrete in different consistency. *Advanced Materials Research*, pp.1224-1228.
- Donson, C. J. and Rajagopalan, K. S. 1979. Field Tests Verify Temperature Effects on Concrete Strength. *Concrete International*, 1, No. 12, pp. 26-30.
- Fattuhi, N. I. The setting of mortar mixes subjected to different temperatures, *Cement and concrete Research*, 1985.
- Gambhir, M. L. 2009. *Concrete Technology*. Tata McGraw Hill Education Private Limited, 7 West Patel Nagar, New Delhi-110008.
- Mittflacher, M. 1983. Effect of hot weather conditions on the strength performance of set-retarded field concrete, in *Temperature Effects on Concrete*. ASTM Sp. Tech. Philadelphia, Publ. No. 858. Pp. 88-106.
- Neville, A. M. 2000. *Properties of concrete*. Pitman Publishing Ltd, 39 Parker Street, London.
- Shetty, M. S. 1982. *Concrete Technology*. S. Chand & Company Ltd, Ram Nagar, New Delhi-110055

FLEXURAL RESPONSE AND CORROSION PERFORMANCE OF FERROCEMENT PANEL

Maria Shirin Anita¹ and Md. Harunur Rashid²

¹ Department of Civil Engineering, Khulna University of Engineering and Technology, Bangladesh, e-mail: mariashirin17@gmail.com

² Department of Civil Engineering, Khulna University of Engineering and Technology, Bangladesh, e-mail: hafin02@gmail.com

ABSTRACT

This research work was carried out to investigate the performance of ferrocement as infill wall panel in building structures. For this, five types of panel were casted and tested to find out the flexural strength, deformation and corrosion of ferrocement panel. Panels are constructed to find out the mechanical properties of ferrocement in size of 0.3m×0.3m having 30mm and 65mm thickness for single and double layer wire mesh respectively. Samples of 0.3m × 0.3m size with single and double mesh layer were also casted to found out the corrosion effect. To observe the effect of temperature on ferrocement panel, another series of specimens were casted as corrosion sample were kept in 105°C in the oven for 12 hours. Then removed and stored other 12 hours in air and water of a cycle, total 45 such cycles was completed. The test results show that the flexural performance of single layer and double layer mesh specimen under corrosion control reduce 20% and 10% respectively when compared with the specimen kept in controlled condition. Again test results of temperature effect test show, flexural strength of single layer mesh specimen in air cooling condition reduce 30% and specimen in water cooling condition reduce 14%, for double layer mesh specimen. Double layer mesh specimen exhibits greater flexural strength than single layer mesh specimen.

Keywords: Ferrocement, Flexural Strength, Corrosion, Temperature Effect, Wire mesh.

1. INTRODUCTION

The ferrocement is a type of reinforced concrete thin elements constituted by cement mortar and woven wire mesh with relatively small diameter. According to ACI "It is a type of thin wall reinforced concrete commonly constructed of hydraulic cement mortar reinforced with closely spaced layers of continuous and relatively small diameter wire mesh; the mesh may be made of metallic or other suitable materials" (ACI 549R, 1997; ACI-549 2R, 2004). As ferrocement is made of same cementitious materials used in reinforced concrete (RC), it can be widely used as strengthening material for rehabilitation works in any RC structure (Zamin, et al, 2010). According to some previous works the engineering properties of ferrocement structure are equivalent to normal concrete, though in some applications, it performs better. The closely-spaced and homogeneously-distributed reinforcement transform the brittle concrete material into an elastic composite and is regarded as highly flexible construction material possessing unique properties of strength and serviceability. The serviceability and the achievement of ferrocement as a structural material depend upon its durability (Mathews, et al, 1993). The durability of a ferrocement compound may be defined as its capability to resist cracking and any other process of destruction, weathering action, chemical attack, abrasion, (Ramesht, et al, 1993).

The tensile strength capacity of ferrocement panel is a function of the volume of reinforcement used in the panel. A ferrocement element subjected to tensile stress behaves something like linear elastic material until the first crack appears. After this, the ferrocement

element will be faced multiple cracking and eventually continuing to a point where the mesh starts to experience yielding. In this stage, the number of cracks will continue to grow with the increase in the tensile force. The specific surface area of ferrocement element has been found to influence the first crack in tension, as well as the width of the cracks. The maximum stress at first crack for ferrocement element increases in proportion to the specific area of the element. The strength behavior of ferrocement panel under compression is depended on the properties of cement mortar. (Clear, April 1973)

Bangladesh is a tropical country where three distinct seasons are present, a hot, humid summer from March to June; a cool, rainy monsoon season from June to October; and a cool, dry winter from October to March. In general, maximum summer temperatures range between 30°C and 40°C. April is the warmest month in most parts of the country. January is the coldest month when the average temperature for most of the country is about 10°C. Concrete expands when heated and contracts when cooled, and ferrocement also behave as like the concrete. So this temperature variation causes thermal expansion and contraction of ferrocement and may cause for thermal cracking.

Corrosion of wire mesh in ferrocement is one of the major deterioration causes in the structure. The entrance of chloride ions and carbon dioxide to the steel surface is the most important causes of corrosion initiation of steel wire mesh in ferrocement panel. After initiation of the corrosion process, the corrosion products recognized as red-brown dust (hydrous ferric oxide $Fe_2O_3 \cdot 3H_2O$) are usually deposited in the restricted space in the concrete around the mesh. Their formation within this restricted space sets up expansive stresses, (the corrosion products resulting from the corrosion of steel wire mesh occupy a volume equal to three to six times that of the original level) which may causes cracks, creates internal pressure and spall the concrete cover. According to R.Elavarasan (2016) this, in turn, results in enormous losses, direct and indirect, all over the world.

Nowadays this is an emerging issue to find out the effect of corrosion and temperature along with the mechanical properties of ferrocement panel. Wire mesh was used as reinforcement in one and two layers embedded with thin cement composite panels. Some samples were subjected to a corrosive environment under controlled condition and other were kept under thermal effect. After 60 days under controlled condition

2. METHODOLOGY

2.1 Material Properties

The properties of used materials, such as specific gravity, absorption, fineness modulus and unit weight were done according to ASTM C128, ASTM C128, ASTM C136, ASTM C29 testing standards respectively in the material lab of the Department of Civil Engineering of KUET, Bangladesh. River bed sand was used as fine aggregate and properties of this are shown in Table 1. Wire mesh available in the local market was used to prepare the sample. The diameter of mesh wire is 1mm and consisted of a square opening of 10.0 mm x 10.0 mm. Portland Composite Cement was used as binding materials to prepare the specimens.

Table 1: Properties of Fine Aggregate

Unit Weight (Kg/m ³)	Voids (%)	Moisture content (%)	specific gravity	Absorption	F.M value
1487.98	23.14%	1.17%	2.04	4.17%	3.9

2.2 Specimen Preparation

Two types of 20 numbers and 24 numbers specimens were prepared for corrosion test and temperature effect measurement respectively. The specimens are designated as type A and type B for corrosion and temperature effect respectively. Size of the specimen was 0.3m x 0.3m and the thickness was 30mm and 65mm for single and double layers of wire mesh.

For the preparation of specimen, sufficient numbers of the wooden frame were prepared. Steel cutting scissor was used to cut and prepare the mesh according to the size and flat on the wooden platform by hammering. A typical view of the frame, wire mesh, and electric wire assembling and finished sample are shown in Figure 1 and 2.

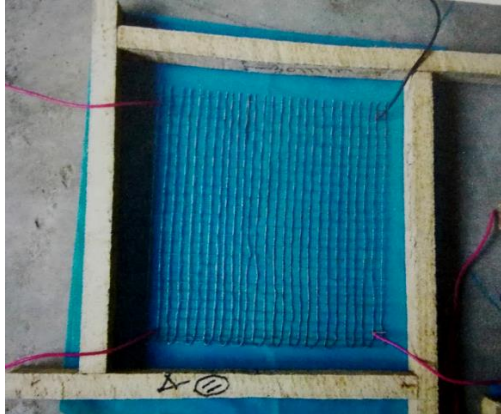


Figure 1: Spcimen ready for casting



Figure 2: Specimen after casting

All corners of the wire mesh were attached with electric wire for the specimens which were kept under corrosion test. After completing all necessary arrangements, the mortar was well mixed, placed and well compacted to ensure a homogeneous body shown in figure 1 and 2. The mixing proportion of cement sand is used 1:2 and water were used 40% of the cement weight. After 24 hours of specimen preparation, the frame was removed and the specimen was transferred to water chamber for curing up to 28 days. general information of samples with identity shown in Table 2.

Table 2; Sample Description

Sample No	Length(mm)	Width(mm)	Thickness(mm)	Mesh layer
A	300	300	30	Single
B	300	300	65	Double

2.3 Corrosion Setup

For this experiment, a water tub was prepared temporarily with bricks and thick polythene paper. Total 20 numbers of the sample are placed in the water tub at a time. The samples were tied by a thin jute rope so that the sample can rest in the position easily. Then the water tub was filled with water. A copper plate was placed in water and electrically connected to the wire mesh through adapter As shown in figure 4 and 5.

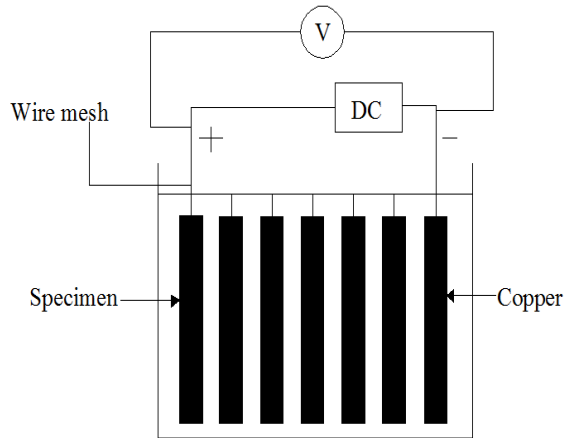


Figure 4: Current Application Diagram



Figure 5: Specimens in Corrosion Cell

The current was applied from an external AC source to the cell through the adapter. Initially, 3 volts was supplied, however, the measured output voltage at the initial time was 2.56 volt and it was varied from 2.35 to 2.65 until 4 weeks. The adapter had one end connected to the copper plate in the water and another end is connected to the wire mesh in the specimen via an electric wire. Samples were ready for testing after 60 days in the corrosion chamber.

2.4 Temperature Effect

To find out the temperature effect 24 numbers of the sample were prepared for single layer and other 24 nos for double layer wire mesh. Samples were tested under different condition shown in Table 3

Table 3: Specimen designation for testing under different condition

Normal condition		Temperature effect			
Single layer mesh (A)	Double layer mesh (B)	Single layer mesh (A) Specimen cooled in air	Single layer mesh (A) Specimen cooled in water	Double layer mesh (B) Specimen cooled in air	Double layer mesh (B) Specimen cooled in water
A-9	B-9	A-1	A-3	B-1	B-3
A-10	B-10	A-2	A-4	B-2	B-4
A-11	B-11	A-5	A-7	B-5	B-7
A-12	B-12	A-6	A-8	B-6	B-8

Two number of samples were tested under each group and provide the average result in this work for single and double layer mesh. To observe temperature effect 32 samples were kept in 105°C in the oven for 12 hours. After removing from oven 16 samples were kept in room air and rest samples were quenching for 10 minutes and then stored in room air for another 12 hours. Heating in the oven was conducted at night and other works at day time, confirm a cycle. 45 such cycles were performed to find out the temperature performance of ferrocement panel. In each cycle 20 pictures were taken just after removed from the oven, quenching and before placed in the oven again.

2.5 The Flexure Test Procedure

For testing, the specimens 3-point flexure test was performed. The force in applied by means of loading pins. The ferrocement wall panels were loaded under three-point bending with a shear span of 8 inches. A load was applied at mid of the shear span by UTM (Universal testing machine). A deformation gauge was attached to the mid of the specimen.

Deformation was measured at the interval of 0.5 KN increased of the load. The configuration provides a uniform loading of the specimen and prevents the frictions between the specimen and the supporting point.

3. RESULT AND DISCUSSION

The results of the tested specimens in flexure is given below.

3.1 Flexure Test Results for Sample Under Corrosion Control

Figure-6 shows that flexural strength of specimen A is 26 percent reduced due to the effect of corrosion. However, for specimen B the flexural strength reduced by an amount of 12 percent due to the corrosion shown in Figure 7. The specimen B is better than A in both under normal and corrosion condition. These results exhibit that the flexural strength of specimen in normal condition is more than the specimen kept under corrosive environment and specimen with double layer mesh gives more flexural strength than the specimen with single layer mesh.

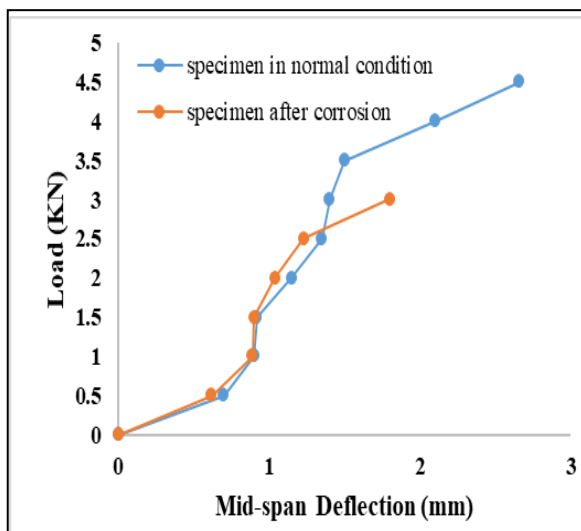


Figure 6: Load and deflection for specimen A

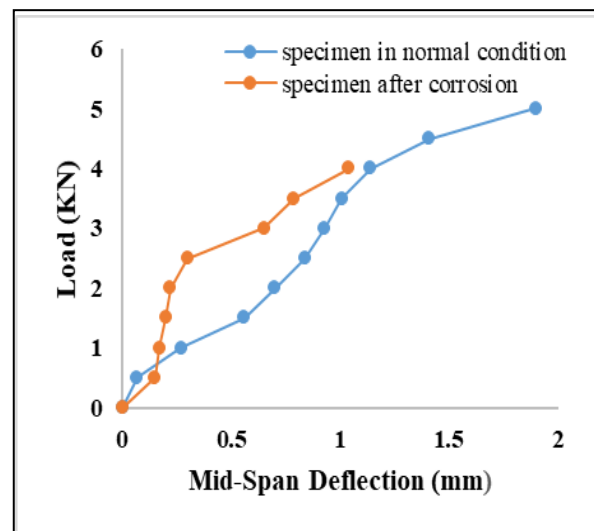


Figure 7: Load and deflection for specimen B

3.2 Cracking Behaviour of Samples Under Temperature Effect

Cracks were found in samples having single layer wire mesh (type A) after 45 cycles. However, no visible cracks were found up to 60 cycles for double layer mesh sample (type B) indicates double layer mesh element is more durable than single layer mesh element. Typical images of sample A under different type cooling conditions are shown in Figure 8.

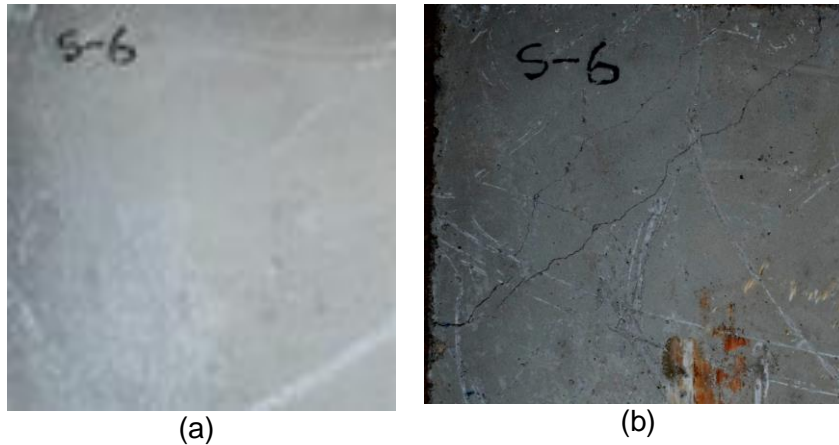


Figure 8: Ferrocement Specimen Type A after 45 cycles (a) cooled in room (b) Quenched and cooled in room.

3.3 Flexure Test Results for Sample Under Temperature Effect

Flexural performance of single layer mesh specimen exhibits about 43% and 48% strength loss when cooled in normal room environment and quenched respectively due to temperature effect is shown in Figure 9. However, in case of double-layer wire mesh in ferrocement panel, the flexural capacity droops about 32% for both air and water cooling condition. It may be concluded here that the double layer wire mesh exhibits better performance when compared to single layer mesh element.

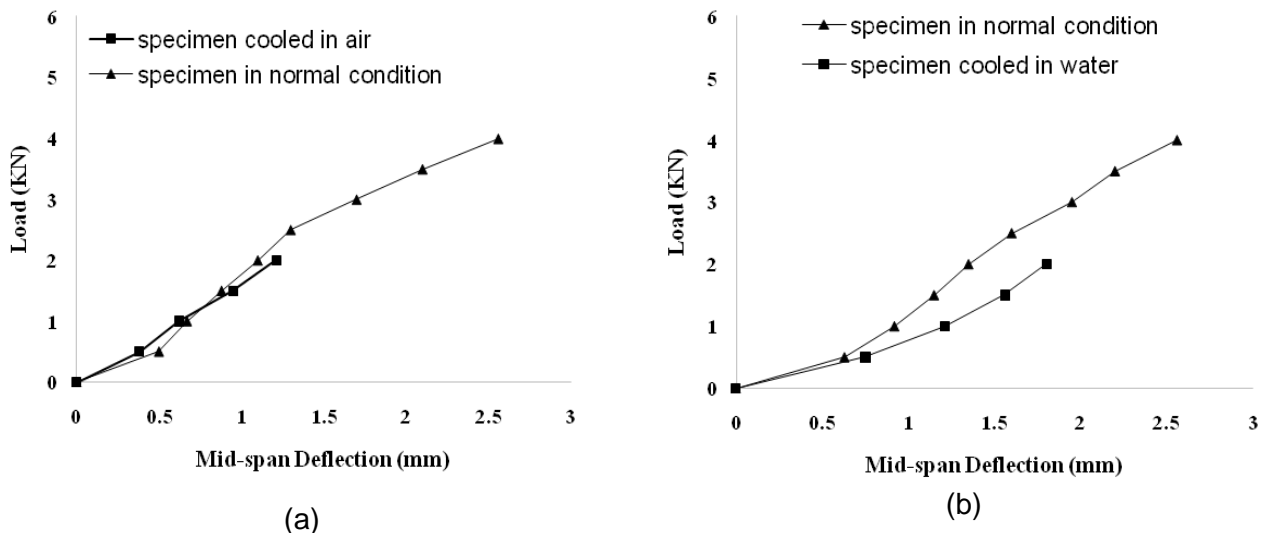


Figure 9: Flexural performance of specimen "A" after temperature effect (a) cooled in air (b) Quenched and then cooled in air

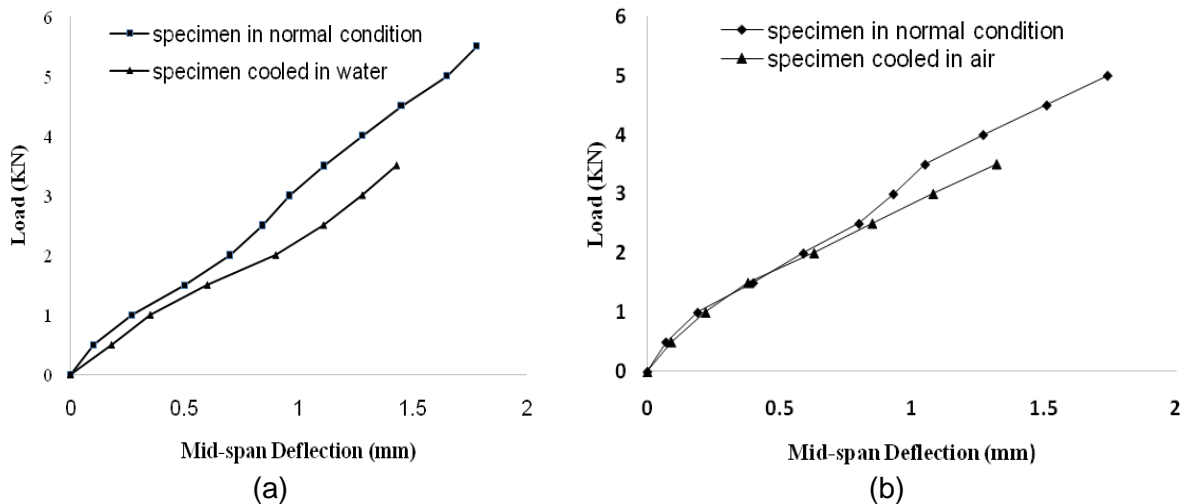


Figure 10: Flexural performance of specimen “B” after temperature effect (a) cooled in air (b) Quenched and then cooled in air

4. CONCLUSIONS

From this experiment, the following conclusion can be drawn on the performance of ferrocement panel under different condition.

Flexural strength of single and double layer wire mesh specimens are 26% and 12% lesser compared to the controlled specimen. These results conclude that the flexural strength of specimen in normal condition is more than the specimen kept under corrosive environment and specimen with double layer mesh gives better performance compared to the single layer.

Flexural performance of single layer mesh specimen exhibits about 43% and 48% strength drops when cooled in normal room environment and quenched respectively. However, in case of double-layer wire mesh, the flexural capacity droops about 32% for both air and quenched condition. It may be concluded here that the double layer wire mesh exhibits better performance than the single layer mesh elements.

REFERENCES

- Clear, K. a. (April, 1973). *Time-to- Corrosion of Reinforcing Steel in Concrete Slabe, V.1 :Effect of Mix Design and Construction*. Washington, DC: FHWA-RD- 73-32, Federal Highway.
- G. G. Carette K. E. Painter, V. M. (7/1/1982). Sustained High Temperature Effect on Concretes Made With Normal Portland Cement, Normal Portland Cement and Slag, or Normal Portland Cement and Fly Ash. *Concrete International*.
- Mhadeshwar, S. N. (June-2017). Experimental Performance, mathematical modelling and development of Stress Block Parameter of Ferrocement Beams with Rectangular Trough Shaped Skeletal Steel. *International Research Journal of Engineering and Technology (IRJET)*.
- R.Elavarasan. (March 2016). Experimental Study on Flexural Strength of Wire Mesh Concrete Slab. *International Journal of Mathematical Sciences and Engineering (IJMSE)*.
- ACI Committee 5492R (2004). “Report on Thin Reinforced Cementitious Products”, Farmington Hills, Michigan. ACI 5492R-04.
- ACI Committee 549R (1997). “State-of-the-Art Report on Ferrocement”, Manual of Concrete Practice, ACI, Farmington Hills, Michigan ACI 549R-97
- Zamin Bin Jumaat, M., Humayun Kabir, M. And Obaydullah, M. (2010). “Structural Performance of Reinforced Concrete Beams Repairing from Spalling”, *European Journal of Scientific Research*, 45:89-102

Mathews, M.S., Sudhakumar, J., and Jayasree, P. (1993). "Durability Studies on Ferrocement",
Journal of Ferrocement, 23, 15-23.

Ramesht, M.H., and Jafar, M.I. (1993). "The Monitoring of Reinforcement Corrosion in Ferrocement",
Journal of Ferrocement, 23, 289 -299.

ACCIDENTS ON CONSTRUCTION SITES IN BANGLADESH: A REVIEW

Shakil Ahmed¹, Md. Habibur Rahman Sobuz² and Md. Ikramul Haque³

¹ Student, Dept. of BECM, Khulna University of Engineering & Technology, Khulna, Bangladesh, e-mail: ashakilmondol@gmail.com

² Asst. Professor, Dept. of BECM, Khulna University of Engineering & Technology, Khulna, Bangladesh, e-mail: habibkuet@gmail.com

³ Asst. Professor, Dept. of BECM, Khulna University of Engineering & Technology, Khulna, Bangladesh, e-mail: ikramul3300@gmail.com

ABSTRACT

Bangladesh is facing tremendous accident issue at construction site and it get larger size every year. The statistics of accident at construction site shows us a picture that Bangladeshi construction sector is on most critical situation that need a huge and fast overcome from the current frequently accidental level. An accident leads a project delays, cost overrun and sub-standard product as well as affect economical and infrastructure development of a nation. This research focus on identifying the most crucial causes and analyzing statistical data of accident on construction site and to understand their relative importance (RII). In order to achieve this goal, a set of questionnaire was designed by a comprehensive literature review. The study is find 18 crucial factors of influencing accident on construction site. The key causes of accident based on overall consideration were: lack of personal protective measures, lack of safety awareness among top management, lack of safety awareness among labour, lack of training, non -strict regulation against safety, management commitment and unskilled labour. Accident control is the major concern in the construction industry in this way any endeavor to identify and investigate any approach to prevent and control accident ought to be yell after, henceforth the requirement for the research.

Keywords: Construction Accident; Causes; Construction Safety; Statistical Analysis of Accident; Bangladesh

1. INTRODUCTION

Food, shelter, and clothing are undoubtedly the three basic needs of human being. It is therefore not surprising that the construction industry is the largest industry of the world. Construction sector is one of the most important sectors in the World. The construction industry has earned the 6% of the global GDP and growing (WEF, 2016) in 2016. Bangladesh is one of the newly born developing country. Construction sector plays a significant role on Bangladesh national economy since past few years. In 2016, this industry has earn 7.67% of growth GDP of Bangladesh (Bangladesh Bureau of Statistics, 2016). This industry has a great interaction with the other economic industries as a backward and forward linkage (Bon, 2000). But construction industry is considered as one of the most unsafe and uncertain industrial activities in the country. This is recognized as the most hazardous and uncertainty industry due to its unique nature. Construction industries are also recorded several work- related accidents and injuries for various causes in the construction site. Rate of injury to physical properties and labour in the construction industry is much greater than any other industries in Bangladesh. A great number of people fall victim to injury every year, serious harm and even death often caused by accidents on construction project sites. Construction accident as an unexpected occurrence disordering a planned sequence of a construction project which result to loss of production, injury to personnel, damage to plant and equipment (Lucy at el, 1999). The ILO state that there are about 60,000 fatal accidents happen in the construction sites of the world in each year. Every day about 950 people died and over 720,000 workers get hurt because of occupational accidents (Dilipkumar and Jha, 2016). According to the International Labour Association (ILO),

worldwide appraisals of directly and indirectly about expenses for construction accidents are USD 2.8 trillion, comparable to 4% of the yearly worldwide GDP (Leigh, 2011).

Construction employees have three times more chances of dying and two times of getting injured than any worker of other economic activity (Sousa and Teixeira, 2004). In Bangladesh, the statistics reported that thousands of workers are being injured and killed each year due to the work related accidents, where the construction industry has recorded more than forty percent of the occupational injuries and fatalities (Safety and Rights Society report, 2015). It is necessary to understand that a high proportion of workforce come out from the construction industry that compared to other industrial. This indicates that a large population of global workforce is engaged in occupational injuries and fatalities. The majority of construction injury cases are simply related to poor decision making, which can be prevented through adequate safety culture (Stanley, 2010). It is necessary to determine the specific factors that are effectively important to successful implementation of safety programs to achieve desired predetermined goal. The elements of poor construction safety management find out as lack of education and training, lack of safety awareness, aversion of input safety measures and reckless operation (Tam, 2004). Construction accidents commonly happen on site due to lack of knowledge or training, inappropriate in judgment or carelessness and poor machineries (Coble et al, 1994). The main obstructions of safety implementation are the shortage of skilled workers, workers level, poor management commitment and nature of construction industry (Smallwood, 2000). Rough project schedule, disproportionate approval procedures, low management expertise, inappropriate planning, scarcity of skilled labour, variations and lack of coordination between projects participants are the main hazards to safety performance of a construction project. (Husin et al, 2008). Contributory factors to occur accidents are 70% is of workers, 49% is of work place issues, 56% is of equipment shortcomings, 27% is of material conditions and 84% is of risk management (Haslam et al, 2005).

Un-safety of different temporary structure systems are considered as the major factors of construction accidents. Construction accidents usually occur on a project site due to collapse of construction parts or elements, unsafe working condition, employee behaviours and misuse of machineries and tools. There are no doubt that the adoption of health and safety culture is an important element needed in the construction industry. In this 21st century, the improvement in technological and social sectors have modified the steps and stage of construction works. As a result many other advanced management practices are employed to reduce and eliminating the constructional injuries and fatalities which improve efficiency and effectiveness of construction industry by reducing waste and increasing profit. The adoption of appropriate procedure in safety management can reduce and eliminate the accidents and injuries in construction site. This occurrence is also hamper the schedule, plants, equipment and related properties. Appropriate safety management technique can simplify the project success and organizational sustainability. But negligence of safety practice can result in construction accidents and injuries. These type injuries and fatalities can affect the workers output of project, therefore reducing the probability that the job will be properly executed. Several researchers have proved that the appropriate safety management can improve productivity and occupational safety and health and also reduce the massacre of cost. For all these reason the study about construction safety is important. Construction site accident statistics and data in Bangladesh are not properly and regularly published. Therefore, they are not easily available and not easy to access. However, it is expected that many fatal and non-fatal accidents would be happening everyday due to its characteristics such as unique nature and less controlled over the working environment. But there is no system recommended for aggregating and recording this statistics across the country to done in proper seriousness. This is one of the reasons for not conducting sufficient researches and literature on construction accident and safety. Therefore, this study sets the following objectives of study the existing global and national accidents factors of construction accidents in Bangladesh.

2. METHODOLOGY

The essential data was collected from online sources in distributed media and research papers. The collected data was examined to distinguish the potential causes in the construction industry. A portion of the key data and information was taken specifically from the contextual investigations and some have been anticipated utilizing accessible information sources.

2.1 Data Collection

The nature of this review is required a quantitative methods of data collection. For quantitative approach, review through journal and conference papers, articles, media and others were found effective because of the relative ease of obtaining essential data and information appropriate for achieving the objectives of the study. From the literature scanning 18 vital number of factors were selected and used to design the data collecting sheet to determine the crucial factors of construction accident. To achieve this, a data sheet was designed to get the relative value of 0 to 10 based on importance by reviewing each papers, articles and other sources. Here the value 0 means the factor is not responsible for construction accident according to a specific review. Also 0 represents least important and 10 most important factor that liable the construction accident. Table-1 shows below an example of collecting data from the literature review of one research (kadiri et al, 2014).

Table-1: Sample of data collection sheet for determination of relative importance index

Factors	Relative value of importance										
	0	1	2	3	4	5	6	7	8	9	10
Lack of attention from authority											X
Lack of safety awareness							X				
Errors in judgment or carelessness	X										
Lack of education and training								X			
Reckless action of authority and workers								X			
Poor equipment and their maintenance									X		
Lack of emergency measures		X									
Non-strict execution of safety regulation and operation procedure						X					
Non-definite organization commitments					X						
Poor safety awareness of workers											X
Lack of technical guide							X				
Lack of personal protective measures										X	
Overtime work for workers							X				
Lack of team work or coordination				X							
Act of God or bad weathering	X										
Lack of information flow			X								
Type and nature of construction						X					
Rough project schedule and variations									X		

Sources: SRS annual report (2010), SRS annual report (2011), SRS annual report (2012), SRS annual report (2013), SRS annual report (2014), SRS annual report (2015), kadiri et al (2014), Amaka (2013), Abdul et al

(2008), Building Standard (2013), Farida (2010), OSHE Report Bangladesh (2014), Vhokto (2014), Parves et al (2015), Salma et al (2010), Fabiha et al (2016), Chowdhury and Tanim(2016), Mahbub (2015), Islam et al (2015)

2.2 Data Analysis

This section is to seek the preferences of value on crucial factors responsible for occurring accidents on construction sites. Using the RELATIVE IMPORTANCE INDEX the factors resulting to accidents on construction sites can be achieved according to importance value. To determine the relative ranking of factors the value were then transformed to importance indices based on the formula:

$$\text{RELATIVE IMPORTANCE INDEX} = (\Sigma M)/(HN) \quad (1)$$

In Equation (1), M represents the mean value obtain to each factor by the reviewing which ranging from 0 to 10, H is the highest value (i.e. 10 in the study) and N is the total number of samples of reviewing. Based on equation (1), the relative importance index (RII) can be calculated. And based on the relative importance index (RII) the rank of factors is arranged.

3. RESULT AND DISCUSSION

In Bangladesh the incidents rate of accident on construction site is become a serious national issue and the rate of death for these types of incident is turning into horrible figure. This type of accidents not only takes life but also causes severe damages to construction products, processes and quality. The fatality rate of Bangladesh in construction site is two times than UK and three times than Singapore. Bangladesh faces those problems in few decades but not appropriately come to the media and there are no proper statistics of fatalities of construction sector that have recorded both publicly and privately. However, some of the NGO and government organization has started to collect statistics of accident ton various industries. According to annual reports of Safety and Rights Society (SRS), OHSE reports, newspapers and others documents, the construction accidental death statistics are shown in the Table-2.

Table-2: Statistics of death and injury due to construction accident from 2010-2015

Year	Death (persons)	Injured (persons)
2010	141	1355
2011	183	346
2012	149	433
2013	127	1365
2014	130	432
2015	147	234

Sources: SRS annual report (2010), SRS annual report (2011), SRS annual report (2012), SRS annual report (2013), SRS annual report (2014), SRS annual report (2015), Farida,(2010), OSHE Newsletter (2015), Gazi, (2015), OSHE Annual Report (2013)

In table-2, it is indicated that a huge number of fatality rate exist in the construction sector in Bangladesh. Since 2010 the death and injury rate are still stand at same amount of figure to 2015. There nothing change or improve in the safety management of construction sector.

Workers are the prime contributors and cause of accidents on construction industry. worker are 65.71% responsible for this type of accident in small scale construction project and labourers are the major group of workers that are primarily affected about 60% by these accidents (Kadiri et al, 2014). A group of workers are worked either been paid on a daily or finish and go system creates an environment in which these workers carelessly and impatiently carryout their work thereby ignoring safe and standard working practices and they are creating traditional environments in which accidents are likely to occur. In this study from literature review it has been made figure-1(data is calculated from the analysis of accident on construction site at 2010-2015 excluding Rana Plaza and Tazner Garments) containing the statistics of accidents on construction site.

From the scan of literature review, 18 factors are selected and collect their each relative importance value from reviewing various sources. The relative importance ranking made by the relative importance index formula is shown in Table-3 below.

Table-3: Factors responsible for occurring construction accident in Bangladesh

Factors	RII	Rank
Rough project schedule and variations	1.70	9 th
Lack of safety awareness	4.47	2 nd
Errors in judgment or carelessness	3.16	5 th
Overtime work for workers	1.43	10 th
Lack of education and training	4.26	3 rd
Reckless action of authority and workers	2.04	8 th
Poor equipment and their maintenance	2.58	6 th
Lack of emergency measures	0.67	14 th
Lack of information flow	0.16	17 th
Non-strict execution of safety regulation and operation procedure	2.36	7 th
Non-definite organization commitments	0.77	13 th
Poor safety awareness of labour	4.02	4 th
Lack of technical guide	1.22	11 th
Lack of attention from authority	4.74	1 st
Lack of personal protective measures	1.09	12 th
Type and nature of construction	0.31	16 th
Lack of team work or coordination	0.44	15 th
Act of God or bad weathering	0.10	18 th

Table-3 admits the five most pivotal factors influencing safety management and liable for accidents in construction projects lack of attention from authority, lack of safety awareness, lack of education and training, poor safety awareness of labours, errors in judgment or carelessness. The results show that management authority's attention is very essential for effective safety management to reduce accident rate. Organization administrators assume an essential part in the definition and execution of safety practices in the working environment and representatives admire them for direction and demonstrating. The lack safety awareness is ranked second, the safety culture in the sector is 'much the same as some other sector ... which helps with reducing dangers required to the workers' safety and life, in this way increasing the awareness among workers with the help of positive initiative

and key arranging from the administration (Bernard, 2011). Lack of education and training is ranked third, this is generally accepted that it is can greatly influence the safety management in projects education and proper training of worker a crucial aspect in project implementation. It is very essential to worker that he is very well known with materials or equipment which he used his regular work. He could completed the assigned work with appropriate and safe procedure. Poor safety awareness of labour is the fourth important factor that influence the construction accident. Lack of safety awareness led a labour to indirectly discourage to take personnel safety measure and things to do with safe and healthy ways. Errors in judgment or carelessness is the fifth important factor which liable for occurring construction accident. It is referred universally as the most vital factor for affecting safety management of the project and also have the effect on project implementation greatly. The least important factor is concerned as act of God or bad weathering. It has influence on project in various ways as create risky environment for movement and transportation. The unpredictability and power of the weather can create unforeseen problems which may occur accident. It is find out from literature review that lack of information flow and nature of the work both can play little significant influence of occurring accidents on construction sites.

4. CONCLUSIONS

Construction accident is the most important fact in recent era that affect a construction project in various ways and run the project adversely. There 18 number of influencing factor are selected by literature scanning for this study. Lack of proper attention from authority, lack of safety awareness and lack of expertise/training are the main causes of accidents. To ensure a safe, healthy and accident free construction industry, authority must understand, undertake and implement all or some of the following measures which reduce the factors by continuous supervision and inspection by safety officials, train the workers professionally and accurate use of safety measures and work procedures. The authority should take necessary steps to reduce the various lack of management to prevent accident on construction site. The study discloses that safety issues are the fundamental to achieve project success. More so, it has also shown the critical factors to be treated in managing safety issues and successful project completion. We analysed about 18 factors of construction accident in this study if someone will take more number of factors and analyse them it will be more effective to the treatment of construction accident in our country. It will very effective to study or review more number of sources likes journal, research paper, newspapers, reports, article, blog and website to collect the data of this paper. It will give a more accurate figure of factors as well as their importance index. The study will be more effective if more factors of accident in construction site are analysed by visiting site and take response from the workers and victims.

REFERENCES

- A.P.C. Chan, C. M. T. (2000). Factors affecting the quality of building projects in Hong Kong. *International Journal of Quality and Reliability Management*, 17(4/5), 423-441.
- Abdul Rahim Abdul Hamid, M. Z. A. M., Bachan Singh. (2008). Causes of accidents at construction sites. *Malaysian Journal of Civil Engineering* 20(2), 242 - 259.
- Ahmed, G. T. (2015, 08, March, 2015). Construction brings highest worker deaths this year: survey, *The Daily star*.
- Bangladesh Occupational Safety, H. a. E. F. (2013). *OSHE's Workplace Accident Survey Report-2013*. Dhaka, Bangladesh: Bangladesh Occupational Safety, Health and Environment Foundation
- Bangladesh Occupational Safety, H. a. E. F. (2015). *OSHE's Workplace Accident Survey Report-2015*. Dhaka, Bangladesh: Bangladesh Occupational Safety, Health and Environment Foundation
- Bangladesh Occupational Safety, H. a. E. F. O. (2014). *OSHE's Workplace Accident Survey Report*. January 09, 2014, Dhaka, Bangladesh.
- BBS. (2016). *Bangladesh Bureau of Statistics annual report-2016* (Publication, Trans.). <http://www.bbs.gov.bd/>: Bangladesh Bureau of Statistics, Dhaka, Bangladesh.

- Bernard, S. (2013). Importance of Safety Culture in Construction. www.essaytube.com, May 12th, 2013.
- Biswas, V. K. (2014). Socio-Economic Background of Construction Workers: A Study on Dhaka City. *World Vision Research Journal*, 8(1), 82-91.
- Fabiha Tasnim, I. R., Monica Sharfin Rahman and Ridwan Islam. (2016). A Review on Occupational Health Safety in Bangladesh with Respect to Asian Continent. *International Journal of Public Health & Safety*, 1(1).
- G., K. Z. O. N. T. A. G. K. O. T. O. E. A. S. P. O. A. (2014). Causes and Effects of Accidents on Construction Sites (A Case Study of Some Selected Construction Firms in Abuja F.C.T Nigeria). *IOSR Journal of Mechanical and Civil Engineering (IOSR-JMCE)*, 11(5 Ver. I (Sep- Oct. 2014)), 66-72.
- Jama, M. U. A. M. (2015). Safety management issues in construction industry of Bangladesh. (Master in Engineering thesis programe postgraduate), Bangladesh University of Engineering And Technology, Dhaka, Bangladesh.
- Khanom, M. F. (2010). Occupational Accident Statistics in Bangladesh: Reality, problems and challenges. Dhaka, Bangladesh: Bangladesh Occupational Safety, Health and Environment Foundation.
- Leigh, J. P., Waehrer, G, Miller, T R and McCurdy, S A. (2006). Costs differences across demographic groups and types of occupational injuries and illnesses. *American Journal of Industrial Medicine*, 49(10), (845-853).
- M. H. Islam, S. Y. M. a. M. R. K. (2015). Construction Safety Practice in Bangladesh: A Case Study in KUET, Mirerdanga and Teliganti Union. Paper presented at the International Conference on Recent Innovation in Civil Engineering for Sustainable Development, DUET - Gazipur, Bangladesh.
- N.H. Husin, H. A., K. Jusoff. (2008). Management of Safety for Quality Construction. *Journal of Sustainable Development*, 1(3), 41-47.
- Ogwueleka, A. C. (2013). A review of safety and quality issues in the construction industry. *Journal of Construction Engineering and Project Management*, 3(3), 42-48.
- Parvez Ahmed Sharif, M. E. I. a. R. A. K. (2015). The international journal of business & management. *The International Journal of Business & Management*, 3(5), 214-226.
- Patel, D. A. J., Kumar Neeraj. (2016). AN ESTIMATE OF FATAL ACCIDENTS IN INDIAN CONSTRUCTION. Paper presented at the Proceedings of the 32nd Annual ARCOM Conference, 5-7 September 2016, Manchester, UK.
- R. a. Haslam, S. A. H., A. G. F. Gibb, D. E. Gyi, T. Pavitt, S. Atkinson, and A. R. Duff. (2005). Contributing factors in construction accidents. *Appl. Ergon.*, 36, 401-415.
- R.I. Coble, C. J. K. (1994). The environment as a construction Safety Concern. Paper presented at the Proceedings of the 5th Annual Rinker International Conference focusing on Construction Safety and Loss Control, Florida.
- S. Sousa, J. T. (2004). Prevention measures to reduce risk of falling from heights. Paper presented at the IX National Symposium of ISMAI, Porto, Portugal.
- Salma A. Iqbal, M. I., Md. Zubair Taufiq and Md. Shamim Ahmed. (2010). Identification of occupational injury among the workers of selected cement industries in Bangladesh: a case study. *Journal of Chemical Engineering, IEB*, 25(1), 22-28.
- Smallwood, J. J. (2000). The holistic influence of design on construction health and safety (H&S): General contractor (GC) perceptions. Paper presented at the Proceedings of the Designing for Safety and Health Conference, London, UK.
- SRS. (2010). Safety and Rights Society Annual report: Workplace deaths in Bangladesh in 2010. Dhaka, Bangladesh: Safety and Rights Society.
- SRS. (2011). Safety and Rights Society Annual report: Workplace deaths in Bangladesh in 2011. Dhaka, Bangladesh: Safety and Rights Society.
- SRS. (2012). Safety and Rights Society Annual report: Workplace deaths in Bangladesh in 2011. Dhaka, Bangladesh: Safety and Rights Society.
- SRS. (2013). Safety and Rights Society Annual report: Workplace deaths in Bangladesh in 2013. Dhaka, Bangladesh: Safety and Rights Society.
- SRS. (2014). Safety and Rights Society Annual report: Workplace deaths in Bangladesh in 2014. Dhaka, Bangladesh: Safety and Rights Society.
- SRS. (2015). Safety and Rights Society Annual report: Workplace deaths in Bangladesh in 2015. Dhaka, Bangladesh: Safety and Rights Society.
- Stanley, J. (2010). The causes of construction accidents and what to do about them: Workplace Safety Blog.

- Tanim, M. F. C. a. T. R. (2016). Industrial Accidents in Bangladesh Apparel Manufacturing Sector: An Analysis of the Two Most Deadliest Accidents In Histor. *Asian Journal of Social Sciences and Management Studies*, 3(2), 115-126.
- WEF. (2016). Industry Agenda Shaping the Future of Construction: A Breakthrough in Mindset and Technology. www.Weforum.org.

APPLICABILITY OF UNSTEADY RANS FOR PREDICTING FLOW FIELDS AROUND CYLINDERS

Md. N Haque

¹Assistant Professor, Department of Civil Engineering, East West University, Bangladesh, e-mail: naimul@ewubd.edu

ABSTRACT

Accurate prediction of aerodynamic response mostly depends on the accurate modelling of turbulence. A number of turbulent modelling has been proposed over the years and each of them has its own merits and demerits. Unsteady RANS with $k-\omega$ -SST turbulence model is one of the popular simulation techniques which is computationally less expensive as compared to the others. In the present study, the performance of unsteady RANS is checked for other bluff bodies such as rectangular ($R = \text{width/depth} = 3$) and circular cylinders at Reynolds number (Re) of 1.2×10^4 . Simulations were conducted for a rectangular cylinder with a side ratio (R) of 3 and circular cylinders by using an open source code called OpenFOAM. The mean and rms values of steady state force coefficients were evaluated and compared with the previous experimental data. The mean pressure coefficients were also calculated at the bluff body surface. It was found that the unsteady RANS with $k-\omega$ -SST turbulence model can efficiently predict the aerodynamic responses around the selected bluff bodies.

Keywords: Unsteady RANS; rectangular cylinder; circular cylinder, force coefficient and pressure coefficient etc.

1. INTRODUCTION

Prediction of accurate wind load on structure is one of the most important engineering challenges. In conventional way, wind tunnel experiment is carried out to predict the wind load or aerodynamic responses of the structure. Wind tunnel is a reliable method of predicting wind loads on structure. However, wind tunnel is quite expensive and model setup procedure is also complicated. Moreover, through wind tunnel experiment one can obtain result in a limited location only. In contrary to wind tunnel experiment, Computation Fluid Dynamics (CFD) has overcome most of these limitations. Now-a-days, CFD has drawn attention of researchers of various fields and it is being used as a research tool. However, obtaining an accurate result through CFD simulation is not straightforward. To obtain an accurate result, users need to pay attention for a number of critical issues, such as turbulence model, numerical schemes, boundary condition, domain size, temporal and spatial discretization etc. Sufficient background studies required to be carried out for these issues to produce recommendations and proper guidelines regarding those issues.

Most of these issues were rigorously addressed in the literature (Murakami and Mochida 1989; Yu and Kareem 1996, Rodi, Ferziger, Breuer, & Pourquie, 1997; Rodi 1997; Sohankar, Davidson and Norberg, 1998) and their influences on numerical results were investigated. However, still some issues need further analysis. For the selection of two-equation based turbulence model for two-dimensional simulation, it already known that $k-\omega$ -SST turbulence model has superiority than the other models. The applicability and performance of this model has also been checked in bluff body and bridge aerodynamics fields (Mirnada, Patruno, Ubertini & Vairo, 2014; Patruno, 2015 and Haque, Katsuchi, Yamada & Nishio, 2015). The flow behaviour around rectangular cylinders can be divided into three categories (Deniz and Staubli, 1997). The first category is the rectangular bluff section (Side ratio, $R \leq 2$) where the flow separates at the leading edge without any flow reattachment and vortices form at the

leading edge (LEV). For the rectangular cylinder with side ratio (R) in between 2 to 5, the flow reattaches intermittently at the side face of the body and the impinging leading edge vortices form (ILEV). The third category is the elongated bluff section ($R \geq 5$) where the flow reattaches at the side surfaces and trailing edge vortices form (TEV). In previous studies the performance and applicability of $k-\omega$ -SST was mainly checked for predicting aerodynamic responses of rectangular bluff sections of first and third categories. Therefore, it is also important to check the performance and applicability of $k-\omega$ -SST turbulence model for the remaining (second category) category of semi-bluff sections (ILEV). Moreover, the effect of other issues such as boundary condition, domain size, temporal and spatial discretization etc. on results depends on the selection of turbulence model. If the turbulence model changes, their effects on numerical results also changes. In past studies the influence of those issues were mainly checked for the other turbulence models, especially for the LES. Later, Haque et al. (2015) investigated the effects of spatial discretization on results and proposed guidelines for selecting appropriate grid resolution for $k-\omega$ -SST turbulence model. No research was dedicated to investigate the effect of domain size or to provide some guidelines to select the domain size using the $k-\omega$ -SST turbulence model.

In the present study detail domain sensitivity analysis is carried out for a rectangular cylinder using $k-\omega$ -SST turbulence model. The influence of upstream, downstream and height of the domain is varied and their influences on aerodynamic force coefficients are presented. The performance and applicability of unsteady RANS with $k-\omega$ -SST turbulence model is also checked for the rectangular cylinder with side ratio (R) of 3 where partial or intermittent flow reattachment occurs by comparing the results with past experimental data. Along with this the performance and applicability of $k-\omega$ -SST turbulence model is also checked for a circular cylinder with smooth surface.

2. NUMERICAL MODEL AND SETUP

Flow is assumed to be two dimensional, unsteady and incompressible in nature. The flow around the object is modelled by Reynolds-Averaged Navier-Stokes (RANS) equation. The governing equations are shown as follows;

$$\frac{\partial U_i}{\partial x_i} = 0 \quad (1)$$

$$\rho \frac{\partial U_i}{\partial t} + \rho U_j \frac{\partial U_i}{\partial x_j} = -\frac{\partial P}{\partial x_i} + \frac{\partial}{\partial x_j} (2\mu S_{ij} - \overline{\rho u'_j u'_i}) \quad (2)$$

The vectors U_i and x_i are velocity and position respectively, t is time, P is the pressure, ρ is the density, μ is the molecular viscosity and S_{ij} is the strain rate of tensor. Due to time averaging process, the new variable $\overline{\rho u'_j u'_i}$ appears, which is known as Reynolds stress. It needs modelling to close the equation. Turbulence modelling is attained by $k-\omega$ -SST model (Menter, 1994). An open source Finite Volume code OpenFOAM (V2.2.0) is used to evaluate the flow field numerically. The flow is discretized spatially by a structured non-uniform grid arrangement based on the recommendation given by Haque et al. (2015). Figure 1 shows the grid system. To confirm the stability during simulation, time step (Δt) is selected such that courant number (C_o) doesn't exceed 0.8. All the simulations are conducted for 600 non-dimensional time unit and during response analysis first 200 non-dimensional times unit data are ignored from the stability point of view. A uniform flow (Along the flow, $u=1$, across the flow, $w=0$) is prescribed at the inlet as a boundary condition. At the outlet, Neumann boundary condition is applied. At the top and bottom wall of the domain, slip boundary condition is implemented. No-slip and no-penetration boundary conditions are prescribed on the solid walls around the object.

3. RESULTLS AND DISCUSSION

3.1 Domain Sensitivity Analysis

At the present work, a detail domain sensitivity analysis is conducted at high Reynolds number of 1.2×10^4 for side ratio (R) of 3 (B/D) with the $k-\omega$ -SST turbulence model. In domain sensitivity analysis, upstream length (X_u), downstream length (X_d) and height (H) of the domain are changed and global response of the body is observed. All the dimensions are normalized with the height (D) of the object. All three chosen lengths are varied from 5 to 40 when one parameter is being changed; other two parameters are kept constant at the basic value as shown in Figure 2. Figure 3 shows the mean and root mean square (rms) values of steady state force coefficients for normalized distance of interest. As can be seen from the figure that all the response parameters become stable when the upstream distance (X_u) exceeds a value of 15. But a value less than 10 affects the response significantly. Sohankar and his associates (Sohankar, Davidson & Norberg, 1995 and Sohankar, Norberg & Davidson, 1996) recommended a normalized upstream distance of 10 to get independent result, which is a bit liberal according to the present investigation. Similarly, for the case of height of the domain (H), when the value exceeds 25 units all the responses become stable and no correction for blockage is required. No significant effect of outlet location is found on the mean results except rms. A normalized downstream length of more than 25 units would be a recommended value to keep outlet disturbance away from after body when Neumann type outlet boundary condition is used.

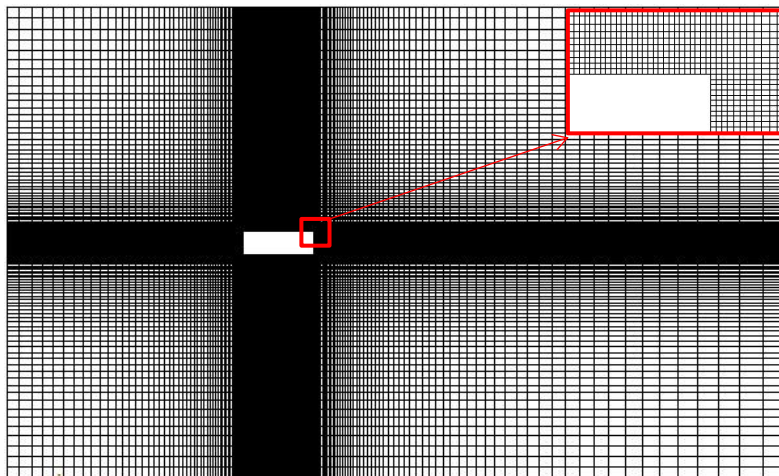


Figure 1: Non-uniform spatial discretization of the doamin

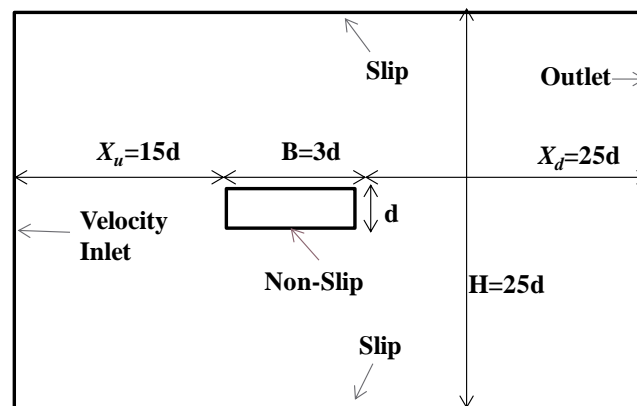


Figure 2: Boundary condition and domain size

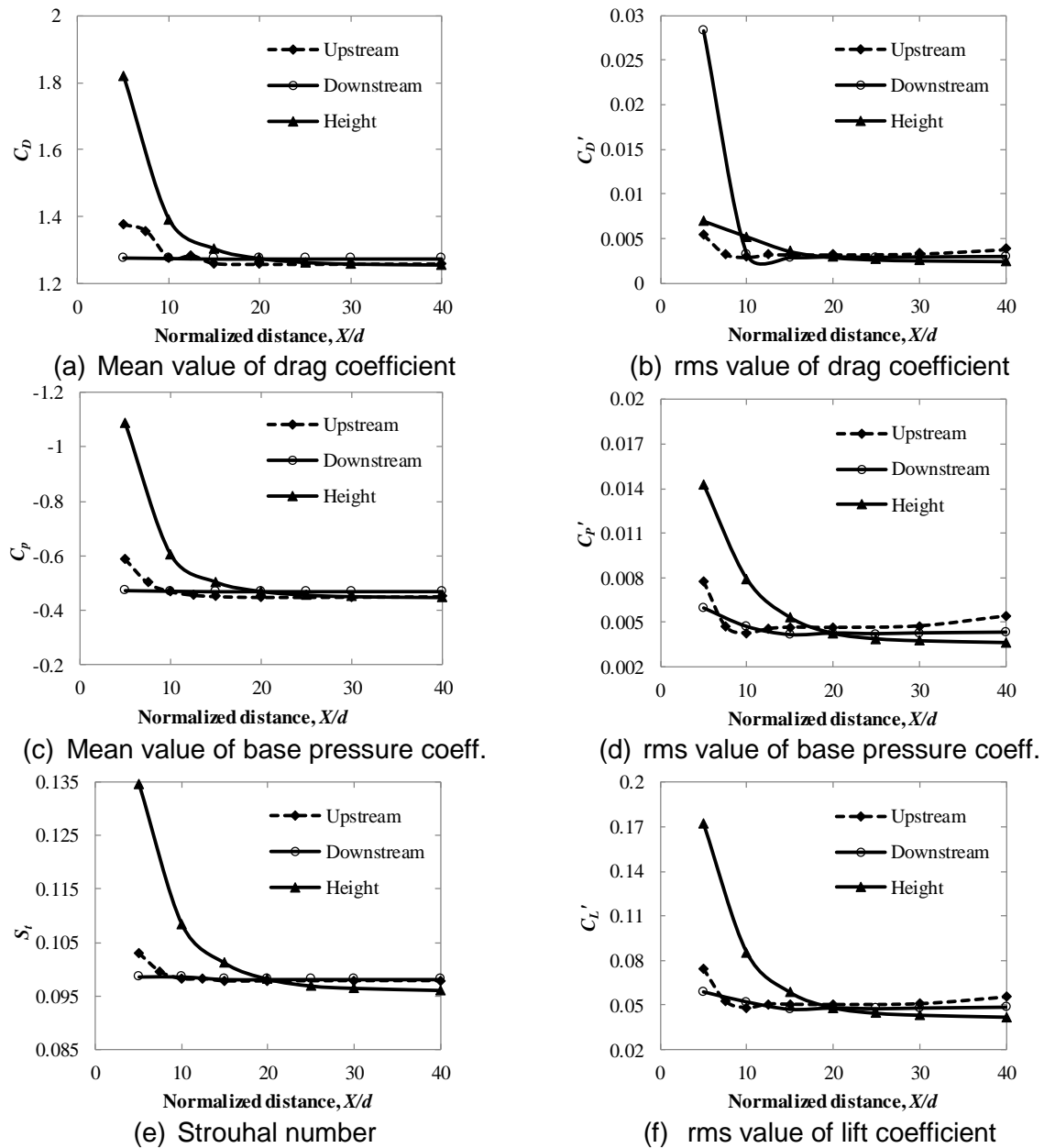


Figure 3: Influence of domain size on steady state aerodynamic force coefficient

3.2 Aerodynamic Response of Rectangular Cylinder (R of 3)

To check the performance and applicability of unsteady RANS with $k-\omega$ -SST turbulence model for predicting aerodynamic response of semi-bluff section with ILEV, simulation is conducted for a rectangular cylinder of side ratio, $R=3$. Table 1 compares the calculated steady state force coefficients with the experimental data. As can be seen the calculated drag force coefficient is very close to the experimental one. Similar to the drag force, the present turbulence model could predict the Strouhal number (S_t) very close to the experimental one. For better comparison of the obtain results, Figure 4 compares the surface pressure coefficients with the experimental data. The $k-\omega$ -SST turbulence model grasps the surface pressure distribution quantitatively. Small discrepancy can be noticed at the top surface leading edge corner. However, except that the present turbulence could predict the aerodynamic responses quite efficiently.

Table 1: Aerodynamic characteristics of rectangular cylinder with a side ratio (R) of 3 at $Re=1.2 \times 10^4$

	C_d	C_L'	S_t
Current CFD	1.28	0.349	0.125
Exp. of Nakaguchi, Hashimoto & Muto(1968) at $Re=2-6 \times 10^4$	1.25		
Exp. of Norberg (1993) at $Re=4 \times 10^4$	1.24		0.155

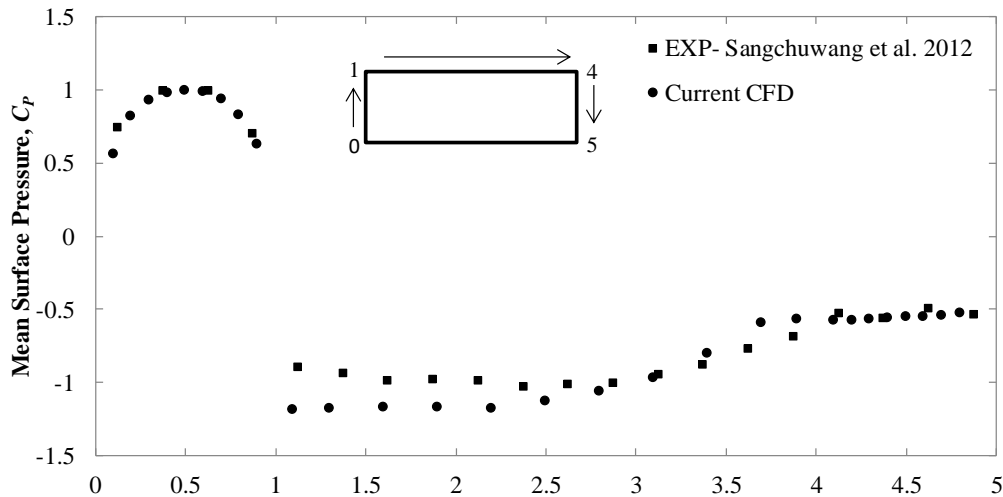


Figure 4: Surface pressure distribution around rectangular cylinder (R of 3) at Re 1.2×10^4 . Experimental work: Sangchuwang, Yamada & Katsuchi, 2012.

3.3 Aerodynamic Response of Circular Cylinder

The performance and applicability of is also checked for the circular at Reynolds number (Re) of 1.2×10^4 . Table 2 shows the calculated steady state force coefficients. The current simulation also could predict the aerodynamic responses with reasonable accuracy. Figure 5 compares the mean surface pressure around circular cylinder with previous experimental work. The $k-\omega$ -SST maps the mean pressure accurately but a slight discrepancy at the flow separation point can be found. One important reason could be limitation of the turbulence model itself and another reason could be the variation of Reynolds number between the present and experimental one.

Table 2: Aerodynamic characteristics of circular cylinder at $Re=1.0 \times 10^4$. Previous works: Cantwell and Coles (1983) at $Re=1.5 \times 10^4$, Wieselsberger (1921) at $Re=1.5 \times 10^4$, Ribner and Etkin (1958) at $Re=1.5 \times 10^4$, Mustto and Bodstein (2011) at $Re=4 \times 10^4$.

	C_D	C_D'	C_L	C_L'	S_t
Current CFD	1.48	0.078	0.00377	1.128	0.191
Exp. (Cantwell & Coles 1983)	1.18				
Exp. (Wieselsberger 1921)	1.16				
Exp. (Ribner & Etkin 1958)					0.191
Numerical (Mustto & Bodstein 2011)					0.177

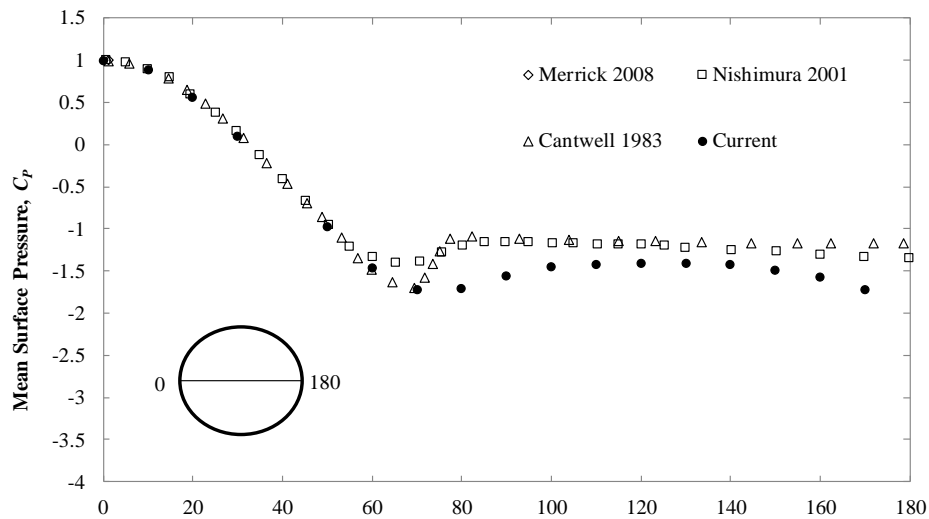


Figure 5: Surface pressure distribution around circular cylinder at $Re=1.2 \times 10^4$. Experimental results are: Merrick & Bitsuamlak (2008) at $Re=2.8 \times 10^5$; Nishimura & Taniike (2001) at $Re=6.1 \times 10^4$; Cantwell & Coles (1983) at $Re=1.4 \times 10^5$

4. CONCLUSIONS

In the present paper, the performance and applicability of $k-\omega$ -SST turbulence is checked for simulating aerodynamic responses of semi-bluff section. Domain sensitivity analysis is carried out and simulations are performed for circular cylinders as well. Steady state force coefficients and surface pressure distribution are calculated and compared with the experimental results. Based on the observation and discussion, the following important conclusions are drawn,

- i) For 2D RANS simulation with $k-\omega$ -SST turbulence model, inlet of the domain should be located at least 15D upstream of the object, outlet should be more than 20D downstream of the object and height of the domain should be at least 25D. A value less than 10D for upstream, 15D for downstream and 20D for height of the domain would alter the steady state responses significantly.
- ii) It can be concluded that the Unsteady RANS with $k-\omega$ -SST turbulence model can predict the mean aerodynamic responses around the semi-bluff bodies having ILEVs both qualitatively and quantitatively. The Unsteady RANS failed to predict the responses accurately at the location of flow separation. Therefore, when this method is adopted to obtain the aerodynamic responses of bluff bodies with more complex shapes, especial care should be taken during the time of explaining the aerodynamic responses.

REFERENCES

- Cantwell, B. and Coles, D. (1983). An experimental study of entrainment and transport in the turbulent near wake of a circular cylinder. *Journal of Fluid Mechanics*, 136, 321–374.
- Deniz, S. and Staubli, T. (1997). Oscillating rectangular and octagonal profiles: interaction of leading- and trailing-edge vortex formation. *Journal of Fluids and Structures*, 11, 3-31.
- Haque, M.N., Katsuchi, H. Yamada, H. and Nishio, M. (2015). Strategy to develop efficient grid system for flow analysis around two-dimensional bluff bodies. *KSCE Journal of Civil Engineering*, 20(05), 1-12.

- Merrick, R. and Bitsuamlak, G.T. (2008). "Control of flow around a circular cylinder by the use of surface roughness." 4th International Conference on Advances on Wind and Structures (AWAS08), 29-31 May 2008, Jeju, Korea.
- Miranda, S.D., Patruno, L., Ubertini, F. and Vairo, G. 2014. On the identifications of the flutter derivatives of bridge deck via RANS turbulence models: Benchmarking on rectangular prisms. *Engineering Structures*, 76, 359-370.
- Murakami, S. and Mochida, A. (1995). On turbulent vortex shedding flow past 2D square cylinder predicted by CFD. *Journal of Wind Engineering and Industrial Aerodynamics*, 54-55,191-211.
- Mustto, A.A. and Bodstein, G.C.R. (2011). Sub-grid scale modeling of turbulent flow around circular by mesh-free vortex method. *Engineering Application of Computational Fluid Mechanics*, 5(2), 259-275.
- Nakaguchi, H., Hashimoto, K., Muto, S., (1968). An experimental study on aerodynamic drag of rectangular cylinders. *J. Japan Soc. Aeronaut. Space Sci.* 16,1-5 (in Japanese).
- Nishimura, H. and Taniike, Y. (2001). Aerodynamic characteristics of fluctuating forces on a circular cylinder. *Journal of Wind Engineering Industrial Aerodynamics*, 89,713-701.
- Norberg, C. (1993). Flow around rectangular cylinders: pressure forces and wake frequencies. *Journal of Wind Engineering and Industrial Aerodynamics*, 49,187-196.
- Patruno, L. (2015). Accuracy of numerically evaluated flutter derivatives of bridge deck sections using RANS: Effects on the flutter onset velocity, *Engineering Structures*, 89, 49-65.
- Ribner, H.S. and Etkin, B. (1958). "Noise research in Canada." Proc. 1st International Congr. Aero. Sci., Madrid, Pagamon press, London,1958.
- Rodi, W., Ferziger, J., Breuer, M., and Pourquie', M. (1997). Status of Large- Eddy Simulations: Results of a Workshop, *ASME Journal of Fluids Engineering*, 119, 248–262.
- Sangchuwong, P., Yamada, H. and Katsuchi, H. (2012). Study on turbulence effects on flow fields around sharp-edged bluff bodies. *Journal Structural Engineering (JSCE)*, 59A, 627-636.
- Sohankar, A., Davidson, L., Norberg, C. (1995). "Numerical simulation of unsteady flow around a square two-dimensional cylinder." Proc. Twelfth Australasian Fluid Mechanics Conf. 10-15 December, 1995, Sydney, Australia, 517-520.
- Sohankar, A., Norberg, C., Davidson, L. (1996). "Numerical simulation of unsteady low-Reynolds number flow around a rectangular cylinder at incidence." Proc. 3rd Int. Colloq. on Bluff Body Aerodynamics and Applications, July 28- 1 August 1996, Virginia, USA.
- Sohankar, A., Davidson, L., and Norberg, C. (1998). Low- Reynolds- number flow around a square cylinder at incidence: study of blockage, onset of vortex shedding and outlet boundary condition. *International Journal for Numerical Methods in Fluids*, 26, 39-56.
- Wieselsberger, C. (1921). Neuere feststellungen .uber die gesetze des fl. ussigkeits und luftwiderstands, *Phys. Z.* 22, 321–328.
- Yu, D., Kareem, A., (1996). Two-dimensional simulation of flow around rectangular prisms. *Journal of Wind Engineering and Industrial Aerodynamics*, 62, 131-161.

THE EFFECT OF FIRE ON THE STRENGTH OF CONCRETE MATERIAL

HM Iqbal Mahmud¹, MD Kawser Babu Raju² and Md Lokman Hosen³

¹ Associate Professor, Khulna University of Engineering & Technology, Bangladesh,
e-mail: iqbal.mahmud@ce.kuet.ac.bd

² Undergraduate Student, Khulna University of Engineering & Technology, Bangladesh,
e-mail: kawserahmed1201114@gmail.com

³ Undergraduate Student, Khulna University of Engineering & Technology, Bangladesh,
e-mail: mlh1201073@gmail.com

ABSTRACT

Structural members exposed to fire may damage considerably and loss its durability even may collapse due to failure of the member of a building. This work presents the results of an experimental investigation of the effect of fire on the strength of concrete. Cylindrical and beam specimens were prepared and burnt in fire for a duration of one hour, without any imposed load during the burning. In both cases, two systems were followed for cooling the samples, (i) natural cooling in air (ii) forced cooling in water. Afterward the compressive and flexural strength of the specimens were examined. Surface cracking pattern and spalling in the specimens due to burning were also investigated. The result shows that the strength of concrete was considerably reduced due to burning in fire. The compressive strength of cylindrical specimens was decreased 60% and 44%, respectively, for forced and natural cooling of the specimens. In case of beam samples, the flexural strength was decreased 69% and 60%, respectively, for the forced and naturally cooled specimens. This research also reveals that the specimen cooled in air showed better performance compared to that cooled in water.

Keywords: Concrete, compressive strength, fire, natural cooling, forced cooling.

1. INTRODUCTION

The recent fire incidents are alarming the risk of fire and safety issues in Bangladesh. It is one of the major causes of huge damage and losses of properties in Bangladesh (Digester report, 2013). For building construction, concrete is one of the main load carrying parts of a reinforced concrete structure. However, the strength of concrete is significantly affected due to high temperature of fire. This may causes in undesirable structural failures (Ali et al., 2004; Georgali and Tsakiridis, 2005 and Xiao et al., 2005). During a fire, the temperature may reach up to 1100°C in buildings and even up to 1350°C in tunnels (Hager, 2013). The exposure of concrete structural elements to high temperature leads to significant losses in its structural capacity due to the reduction in its strength of the concrete and most importantly due to loss of bond between aggregate and binding materials (Khalaf, 2017). So, the information on the degree of strength degradation is required for structural design of fire safety and structural repair after a fire incident. This evaluation of degree of deterioration of the concrete properties will enable engineers to decide whether a structure after exposure to high temperatures can be repaired rather than required to be demolished. Another essential concern is cooling of the concrete member during or after a fire incident. The method of cooling of a hot concrete member may affect its strength. If a concrete member is cooled slowly or naturally in air, the property of it may differ from that one cooled immediately in water. Because due to sudden cooling in water thermal stress is developed in the concrete. Thus, it is necessary to investigate the mechanical properties of concrete to predict about its lifetime and durability after a fire hazard. Hence, this study aims to investigate the effect of fire on the mechanical properties of concrete. The specific objectives of this study can be listed as below.

1. To investigate the effect of burning of concrete specimens in fire by testing the compressive and flexural strength of the burnt specimens.
2. To investigate the effect of cooling process on the hot specimens after burning in fire.
3. To investigate the physical effects of fire (spalling, cracks etc.) on the specimens.

2. METHODOLOGY AND EXPERIMENTAL PROGRAM

2.1 Materials

For the preparation of concrete, ordinary Portland cement, sylhet sand (fine aggregate) and locally available stone chips were used. The nominal size of the coarse aggregate was 19 mm. The properties of fine and coarse aggregates are presented in Table 1.

Table 1: Material properties.

Materials	Properties	Value
Coarse Aggregate	Specific Gravity	2.45
	Absorption, %	3.34
	Unit Weight, Kg/m ³	1510
Fine Aggregate	Specific Gravity	2.54
	Absorption, %	2.74
	Fineness Modulus	2.65
	Unit Weight, Kg/m ³	1615

2.2 Preparation of test Specimens

The casting of specimens was completed with a mix ratio of 1:1.5:3, giving a water to cement ratio of 0.635 with target strength of 3500 psi (24 MPa). At each time of casting of concrete specimen slump was determined and it was within 100-120 mm. Nine cylindrical specimens of diameter 100 mm and height 200 mm were prepared to determine the compressive strength of concrete after burning in fire. Among these nine specimens, three specimens were used as the reference specimens (virgin specimen), which were tested without burning in fire and other six specimens were burnt in fire. Out of six specimens, which were burnt in fire, three were cooled naturally in air and three were cooled forcedly in water. Similar to the cylindrical specimens, nine numbers of beam specimens of 100 × 100 mm cross section and 450 mm long were casted to examine the flexural strength of concrete. Among the nine specimens, three were kept for testing without burning (virgin specimens) and six were kept for burning in fire. Among the six specimens, which were kept for burning, three were cooled naturally in air and three were cooled forcedly in water.

2.3 Burning of the specimens



(a)



(b)

Figure 1: Placing the specimens in the fire chamber; (a) cylindrical specimens, (b) beam specimens.

A fire chamber was prepared to burn the samples in fire as shown in Figure 1. The chamber was in a dimension of 500×500×600 mm. The specimens were kept inside the chamber and fire was produced by dry wood. The wood was placed by layer so that the sufficient oxygen could flow during fire. Then specimens were placed on a platform prepared by steel placing above the layer of fire wood. The fire temperature during burning of the specimens was about 800 – 1000°C. For both cases, the specimens were burnt in fire for a duration of one hour, without any imposed load on the specimens during the burning.

2.4 Cooling of the specimens

After burning the specimens, they were cooled in two processes. Among the six cylindrical specimens, three were immersed in water immediately after burning in fire and three were kept in open air for natural cooling. The first process of cooling represents the immediate cooling of the specimens which is resemble to the application of water in a building for the suppression of fire by the fire-fighters during a fire incident in that building and the second process resembles to the cooling of the structural members of a building after a fire incident without any application of water or any other fire suppression agent. The same two cooling processes were applied to beam specimens.

2.5 Testing of the specimens

After performing the burning and cooling processes, the specimens were tested in the laboratory. The cylindrical specimens were crushed by compressive testing machine and the ultimate capacity of the samples was recorded. The flexural strength of concrete beams was determined by testing the specimens following the three point loading test method. The results are summarised in the following sections.

3. RESULTS AND DISCUSSIONS

3.1 Compressive strength of the cylindrical specimens

In this study, nine cylindrical specimens were tested and the compressive strength of concrete was determined. Among the nine specimens, as described in the previous section, three were tested without burning (virgin sample), six samples were burnt in fire. The specimens were burnt for 60 minutes. After the burning the specimens in fire, three were kept in open air for natural cooling and three were immersed in a water chamber for immediate cooling. Afterward, the specimens were tested in compression testing machine and the results are summarised in Table 2.

Table 2: Test results of compressive strength of the cylindrical specimens.

Test condition		Sample No	Compressive Strength (MPa)	Average Compressive Strength (MPa)	Average % Loss of Strength with Respect to the Virgin Sample
Samples without burning in fire	Virgin sample	1	23.17	23.33	—
		2	23.44		
		3	22.95		
Samples burnt in fire	Natural cooling	1	14.63	12.95	44%
		2	12.40		
		3	11.82		
	Forced cooling	1	10.24	9.25	60%
		2	9.13		
		3	8.51		

The strength of samples, burnt and cooled at different ways, was compared to that of the virgin sample and presented in Figure 2. In the analysis it has been observed that the

strength of concrete was decreased considerably due to the burning in fire. The average compressive strength of the unburnt specimens was 23.33 MPa, whereas this strength for burnt samples was only 12.95 and 9.25 MPa, for naturally and forcedly cooled specimens, respectively. The average percent loss of strength due to burning in fire was 44% and 60%, for naturally and forcedly cooled specimens, respectively.

This study also reveals that the specimens cooled in air showed better strength compared to that cooled in water. The possible reason is that due to sudden cooling in water, the outer surface of the sample was cooled immediately but the inner part of the sample was in high temperature. As a result, thermal stress was developed in the sample which may lead to crack in the specimens. However, this requires further detail investigation to examine the specific reason for degradation of strength due to sudden cooling of hot concrete specimens in water.

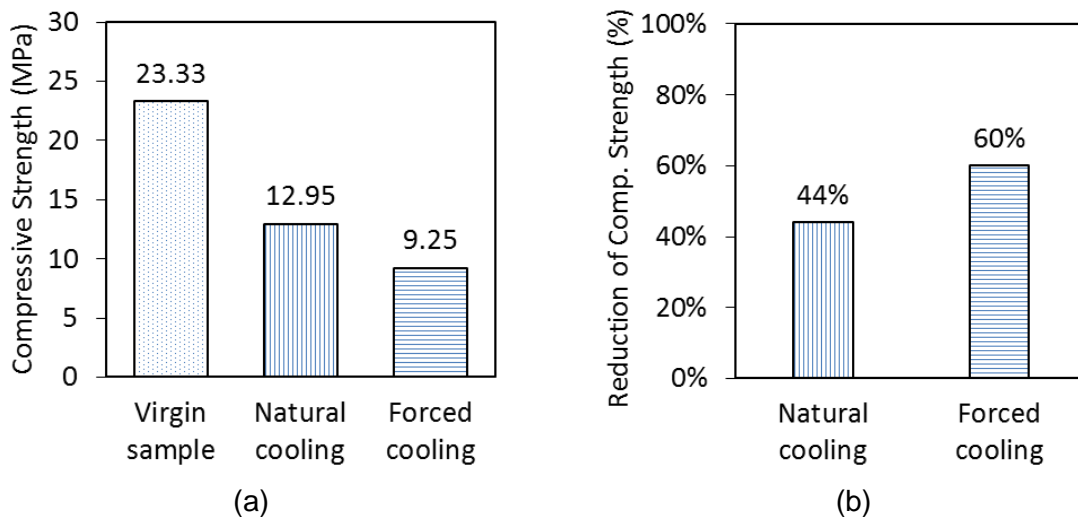


Figure 2: Comparison of test results of compressive strength of cylindrical specimens at different conditions; (a) compressive strength, (b) reduction of compressive strength.

3.2 Flexural strength of the beam specimens

Nine beam specimens were tested and the flexural strength of concrete was determined. The flexural strength from the tests of the specimens at ambient temperature and after exposed to fire at high temperature are presented in Table 3.

Table 3: Test results of flexural strength of the beam specimens.

Test Condition		Sample No	Flexural Strength (Mpa)	Average Flexural Strength (Mpa)	Average % Loss of Strength with Respect to the Virgin Sample
Specimens without burning in fire	Virgin sample	1	6.80	6.40	-
		2	6.45		
		3	5.98		
Specimens burnt in fire	Air cooling	1	2.90	2.55	60%
		2	2.48		
		3	2.28		
	Water cooling	1	2.27	2.00	69%
		2	2.02		
		3	1.85		

In the analysis, it has been observed that the strength of the specimens was significantly reduced due to burning in fire. The effect of cooling process on the strength of beam was also examined in the experiment, as it was done in the cylindrical specimens. In the analysis it has been found that the average flexural strength was 6.4 MPa at ambient temperature whereas this value was 2.55 MPa and 2.0 MPa for naturally and forcedly cooled specimens, respectively. Due to burning in fire, the flexural strength was reduced about 60% and 69% for natural cooling and forced cooling of the specimens, respectively. The result also reveals that due to sudden cooling of the sample in water, the strength of the concrete reduced more than the sample cooled slowly in natural air. The comparison of results is also presented graphically in Figure 3.

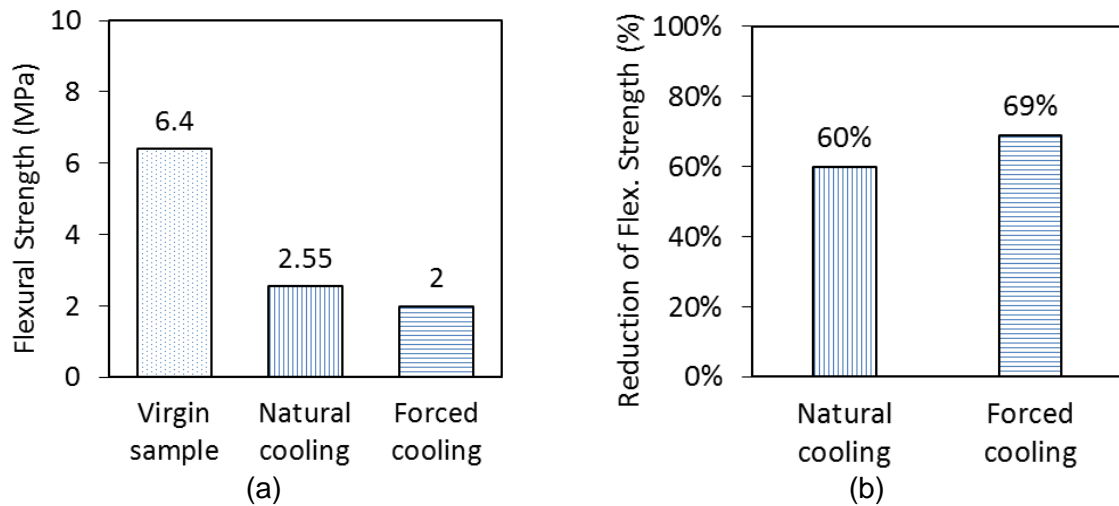


Figure 3: Comparison of test results of flexural strength of beam specimens at different conditions; (a) flexural strength, (b) reduction of flexural strength.

3.3 Spalling and cracks in the specimens

Spalling and cracking are common phenomenon in concrete during burning in. As concrete is not a product of a single material, when it is exposed to fire or high temperature, cracks develop in it due to the thermal incompatibility among the individual ingredient of concrete (i.e. coarse aggregate, fire aggregate and cement). Spalling results in loss of volume in concrete member and reduction in the load bearing capacity of the member. These phenomena were also observed in our experiment during the burning of the samples and shown in Figures 4. In the analysis, it has been found that the affected average surface area and volume of spalling in the tested specimens were 4% and 2.5%, respectively, for cylindrical specimen. Similarly, the reduction of area and volume was found to be about 0.64% and 0.52%, respectively, for the beam specimen.



Figure 4: Spalling and cracks in specimens; (a) spalling in cylindrical specimen, (b) cracks in beam specimen.

4. CONCLUSIONS

This study was aimed to evaluate the behaviour of concrete beam exposed to fire. The effect of cooling process on the burnt specimens of concrete was also investigated. Nine cylindrical and nine beam specimens of concrete were prepared for test. Among the nine cylindrical specimens, three were used as virgin specimens, which were tested without burning in fire and six specimens were burnt in fire. To examine the effect of cooling process, out of six specimens burnt in fire, three were cooled naturally in air and three were cooled immediately in water. The natural cooling in air represents the slow process of cooling and forced cooling in water represents immediate cooling which is resemble to the suppression of fire by the fire-fighters during a fire incident in a building. Same procedure was also followed for the nine beam specimens. Subsequently, all of the specimens were tested in the compression testing machine.

The result shows that both compressive and flexural strength of concrete were reduced significantly due to burning in fire. The strength of concrete was also affected by the cooling process of the sample. It has been found that the strength of concrete was reduced more due to immersion in water compared to the samples cooled naturally in air. The compressive strength of concrete was reduced about 60% and 44% for forced cooling and natural cooling, respectively, compared to that of the unburnt specimen. In case of the beam specimens, the flexural strength of concrete was reduced, due to burning in fire, about 60% and 69%, for natural cooling and forced cooling of the samples, respectively. The spalling of concrete due to burning in fire was 2.61% and 0.52% in volume of the specimen for cylindrical and beam specimen, respectively. Further study is recommended to examine the effect of fire on reinforced concrete beam.

ACKNOWLEDGEMENTS

The authors want to express gratefulness to the technicians of the Engineering Materials Laboratory of Department of Civil Engineering, Khulna University of Engineering & Technology, for their warmth cooperation.

REFERENCES

- Ali, F., Nadjai, A., Silcock, G. and Abu-Tair, A. (2004). "Outcomes of a major research on fire resistance of concrete columns." *Fire Safety Journal*, Vol. 39, pp. 433–445.
- Department of Disaster Management. (2013). "Disaster Report." Ministry of Disaster Management & Relief, Government of the People's Republic of Bangladesh, pp. 60.
- Khalaf, J. (2017). "Development of non-linear bond stress-slip models for reinforced concrete structures in fire." *PhD thesis*, Brunel University, London.
- Georgali, B. and Tsakiridis, P.E. (2005). "Microstructure of fire-damaged concrete - A case study." *Cement and Concrete Composites*, Vol. 27, pp. 255–259.
- Hager, I. (2013). "Behaviour of cement concrete at high temperature." *Bulletin of the Polish Academy of Sciences: Technical Sciences*, 61(1), pp. 145-154.

RE-STRENGTHENING OF REINFORCED CONCRETE (RC) BEAM USING NEAR SURFACE MOUNTED (NSM) STEEL RE-BARS

Mohammad Nurul Mobin¹ and Md.Foisal Haque²

¹ Graduate Student, Dhaka University of Engineering & Technology, Gazipur, Bangladesh, e-mail: nurul9901@gmail.com

² Graduate Student, Dhaka University of Engineering & Technology, Gazipur, Bangladesh, e-mail: mfh.civil@gmail.com

ABSTRACT

Strengthening of structures has become a highly sought after solution to improve inadequate, weak structures. Strengthening of reinforced concrete (RC) members using externally bonded reinforcement (EBR) is a well established technology that is in widespread use. However, near surface mounted (NSM) reinforcement technique is a promising alternative due to several key advantages in terms of bonding and protection. This paper presents a study on the flexural behavior of NSM steel strengthened RC beams made of brick aggregate concrete. Four-point bending tests were carried out up to failure on four rectangular RC beams, each of 150 mm width, 200 mm depth and 2100 mm length. One beam was left un-strengthened to act as the control beam. All other beams were strengthened with different ratios of steel reinforcements, of them two used epoxy adhesive as bonding material, while for the other two beams cement paste was used. Yield and ultimate strengths, flexural failure modes, effect of adhesives, cracking behavior and ductility are reported and discussed based on measured load and deflection. The test results show that flexural strength increased up to 102.4%, excellent ductility and ductile failure mode.

Keywords: Retrofitting, flexural strengthening, RC, NSM, Steel, cement paste, epoxy, Brick chips.

1. INTRODUCTION

Strengthening of existing structures or structural elements becomes a necessity due to ageing, environmentally induced degradation, poor initial design and/or construction, lack of maintenance, seismic upgrade and meeting new code requirements (*fib Bulletin 14*, 2001). In a frame structure, the chief load carrying members are beams and columns. That is why RC beam strengthening is an important issue of structural upgrading. Quite a few techniques have been developed over the years to strengthen or retrofitting of RC beams. One method, that is widely used to strengthen the deficient flexural strength of RC beams is Externally Bonded Reinforcement (EBR) technique. The technique originally pioneered simultaneously in South Africa and France in the 1960s (Fleming & King, 1967) requires adhering additional reinforcements like steel plates or fibre reinforced polymers (FRP) laminates. Although capable of achieving significantly higher capacity, EBR method has some major shortcomings. Firstly, the reinforcements are exposed which makes it vulnerable to rusting (in case of steel), fire, vandalism and other thermal, environmental and mechanical damage (Hosen *et al*, 2014). At the same time there is a high possibility of brittle failure like debonding and delamination. All these weaknesses adversely affect the durability and prevents achieving the full capacity of strengthening reinforcements (Brena *et al*, 2001; Hawileh *et al*, 2014).

Another promising strengthening technique is Near Surface Mounting (NSM) reinforcement. The idea of NSM reinforcement started in Europe by using steel bars between 1940 and 1950 (Bournas & Traintafillou, 2008). The NSM technique involves cutting grooves into the concrete cover and bonding the bars into the grooves by using appropriate adhesive material such as epoxy resin or cement mortar (Petrina, 2009). The advantage of NSM over

EBR is that the concrete cover and adhesive provide protection against corrosion, fire, vandalism and mechanical damage (Wuertz, 2013). Another advantage of NSM technique is that it can be implemented in the negative moment regions unlike the EBR method (El-Hacha & Rizkalla, 2004). Also, the NSM technique can delay the debonding of the reinforcement, compared to EBR method while retaining all the advantages the latter offers. The use of FRP composites though very popular in enhancing the capacity to large extent (El-Hacha & Rizkalla, 2004; De Lorengis & Nanni, 2002), also suffer from certain disadvantages: low ductility, strain incompatibility with concrete, not readily available and extra large cost of both reinforcing and adhesive materials. Due to availability of steel bars combined with its economy, sufficient strength, excellent ductility, long-term durability, good bond performance and strain compatibility with concrete (Rahal & Rumaih, 2011), also acquaintance of the local people to work with, NSM with steel bars has all the ingredients to become a very suitable proposition. NSM strengthening using steel bars has been used on masonry buildings and arch bridges (Garrity, 2001; Asplund, 1949). Crushed bricks are extensively used in Bangladesh for concrete making due to its economy and availability. Due to satisfactory performances of such concrete (Akhtaruzzaman & Hasnat, 1983), the beams under investigation will use crushed bricks as coarse aggregates.

Ductility is the ability of a material to undergo plastic (non-reversible) deformation before failure. Ductility is an essential property of a structure which gives ample warning before any impending failure thus catastrophic losses can be avoided. So, identifying the strengthening material which gives better ductility is important. Ductility is generally measured by the ratio of the ultimate deformation to that at the first yielding of steel reinforcement (strain = 0.002).

In this paper the structural behaviour of RC beams strengthened with NSM steel bars and exposed to flexural loading is investigated. The test variables are strengthening reinforcement ratio, adhesive materials and yield and ultimate strength. Load and deflection are analysed to understand cracking behaviour, failure modes and ductility of the tested beams.

2. EXPERIMENTAL PROGRAMME

2.1 Specimen Geometry and Reinforcement

The beams were designed as under reinforced beams to initiate failure in flexure, in accordance with the BNBC2006. The cross-sectional dimensions of the beams were 150 mm x 200 mm and the length of the beams was 2000 mm with 1350 mm as the effective span. The main flexural reinforcement consists of 2-8mm bars with 2-6mm bars used for compression steel and to help form the cages. The shear reinforcement consists of 8mm stirrups spaced 75mm center to center throughout the span. This excessive shear reinforcement was used to eliminate any possibility of Shear failure.

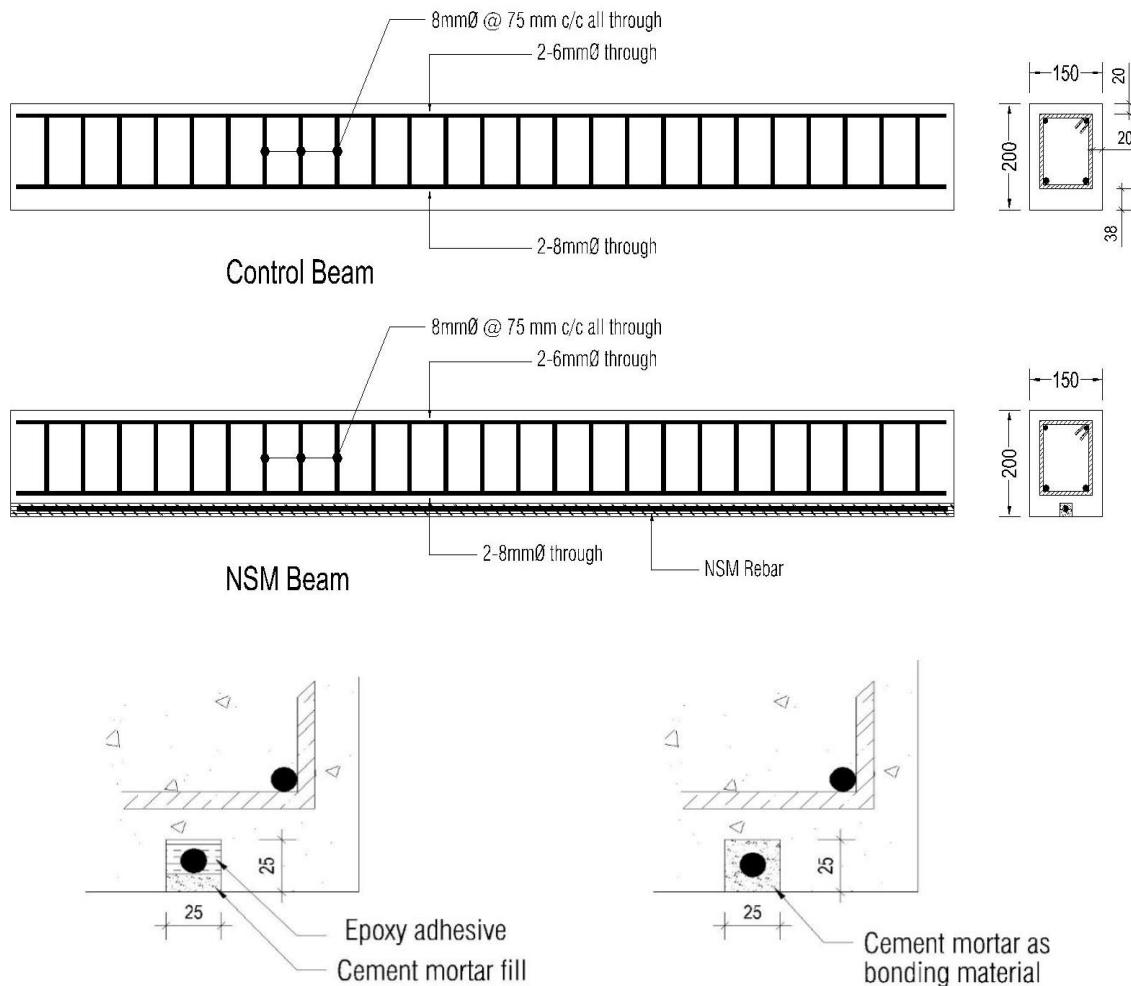
The materials of the present experimental program are concrete, steel reinforcing bars, epoxy adhesive. The mechanical properties of epoxy adhesive have been provided by the manufactures. Whereas, tensile tests for both the longitudinal and transverse steel reinforcement and compression tests for the concrete 100 mm x 200 mm cylinders were done in the laboratory.

2.2 Experimental Matrix

A total of five RC beam specimens were tested. The first beam specimen was the control beam with no strengthening and the remaining beam specimens were strengthened with steel bars of different diameters.

Table 1: Experimental Matrix

Beam ID	Strengthening Type	Bonding Material
CB-1 (control beam)	n/a	n/a
A-1	1-8 mm NSM steel bar	Epoxy adhesive
A-3	2-8 mm NSM steel bar	Epoxy adhesive
A-4	1-8 mm NSM steel bar	Cement mortar
A-5	2-8 mm NSM steel bar	Cement mortar



NSM Detailing
Figure 1: Details of Specimen

2.3 Material Properties

All the beam specimens were cast using normal concrete using Portland Composite Cement (PCC), coarse sand (FM > 2.5) as fine aggregates and crushed brick chips (20mm downgraded) as coarse aggregate. Fresh tap water was used to hydrate the concrete mix during the casting and curing of the beams, cubes, prisms and cylinders. The concrete mix ratio was 1:1.5:3 with a water/cement ratio (w/c) of 0.50 which required 193 kg/m³ of water, 654 kg/m³ of fine aggregate, 1186 kg/m³ of coarse aggregate and 386 kg/m³ of PCC. The 28

day's average compressive strength of the concrete was 28.67 MPa based on tests of three 100 mm x 200 mm concrete cylinders. The yield and ultimate strength of ϕ 8 mm steel bar was 446.76 MPa and 601.77 MPa respectively. The average yield and failure stress of the ϕ 10mm bar were 432.54MPa and 568.44 MPa, respectively. The modulus of elasticity for all bars was 200 GPa.

A two-part epoxy named Adesilex PG2 SP was used to bond the NSM bars to the specified Beams. The mixing procedures were followed as specified by the manufacturer to ensure a good bond to the concrete surface.

Table 2: Properties of Adesilex PG2 SP Epoxy

Strength Type	Strength (Mpa)	Final Hardening
Compressive Strength	80	7 days
Tensile Strength	30	
Flexural Strength	40	

2.4 Strengthening Procedure

In the NSM technique strengthening bars are placed into grooves cut into the concrete cover of the RC beams and bonded using epoxy adhesive groove filler. In this investigation, prior to the casting of experimental beams, 25mm x 25mm wooden rods of 2m length was placed to form grooves for NSM. A hammer and a hand chisel were used to chisel out the wooden rods and remove any remaining concrete lugs and to roughen the lower surface of the groove. The grooves were cleaned with a wire brush and water jet. The details of the grooves are shown in Figure 1.

To install the NSM bars on the beams using epoxy, the grooves were filled slightly more than one fourth depths, and then the bars were pushed into the grooves so that they were sufficiently surrounded by epoxy. More epoxy was then used to completely drown the bars into the adhesive paste. After that, the epoxy was allowed to sit for 24 to 36 hours to ensure proper curing and bonding. Finally, the remaining portions of the grooves were filled with cement mortar scraped off using trowel until flushed with the soffit of the beam. The mortar was cured for seven days.

For the beams in which cement is to be used as bonding material for NSM rebars, cement paste was made by mixing cement and water. The grooves were filled slightly more than halfway full, and then the bars were pushed into the grooves so that they were sufficiently surrounded by the cement paste. Excess paste was then used until it was flushed using trowel with the soffit of the beam. Once finished, the cement paste was cured for seven days to ensure proper bonding.

2.5 Experimental Set-up & Procedures

The flexural tests were performed in the material testing laboratory at DUET. The beams were loaded in four-point bending using a spreader beam of 450mm long effective span and a 250 KN beam testing machine. The loading jack was supported by two structural steel support columns and the columns were fastened to the laboratory RC strong floor. The actuator is controlled by a servo-electro hydraulic system operated by the technical staff. A load cell was placed under the centre of main loading point and at the top of spreader beam to measure the applied loads. Figure 2 shows the experimental test setup.

Two ten inches long linear variable differential transducer (LVDT) sensors were placed at mid-span on the top of the beams to measure deflection at mid-span. All of the instrumentation was wired into a channel data acquisition system called Megadac 200, a

system developed by MTS. The data was recorded every 2 seconds. Before each test, the data acquisition system was reshuffled to zero value to ensure that is recording data and recording it correctly. The beams were loaded at a rate of 2kN per minute. After completing each test, the data was transferred from the data acquisition system to Microsoft Excel for analysis.

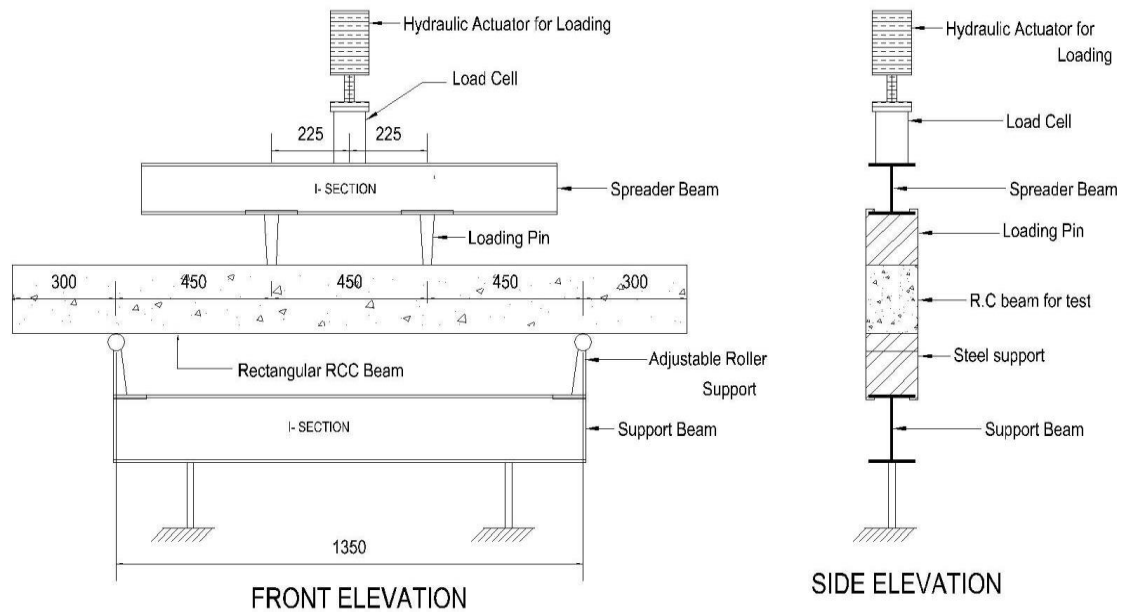


Figure 2: Experimental test setup



Figure 3: Typical loading arrangement

3. RESULTS & DISCUSSIONS

3.1 Mode of Failure:

The control beam CB1 failed in a ductile concrete crushing failure mode, which is steel yielding first followed by crushing of the concrete. The failure modes of all the other beams i.e. A1, A3, A4 and A5 followed the same pattern. The cracking pattern was similar for all the beams. At first, a fine flexural crack developed under one of the two loading pins originating at the bottom of the beam. As the external load increased, additional cracks developed at the neutral axis or beyond the neutral axis, with a notable increase in the deflection of the beam.

3.2 Load & Deflection

Control Beam (CB-1):

The test results show that the beam achieved a maximum load of 50.4 kN with a maximum deflection of 31.4 mm. The beam reached yielded at 33.6 kN with 3.22 mm deflection. Figure 4 shows the beam after testing and the concrete crushing that occurred at failure.



Figure-4: CB-1 after testing

Beams with NSM Bars using Epoxy adhesive (A1 & A3):

The test result showed that the beam A1 yielded at 56 kN having a deflection of 3.76 mm and failed at a maximum load of 82 kN which corresponds to a maximum deflection of 41.4 mm. Beam A3 yielded at 73.6 kN and failed at 102 kN with corresponding deflections of 3.76 mm and 45.42 mm, respectively.



Figure-5: A-1 after testing



Figure-6: A-3 after testing

Beams with NSM Bars using cement paste (A4& A5): The beam A4 yielded at 54.4 kN having a deflection of 4.06 mm and failed at a maximum load of 70.8 kN which corresponds to a maximum deflection of 42 mm. Beam A5 yielded at 70.4 kN and failed at 96.4 kN with corresponding deflections of 3.66 mm and 36.7 mm, respectively.



Figure-7: A-4 after test



Figure-8: A-5 after test

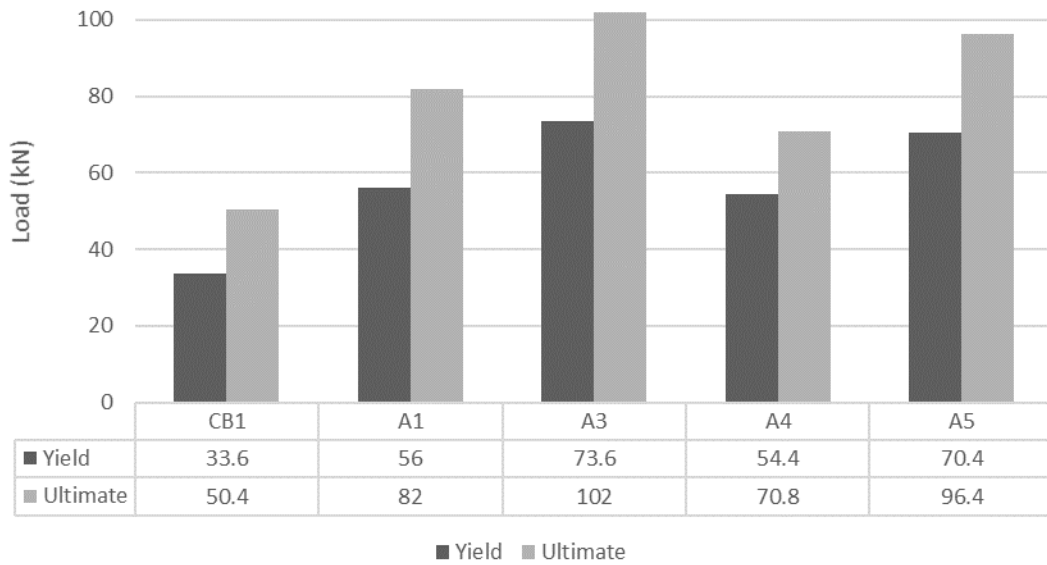


Figure-9: Yield and Ultimate load of beams

Table-3: Capacity of test specimens

Beam ID	Yield Load (KN)	Ultimate Load (KN)	Increase in Capacity (%)	Failure mode
CB1	33.6	50.4	0.00	Ductile
A1	56	82	62.7	Ductile
A3	73.6	102	102.4	Ductile
A4	54.4	70.8	40.47	Ductile
A5	70.4	96.4	91.27	Ductile

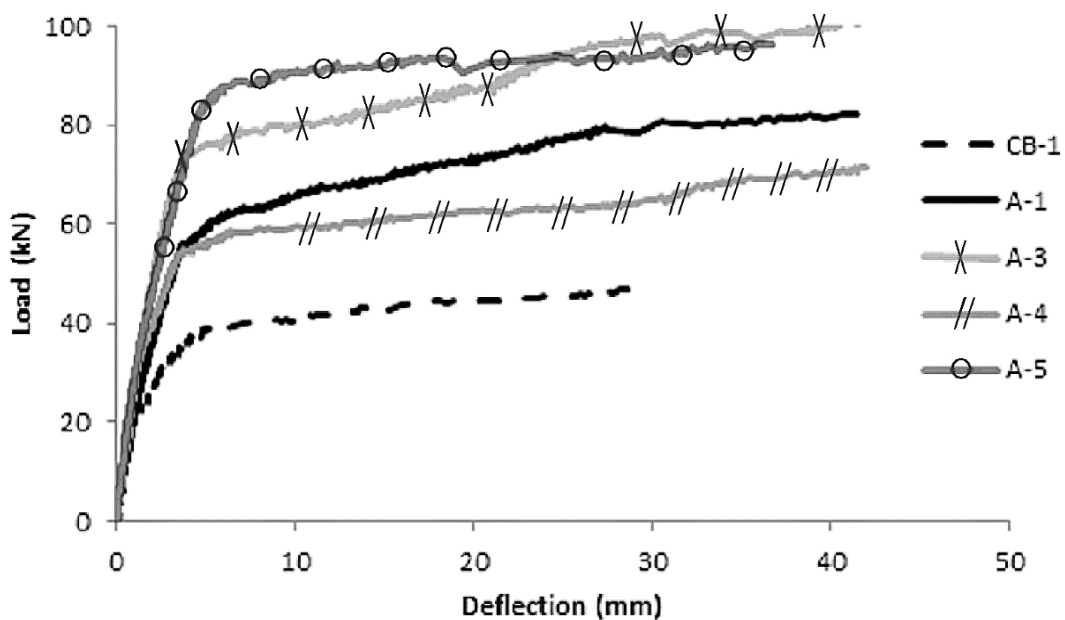


Figure-10: Load- Midspan Deflection of Beams

3.3 Ductility:

Table-4: Ductility of tested beams

Beam ID	Δy (mm)	Δu (mm)	Ductility, μ	Ductility increase, $\Delta\mu$
CB-1	3.22	31.4	9.75	0
A-1	3.76	41.4	11.01	1.26
A-3	3.76	45.42	12.08	2.33
A-4	4.06	42	10.34	0.59
A-5	3.66	36.7	10.03	0.28

In this study deflection ductility, was examined and are presented in Table 4. The deflection ductility index is expressed as the ratio between the deflection at ultimate load (Δu is the mid-span deflection at ultimate load) and the yield load (Δy is the midspan deflection at yield load). The deflection ductility index was increased by 12.93%, 23.9%, 6.05% and 2.87% for A-1, A-3, A-4 and A-5 respectively over the control beam. Overall, all the strengthened beams showed very good ductility.

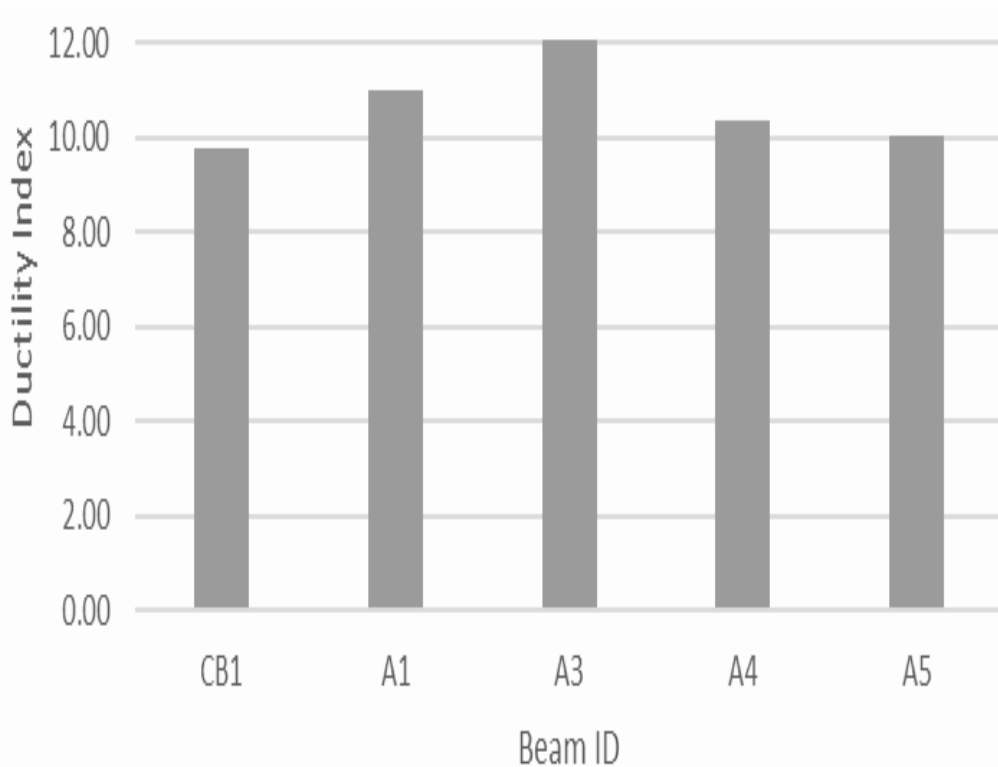


Figure-11: Ductility of Beams

3.3 Comparison of adhesives:

In terms of yield load epoxy does not show any advantage over cement as adhesive material. However, the epoxy used beams (A-1 and A-3) showed higher ultimate load than similarly configured beams which used cement paste as bonding material (A-4 and A-5). Also, when the adhesive changes from epoxy to cement paste, the beam shows lower ductility. These behaviours are expected due to the fact that epoxy possesses much higher strength than the cement paste.

4. CONCLUSION

The investigation carried out in this paper on RC beams strengthened by NSM steel reinforcement either with epoxy adhesive or cement paste has shown that this is a very effective strengthening technique. The following conclusions can be derived from the experimental results: -

- The mode of failure observed in all strengthened beams was ductile concrete crushing.
- Increasing the amount of NSM steel reinforcement from 50.26 mm² to 100.53 mm² increased the ultimate load capacity from 62.7% to 102.4% over control beam.
- Beams strengthened with NSM steel reinforcement have significantly increased yield and ultimate capacities with very good ductility.
- The use of cement paste as an alternative to epoxy adhesive shows adequate strength and ductility, hugely reduces the cost with slight reduction of performance.
- The NSM steel reinforcement enhances the load-deflection response of the RC beams. At any load level, the deflections of the strengthened beams were less than that of the control beam.
- The NSM strengthening technique using steel reinforcement and cement paste offers a very cheap but effective solution compared to any other strengthening technique.

ACKNOWLEDGEMENTS

Special thanks to Professor Dr. Md. Mozammel Hoque, thesis supervisor, and Professor Dr. Abdul Kader for their supervision and guidance throughout the whole experimental process. Also thanks to all the staffs of concrete and material testing laboratory for their sincere effort.

REFERENCES

- Akhtaruzzaman, A.A., & Hasnat, A. (1983). *Properties of concrete using crushed brick as aggregate*. Concrete international. 1983.
- Asplund, S. (1949). *Strengthening bridge slabs with grouted reinforcement*. in *ACI Journal Proceedings*. 1949. ACI.
- BNBC-2006. *Ultimate Strength Design of Reinforced Concrete Structures*. Chapter -6, Part-6.
- Bournas, D.A., & Traintafillou, T.C. (2008). *Flexural strengthening of RC columns with near surface mounted FRP or stainless-steel reinforcement: experimental investigation*. The 14th World Conference on Earthquake Engineering, October 12-17, 2008, Beijing, China, p2
- Brena, S.F., et al., (2003). *Increasing flexural capacity of reinforced concrete beams using carbon fiber reinforced polymer composites*. ACI Structural Journal, 2003, 100(1).
- De Lorenzis, L. and Nanni, A. (2002). *Bond between Near-Surface Mounted Fiber Reinforced Polymer Rods and Concrete in Structural Strengthening*. ACI Structural Journal. 99(2): 123-132
- fib Bulletin 14: Task Group 9.3 FRP (Fibre Reinforced Polymer) reinforcement for concrete structures. *Design and use of externally bonded fibre reinforced polymer reinforcement (FRP EBR) for reinforced concrete structures*. July, 2001.
- Fleming, C. J., & King, G. E. M. (1967). *The Development of structural adhesives for three original uses in South Africa*. RILEM Paris, 75-92.
- Garrity, S. (2001). *Near-surface reinforcement of masonry arch highway bridges*. in *Proceedings 9th Canadian Masonry Symposium*, Fredericton. 2001.
- El-Hacha, R. and S.H. Rizkalla (2004), *Near-surface-mounted fiber reinforced polymer reinforcements for flexural strengthening of concrete structures*. ACI Structural Journal, 2004. 101(5).
- Hawileh, R.A., et al. (2014) *Behavior of reinforced concrete beams strengthened with externally bonded hybrid fiber reinforced polymer systems*. *Materials & Design*, 2014. 53: p. 972-982.
- Hosen, M. A. et al. (2014). *Flexural Strengthening of RC Beams with NSM Steel Bars*. International Conference on Food, Agriculture and Biology (FAB-2014), Kuala Lumpur (Malaysia), June 11-12, 2014.
- Petrina, D.A. (2009). *Strengthening of Reinforced Concrete Beams using Anchored Near Surface Mounted Bars*. McMaster University. 2009.

NUMERICAL MODELING AND FINITE ELEMENT ANALYSIS OF SHS COLUMNS RETROFITTED WITH CFRP WRAPPINGS

U. Devi¹, M. M. Rahman², M. F. Rabby³ and M. H. Talukdar⁴

¹ Ph.D. Candidate, North Carolina State University, U.S.A., e-mail: urmidevi_buet07@yahoo.com

^{2, 3, 4} Researcher & Structural Engineer, Ahsanullah University of Science and Technology, Bangladesh, e-mail: maksud.ce.aust@gmail.com

ABSTRACT

This paper presents a numerical modeling and finite element analysis on the behavior of steel hollow section (SHS) columns strengthening with Carbon Fibre Reinforced Polymer (CFRP) wrappings, engaging FEA software ABAQUS 6.14-4. A three dimensional finite element model of steel SHS column was developed using both shell and solid element considering both material and geometric nonlinearities whereas CFRP wrappings with different orientations were incorporated in the model with both conventional (S4R) and continuum shell (SC8R) element to capture actual behavior of CFRP retrofitted SHS column. The proposed numerical model was then incorporated into the ABAQUS to simulate some of the experimental studies found in relevant literatures. It has been found that good agreement exists between numerical analysis and past experimental results, which has established the acceptability and validity of the proposed finite element model to carry out further investigation.

Keywords: Retrofitting, SHS columns, CFRP strips, Finite Element

1. INTRODUCTION

In recent days after experiencing a number of severe earthquakes in Bangladesh and also in nearby country Nepal, people have become more concerned about the rehabilitation of retrofitting of the existing structures. For this reason, the use of Carbon Fiber Reinforced Polymer (CFRP) materials is gaining popularity day by day for repairing of steel structures compared to other conventional retrofitting techniques (Devi and Amanat, 2015; Shaat and Fam, 2006). Since the column is the most important element of the structure, so through retrofitting of columns using CFRP, the whole structure may perform better. In recent years, steel hollow section (SHS) columns have become a great topic of research. Recent research of steel CFRP composite section includes investigating the behavior of axially loaded short and long square hollow structural section (HSS) columns strengthened with carbon fibre reinforced polymer (CFRP) sheets by Shaat and Fam (2006), behavior of steel SHS strengthened with CFRP under large axial deformation by Bambach and Elchalakani (2007), axial capacity and design of thin-walled steel SHS strengthened with CFRP by Bambach MR, et al. (2009), CFRP strengthening of rectangular steel tubes subjected to end bearing loads by Fernando et al. (2009), a numerical finite element investigation on the behavior of steel square hollow structural section (HSS) columns strengthened with CFRP by Devi, U. and Amanat, K.M. (2015). Although such experimental studies provide satisfactory results regarding retrofitting, more research is required in this field. Due to the huge expense of such experiments, numerical studies are being preferred nowadays. This paper focused on developing a three-dimensional finite element model to investigate the behavior and axial strength of SHS columns retrofitted using CFRP wrappings. The proposed model is then used to simulate the experimental results from Bambach and Elchalakani (2007).

2. FINITE ELEMENT METHODOLOGY

In this section, the extensive details of finite element methodology of the experimental study conducted by Bambach and Elchalakani (2007) have been discussed thoroughly. ABAQUS 6.14-4 has been used for numerical modeling. Details of element selection, material modeling boundary conditions and typical results with deflected shapes are included in this section.

2.1 Finite Element Modeling

In this study, Finite Element Analysis (FEA) has been carried out using ABAQUS 6.14-4 since this software allows for reducing time, effort, and material costs involved with trial and error manufacturing techniques.

2.2.1 Geometric Properties in Finite Element Model

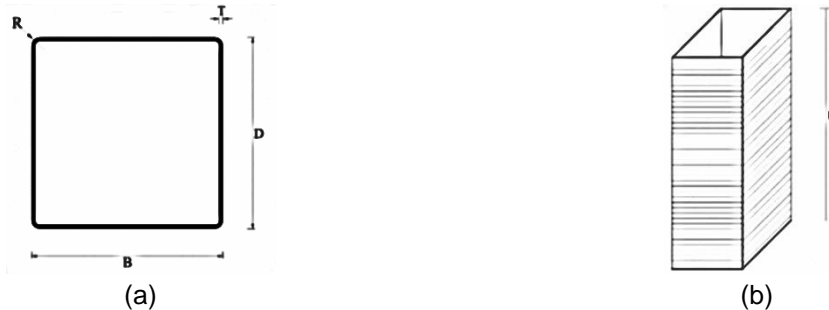


Figure 2.1: Geometric Properties of Finite Element Modeling (Bambach and Elchalakani, 2007)
(a) Cross-Sectional Dimensions (b) Longitudinal Dimension

In Figure: 2.1 Geometry has been incorporated as defined in the experimental model of Bambach M.R. and Elchalakani M. (2007). Two cross-sectional dimensions are designated as shown in Figure: 2.1, where, “B” stands for width, “D” stands for depth, “L” stands for length of SHS column, “T” stands for thickness and “R” stands for outer corner radius. Geometric properties of SHS columns are shown in the following Table 2.1.

Table 2.1: Dimensions of Simulated Models of Steel SHS Column (Bambach and Elchalakani, 2007)

Item	Column Section	B (mm)	D (mm)	L (mm)	T (mm)	R (mm)
SHS Column	SHS 100x100x2	100	100	300	2	4
	SHS 75x75x2	75	75	225		2
	SHS 65x65x2	65	65	195		4
	SHS 50x50x2	50	50	150		2
CFRP for SHS 100x100x2	1T1L	100.68	100.68	300	0.17	4.34
	2T2L	101.36	101.36			4.68
CFRP for SHS 75x75x2	1T1L	75.68	75.68	225	0.17	2.34
	2T2L	76.36	76.36			2.68
CFRP for SHS 65x65x2	1T1L	65.68	65.68	195	0.17	4.34
	2T2L	66.36	66.36			4.68
CFRP for SHS 50x50x2	1T1L	50.68	50.68	150	0.17	2.34
	2T2L	51.36	51.36			2.68

The geometry of CFRP layers has also been defined. Based on the experimental study (Bambach and Elchalakani, 2007), each CFRP layer is 0.17mm thick. CFRP layers have been placed around the SHS column. In one case, two CFRP layers have been placed, one is laid transversely around the Steel SHS column perpendicular to the direction of axial load and the other is laid longitudinally i.e. in the direction of axial load. It is designated as 1T1L as per the experimental study. Similarly, geometry for 2T2L has also defined in finite element modeling. In the experimental setup, CFRP sheets were overlapped by 20mm. But for simplification of finite element modeling, the overlapping of CFRP sheets has not been considered. The geometry of CFRP layers has been summarized in Table 2.2.

Table 2.2: Dimensions of Simulated Models of CFRP Layers (Bambach and Elchalakani, 2007)

Item	Designation	Orientation	B1 (mm)	D1 (mm)	T (mm)	L (mm)	R (mm)
CFRP Layers for SHS 100x100x2	1T1L	Transverse Layer	100.34	100.34	0.17	300	4
	1T1L	Longitudinal Layer	100.68	100.68			
	2T2L	Transverse Layer 1	100.34	100.34			
	2T2L	Longitudinal Layer 1	100.68	100.68			
	2T2L	Transverse Layer 2	101.02	101.02			
	2T2L	Longitudinal Layer 2	101.36	101.36			
CFRP Layers for SHS 75x75x2	1T1L	Transverse Layer	75.34	75.34	0.17	225	2
	1T1L	Longitudinal Layer	75.68	75.68			
	2T2L	Transverse Layer 1	75.34	75.34			
	2T2L	Longitudinal Layer 1	75.68	75.68			
	2T2L	Transverse Layer 2	76.02	76.02			
	2T2L	Longitudinal Layer 2	76.36	76.36			
CFRP Layers for SHS 65x65x2	1T1L	Transverse Layer	65.34	65.34	0.17	195	4
	1T1L	Longitudinal Layer	65.68	65.68			
	2T2L	Transverse Layer 1	65.34	65.34			
	2T2L	Longitudinal Layer 1	65.68	65.68			
	2T2L	Transverse Layer 2	66.02	66.02			
	2T2L	Longitudinal Layer 2	66.36	66.36			
CFRP Layers for SHS 50x50x2	1T1L	Transverse Layer	50.34	50.34	0.17	150	2
	1T1L	Longitudinal Layer	50.68	50.68			
	2T2L	Transverse Layer 1	50.34	50.34			
	2T2L	Longitudinal Layer 1	50.68	50.68			
	2T2L	Transverse Layer 2	51.02	51.02			
	2T2L	Longitudinal Layer 2	51.36	51.36			

2.2.2 Material properties in finite element model

2.2.2.1 Steel SHS Tube

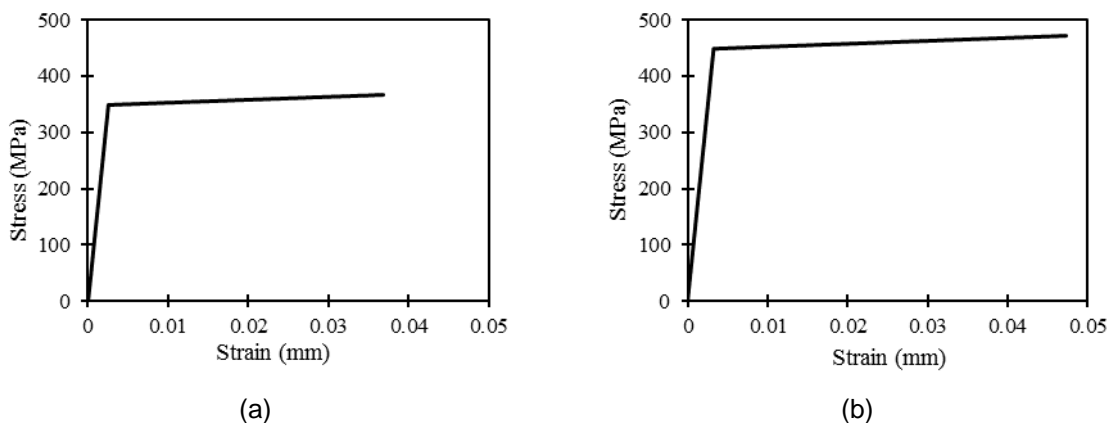


Figure 2.2: Stress-Strain Curve for Steel SHS Column from Coupon Test (Bambach and Elchalakani, 2007) (a) for SHS50x50x2, SHS65x65x2 & SHS75x75x2 (b) for SHS 100x100x2

For capturing the actual behavior of SHS column retrofitted with CFRP layers, material properties should be incorporated carefully in finite element modeling. The material property of steel SHS column has been considered as a linear and isotropic material. Young's and Poisson's ratio of steel

SHS column have been taken, except for Steel SHS 100x100x2, 138.285 GPa and 0.3 respectively. Whereas for Steel SHS 100x100x2, Young's modulus has been taken 200 GPa. The yield stress of SHS column has been taken 350 MPa for all sections, except for SHS section 100x100x2, where yield stress has been taken 450 MPa. The stress-strain curve has been incorporated in Figure 2.2 as per the Coupon test provided by Bambach M.R. and Elchalakani M (2007).

2.2.2.2 CFRP Layers

High strength CFRP materials have been used for retrofitting. In one case, it has been considered linear elastic and isotropic material. In the second case, it has been considered linear elastic and lamina material.

Table 2.1: Material properties of CFRP Layer

Item	Young's Modulus	Poisson's Ratio
CFRP	230 GPA	.3

2.2.3 Element selection

Steel SHS column has been modeled using 4-node, quadrilateral, and stress/displacement shell element with reduced integration and large strain formulation which can be found in ABAQUS 6.14-4 as S4R type. In another case, it is also modeled using 8-node linear brick, reduced integration with hourglass control which can be found in ABAQUS 6.14-4 as C3D8R. To capture the actual behavior, CFRP is modeled by using element S4R and SC8R both. The thickness is determined from the element nodal geometry.

2.2.4 Section assignment

For steel SHS sections both homogeneous solid and homogeneous shell sections have been used for modeling. For CFRP sections, homogeneous shell sections and composite shell sections have been incorporated.

2.2.5 Steel-CFRP and CFRP-CFRP interaction

In this finite element modelling, Steel-CFRP and CFRP-CFRP interface have been assumed perfect bonding. For this, tie constraints have been incorporated in the modeling. A tie constraint allows fusing together two regions even though the meshes created on the surfaces of the regions may be dissimilar. A surface-based tie has been adopted. In Steel-CFRP interface, Steel SHS outer surface has been used as master surface whereas, the inner surface of first CFRP layer has been used as slave surface. Again in CFRP-CFRP interface, the outer surface of CFRP layer near SHS column has been considered master surface and the inner surface of CFRP layer far from SHS has been taken as slave surface.

2.2.6 Boundary conditions and loading

2.2.6.1 Boundary Conditions

Boundary condition has been applied as per the experimental study (Bambach M.R. and Elchalakani M., 2007). According to experimental setup ends of the composite SHS were ground square and the CFRP was minimally hand ground at the ends platens of the testing machine. To capture this condition, one end of the steel SHS column has been considered fixed. Also, in one of the case studies, translation in the X and Y –direction has been restrained to avoid the rotation about Z-axis.

2.2.6.2 Load application

Displacement controlled loading has been incorporated into the finite element model. Displacement is applied at the opposite of fixed end at one node in the Z-direction.

2.2.7 Solution strategy

Both the Newton-Raphson method and Arc-Length method have been used for the solution. In this study, it has been seen that the result of Newton-Raphson and Arc-Length method is quite similar. But with Arc-Length method, large range of results can be obtained. So, ultimately study has been conducted using the Arc-Length method only.

2.2.8 Figures from finite element modeling

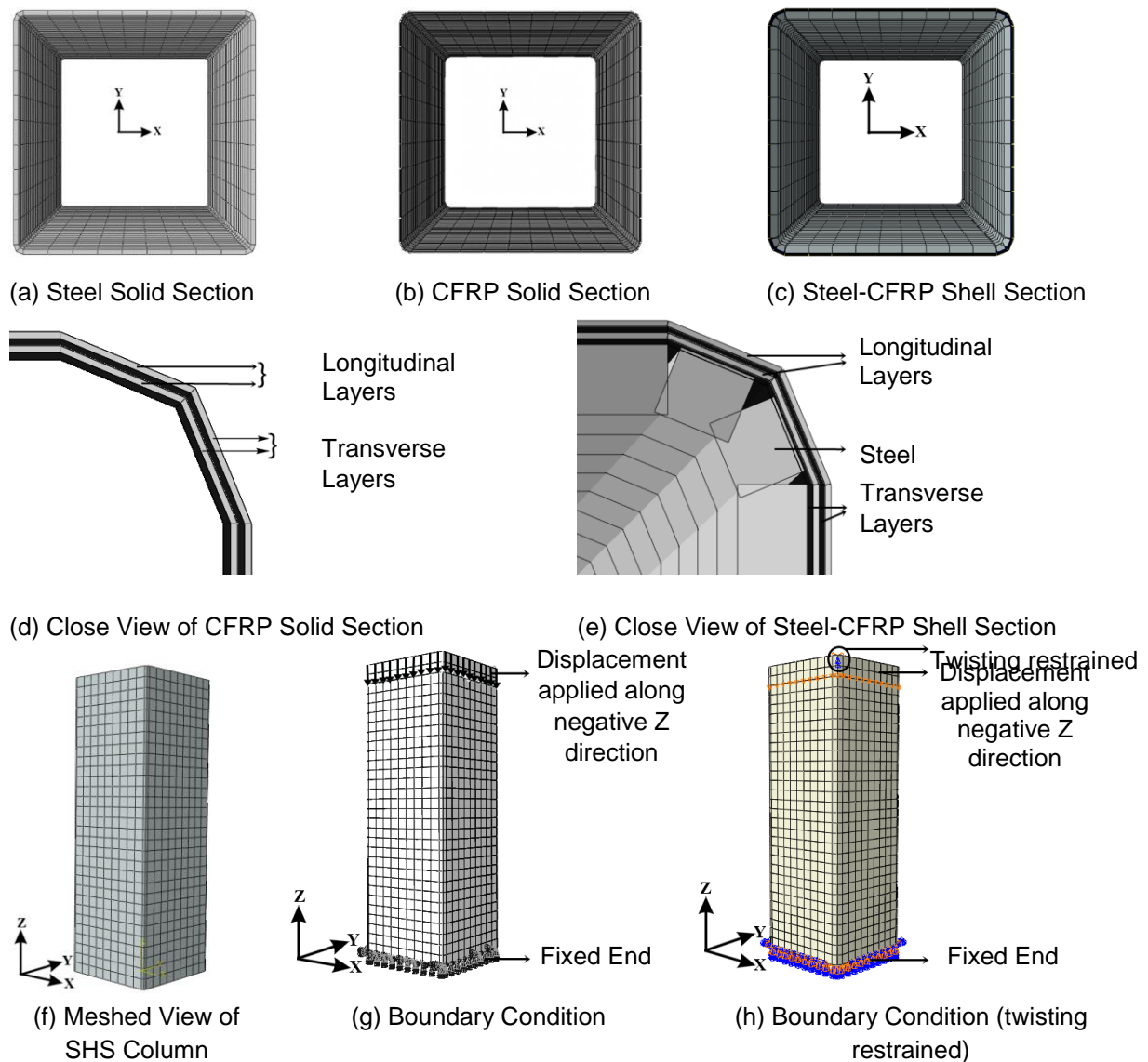


Figure 2.3: Figures from finite element modeling

3. EXPERIMENTAL MODEL VERIFICATION (BAMBACH AND ELCHALAKANI, 2007)

In this section, the results of the numerical simulations and the tests are compared, and the sensitivity of the models to the key modeling parameters, particularly the imperfection amplitudes, are examined. Comparisons with the test results are made to assess the accuracy of the models and verify their suitability for performing parametric studies.

3.1 Verification of experimental result

Verification was done using the experimental study conducted by M. R. Bambach and M. Elchalakani (2007). SHS 50x50x2, SHS 65x65x2, SHS 75x75x2, SHS 100x100x2 sections taken for verifications. For verifying the proposed models, different combinations of elements and/or modeling techniques have been considered. Tabular representations of verification for section for different case studies are shown in Table: 3.1

Table 3.1: Details of Different Case Studies Considered for Verification

Cases	Steel SHS			CFRP layers			Interaction
	Element	Material	Section	Element	Material	Section	
Case 1	S4R	Elastic, Isotropic	Shell, Homogenous		Not Applicable		Not Applicable
Case 2	S4R	Elastic, Isotropic	Shell, Homogenous	S4R	Elastic, Isotropic	Shell, Composite	Tie
Case 3	C3D8R	Elastic, Isotropic	Solid, Homogenous	SC8R	Elastic, Isotropic	Shell, Composite	Tie
Case 4	S4R	Elastic, Isotropic	Shell, Homogenous	SC8R	Elastic, Isotropic	Shell, Composite	Tie
Case 5	S4R	Elastic, Isotropic	Shell, Homogenous	S4R	Elastic, Isotropic	Shell, Composite	Tie (with extra DOF for rotation off about z-axis)
Case 6	C3D8R	Elastic, Isotropic	Solid, Homogenous	SC8R	Elastic, Isotropic	Shell, Composite	Tie (with extra DOF for rotation off about z-axis)
Case 7	S4R	Elastic, Isotropic	Shell, Homogenous	SC8R	Elastic, Isotropic	Shell, Composite	Tie (with extra DOF for rotation off about z-axis)

Parametric key results related to case studies are shown in following figures.

Now the graphical representation of verification of experimental studies for various sections and for various combinations is shown in the following Figure: 3.1 - 3.52.



Fig 3.1: SHS 50x50x2 – Case 1

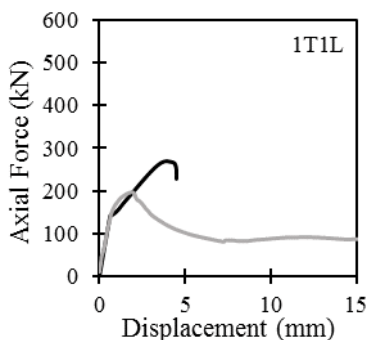


Fig 3.2: SHS 50x50x2 – Case 2

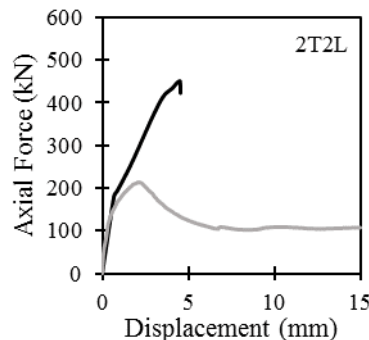


Fig 3.3: SHS 50x50x2 – Case 2

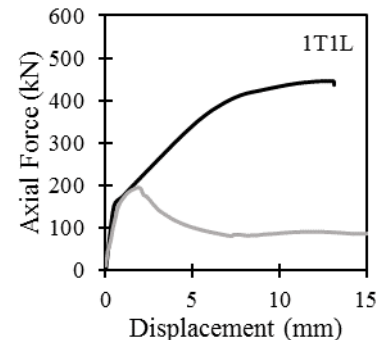


Fig 3.4: SHS 50x50x2 – Case 3

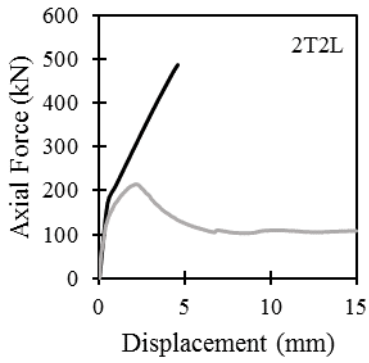


Fig 3.5: SHS 50x50x2 – Case 3

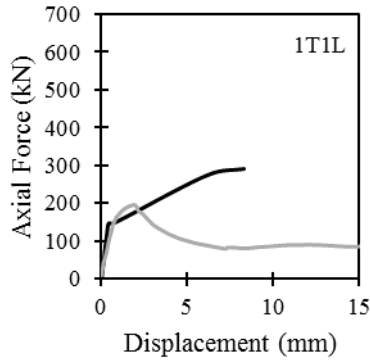


Fig 3.6: SHS 50x50x2 – Case 4

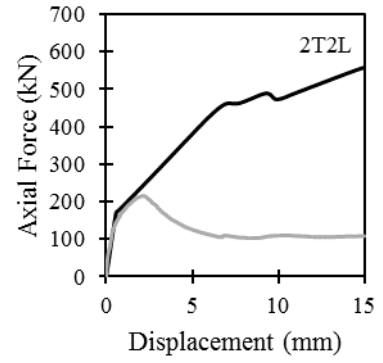


Fig 3.7: SHS 50x50x2 – Case 4

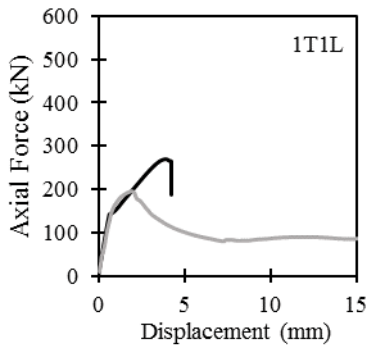


Fig 3.8: SHS 50x50x2 – Case 5

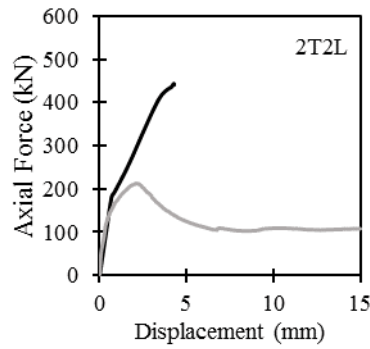


Fig 3.9: SHS 50x50x2 – Case 5

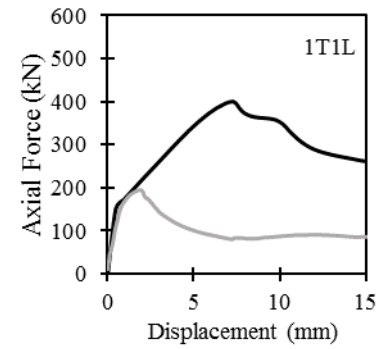


Fig 3.10: SHS 50x50x2 – Case 6

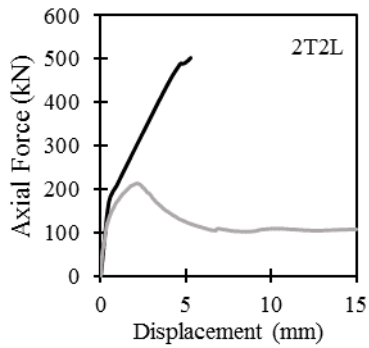


Fig 3.11: SHS 50x50x2 – Case 6

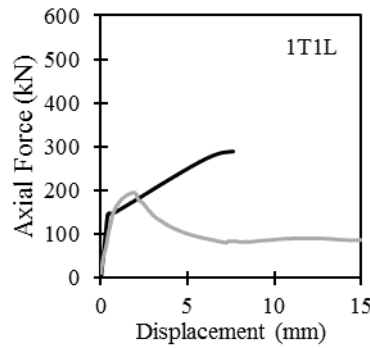


Fig 3.12: SHS 50x50x2 – Case 7

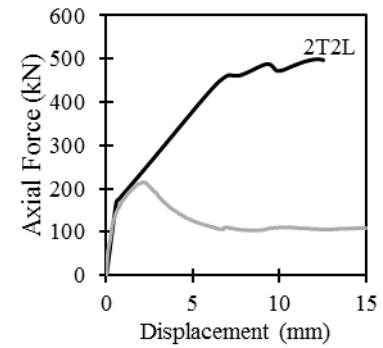


Fig 3.13: SHS 50x50x2 – Case 7

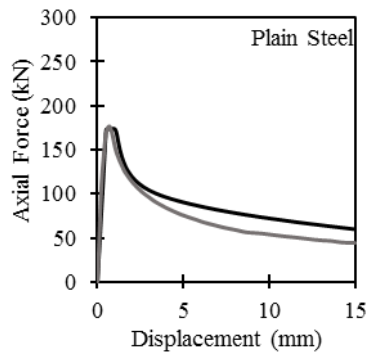


Fig 3.14: SHS 65x65x2 – Case 1

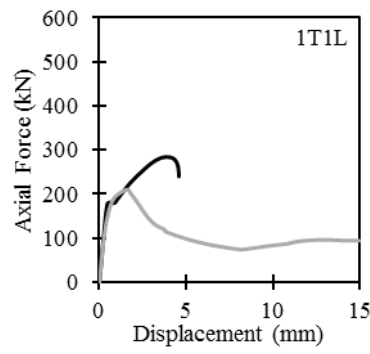


Fig 3.15: SHS 65x65x2 – Case 2

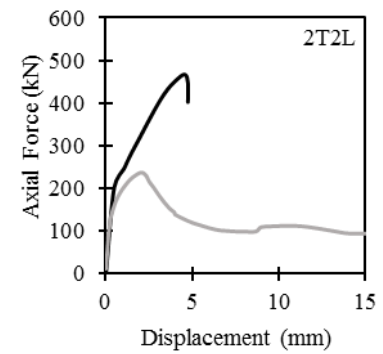


Fig 3.16: SHS 65x65x2 – Case 2

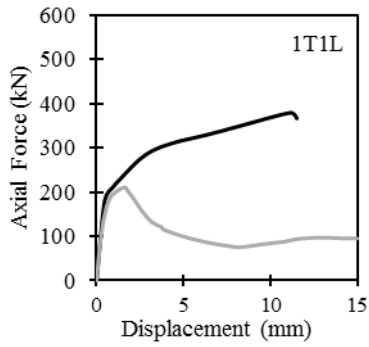


Fig 3.17: SHS 65x65x2 – Case 3

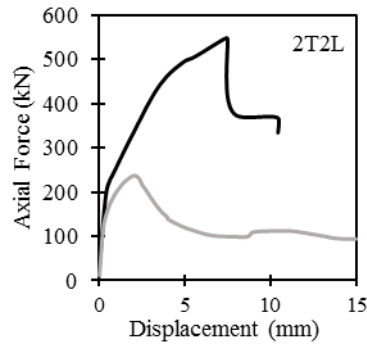


Fig 3.18: SHS 65x65x2 – Case 3

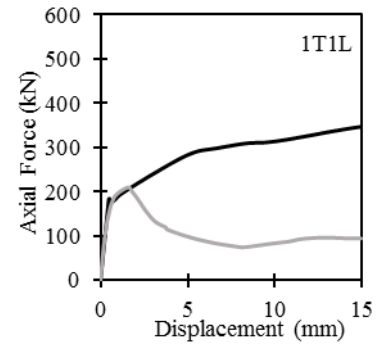


Fig 3.19: SHS 65x65x2 – Case 4

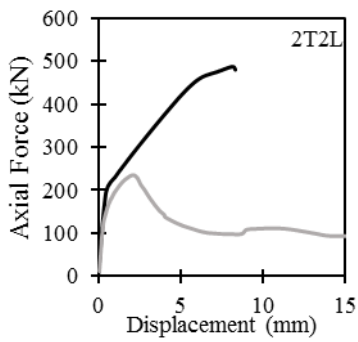


Fig 3.20: SHS 65x65x2 – Case 4

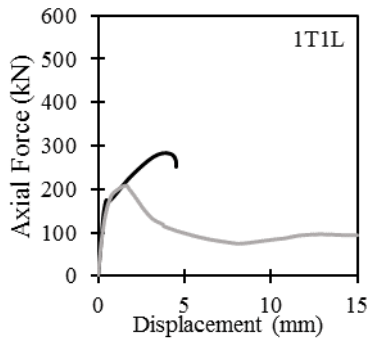


Fig 3.21: SHS 65x65x2 – Case 5

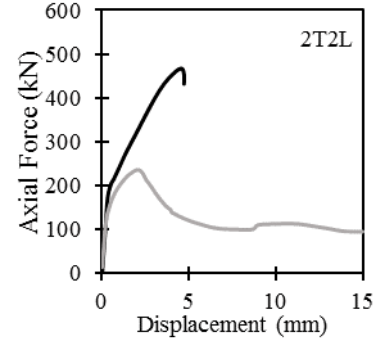


Fig 3.22: SHS 65x65x2 – Case 5

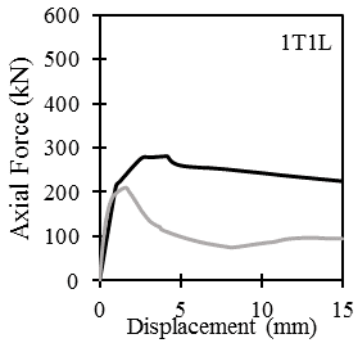


Fig 3.23: SHS 65x65x2 – Case 6

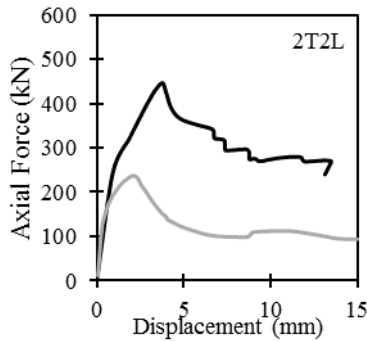


Fig 3.24: SHS 65x65x2 – Case 6

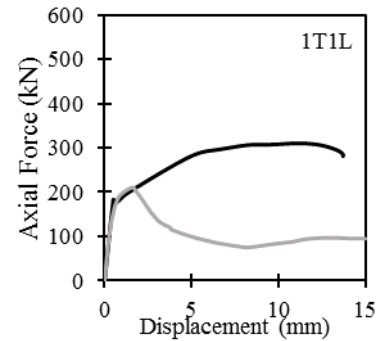


Fig 3.25: SHS 65x65x2 – Case 7

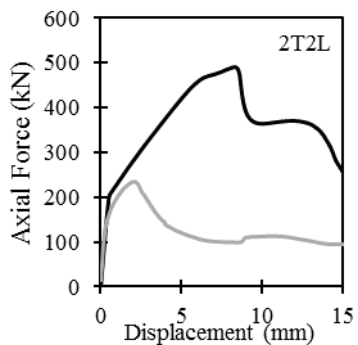


Fig 3.26: SHS 65x65x2 – Case 7

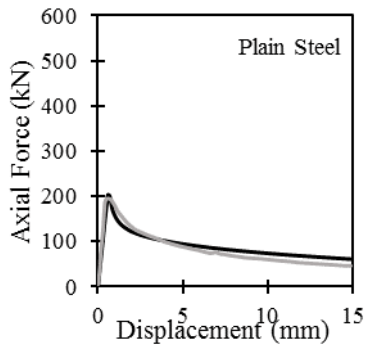


Fig 3.27: SHS 75x75x2 – Case 1

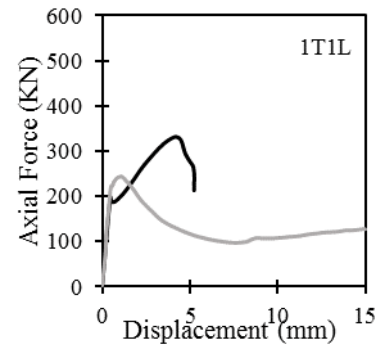


Fig 3.28: SHS 75x75x2 – Case 2

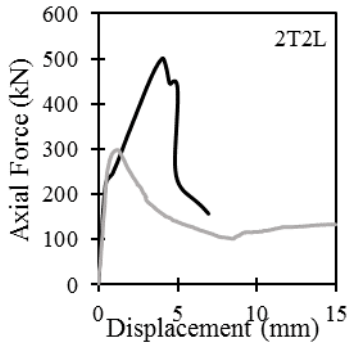


Fig 3.29: SHS 75x75x2 – Case 2

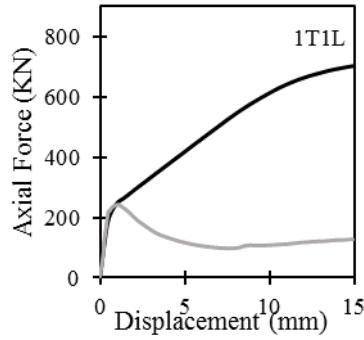


Fig 3.30: SHS 75x75x2 – Case 3

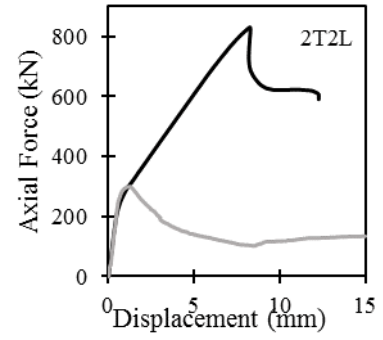


Fig 3.31: SHS 75x75x2 – Case 3

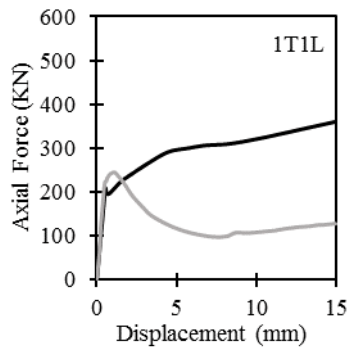


Fig 3.32: SHS 75x75x2 – Case 4

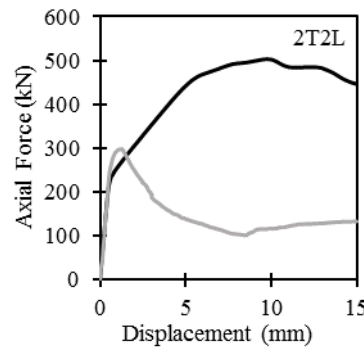


Fig 3.33: SHS 75x75x2 – Case 4

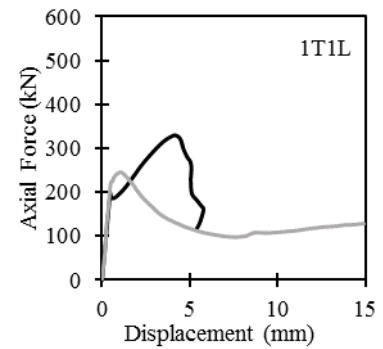


Fig 3.34: SHS 75x75x2 – Case 5

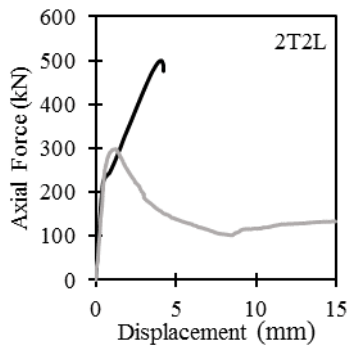


Fig 3.35: SHS 75x75x2 – Case 5

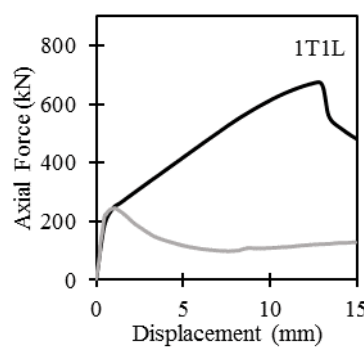


Fig 3.36: SHS 75x75x2 – Case 6

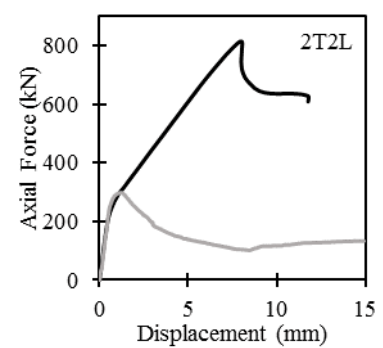


Fig 3.37: SHS 75x75x2 – Case 6

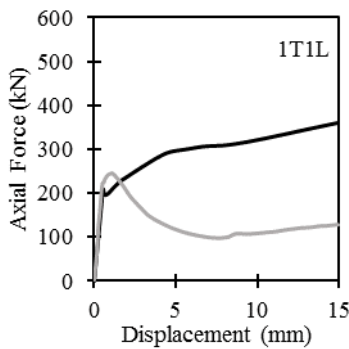


Fig 3.38: SHS 75x75x2 – Case 7

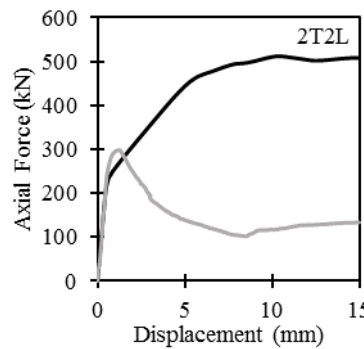


Fig 3.39: SHS 75x75x2 – Case 7

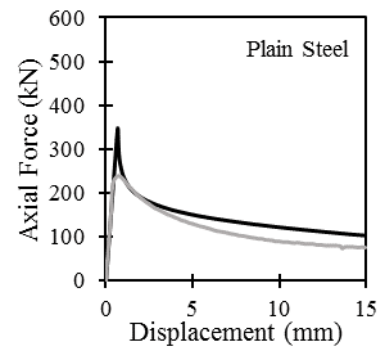


Fig 3.40: SHS 100x100x2 – Case 1

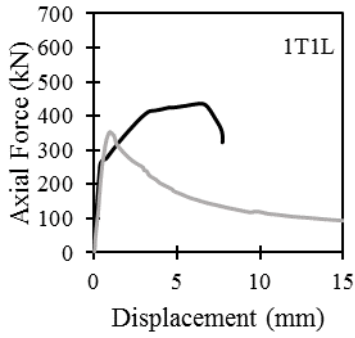


Fig 3.41: SHS 100x100x2 – Case 2

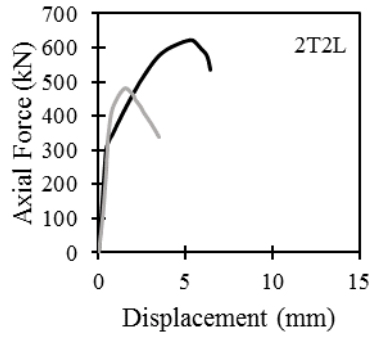


Fig 3.42: SHS 100x100x2 – Case 2

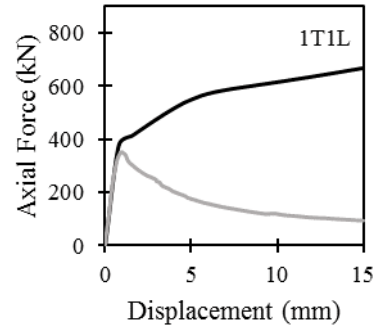


Fig 3.43: SHS 100x100x2 – Case 3

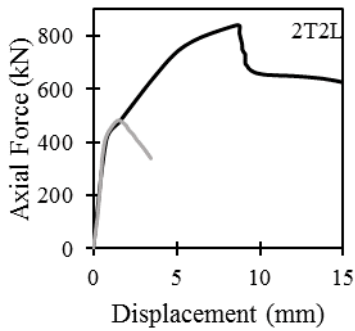


Fig 3.44: SHS 100x100x2 – Case 3

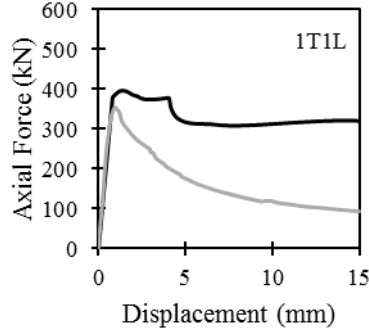


Fig 3.45: SHS 100x100x2 – Case 4

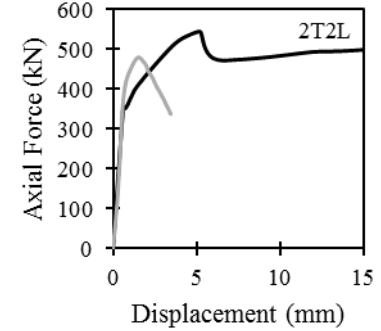


Fig 3.46: SHS 100x100x2 – Case 4

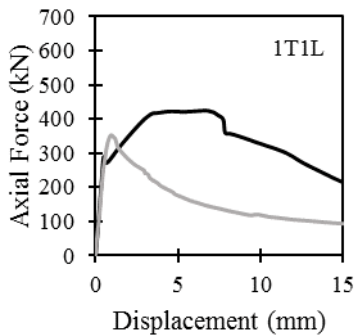


Fig 3.47: SHS 100x100x2 – Case 5

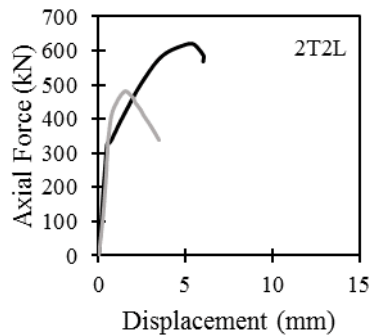


Fig 3.48: SHS 100x100x2 – Case 5

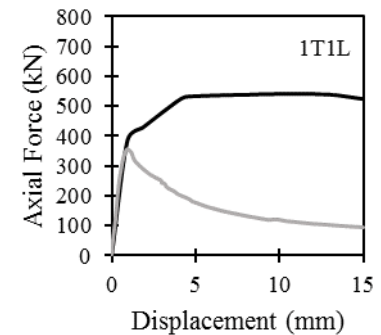


Fig 3.49: SHS 100x100x2 – Case 6

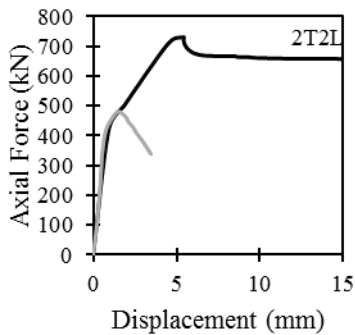


Fig 3.50: SHS 100x100x2 – Case 6

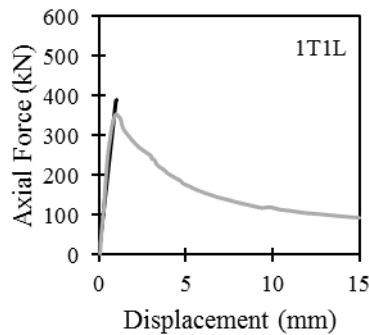


Fig 3.51: SHS 100x100x2 – Case 7

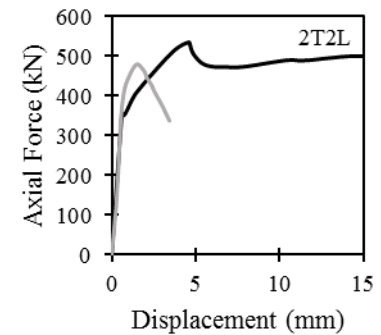


Fig 3.52: SHS 100x100x2 – Case 7

Tabular representation of verification of maximum experimental load with maximum numerical load is shown in the following Table 3.2

Table 3.2: Comparison between Experimental and Numerical Results

Section	Designation	Case	Experimental Load (KN)	Numerical Load (KN)	Experimental Load/ Numerical Load
50x50x2	Plain Steel	Case 1	181.8	133.561	1.361
50x50x2	1T1L	Case 2	201.0	269.257	0.746
		Case 3		445.083	0.452
		Case 4		292.718	0.687
		Case 5		269.222	0.747
		Case 6		400.214	0.502
		Case 7		290.004	0.693
		50x50x2		2T2L	Case 2
Case 3	486.434		0.438		
Case 4	556.654		0.383		
Case 5	442.789		0.481		
Case 6	503.731		0.423		
Case 7	498.543		0.427		
65x65x2	Plain Steel		Case 1		176.6
65x65x2	1T1L	Case 2	209.1	283.089	0.739
		Case 3		378.734	0.552
		Case 4		349.666	0.598
		Case 5		281.984	0.742
		Case 6		281.861	0.742
		Case 7		311.32	0.672
		65x65x2		2T2L	Case 2
Case 3	547.274		0.429		
Case 4	486.022		0.483		
Case 5	464.827		0.505		
Case 6	446.615		0.526		
Case 7	489.873		0.480		
75x75x2	Plain Steel		Case 1		198.4
75x75x2	1T1L	Case 2	242.7	330.238	0.735
		Case 3		719.123	0.337
		Case 4		414.979	0.585
		Case 5		330.116	0.735
		Case 6		674.82	0.360
		Case 7		373.919	0.649
		75x75x2		2T2L	Case 2
Case 3	830.408		0.357		
Case 4	503.528		0.589		
Case 5	499.461		0.594		
Case 6	813.58		0.364		
Case 7	510.667		0.581		
100x100x2	Plain Steel		Case 1		238.4
100x100x2	1T1L	Case 2	354.1	436.204	0.812
		Case 3		751.053	0.471
		Case 4		397.06	0.892
		Case 5		423.979	0.835
		Case 6		540.712	0.655
		Case 7		389.48	0.909
		100x100x2		2T2L	Case 2
Case 3	841.281		0.572		
Case 4	545.092		0.882		
Case 5	620.663		0.775		
Case 6	731.535		0.657		
Case 7	536.342		0.897		

Deflected shape for section SHS 100 x 100 x 2 is shown in Figure: 3.53. From the graphical and tabular representation of verification and the deflection pattern of the simulated SHS sections, it is observed that case 5 shows good agreement with the experimental study. That is, if the Steel SHS is modeled using S4R and CFRP layers are modeled using S4R, then a ratio of more than 0.5 has been achieved between experimental peak load and numerical peak load i.e., there is less deviation from the experimental load. Also by observing the deflection pattern and graphical representation of the of the simulated SHS sections, it is found that case 6 also shows good agreement with the experimental study. That is, if the Steel SHS is modeled using C3D8R and CFRP layers are modeled using SC8R, then a deflected shape similar to the experimental study has been found and. Thus these verified models can be used for further parametric studies of SHS sections retrofitted with CFRP wrapping.

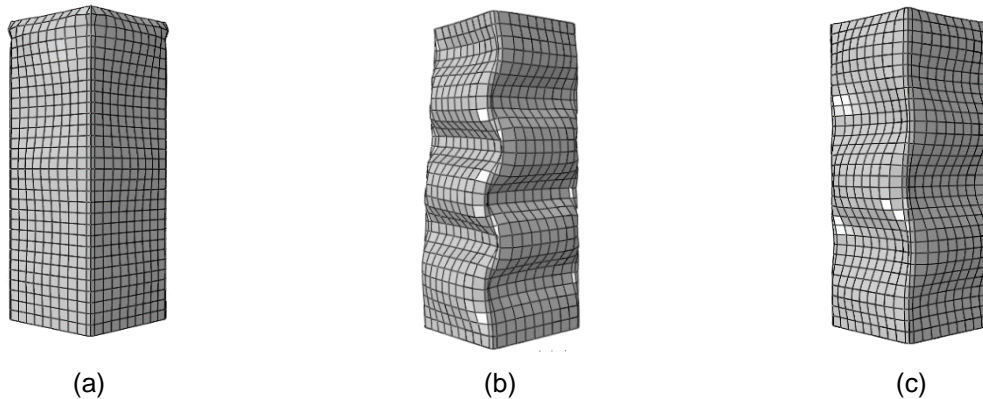


Figure 3.53: Deflected Shape for Section SHS 100 x 100 x 2 (a) Case 5 - 1T1L (b) Case 6 - 1T1L (c) Case 7 - 1T1L

4. CONCLUSION

In this study, a three-dimensional finite element model to investigate the behavior and axial strength of SHS columns retrofitted using CFRP wrappings has been developed. Finite element analysis has been conducted on the model and the result from this analysis has been verified with the experimental result. In this section, summarization of the findings of the whole finite element analysis is shown.

4.1 Outcomes of the study

Outcomes of the present study are listed below:

1. The experimental study conducted by Bambach and Elchalakani (2007) has been successfully verified with the 3D finite element model developed using ABAQUS 6.14-4.
2. From the graphical and tabular representation of verification, it is observed that case 5 shows good agreement with the experimental study. That is, if the Steel SHS is modeled using S4R and CFRP layers are modeled using S4R, CFRP material property is defined as elastic isotropic and translation along X-axis & Y-axis is restricted for one node at loading set for avoiding the rotation about Z-axis, then a good agreement has been found between numerical and experimental results. This model can be used for further parametric studies.
3. It has also been found that case 6 shows good agreement with the experimental study in regard to the deflection pattern and graphical representation. That is, if the Steel SHS is modeled using C3D8R and CFRP layers are modeled using SC8R, CFRP material property is defined as elastic isotropic and translation along X-axis & Y-axis is restricted for one node at loading set for avoiding the rotation about Z-axis, then a deflected shape similar to the experimental study has been found. This model can also be used for further parametric studies.
4. In this study, damage property was not assigned to the CFRP materials and the interface between Steel and CFRP has been assumed as perfectly bonded which may have resulted in poor agreements between numerical and experimental study especially in the post-peak regime for many cases.

4.2 Future recommendations

1. In this study, damage property of the CFRP material has not been considered. So further study can be conducted incorporating the detailed damage modeling of CFRP materials.
2. In this study, perfect bonding between adjacent two layers has been assumed. In future, cohesive bonding between the layers can be considered to achieve a more accurate result.
3. A parametric study needs to be done by varying different parameters of the proposed finite element model.

REFERENCES

- Bambach, M. R. and Elchalakani, M. 2007. "Plastic mechanism analysis of steel SHS strengthened with CFRP under large axial deformation". *Thin-Walled Structures*, 45(2), pp. 159-170.
- Bambach M. R.; Jama H. H. and Elchalakani M. 2009. "Axial capacity and design of thin-walled steel SHS strengthened with CFRP". *Thin-Walled Structures* Volume 47, Issue 10, pages 1112–1121.
- Devi U. and Amanat K. M. 2015. "Non-Linear Finite Element Investigation on the Behavior of CFRP Strengthened Steel Square HSS Columns under Compression". *International Journal of Steel Structures*, 15(3), p. 671-680.
- Fernando D.; Yu T.; Teng J. G. and Zhao X. L. 2009. "CFRP strengthening of rectangular steel tubes subjected to end bearing loads: Effect of adhesive properties and finite element modeling". *Thin-Walled Structures* 47, pp. 1020–1028.
- Shaat, A. and Fam, A. 2006. "Axial loading tests on short and long hollow structural steel columns retrofitted using carbon fiber reinforced polymers". *Canadian Journal of Civil Engineering*, 33(4), pp. 458-470.

BONDING STRENGTH BEHAVIOR OF CONCRETE USING GRANULAR WASTE PLASTIC AS A PARTIAL REPLACEMENT OF SAND

Md. Yeasin Arafat¹ and Mohammad Tarequul Alam²

¹ Undergraduate student, Department of Civil Engineering, Chittagong University of Engineering & Technology, Bangladesh, e-mail: yea5in.4arafat@gmail.com

² Assistant Professor, Department of Civil Engineering, Chittagong University of Engineering & Technology, Bangladesh, e-mail: mtalamcuet@gmail.com

ABSTRACT

Concrete is one of the most common materials used in the construction industry throughout the world. Excessive extraction of natural aggregates, due to the rapid growth of concrete construction resulted in the search for alternative source of concrete aggregate. The aim of the study is to investigate the influence of plastic waste granular on the bonding between steel and concrete. Also to observe the variation of compressive strength of concrete using granular waste plastic compared to the conventional concrete. The test specimens were made from concrete of grade 20 MPa and granulated waste plastic were used as partial replacement of 0%, 5%, 10% and 15% by weight of natural fine aggregate (sand). For pull out loading test 12mm, 16 mm, 20 mm and 25 mm \varnothing rebar were used incorporating 0%, 5%, 10% and 15% plastic granular. From the study, it was observed that the variation of compressive strength is very little up to 5% replacement level. Beyond 5% replacement level compressive strength reduces rapidly with the increment of granular plastic replacement. The bonding stress between steel and concrete decreases for 12mm, 16mm, 20mm and 25mm bars respectively as about 5 to 7% with 5% replacement level, 15 to 20% with 10% replacement level and 20 to 30% with 15% replacement level. The variation is less for small \varnothing bars and it increases for higher \varnothing bars.

Keywords: Recycling plastic waste, Bonding strength, Pull out test, Waste management, PET fiber.

1. INTRODUCTION

Due to rapid industrialization & urbanization all over the world, lots of infrastructure developments are taking place. This process has thrown questions to mankind to solve the problems generated by this growth. One of the important problem is the acute shortage of constructional materials. Big attention is being focused on the environment and safe guarding natural resources and recycling of waste materials (Thosar, Husain, 2017). For solving the disposal of large amount of recycled plastic material, reuse of plastic in concrete industry is considered as the most feasible application (Yadav, 2008). Plastic waste is one of the fastest growing waste products throughout the world. Every year more than 500 billion plastic bags are used all over the world (Thosar, Husain, 2017). According to World Watch institute (2015) about 299 million tons of plastic waste were produced in 2013. Disposal of plastic waste in environment is considered to be a big problem due to its very low biodegradability and presence in large quantities. In recent time use of such industrial waste from polypropylene (PP) and poly ethylene terephthalate (PET) were studied as alternative replacements of a part of the conventional aggregates of concrete. If plastic wastes can be mixed with the concrete mass in some quantity Orin some form, without affecting the fundamental and other properties of concrete with slight negotiation in strength, large quantities of plastic waste can be consumed to solve disposal problem of plastic waste.

Reinforced concrete is an integral part of construction work all over the world. It behaves as a composite member when reinforcing bars and concrete residing together and they offer better stiffness and durability than conventional concrete. These fundamental properties

depend on the bond behavior between steel and concrete (Paul et al., 2013). If plastic waste granular is to be used in reinforced concrete then the bonding between steel and plastic is of great concern. The main objectives of this study are to investigate the influence of plastic waste granular on steel-concrete bonding and to observe the variation of compressive strength of concrete made by adding plastic granular. Ultimately, the aim of this project is to explore the possibility of recycling plastic waste material to check the variation of the mechanical properties of Reinforced Concrete.

2. METHODOLOGY

At first Literature review was completed from Journals, Books and internet. Then primary estimation for materials was made and required materials were collected. Various properties of the materials were tested and according to that mix ratio was calculated using ACI mix design. Then the specimens were cast and cured for specified curing period. After that compressive strength test and pull out test were executed.

2.1 Materials

Ordinary Portland Cement (OPC), locally available fine sand was used for casting the specimens. Brick chips made from first class bricks were used as coarse aggregate. Plastic waste products were collected, washed thoroughly and then dried. Then these were shredded and grinded to achieve required fineness.

2.1.1 Coarse aggregate

First class brick chips were used as coarse aggregate. Specific gravity, Unit weight and absorption capacity were found 2.08, 1200 kg/m³, 12% respectively. Maximum aggregate size was 20mm.

2.1.2 Fine aggregate

Local sand (fine sand) was used as fine aggregate. Specific gravity, Unit weight, absorption capacity and fineness modulus were 2.48, 1600 kg/m³, 3.26% and 1.36 respectively.

2.1.3 Binder

Ordinary Portland Cement (OPC) was used as binding material. Specific gravity, initial setting time and final setting time were found 3.15, 48 minutes and 240 minutes respectively.

2.1.4 Plastic granular

Specific gravity, Unit weight and Fineness Modulus of plastic waste granular were found 0.93, 593 kg/m³ and 2.74.

2.2 Concrete mix design

The ACI Standard 211.1 was followed for reference mix design of M20 grade concrete. The mix ratio was found 1:1.37:2.92 with w/c ratio of 0.59.

Table 1: Mix Proportion for each m³ of concrete

Plastic (%)	Water (kg)	Cement (kg)	Sand (kg)	Brick chips (kg)	Plastic Granular (kg)
0	183.62	346.49	476.39	1010.89	0
5	183.62	346.49	452.57	1010.89	23.82
10	183.62	346.49	428.75	1010.89	47.64
15	183.62	346.49	404.93	1010.89	71.46

2.3 Test specimens

For compressive strength test, cylindrical specimens of dia 150mm (6") and height 300mm (12") were used. Three specimens were used for each of the percentage of sand replacement (0%, 5%, 10% and 15%). Twelve groups of concrete cylinder of same size were used for pull out test. 12mm, 16mm, 20mm and 25mm deformed bars were used as reinforcement. For each diameter of rebar four groups of cylinder with plastic level of 0%, 5%, 10%, 15% were used. Embedded length of the bars were $12x d_b$ (bar diameter). All the tests were conducted after a curing period of 28 days.

2.4 Bond stress & Direct pull out test

The transfer of axial force from reinforcing steel bar to the surrounding concrete produced from the development of tangential stress components along the contact surface. The stress acting parallel to the bar along the interface is called bond stress. For the reinforced concrete material, it is necessary to create suitable bond between steel bars and surrounding concrete. Bond ensures that there is little or no slip of the steel bars relative to the concrete and the means by which stress is transferred across the steel-concrete. Bond resistance is made up of chemical adhesion, friction and mechanical interlock between the bar and surrounding concrete.

The direct pullout test was conducted using Universal Testing Machine. This method was adopted in this study to evaluate the bond performance of steel-reinforced concrete for various diameters (12 mm, 16 mm, 20 mm and 25 mm) and degrees of plastic granular (0%, 5%, 10% and 15% replacement of sand). This testing set up and procedure is different from ASTM C900-15 setup. However, the test was adopted in this study because it is simpler, more convenient and costs less compared with other tests. This test setup is also practical as it represents the main longitudinal reinforcement, which is mostly subjected to tensile forces in a reinforced concrete beam (Rakib, Morshed, 2016).

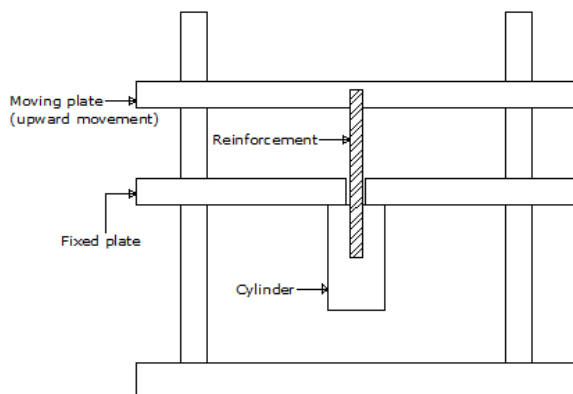


Figure 1: Schematic diagram of direct pull out test.

The schematic diagram of the test is shown in Figure 1. In the test conducted, the specimens were positioned in a Universal Testing Machine. Concrete cylinder was kept below the fixed plate that has a hole in the center where the bar can pass through. The reinforcement was entered through the hole of the fixed plate and reached to the moving plate where it was gripped by clamp. Force was applied by the upward movement of the moving plate and force was measured using the scale of Universal Testing Machine.

2.4.1 Bond stress calculation

Bond stress is calculated as average stress between the reinforcing bar and the surrounding concrete along the embedded length of the bar. In general, the bond stress corresponding to the maximum pull out load can be regarded as the bond strength or the ultimate bond (ACI Committee 2002). The criterion of ultimate bond strength is characterized by its clear definition and simplicity in bond strength interpretation (Hadi, 2008). For uniform bond, the bond stress S can be expressed as:

$$S = P_{\max} / (\pi \times L \times d_b) \quad (1)$$

Where, P_{\max} = maximum pull out load

d_b = diameter of the bar

L = Embedded bar length = $12 d_b$

Equation (1) was employed in present calculation of bonding stress between the embedded steel bar and the surrounding concrete for the specimen.

3. RESULTS & DISCUSSIONS

3.1 Results and Graphs

3.1.1 Uniaxial Compressive Strength test

The compressive strength results are shown in the Table 2 below. All the strengths are average of three values of compressive strength for each plastic level. All the specimens were made from concrete of grade 20 MPa and tested after 28 days curing period.

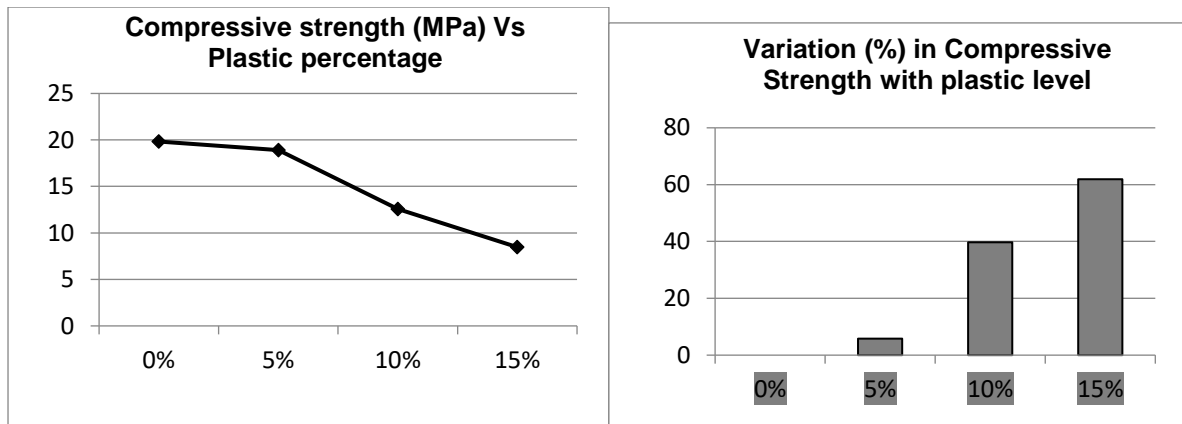
3.1.2 Table 2: Compressive strength test data

% of sand replaced	Average compressive strength (MPa)
0%	19.83
5%	18.91
10%	12.58
15%	8.47



Figure 2: compressive failure at 15% replacement level

Figure 2 shows the failure of concrete specimen under compressive load at replacement level of 15%. From figure this is evident that incorporation of plastic makes the concrete ductile. The specimen deformed significantly before failure. Figure 3 shows that the compressive strength of concrete reduces gradually with the increment of plastic granular as fine aggregate. Up to 5% replacement level the reduction is within 5%. But beyond 5% compressive strength decreases significantly up to 60%. This is due to poor bonding between plastic granular and cement paste.



• Figure 3: Variation of compressive strength with plastic level.

3.1.3 Direct Pull out test

Bond stress between steel and concrete for different bar diameters (12 mm, 16mm, 20 mm and 25 mm) incorporating various plastic levels (0%, 5%, 10% and 15%) are tabulated in Table 3 below. All the specimens were made from concrete of grade 20 MPa and tested after a curing period of 28 days.

Table 3: Direct pull out test data

Bar diameter	Average Bond stress (MPa) for various replacement levels			
	0%	5%	10%	15%
12 mm	14.64	13.26	11.91	10.47
16 mm	10.24	9.6	8.59	7.83
20 mm	8.05	7.56	6.76	6.09
25 mm	6.52	6.04	5.47	5.13

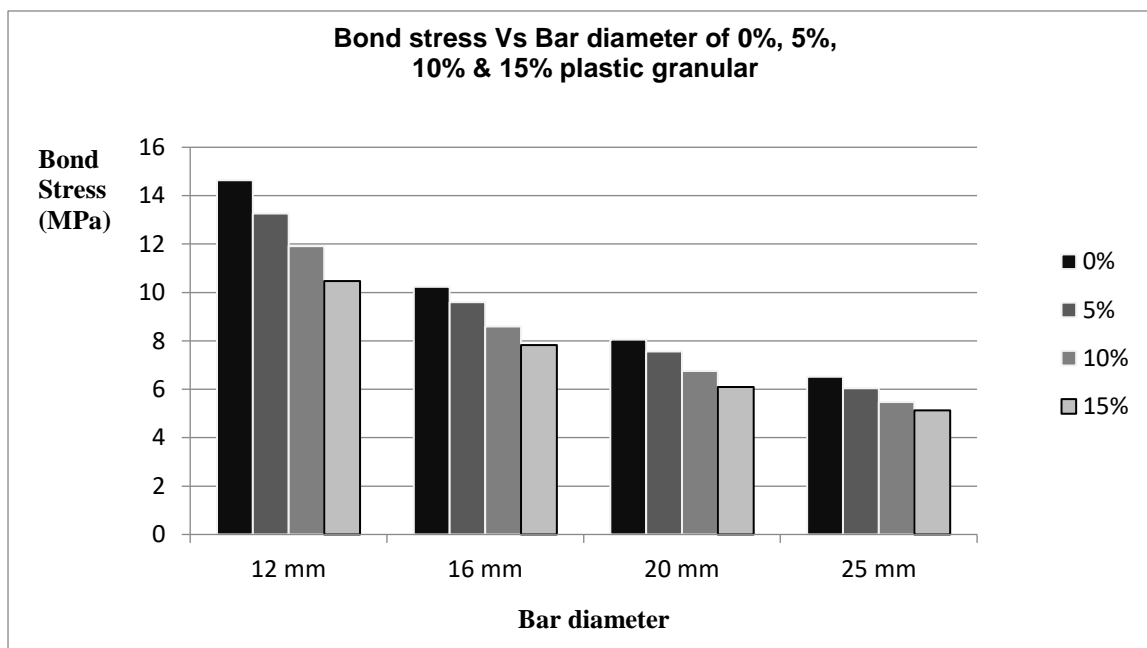


Figure 4: Bonding stress Vs Bar diameter of 0%, 5%, 10% & 15% plastic granular.

Figure 4 shows the variation of bond stress of specimens with different bar diameters for sand replacement level of 0%, 5%, 10% and 15%. Bond stress decreases with the increase

in diameter of steel bar. From graph, it is clear that plastic granular has influence on the bonding between steel and concrete. All the specimens failed by splitting or crushing of concrete. For all diameter bars the bond stress reduces with the plastic level. The possible reason behind this reduction is the poor bonding between steel and plastic material. Chemical adhesion is completely absent in this case. So the mechanical interlock is very poor.

4. CONCLUSIONS

Following conclusions can be drawn based on the results observed from this study:-

- The value of compressive strength of concrete is observed to decrease 5% up to a replacement level of 5%. But beyond that it decreases rapidly by 40% and 60% for 10% and 15% plastic granular.
- The bonding stress between steel and concrete decreases for 12mm, 16mm, 20mm and 25 mm respectively as about 5 to 7% with 5% replacement level, 15 to 20% with 10% replacement level and 20 to 30% with 15% replacement level.
- Bond stress decreases significantly with plastic granular used as partial replacement of sand. So introduction of plastic granular in Reinforced concrete is not safe and should not be recommended.
- Introduction of plastics in concrete tends to make concrete ductile, hence increasing the ability of concrete to significantly deform before failure. This characteristic makes the concrete useful in situations where it will be subjected to harsh weather such as expansion and contraction, or freeze and thaw.

ACKNOWLEDGEMENTS

The authors would like to acknowledge the support of the Department of Civil Engineering, Chittagong University of Engineering & Technology for providing the facilities and expertise to carry out this research. Authors convey their special thanks to Professor Dr. Md. Moinul Islam, Department of Civil Engineering, Chittagong University of Engineering & Technology for being extremely helpful.

REFERENCES

- Worldwatch Institute (2015)- www.plastic-pollution.org
- Hadi, MNS 2008, 'Bond of high strength concrete with high strength reinforcing steel', The Open Civil Journal, vol. 2, pp. 143-147.
- ACI Committee 318, 2002, 'Building Code Requirements for Structural Concrete', American Concrete Institute (ACI 318-02) and Commentary (318R-02), USA.
- Thosar P.C. & Dr. Husain M. (2017)- "Reuse of Plastic waste as Replacement of sand in concrete"- International Conference on Recent Trends in Engineering & Science (ICRTES 2017) Volume 6, Special issue 1
- Paul, B. K., Saha, G. C., Saha, K. K., Rashid, M. H. (2013)-"Effect of Casting temperature on Bond stress of reinforced concrete structure." Global Journals Inc. (USA), Double Blind Peer Reviewed International research journal, volume 13 issue 2 version 1.0.
- Md. Rakib and Abu Zakir Morshed (2016) – "Effect of rebar corrosion on bond stress-slip behavior in Reinforced concrete." 3rd International Conference on Civil Engineering for Sustainable Development (ICCESD 2016).
- Yadav I. S. (2008)- "Laboratory investigation of the properties of concrete containing recycled plastic aggregates"

EFFECT OF DIFFERENT BRACING SYSTEMS ON THE STRUCTURAL PERFORMANCE OF STEEL BUILDING

Md. Ahasan – ul – Haque¹, Md. Atik Masum², Md. Muhtadi Ratul³,
Zasiah Tafheem⁴

¹ Student, Department of Civil Engineering, Ahsanullah University of Science and Technology, Dhaka, Bangladesh. e-mail: ahasanridoy13@yahoo.com

² Student, Department of Civil Engineering, Ahsanullah University of Science and Technology, Dhaka, Bangladesh. e-mail: atik.masum007@gmail.com

³ Student, Department of Civil Engineering, Ahsanullah University of Science and Technology, Dhaka, Bangladesh. e-mail: mdratul619@gmail.com

⁴ Assistant Professor, Department of Civil Engineering, Ahsanullah University of Science and Technology, Dhaka, Bangladesh. e-mail: zasiah.ce@aust.edu

ABSTRACT

The present study focuses on the study of the structural performance of steel building with different bracing systems. The effectiveness of various types of bracing system on the structure has also been investigated. For this study, a ten storied commercial steel building has been designed, and then analyzed under lateral loading. The structural performance of the steel building has been investigated using different types of bracing system such as crossed bracing, V-type bracing, and eccentric bracing. A comparative study has been done on story displacement, story drift, moments on beam between braced and un-braced structures at different floor level. From the study, it has been found that in case of crossed braced structure lateral displacement is reduced by 41% which is the largest one and thus significantly contributes to greater structural stiffness. Finally, it can be said that cross diagonally braced structure shows better structural performance among all the structures considered here under similar circumstances.

Keywords: Steel Building, bracing system, story displacement, story drift.

1. INTRODUCTION

Bracing is one of the most widely used lateral load resisting systems in multi-storied buildings. Bracing is a highly efficient and economical method of resisting horizontal force in a frame structure. Braced frame is a structural system, which is designed primarily to resist wind loads and earthquake forces. Braced frames can be an effective system for seismic retrofit due to their high stiffness. Braced frames are almost always composed of steel members. The beams and columns that form the frame carry vertical loads, and the bracing system carries the lateral loads. Braced frames reduce lateral displacement, as well as the bending moment in columns. Steel bracing is economical, easy to erect, occupies less space and has flexibility to design for meeting the required strength and stiffness. It allows obtaining a great increase of lateral stiffness with a minimal added weight, and so it is very effective for existing structure for which the poor lateral stiffness is the main problem.

A comparative study has been made by Tafheem & Khusru, 2013; Khusru & Tafheem, 2014 to understand the effect of different types of bracing system on the structure. By considering both the economy and lateral stiffness, the chevron (V-type) bracing with angle section has been found the most suitable one for the building studied. Traditional chevron-braced (V- and inverted-V-braced) frames have been shown to have very undesirable post buckling behaviour characterized by beam flexure rather than truss action (Khatib et.al., 1988).

Eccentric bracings reduce the lateral stiffness of the system and improve the energy dissipation capacity. Due to eccentric connection of the braces to beams, the lateral stiffness of the system depends upon the flexural stiffness of the beams and columns, thus reducing the lateral stiffness of the frame. The vertical component of the bracing forces due to earthquake causes lateral concentrated load on the beams at the point of connection of the eccentric bracings. EBFs have been used as this have a well-established reputation as high-ductility systems and have the potential to offer cost-effective solutions in moderate seismic region. (Viswanath, K.G et.al., 2010)

The primary focus of this study is to find the most effective bracing system for steel building under lateral loads and also to compare the structural performance between unbraced and different types of braced structures. To achieve this goal, a ten storied steel building has been designed, which is located in Dhaka, Bangladesh. All loads are applied according to Bangladesh National Building Code (BNBC). All the models have been developed for similar loading scenario using different braced conditions. Four building models have been created: one is unbraced structure and other three are braced structures; X-braced structure, V-braced structure and eccentric braced structure. A comparative study among all structural systems has also been done. Comparison of story displacement, story drift and moment of a beam for both braced and unbraced structures has been carried out.

2. METHODOLOGY

Ten storied steel building has been analyzed and designed using ETABS V.15.2 by following provisions and specifications as per Bangladesh National Building Code (BNBC), 2006. The dimension of the longitudinal direction is 90 feet and transverse direction is 45 feet. The height of the building is 100 feet (10ft of each story). There are six spans in long direction and three spans in short direction having 5inch slab. The building layout plan has been given in the following Figure 1.

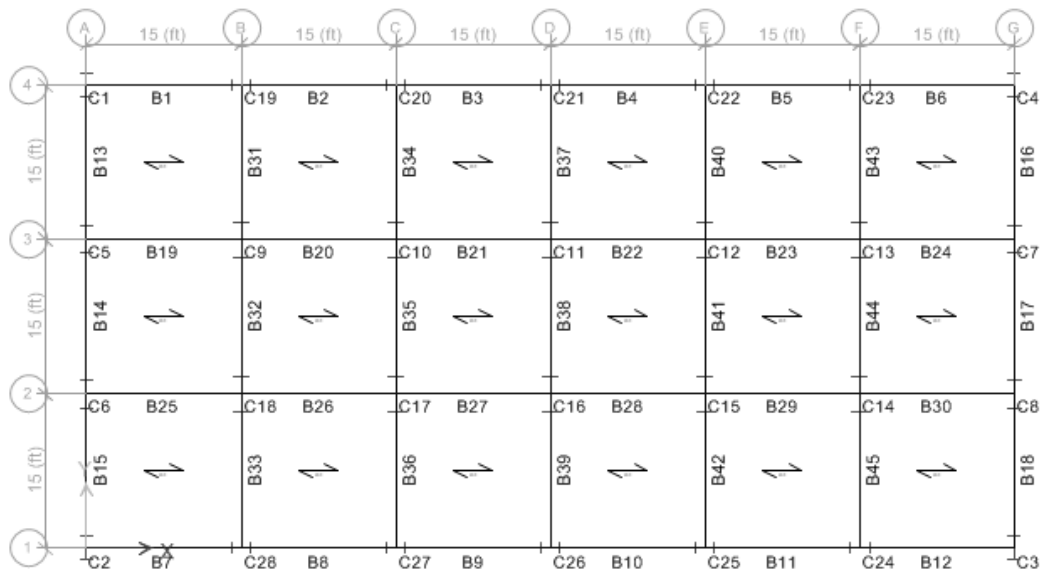


Figure 1: Column and Beam layout of the studied steel building

For simplification of study W24 section has been selected for corner columns, W18 for long direction exterior column, W27 for short direction exterior columns and W36 has been selected for interior columns. Table 1 shows the dimension of all columns.

Table 1: Column sections used in the model

COLUMN ID	Wide Flange Section
C1,C2,C3,C4	W24x370
C19,C20,C21,C22,C23,C24,C25,C26,C27,C28	W18x311
C5,C6,C7,C8	W27x539
C9,C10,C11,C12,C13,C14,C15,C16,C17,C18	W36x652

In case of beam design, W12 section has been used. Table 2 shows the dimension of all beams.

Table 2: Beam sections used in the model

BEAM ID	Wide Flange Section
B13,B14,B15,B16,17,B18,B31,B32,B33, B34,B35,B36,B37,B38,B39,B40,B41,B42, B43,B44,B45	W12x96
B2,B3,B4,B5,B8,B9,B10,B11	W12x152
B1,B6,B7,B12,B20,B21,B22,B23,B26,B27, B28, B29	W12x210
B19,B24,B25,B30	W12x230

All type of dead loads subjected to the structures are defined as per BNBC code. The super-dead loads are floor finish (FF), partition wall (PW) which act along with the self-weight.

Table 3: Dead load and live load

Name of Load	Value	Unit
Dead(FF and PW)	35	psf
Cladding Load	0.25	Kip/ft
Live Load	40	lb/ft ²

For the analysis, the wind and earthquake loading have been calculated as set forth by the provision of Bangladesh National Building Code (BNBC, 2006). According to the following Tables 4 and 5, different coefficients and parameters have been used for the wind (W) and earthquake (EQ) loading that have been applied to the structure.

Table 4: Different coefficients taken into account for the calculation of seismic load

Name	Symbol	Value	Description
Seismic Zone Coefficient	Z	0.15	Zone 2 (Dhaka)
Structural Importance Coefficient	I	1	Standard occupancy Structure (Commercial-Office)
Site Coefficient	S	1.5	Soli profile type S3
Response Modification Co-efficient	R	12	Special Moment Resisting frame

Table 5: Coefficients or parameters taken into account for the calculation of wind load

Name	Symbol	Value	Description
Terrain Exposure Category	A	---	Urban and sub-urban areas
Basic wind speed	V_b	210 km/hr	Dhaka city
Structural Importance Coefficient	C_i	1	Standard occupancy Structure

All structural models consist of same beam-column layout as architectural design are same for each. In the present study, one unbraced and three braced building structures such as X braced, V braced, eccentric braced structures have been modeled which are shown in Figure 2.

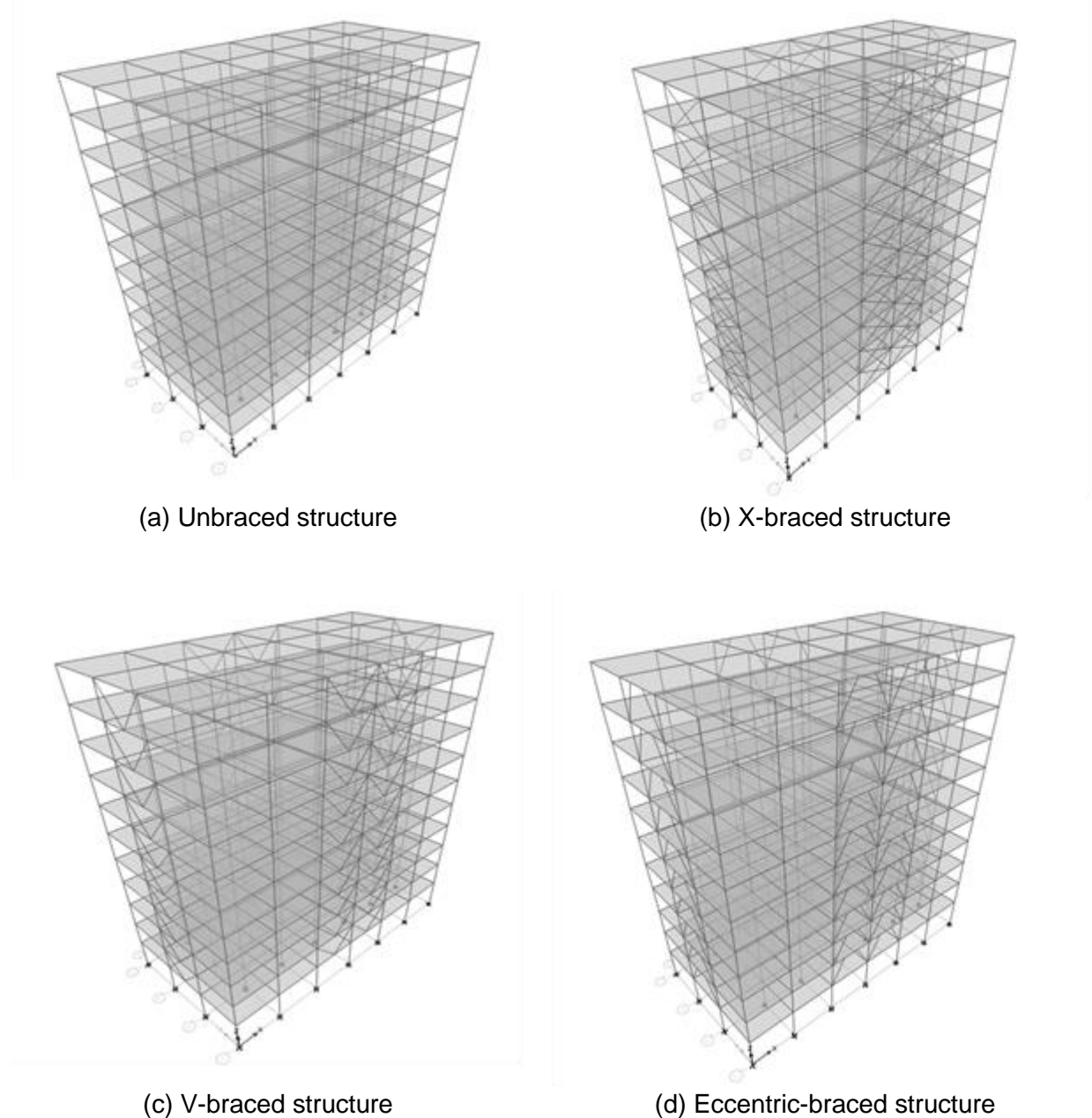


Figure 2: Different types of braced and unbraced structures

3. RESULT AND DISCUSSION

All the displacement values of all 4 structures are plotted in Figure 3 and Figure 4 along both X-direction and Y-direction respectively.

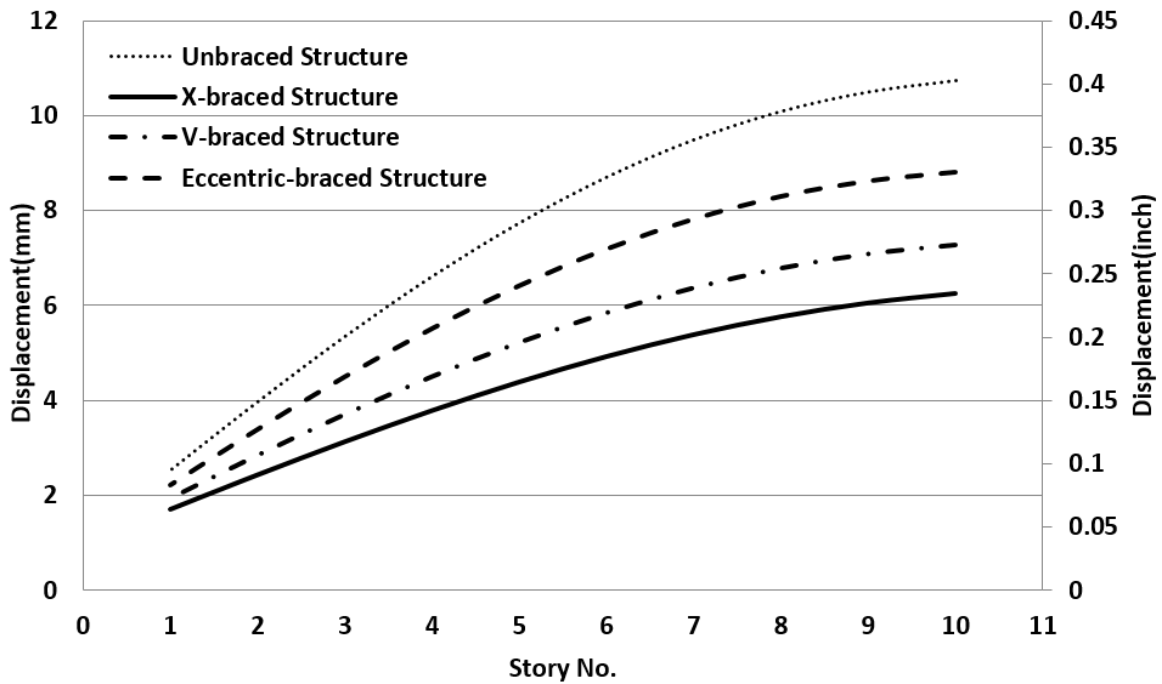


Figure 3: Displacement along X-direction for unbraced, X braced, V braced and eccentric braced structure

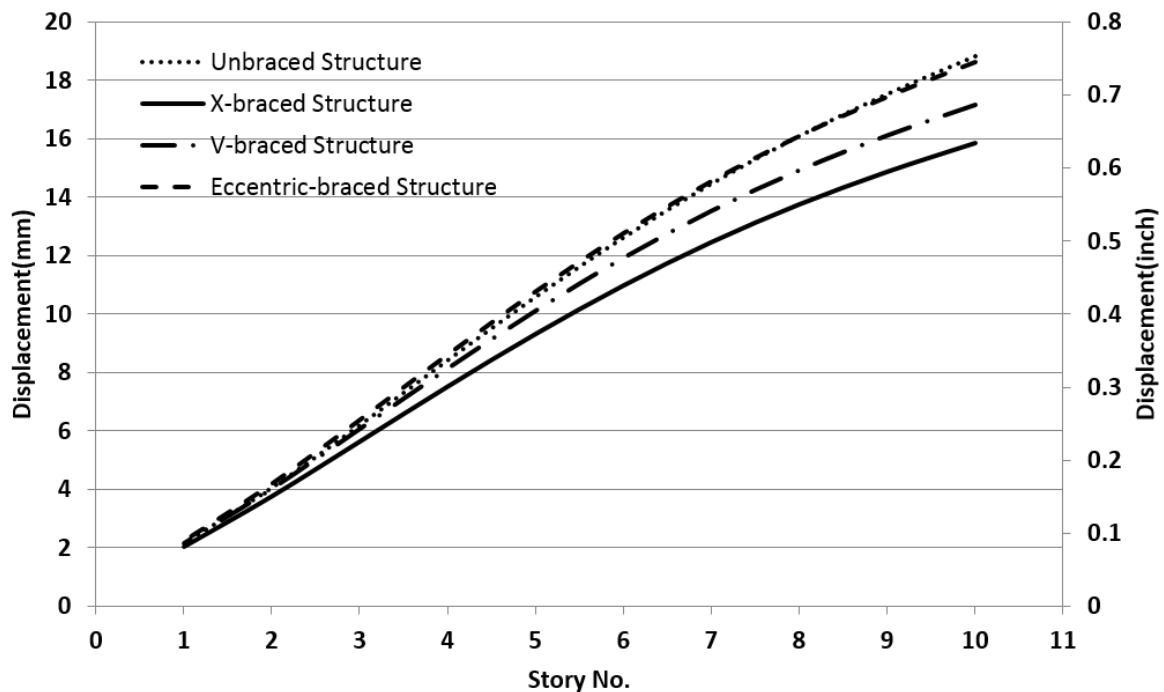


Figure 4: Displacement along Y-direction for unbraced, X braced, V braced and eccentric braced structure

From Figure 3, it is found that in X-direction and at the top floor the reduction in maximum displacement for X-braced structure is 41.7% while compared to unbraced structure followed

by 32.2% for V-Braced structure and 17.9% for eccentric-braced structure. From Figure 4, it has been found that in Y-direction for roof (10th floor) the reduction in maximum displacement for X-braced structure is 15.6% in comparison to unbraced structure followed by 8.8% for V-Braced structure and 0.8% for eccentric-braced structure.

The drift values for all 4 structures are also plotted in Figure 5. It has been observed that at the 3rd floor the values of story drift are maximum in case of all structures and the reduction in story drift values for X-braced structure is 55.7% while compared to unbraced structure followed by 33.7% for V-Braced structure and 16.7% for eccentric-braced structure.

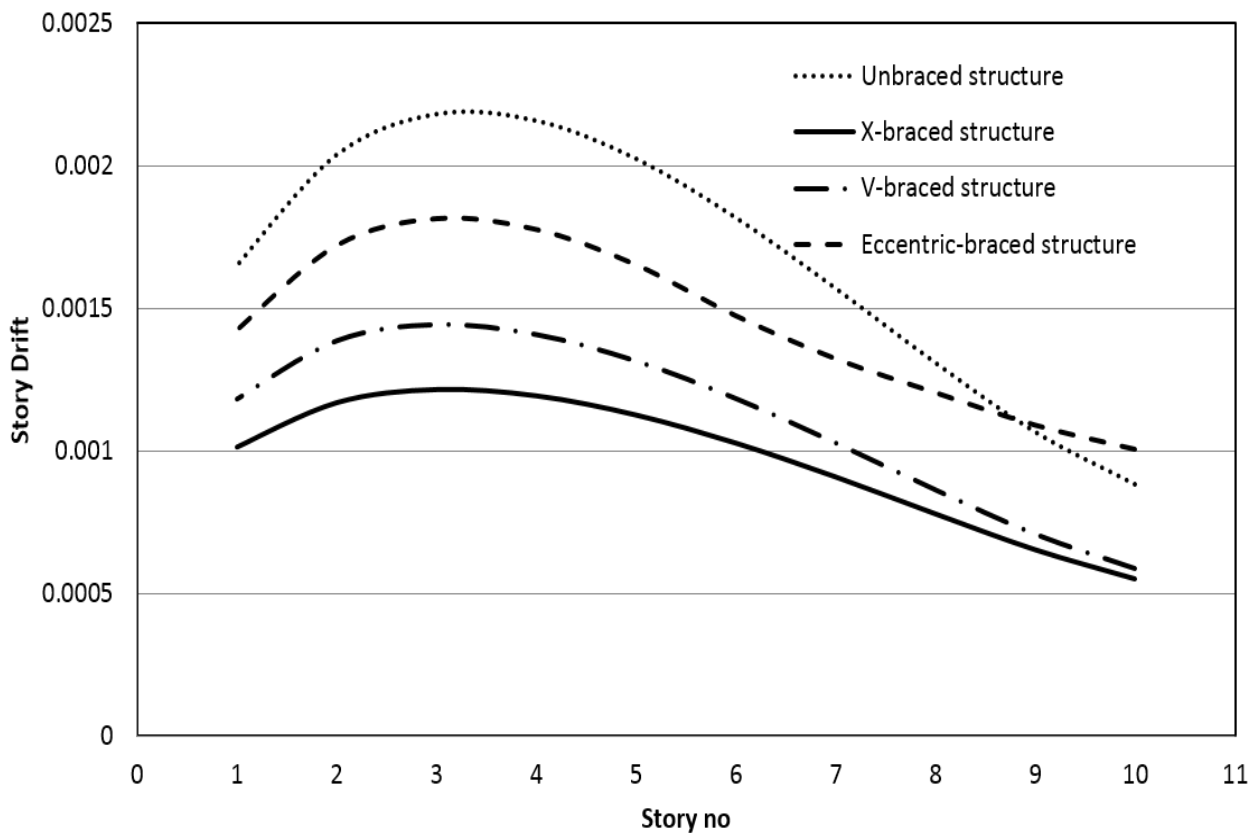


Figure 5: Story Drift of unbraced, X braced, V braced and eccentric braced structures

For the moment of a beam, the beam B13 has been considered and the highest positive or negative moment values of beam B13 were plotted in Figure 6. The moment value of the beam (B13) is lower in X-braced structure than other structures up to eighth floor and almost similar at ninth and top floor.

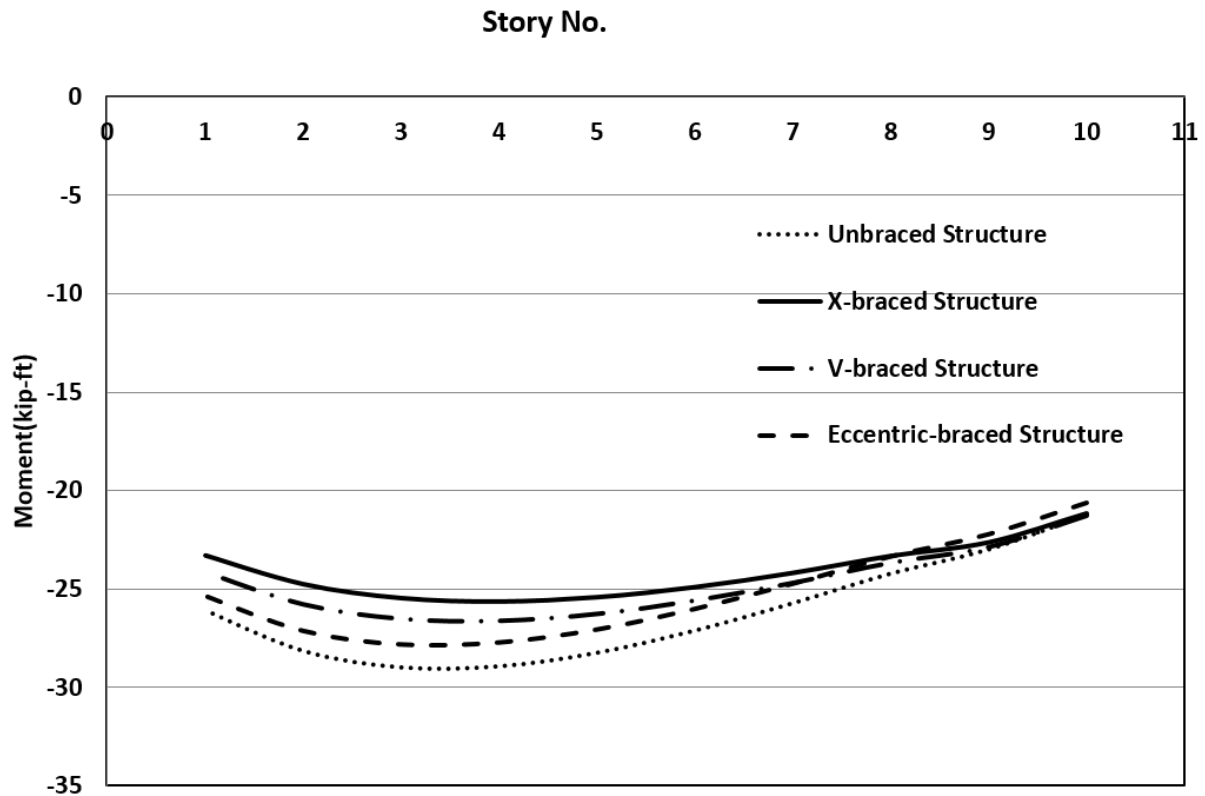


Figure 6: Moment of beam (B13) of Unbraced, X braced, V braced and Eccentric braced Structure

4. CONCLUSIONS

The findings of the present study are given below.

- In case of story displacement in X-direction, unbraced structure shows the maximum value of 0.422283 inch which is within BNBC limit. The maximum reduction in displacement value is 41.7% for X-braced structure in comparison to unbraced structure followed by 32.2% for V-Braced structure and 17.9% for eccentric-braced structure.
- In case of story displacement in Y-direction, unbraced structure shows the maximum value of 0.740774 inch which is within BNBC limit. The maximum reduction in displacement value is 15.6% for X-braced structure in comparison with unbraced structure followed by 8.8% for V-Braced structure and 0.8% for eccentric-braced structure.
- In case of story drift, unbraced structure shows the maximum value which is 0.002180. The maximum reduction in drift value is 55.7% for X-braced structure while compared to unbraced structure followed by 33.7% for V-Braced structure and 16.7% for eccentric-braced structure.
- In case of moment for beam (B13), maximum moment at 4th floor for X braced structure is lower than other three structures.

Among all models, braced structure has shown better resistance than unbraced structure. Finally, it has been found that among all the structures considered, X-Braced structure is the best option among all from the structural point of view.

REFERENCES

- Azar, B.B. and Karimi, M.R.B., (2012), Study the effect of using different kind of bracing system on tall steel structure. American journal of scientific research, ISSN 1450-233X, issue 53, pp. 24-34.
- BNBC, Bangladesh National Building Code, 2006.
- Hines, E.M.,(2010), Eccentric braced frame system performance, Structures Congress 2010, pp 1332-1341.
- Khatib, I. F., Mahin, S. A. and Pister, K. S., (1988). Seismic Behavior of Concentrically Braced Steel Frames, Report UCB/EERC 88/01, University of California, Berkeley, CA, US.
- Khusru, S., and Tafheem, Z., (2014) Comparative assessment on structural performance of optimally designed Steel braced buildings under lateral loading, Journal of Civil and Earthquake Engineering (JCEE), Vol. 3, No.1, pp.52-63.
- Nourbahsh, S.M.,(2011), In elastic behavior of braces in steel structure. Master thesis in Civil Engineering, Eastern Mediterranean University, Cyprus.
- Shin, J., (2008), Seismic evaluation of steel moment resisting frame building with different heresies and stiffness models, 14th world conference on earthquake engineering, 2008 Beijing 12-17 October.
- Sullivan, T.J.,(2013), Direct displacement seismic design of steel eccentrically braced frame structure, Bulletin of Earthquake Engineering (2013),volume 11, issue 6, pp. 2197-2231.
- Tafheem, Z, and Khusru, S., (2013), Structural behavior of steel building with concentric and eccentric bracing: a Comparative Study. International Journal of Structural Engineering, volume 4, no 1, pp 12-19.
- Tremblay, R.,(1995), Performance of steel structure during 17 January, 1994 Northridge earthquake. Canadian Journal of Civil Engineering, 1995, Volume 22 Issue 2, pp 338-360.
- Uriz, P.,(2004), Seismic performance assessment of concentrically braced steel frames, 13th world conference on earthquake engineering, Vancouver, B.C, Canada August 1-6, 2004 paper No.1639.
- Viswanath, K.G., Prakash, K.B. and Desai, A. (2010). Seismic Analysis of Steel Braced Reinforced Concrete Frames, International Journal of Civil and Structural Engineering, Vol. 1, No.1, pp. 114-116.

VULNERABILITY ASSESSMENT OF AN EXISTING BUILDING BY DAMAGE PROBABILITY MATRIX BASED ON PUSHOVER ANALYSIS

Mitu Das¹, Md. Jahir Bin Alam² and Mohammad Rafiqul Islam³

¹Student, Department of Civil and Environmental Engineering, Shahjalal University of Science and Technology, Bangladesh, e-mail: mitudas52@gmail.com

²Professor, Department of Civil and Environmental Engineering, Shahjalal University of Science and Technology, Bangladesh, e-mail: jahiralam@yahoo.com

³Assistant Professor, Department of Civil and Environmental Engineering, Shahjalal University of Science and Technology, Bangladesh, e-mail: rafiqul-cee@sust.edu

ABSTRACT:

Bangladesh is extremely vulnerable to earthquake especially the Sylhet city. In order to predict the likely impact of an earthquake on an existing building it is essential to know the seismic vulnerability of that existing building on the affected areas. This paper mainly focus about the procedures of assessing the seismic vulnerability of existing R.C.C buildings in Sylhet city. The objective of the paper is to develop damage probability matrix which represent the vulnerability of a particular structure for our country. First of all, the types of the structures are reviewed and a classification of structure based on the available data with HAZUS technical manual is done. Then the seismic vulnerability will be assessed by pushover analysis using ETABS software (Extended Three Dimensional Analysis of Building System)-version 9.6. After this nonlinear analysis the value of spectral displacement, ultimate capacity and yield capacity can be determined from capacity spectrum curve. Third, the theoretical methodology of the vulnerability analysis using fragility curve parameters given by HAZUS for typical structure are presented and performance of structure is calculated by using capacity spectrum method. At last a damage probability matrix can be formed based on this available data.

Keywords: Seismic vulnerability, damage probability matrix, pushover analysis, spectral displacement, capacity spectrum curve.

1. INTRODUCTION:

Bangladesh is always vulnerable to earthquake. Since the whole Indian subcontinent is situated on the junction of Indo-Australian plate and Eurasian plate, the tectonic evaluation of Bangladesh can be explained as a result of collision of the north moving Indo- Australian plate with the Eurasian plate. Besides, there are several fault zones active in this junction area, which are the sources of earthquake. Sylhet is extremely vulnerable to earthquake especially due to the presence of SubDauki fault zone (Bolt, B.A, 1987) and is located in seismic zone 3 according to BNBC 2006. Recently developed earthquake catalogue for Bangladesh and surrounding areas show 765 earthquakes with $M_s > 4.0$ have occurred from 1865 to 1999 within a 300km radius of Sylhet city (Sharfuddin, 2010). Among these, there are 28 earthquakes with $M_s > 6.0$ which have resulted in over thousands deaths and caused enormous damage to property, assets and infrastructure. It is evident from past fatal earthquakes around the world that the existence of vulnerable building in high intensity areas has in most cases contributed the total human loss. From the studies it was found that, in Sylhet, a larger proportion of buildings are old, non-engineered, without foundation, without continuous lintel and irregular shaped, which are vulnerable to earthquake. On the other hand, most of the new buildings are unplanned and

designed without considering earthquake risk(Ahmed M., Chowdhury, Ahmed, & Rahman, 2005).

In order to predict the likely impact of an earthquake on an existing building it is essential to know the seismic vulnerability of that existing building on the affected areas. Vulnerability assessment is also useful in estimation of consequences of building damage such as casualties and economic losses(Coburn & Spence, 2002). One of the best effective way of assessing seismic vulnerability of an existing building is nonlinear analysis called pushover analysis. This can be done by various software like ETABS, ABAQUS, SAP2000 etc. Through this nonlinear analysis yield and ultimate capacity of a structure can be easily determined which will be helpful to determine the probability of a structure of being vulnerable. Vulnerability assessment of such seismically active area helps local authorities in proper disaster management. In this paper, an attempt has been made to establish a procedure of assessing seismic vulnerability of an existing mid-rise and low rise building for a seismically active area like Sylhet.

2. METHODOLOGY:

Here the methodology adopted by HAZUS is used in this paper. The entire procedure can be divided into eight steps from the input requirement to the development of damage probability matrix.

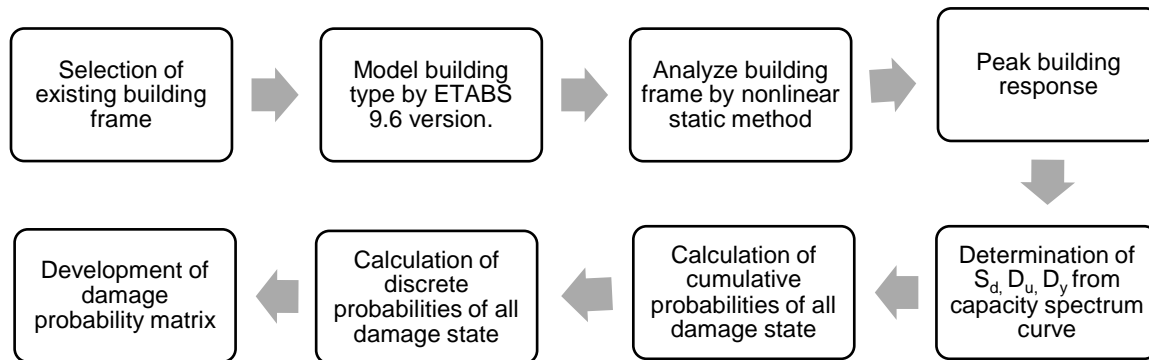


Figure 1: Flow chart of the working procedure

2.1 Building Classification:

The basic model building types are based on FEMA-178 (FEMA, 1992) building classes. Building height subclasses are added to reflect the variation of typical building periods and other design parameters with building height. A listing of structural building types, with corresponding labels, descriptions, and heights, according to HAZUS is provided in Table 1 and used in the development of Damage Probability Matrix.

Table 1: classification based on material and story height (HAZUS-MH, 2003)

NO.	Level	Description	Range	
			Name	Stories
1	C1L	Concrete Moment Frame	Low-Rise	1 - 3
2	C1M		Mid-Rise	4 - 7
3	C1H		High-Rise	8+

2.2 Selection of Building Frame:

The study work has been conducted for two existing building in Sylhet city.

1. One is C1M type normal R.C.C commercial building named “Rahman Mansion”. The floor plan and beam layout is shown in figure 2.
2. Another one is C1L type, flat slab, residential building. The floor plan is given in figure 3.

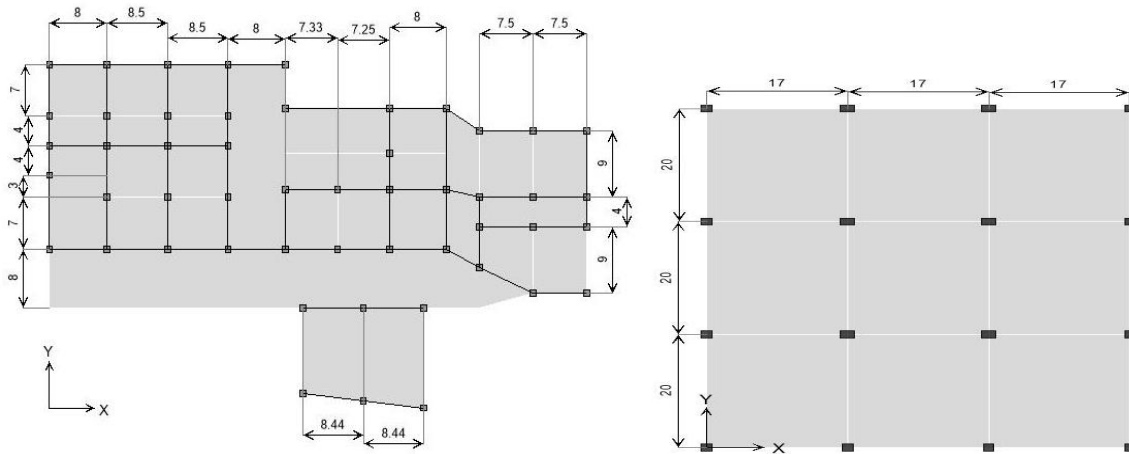


Figure 2: Floor plan of C1M type building Figure 3: Floor plan for C1L type building

2.3 Model Data For Analysis:

Topic	C1M	C1L
Number of storey	5	1
Storey height	10 ft	10 ft
Type of frame	RC moment resisting frame fixed at base.	RC moment resisting frame fixed at base.
Size of corner column	10"×10"	15"×15"
Size of edge and mid column	10"×10"	20"×15"
No of bar of corner column both above and below GL	4 nos 5/8"	-
No of bar of edge and mid column both above and below GL	6 nos 5/8"	-
Typical beam dimension	10"×10"	-
Thickness of slab	4"	6"
Compressive strength of concrete, f_c'	4000 psi.	4000 psi.
Yield strength of steel, f_y'	60000 psi.	60000 psi.
Modulus of elasticity of concrete, E	3600 ksi.	3600 ksi.
Live load on slab	120 psf	40 psf
Floor finish	30 psf	30 psf
Live load on stair	100 psf	-

Earthquake loads are calculated directly by ETABS 9.6 in accordance to UBC-94. The model of these two type of buildings has been shown in figure 4 and 5 which has been established by ETABS-9.6.

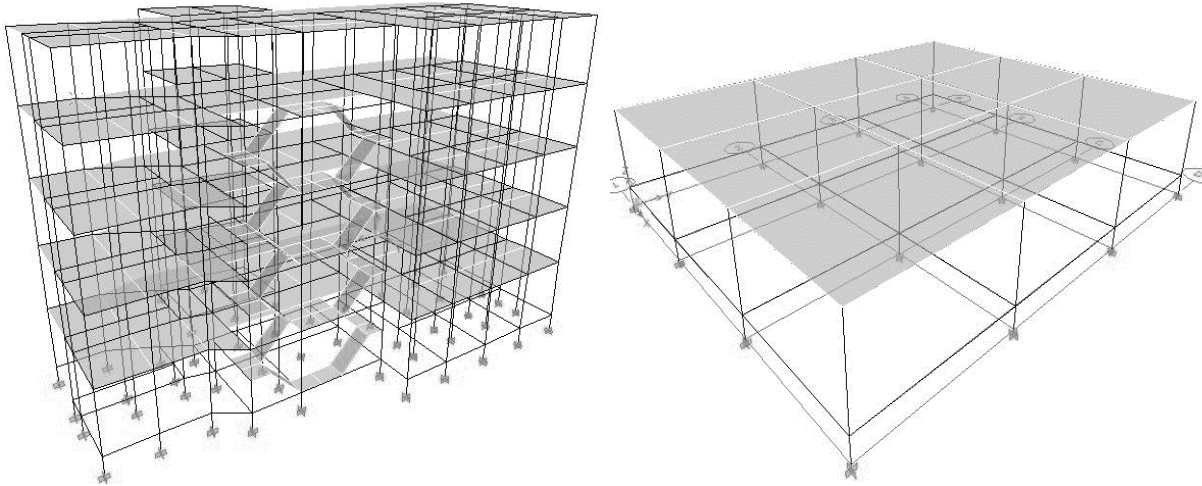


Figure 4: Final model of C1M type building Figure 5: Final model of C1L type building

2.4 Pushover Analysis:

Pushover analysis is a non-linear analysis procedure to estimate the strength capacity of a structure beyond its limit state up to its ultimate strength. It can help demonstrate how progressive failure in building most probably occurs, and identify the mode of final failure. Pushover analysis can be useful under two situation:

- When an existing structure has deficiencies in seismic resisting capacity.
- When a building is to be retrofitted to meet the seismic demands, pushover analysis can show how much where the retrofitting is required and how much.

In ETABS more than one pushover case can be assigned. In this case two pushover cases are used. In first case, gravity loads (dead, live, FF) and in second case, lateral loads (EQ-X, EQ-Y) is used.

The pushover hinges on the model by selecting one or more frame members and assigning them one or more hinge properties and hinge locations is located.

2.4.1 Pushover Curve:

After conducting non-linear analysis pushover curve is formed. Pushover curve is a plot of base shear (V_b) vs roof displacement (Δr_i). Roof displacement is the displacement at the center of mass of the general roof.

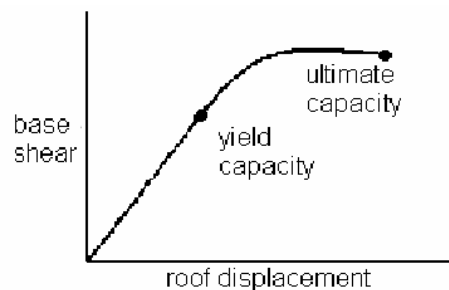


Figure 6: Typical pushover curve

After establishing pushover curve **capacity spectrum method** is used for post processing in this study as detailed in ATC-40.

2.4.2 Capacity Spectrum Curve:

Capacity spectrum curve is a plot of spectral acceleration (S_a) vs spectral displacement (S_d) which is a representation of a structure's ability to resist the seismic demand (Deepak S Bashetty, S. Veeramani, & Dr Krishnamoorthy, 2015). Spectral acceleration is a unit measured in g (acceleration due to earth's gravity) that describes the maximum acceleration in an earthquake on an object. The displacement in a single degree of freedom (SDoF) model due to spectral acceleration is called spectral displacement.

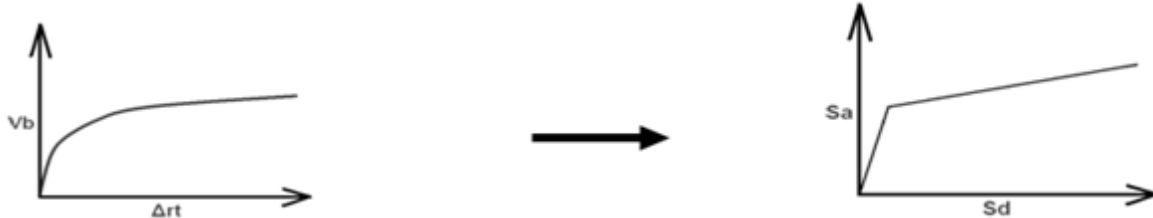


Figure 7: Converting pushover curve to capacity spectrum curve

The multi degree of freedom (MDoF) parameters (V_b and Δr_t) of pushover curve can be converted into single degree of freedom (SDoF) parameters (S_a and S_d) of capacity spectrum curve by the following equations:

$$S_a = (V_b / W) / \alpha_1 \quad (1)$$

$$S_d = \Delta r_t / (PF_1 \times \phi_{1i, roof}) \quad (2)$$

Where,

W = Total dead load of the building

α_1 = Modal mass participation for first natural mode and relates base shear

PF_1 = Modal participation factor for first natural mode and relates displacement to SDoF.

$\phi_{1i, roof}$ = Amplitude of model 1 at level i.

2.4.3 Demand Spectrum Curve:

Demand spectrum curve is a plot of spectral acceleration (S_a) vs spectral displacement (S_d) which is a representation of earthquake ground motion.

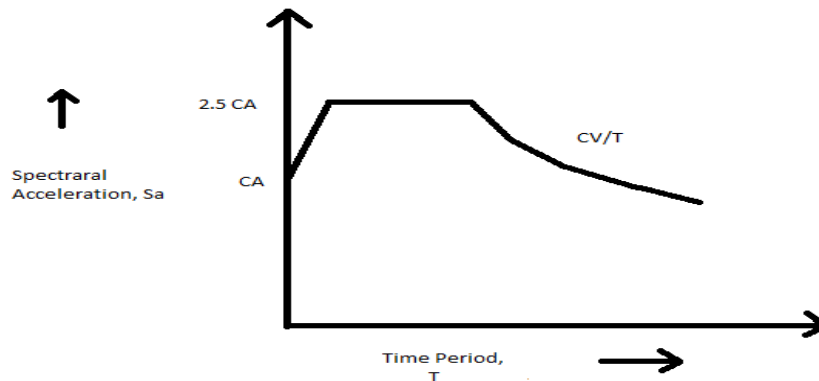


Figure 8: Typical demand spectrum curve

2.5 Performance Point or Peak Building Response:

Intersection point of capacity spectrum curve and demand spectrum curve for effective damping ratio is called performance point. That means, at this point the demand and capacity of a

structure to resist the lateral force produced due to earthquake is met. It represents the maximum inelastic capacity of the structure.

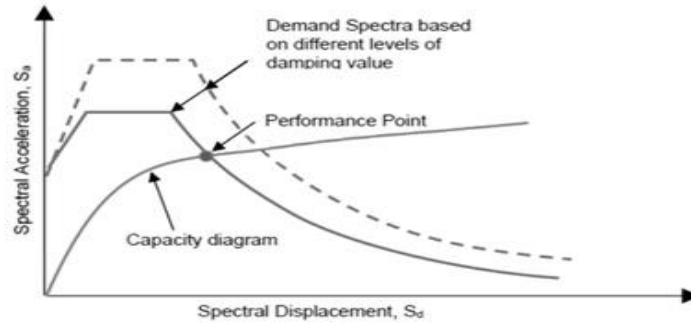


Figure 9: Intersection of capacity spectrum curve and demand spectrum curve

2.6 Determination of S_d , D_y , D_u :

- The data of spectral displacement, and ultimate displacement has been collected at the performance point which can be directly obtained from capacity and demand spectrum curve table.
- But the yield displacement can't be obtained directly from the table like the ultimate displacement. It has to be determined manually from the capacity curve. It is the value upto which the capacity curve remains linear or the slope of the curve remains equal.

2.7 Definition of Damage States:

According to HAZUS, damage states are divided in four classes as shown in Table 2.

Table 2: Damage states thresholds defines with the agreement of capacity spectrum

$Sd1 = 0.7 D_y$	Slight
$Sd2 = D_y$	Moderate
$Sd3 = D_y + 0.25(D_u - D_y)$	Extensive
$Sd4 = D_u$	Complete

Where,

S_d is spectral displacement and suffix 1, 2, 3, 4 show slight damage, moderate damage, extensive damage, and complete collapse respectively.

A_y = yield spectral acceleration

A_u = ultimate spectral acceleration.

D_y = yield spectral displacement

D_u = ultimate spectral displacement.

2.8 Cumulative Damage Probabilities:

For a given damage state, $P[S | S_d]$, $P[M | S_d]$, $P[E | S_d]$, $P[C | S_d]$ a fragility curve is well described by the following lognormal probability density function (Barbat, Lagomarsino, & Pujades, 2002), (HAZUS-MH, 2003).

$$P[ds|Sd] = \varphi\left[\frac{1}{\beta_{ds}} \ln\left\{\frac{S_d}{S_{d,ds}}\right\}\right] \quad (3)$$

Where $S_{d,ds}$ is the threshold spectral displacement and Table 2 shows how the threshold obtain from capacity spectrum (Barbat, Lagomarsino, & Pujades, 2002), β_{ds} is the lognormal standard

deviation parameter which has been described in Table 3. Φ is the standard normal cumulative distribution function and the table has been provided in Table 4 and S_d is the spectral displacement of the structure.

Where,

$P [S | S_d]$ = probability of being in or exceeding a slight damage state, S.

$P [M | S_d]$ = probability of being in or exceeding a moderate damage state, M.

$P [E | S_d]$ = probability of being in or exceeding an extensive damage state, E.

$P [C | S_d]$ = probability of being in or exceeding a complete damage state, C.

Table 3: Structural Fragility Curve Parameters - High-Code Seismic Design Level (HAZUS-MH, 2003)

Type	Slight, β_s	Moderate, β_M	Extensive, β_E	Complete, β_C
C1	0.81	0.84	0.86	0.81
C2	0.68	0.67	0.68	0.81

Table 4: Table of the Standard Normal Cumulative Distribution Function $\Phi (z)$

z	0.00	0.01	0.02	0.03	0.04	0.05	0.06	0.07	0.08	0.09
-3.4	0.00030	0.0003	0.0003	0.0003	0.0003	0.0003	0.0003	0.0003	0.0003	0.0002
-3.3	0.0005	0.0005	0.0005	0.0004	0.0004	0.0004	0.0004	0.0004	0.0004	0.0003
-3.2	0.0007	0.0007	0.0006	0.0006	0.0006	0.0006	0.0006	0.0006	0.0005	0.0005
-3.1	0.0010	0.0009	0.0009	0.0009	0.0008	0.0008	0.0008	0.0008	0.0007	0.0007
-3.0	0.0013	0.0013	0.0013	0.0012	0.0012	0.0011	0.0011	0.0011	0.0010	0.0010
-2.9	0.0019	0.0018	0.0018	0.0017	0.0016	0.0016	0.0015	0.0015	0.0014	0.0014
-2.8	0.0026	0.0025	0.0024	0.0023	0.0023	0.0022	0.0021	0.0021	0.0020	0.0019
-2.7	0.0035	0.0034	0.0033	0.0032	0.0031	0.0030	0.0029	0.0028	0.0027	0.0026
-2.6	0.0047	0.0045	0.0044	0.0043	0.0041	0.0040	0.0039	0.0038	0.0037	0.0036
-2.5	0.0062	0.0060	0.0059	0.0057	0.0055	0.0054	0.0052	0.0051	0.0049	0.0048
-2.4	0.0082	0.0080	0.0078	0.0075	0.0073	0.0071	0.0069	0.0068	0.0066	0.0064
-2.3	0.0107	0.0104	0.0102	0.0099	0.0096	0.0094	0.0091	0.0089	0.0087	0.0084
-2.2	0.0139	0.0136	0.0132	0.0129	0.0125	0.0122	0.0119	0.0116	0.0113	0.0110
-2.1	0.0179	0.0174	0.0170	0.0166	0.0162	0.0158	0.0154	0.0150	0.0146	0.0143
-2.0	0.0228	0.0222	0.0217	0.0212	0.0207	0.0202	0.0197	0.0192	0.0188	0.0183
-1.9	0.0287	0.0281	0.0274	0.0268	0.0262	0.0256	0.0250	0.0244	0.0239	0.0233
-1.8	0.0359	0.0351	0.0344	0.0336	0.0329	0.0322	0.0314	0.0307	0.0301	0.0294
-1.7	0.0446	0.0436	0.0427	0.0418	0.0409	0.0401	0.0392	0.0384	0.0375	0.0367
-1.6	0.0548	0.0537	0.0526	0.0516	0.0505	0.0495	0.0485	0.0475	0.0465	0.0455
-1.5	0.0668	0.0655	0.0643	0.0630	0.0618	0.0606	0.0594	0.0582	0.0571	0.0559
-1.4	0.0808	0.0793	0.0778	0.0764	0.0749	0.0735	0.0721	0.0708	0.0694	0.0681
-1.3	0.0968	0.0951	0.0934	0.0918	0.0901	0.0885	0.0869	0.0853	0.0838	0.0823
-1.2	0.1151	0.1131	0.1112	0.1093	0.1075	0.1056	0.1038	0.1020	0.1003	0.0985
-1.1	0.1357	0.1335	0.1314	0.1292	0.1271	0.1251	0.1230	0.1210	0.1190	0.1170
-1.0	0.1587	0.1562	0.1539	0.1515	0.1492	0.1469	0.1446	0.1423	0.1401	0.1379
-0.9	0.1841	0.1814	0.1788	0.1762	0.1736	0.1711	0.1685	0.1660	0.1635	0.1611
-0.8	0.2119	0.2090	0.2061	0.2033	0.2005	0.1977	0.1949	0.1922	0.1894	0.1867
-0.7	0.2420	0.2389	0.2358	0.2327	0.2296	0.2266	0.2236	0.2206	0.2177	0.2148
-0.6	0.2743	0.2709	0.2676	0.2643	0.2611	0.2578	0.2546	0.2514	0.2483	0.2451
-0.5	0.3085	0.3050	0.3015	0.2981	0.2946	0.2912	0.2877	0.2843	0.2810	0.2776
-0.4	0.3446	0.3409	0.3372	0.3336	0.3300	0.3264	0.3228	0.3192	0.3156	0.3121
-0.3	0.3821	0.3783	0.3745	0.3707	0.3669	0.3632	0.3594	0.3557	0.3520	0.3483

-0.2	0.4207	0.4168	0.4129	0.4090	0.4052	0.4013	0.3974	0.3936	0.3897	0.3859
-0.1	0.4602	0.4562	0.4522	0.4483	0.4443	0.4404	0.4364	0.4325	0.4286	0.4247
-0.0	0.5000	0.4960	0.4920	0.4880	0.4840	0.4801	0.4761	0.4721	0.4681	0.4641
0.0	0.5000	0.5040	0.5080	0.5120	0.5160	0.5199	0.5239	0.5279	0.5319	0.5359
0.10	0.5398	0.5438	0.5478	0.5517	0.5557	0.5596	0.5636	0.5675	0.5714	0.5753
0.2	0.5793	0.5832	0.5871	0.5910	0.5948	0.5987	0.6026	0.6064	0.6103	0.6141
0.3	0.6179	0.6217	0.6255	0.6293	0.6331	0.6368	0.6406	0.6443	0.6480	0.6517
0.4	0.6554	0.6591	0.6628	0.6664	0.6700	0.6736	0.6772	0.6808	0.6844	0.6879
0.5	0.6915	0.6950	0.6985	0.7019	0.7054	0.7088	0.7123	0.7157	0.7190	0.7224
0.6	0.7257	0.7291	0.7324	0.7357	0.7389	0.7422	0.7454	0.7486	0.7517	0.7549
0.7	0.7580	0.7611	0.7642	0.7673	0.7704	0.7734	0.7764	0.7794	0.7823	0.7852
0.8	0.7881	0.7910	0.7939	0.7967	0.7995	0.8023	0.8051	0.8078	0.8106	0.8133
0.9	0.8159	0.8186	0.8212	0.8238	0.8264	0.8289	0.8315	0.8340	0.8365	0.8389
1.0	0.8413	0.8438	0.8461	0.8485	0.8508	0.8531	0.8554	0.8577	0.8599	0.8621
1.1	0.8643	0.8665	0.8686	0.8708	0.8729	0.8749	0.8770	0.8790	0.8810	0.8830
1.2	0.8849	0.8869	0.8888	0.8907	0.8925	0.8944	0.8962	0.8980	0.8997	0.9015
1.3	0.9032	0.9049	0.9066	0.9082	0.9099	0.9115	0.9131	0.9147	0.9162	0.9177
1.4	0.9192	0.9207	0.9222	0.9236	0.9251	0.9265	0.9279	0.9292	0.9306	0.9319
1.5	0.9332	0.9345	0.9357	0.9370	0.9382	0.9394	0.9406	0.9418	0.9429	0.9441
1.6	0.9452	0.9463	0.9474	0.9484	0.9495	0.9505	0.9515	0.9525	0.9535	0.9545
1.70	0.9554	0.9564	0.9573	0.9582	0.9591	0.9599	0.9608	0.9616	0.9625	0.9633
1.8	0.9641	0.9649	0.9656	0.9664	0.9671	0.9678	0.9686	0.9693	0.9699	0.9706
1.9	0.9713	0.9719	0.9726	0.9732	0.9738	0.9744	0.9750	0.9756	0.9761	0.9767
2.0	0.9772	0.9778	0.9783	0.9788	0.9793	0.9798	0.9803	0.9808	0.9812	0.9817
2.1	0.9821	0.9826	0.9830	0.9834	0.9838	0.9842	0.9846	0.9850	0.9854	0.9857
2.2	0.9861	0.9864	0.9868	0.9871	0.9875	0.9878	0.9881	0.9884	0.9887	0.9890
2.3	0.9893	0.9896	0.9898	0.9901	0.9904	0.9906	0.9909	0.9911	0.9913	0.9916
2.4	0.9918	0.9920	0.9922	0.9925	0.9927	0.9929	0.9931	0.9932	0.9934	0.9936
2.5	0.9938	0.9940	0.9941	0.9943	0.9945	0.9946	0.9948	0.9949	0.9951	0.9952
2.6	0.9953	0.9955	0.9956	0.9957	0.9959	0.9960	0.9961	0.9962	0.9963	0.9964
2.7	0.9965	0.9966	0.9967	0.9968	0.9969	0.9970	0.9971	0.9972	0.9973	0.9974
2.8	0.9974	0.9975	0.9976	0.9977	0.9977	0.9978	0.9979	0.9979	0.9980	0.9981
2.9	0.9981	0.9982	0.9982	0.9983	0.9984	0.9984	0.9985	0.9985	0.9986	0.9986
3.0	0.9987	0.9987	0.9987	0.9988	0.9988	0.9989	0.9989	0.9989	0.9990	0.9990
3.1	0.9990	0.9991	0.9991	0.9991	0.9992	0.9992	0.9992	0.9992	0.9993	0.9993
3.2	0.9993	0.9993	0.9994	0.9994	0.9994	0.9994	0.9994	0.9995	0.9995	0.9995
3.3	0.9995	0.9995	0.9995	0.9996	0.9996	0.9996	0.9996	0.9996	0.9996	0.9997
3.4	0.9997	0.9997	0.9997	0.9997	0.9997	0.9997	0.9997	0.9997	0.9997	0.9998

2.9 Discrete Damage Probabilities:

Discrete damage probabilities can be calculated as follows:

Probability of complete damage, $P [C] = P [C | S_d]$

Probability of extensive damage, $P [E] = P [E | S_d] - P [C | S_d]$

Probability of moderate damage, $P [M] = P [M | S_d] - P [E | S_d]$

Probability of slight damage, $P [S] = P [S | S_d] - P [M | S_d]$

Probability of no damage, $P [None] = 1 - P [S | S_d]$

3. RESULTS:

3.1 Results Obtained From Pushover Analysis For C1M Model:

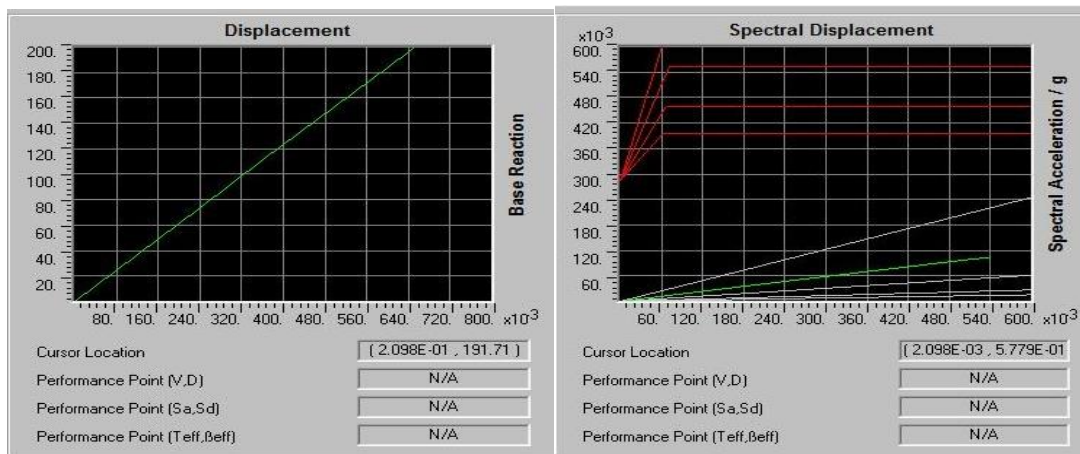


Figure 10: Pushover curve for C1M model Figure 11: Capacity spectrum and Demand spectrum curve for C1M model

Table 5: Pushover Curve Data For C1M Model

File	Step	Displacement	Base Force	A-B	B-IO	IO-LS	LS-CP	CP-C	C-D	D-E	>E	TOTAL
	0	0.0000	0.0000	2200	0	0	0	0	0	0	0	2200
	1	0.2400	74.0557	2199	1	0	0	0	0	0	0	2200
	2	0.3618	111.6309	2186	13	0	1	0	0	0	0	2200
	3	0.6039	185.2674	2184	15	0	0	0	1	0	0	2200
	4	0.6390	195.7270	2183	16	0	0	0	0	0	1	2200
	5	0.6392	196.1143	2179	20	0	0	0	0	0	1	2200
	6	0.6478	198.6822	2179	20	0	0	0	0	0	1	2200
	7	0.6470	198.5111	2200	0	0	0	0	0	0	0	2200

Table 6: Capacity Spectrum Curve and Demand Spectrum Curve Data For C1M Model

File	Step	T _{eff}	β _{eff}	S _d (C)	S _a (C)	S _d (D)	S _a (D)	ALPHA	PF*φ
	0	0.719	0.050	0.000	0.000	2.709	0.535	1.000	1.000
	1	0.719	0.050	0.198	0.039	2.709	0.535	1.628	1.213
	2	0.719	0.050	0.298	0.059	2.709	0.535	1.628	1.213
	3	0.724	0.053	0.500	0.098	2.685	0.524	1.630	1.207
	4	0.725	0.054	0.530	0.103	2.679	0.521	1.631	1.206
	5	0.728	0.058	0.534	0.103	2.643	0.510	1.635	1.196
	6	0.728	0.058	0.542	0.104	2.644	0.510	1.635	1.196

The marked line in the above tables define performance point data. The step in which the value of T_{eff} and β_{eff} is equal or approximately equal to the performance point value obtained from capacity spectrum and demand spectrum curve (figure 11) is defined as step of performance point.

3.2 Results Obtained From Pushover Analysis For C1L Model:

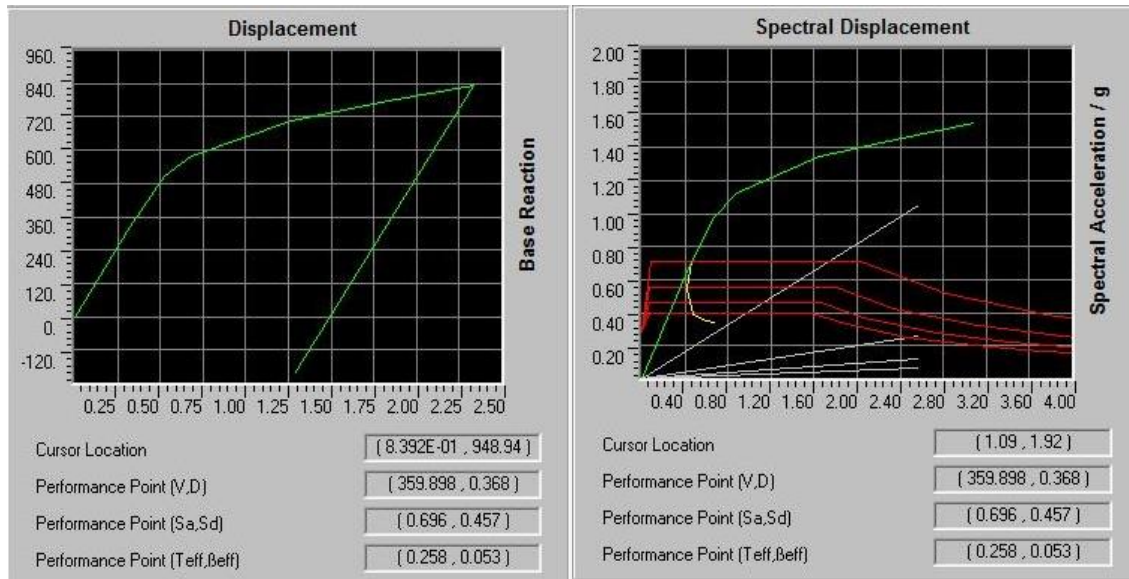


Figure 12: Pushover curve for C1L model Figure 13: Capacity spectrum and Demand spectrum curve for C1L model

Table 7: Pushover Curve Data For C1L Model

File	Step	Displacement	Base Force	A-B	B-IO	IO-LS	LS-CP	CP-C	C-D	D-E	>E	TOTAL
	0	0.0000	0.0000	159	1	0	0	0	0	0	0	160
	1	0.3275	323.5878	124	36	0	0	0	0	0	0	160
	2	0.5278	504.6125	95	61	4	0	0	0	0	0	160
	3	0.6860	579.5488	78	46	31	5	0	0	0	0	160
	4	1.2680	703.5265	75	1	48	36	0	0	0	0	160
	5	1.8389	776.4160	70	4	18	67	0	1	0	0	160
	6	2.3304	831.3887	70	4	18	65	0	2	1	0	160
	7	1.2834	-207.0752	160	0	0	0	0	0	0	0	160

Table 8: Capacity Spectrum Curve and Demand Spectrum Curve Data For C1L Model

File	Step	T _{eff}	β _{eff}	S _d (C)	S _a (C)	S _d (D)	S _a (D)	ALPHA	PF*φ
	0	0.257	0.050	0.000	0.000	0.460	0.712	1.000	1.000
	1	0.257	0.050	0.404	0.626	0.460	0.712	1.366	0.811
	2	0.264	0.065	0.667	0.978	0.444	0.651	1.364	0.791
	3	0.282	0.106	0.880	1.129	0.421	0.540	1.357	0.780
	4	0.354	0.206	1.653	1.346	0.476	0.388	1.382	0.767
	5	0.412	0.240	2.416	1.459	0.584	0.353	1.407	0.761
	6	0.452	0.249	3.094	1.551	0.686	0.344	1.417	0.753

The marked line in the above tables define performance point data. The step in which the value of T_{eff} and β_{eff} is equal or approximately equal to the performance point value obtained from capacity spectrum and demand spectrum curve (figure 13) is defined as step of performance point.

Table 9: Performance Point Data for both model

BuildingBase	Ultimate	Yield	Spectral	Spectral	Effective	Effective
Type	Shear	Displacement	Displacement	Displacement	Acceleration	Time Damping
V (kip)	D _u (in)	D _y (in)	S _d (in)	S _a (g)	Period, Ratio,	T _{eff} (sec) β _{eff}
C1M	195.72700	63900	36180	5300	1030	7250.054
C1L	504.61250	52780	32750	6670	9780	2640.065

Table 10: Calculation of Cumulative Probabilities

C1M							
Damage State	S _d (in)	S _{d,ds}	β _{ds}	X S _d / S _{d,ds}	ln(X)	Y ln(X) / β _{ds}	φ[Y]
Slight	0.530	0.2533	0.68	2.09	0.737	1.08	0.8597
Moderate	0.530	0.3618	0.67	1.46	0.378	0.56	0.7120
Extensive	0.530	0.4311	0.68	1.23	0.207	0.30	0.6179
Complete	0.530	0.6390	0.81	0.83	-0.186	-0.23	0.4091

C1L							
Damage State	S _d (in)	S _{d,ds}	β _{ds}	X S _d / S _{d,ds}	ln(X)	Y ln(X) / β _{ds}	φ[Y]
Slight	0.667	0.2293	0.81	2.91	1.07	1.32	0.9064
Moderate	0.667	0.3275	0.84	2.04	0.71	0.85	0.802
Extensive	0.667	0.3776	0.86	1.77	0.57	0.66	0.7451
Complete	0.667	0.5278	0.81	1.26	0.23	0.28	0.6102

Table 11: Damage Probability Matrix

Model Type	Slight P[S]	Moderate P[M]	Extensive P[E]	Complete P[C]
C1M	0.1477	0.0941	0.2088	0.4091
C1L	0.1044	0.0569	0.1349	0.6102

The damage probabilities of these two buildings can be shown by the following chart:

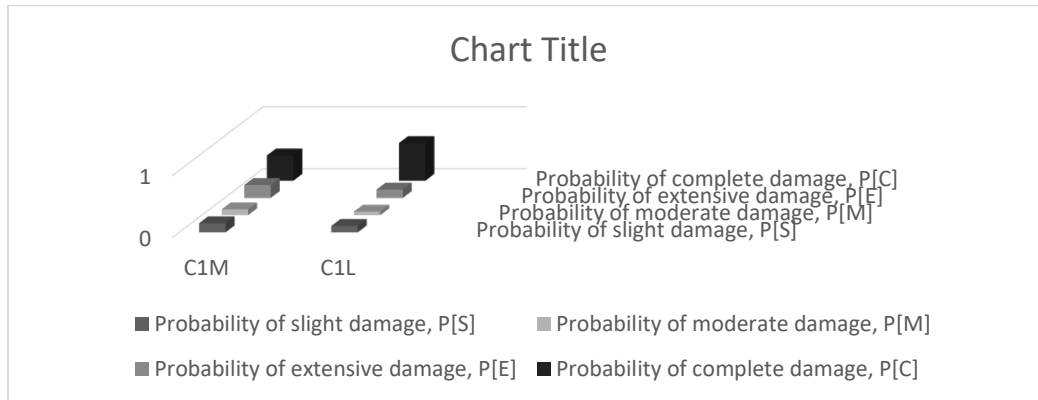


Figure 14: Damage probabilities of both model

4. CONCLUSION:

The probability of being damaged of both the buildings has been determined by pushover analysis. No performance point is available for C1M model. There is no intersection point between the capacity and demand curve as the capacity curve goes very low and demand curve goes very high which means the capacity of the building is very low but demand is very high. Still step 4 has been taken as performance point for C1M model. In this step one hinge forms at the level of $>E$, which represents ultimate collapse and in this stage, gravity loads can no longer be sustained. So, this step can be considered as most critical condition. As yield displacement can't be obtained directly, it has to be calculated manually from capacity curve. From table 3 and 5, it has been seen that, the slope of capacity curve remains equal for C1M model upto step 2 while that of remains equal for C1L model up to step 1. That's why the displacement of those step has been taken as yield displacement for both model respectively. From the above chart it can be understood that, both the buildings are really vulnerable as the probability of being completely damaged is proportionally very high for both these two building. That is how the seismic vulnerability of a mid rise and low rise building can be assessed.

REFERENCES:

- Ahmed M., A., Chowdhury, M. A., Ahmed, M. A., & Rahman, M. S. (2005). probable building damage by earthquake in Sylhet city. *Bangladesh Journal of Environmental Science, Mymensing*.
- ATC-40. (1996). *Seismic evaluation and retrofit of concrete buildings, volume 1*. California: Seismic safety commission.
- Barbat, A. H., Lagomarsino, S., & Pujades, L. (2002). Vulnerability assessment of dwelling buildings. *ResearchGate*. doi:10.1007/1-4020-3608-6_6
- BNBC. (2006). *Bangladesh National Building Code, The Housing and Building Research Institute*. Mirpur, Dhaka, Bangladesh.
- Bolt, B.A. (1987). *site specific study of seismic intensity and ground motion parameters for proposed jamuna river bridge, Bangladesh*.
- Coburn, A., & Spence, R. (2002). *Estimating Human Loss in Earthquake Model*.
- Deepak S Basetty, S. Veeramani, & Dr Krishnamoorthy. (2015). *Performance based seismic analysis of RC buildings*. Manipal Institute of Technology, Department of Civil Engineering, India.
- HAZUS-MH. (2003). *Advance engineering building module*. Department of Homeland Security Emergency Preparedness and Response Directorate FEMA Mitigation Division Washington, D.C.
- Sharfuddin, M. (2010). *Earthquake Hazard Analysis of Bangladesh*.
- Siddiqui, M. Z., Joshi, R., & Ramancharla, P. K. (2007). Estimation of Earthquake Vulnerability of a Structure. *International Conference on National Hazard and Disaster Management*. India.
- Vulnerability Atlas of India. (2007). *Building Materials & Technology Promotion Council Govt. of India*.

SULFATE AND CHLORIDE RESISTANCE PROPERTIES OF PORTLAND CEMENT BLENDS

Abu Zakir Morshed¹, Suraiya Hashi², Nitai Biswas³ and Miftaul Sadik⁴

¹ Professor, Dept. of Civil Engineering, KUET, Bangladesh, azmorshed@ce.kuet.ac.bd

² Graduated Student, Dept. of Civil Engineering, KUET, Bangladesh, suraiyahashiprema@yahoo.com

³ Graduated Student, Dept. of Civil Engineering, KUET, Bangladesh, nitaibiswasts@gmail.com

⁴ Graduated Student, Dept. of Civil Engineering, KUET, Bangladesh, sadikulridan@gmail.com

ABSTRACT

Bangladesh is an alluvial deposited country. More than 53% area is affected by sulfate, salinity and chloride in water and soil. Sulfate can attack cement paste by affecting calcium aluminates in cements and chloride can attack reinforcement by penetrating into the concrete that causes a hazardous damage of existing building. Sulfate and chloride can severely damage the existing building in coastal regions. In this paper durability of cement is evaluated on the basis of strength of mortar cube and concrete cylinder test and the sulfate attack properties of cement is evaluated on the basis of length change of mortar bar specimens during exposure to sulfate solution and the Chloride attack properties is studied by Rapid chloride ion penetration test using Ordinary Portland Cement (OPC), Portland Composite Cement (PCC), 20% FA, 30% FA and 40% FA. The compressive strength of cube specimens in sulfate solution is tested with reference to the water sample. The compressive strength of cube sample exposed to sulfate solution was about 40.6 MPa and 37.2 MPa after 13 weeks and the corresponding linear expansion was obtained about 0.28% and 0.133% for OPC and PCC cement. The compressive strength of the cylindrical specimens was about 16.96 MPa for OPC and 18.34 MPa for PCC at the age of 28 days. The permeability of chloride ion of OPC sample was 22.8% higher than the PCC at the age of 28 days.

Keywords: Blended cement; Sulfate attack; Length change; RCPT

1. INTRODUCTION

Deterioration of concrete by sulfates of an external source is a commonly observed durability problem in concrete structures exposed to seawater, soils or groundwater containing high concentrations of sulfate ions. This durability problem, also known as sulfate attack, occurs after a series of chemical reactions between sulfate ions, cement paste and moisture, (Bosunia & Choudhury, 2001). Sulfate attack is a quite complex process and despite the vast number of research since its identification by USBR in 1908, research on this durability problem is still in progress. Coastal areas in Bangladesh are formed by a delta plain at the confluence of the Ganges (Padma), Brahmaputra (Jamuna), and Meghna Rivers and their tributaries. About 53% of the coastal area is affected by salinity and sulfate in soil and water. Sulfates (for example calcium sulfate, sodium sulfate, and magnesium sulfate) can attack concrete by reacting with hydrated compounds in the hardened cement paste.

Supplementary cementing materials (SCMs) contribute to the properties of hardened concrete through hydraulic or pozzolanic activity to avoid sulfate attack. Typical examples are fly ashes, slag cement (ground, granulated blast-furnace slag), and silica fume. Supplementary cementing materials are often added to concrete to make concrete mixtures more economical, reduce permeability, increase strength, or influence other concrete properties.

Due to high alkalinity of concrete a protective oxide film is present on the surface of steel reinforcement. This protective layer also can be lost due to the presence of chloride in the

presence of water and oxygen. In reality the action of chloride inducing corrosion of reinforcement is more serious than any other reasons. Sulfate attacks the concrete whereas the chloride attacks steel reinforcements. Presence of high amount of sulfate and chloride in soil or water may reduce the design life of structures. Sulfate attack, salt crystallization and Chloride attack are more severe at coastal areas in Bangladesh.

In this study, cement is mixed with different ratio of fly ash (20%, 30% and 40%) and these are tested. After this, a suitable mix ratio is determined to reduce the sulfate attack risk of marine structures and the objects of this experiment are to evaluate the performance of commercially available Portland Composite Cement against chloride attack.

2. METHODOLOGY

Concrete strength is a great variable factor in case of stability. Concrete strength is also dependent on various factors as well as on mortar strength. In this thesis, we all have worked with mortar. For comparison of Portland Composite Cement (PCC), Ordinary Portland Cement (OPC) and cement with different composition of fly ash (20%, 30% and 40%) samples were prepared.

2.1 Materials

Different commercial brand of Ordinary Portland Cement, Portland Composite Cement, cement with 20% fly ash, 30% fly ash and 40% fly ash and local (shyllet) sand from Bangladesh were used in this study. The chemical composition of the material used in this study are summarized below in Table 1.

Table 1: Chemical composition of cementitious materials

Com-pounds	PCC	OPC
	Concentration Unit, %	Concentration Unit, %
SiO ₂	26.735	21.27
Al ₂ O ₃	13.635	5.34
Fe ₂ O ₃	3.500	2.28
CaO	53.489	63.92
MgO	2.552	3.91
SO ₃	1.744	2.32
Na ₂ O	0.123	0.47
K ₂ O	0.907	-
TiO ₂	0.915	-
P ₂ O ₅	0.058	-
MnO	0.221	-

2.2. Mix Design Ratio

The mixture of mortar for casting the cube and bar specimens were completed with a water-cement ratio of 0.485 for blends of Portland cement with pozzolan or slag. 1 part of cement was added to 2.75 parts of sand by mass.

The concrete mix for every cylindrical specimen was based on the weight of materials. The ratio of the concrete mixture was 1 (cement): 2.2 (fine aggregate): 3.5 (coarse aggregate), with a water to cement ratio of 0.6. For casting 20% FA, 30% FA, 40% FA sample the OPC cement were replaced by fly ash. The mix proportion in Kg shows below in Table 2.

Table 2: Mixing composition of samples

Batch No.	Sample type	Cement	Fine aggregate	Coarse aggregate	Fly Ash (FA)
		kg	kg	kg	kg
1	OPC	5.70	12.6	20	-
2	PCC	5.70	12.6	20	-
3	20% FA	4.56	12.6	20	1.14
4	30% FA	4.00	12.6	20	1.71
5	40% FA	3.42	12.6	20	2.28

2.3. Preparation and Test of Cement Mortar Specimens

2.3.1. Strength

Two groups of cube specimens are prepared for testing compressive strength according to ASTM C 109 standards. Each group consists of 21 nos. of cube (2"x2"x2") total 126 nos. of sample. After achieving 20 MPa strength of the samples, one group was immersed in sulfate (5% Na₂SO₄) solution by covering the curing tank with a plate or tape. Each liter of solution contains 50 g Na₂SO₄ dissolved in 900 mL water and diluted with additional distill water to obtain 1 L of solution. The mixing temperature of the solution is 23°C±2°C. The solution must contain pH range of 6.0 to 8.0. The immersed solution need to be cover up so that no air can enter into the container. For immersing the specimens in sulfate solution that is prepared the day before immersion. Compressive strength test was performed at the age of 1, 2, 3, 4, 8 and 13 weeks starting from the day of sulfate immersion.

2.3.2. Length Change

Length change was measured for the bar specimens (250±2.5 mm) with two different set of sample one in water and another one in sulfate solution at 1,2,3,4,8,13 day time interval according to ASTM C 1012 (ASTM, 2004) and ASTM C 157 (ASTM, 2006). Each set of mortar bar consists of 6 nos. of bar. The measurement was performed by a length comparator. The distances between the bolts with the formwork were 250±2.5 mm, the length inside the specimen is 7.5±0.5 mm and outside the specimen is 5 mm. Sample was placed vertically between the two stud at top and bottom. The data of each sample length was then recorded for the two group of specimen. Before the recording of length of a specified sample the base of the comparator in which gage stud on the lower end of the bar fits was cleaned. The length of the mortar specimens was measured in ±0.001 error range with the length comparator device. At the measurements, great cares were taken to calibrate dial indicator and to clean the grooves in which the specimens were put.

2.4. Preparation and Test of Concrete Cylindrical specimens

2.4.1. Strength

Five group of concrete such as OPC, PCC, 20%, 30%, 40% cylinders of diameter 100 mm (4 in) x height 200 mm (8 in) were casted by five batch. From design data 20%, 30%, 40% of Ordinary Portland cement were replaced by Fly Ash separately during casting of 18 cylindrical specimen for compressive strength test. According to mix design without any replacement of cement by Fly Ash, 12 OPC and PCC cylindrical specimen were casted for

compressive strength test. These samples were curing both normal water and Na_2SO_4 water. So, total 60 Nos. of 100 mm (4 in) diameter & 200 mm (8 in) height cylindrical samples were needed for compressive test.

2.4.2. RCPT Sample

Chloride ion penetration test was carried out according to ASTM C 1202 (ASTM, 2006). In this study the penetration was measured in terms of the total passing charge through a slice of cylinder in 6 hrs. For this test a set of cylindrical specimens ($\text{Ø}4$ in. x 6 in.) was prepared with a ratio of 1:2.4:3.35 by weight for each brand of cement. Six different types of samples were prepared for RCPT. OPC, PCC, 20%,30%,40% OPC replaced by Fly Ash samples were prepared. After demolding the sample was cut into $\text{Ø}4$ in. x 2 in. in size after curing with Na_2SO_4 water for the experimental setup. The setup was completed by arranging #100 sieve, voltage supply, multi-meter, cable, M-seal. Then the amount of charge passing and voltage were recorded by multimeter and the temperature was recorded with a thermometer.

3. RESULTS

3.1. Development of compressive strength of concrete

The following Table 3 shows the development of compressive strength of the cement mortar cube against the exposure time in sulfate solution up to the age of 91 days.

The initial strength of OPC, PCC, 20% FA, 30% FA, 40% FA in water was 22.45, 19.47, 21.57, 21.20, 8.43 MPa, respectively and sulfate strength of those was 21.25, 17.93, 19.73, 21.90, 7.93 MPa, respectively. At early age up to 28 days, strength in water solution was higher than the strength in sulfate solution. At the age of 4 weeks (28 days) the maximum strength in sulfate solution was 30% FA about 34.2 MPa and 40% FA showed the lowest strength was about 13.70 MPa. The strength of sulfate solution started to cross the strength of water solution after 28 days. According to ASTM standards 28 days minimum strength need to be 25 MPa. From the table below the compressive strength of both water and sulfate solution were greater than the standards strengths.

Table 3: Development of Compressive strength of mortar cube

Mixture designation	Compressive strength (MPa) in Sulfate					
	7 days	14 days	21 days	28 days	56 days	91 days
OPC	22.45	27.80	31.90	34.20	35.00	35.55
PCC	19.47	25.80	27.07	28.27	30.87	32.43
20% FA	21.57	25.07	25.53	25.83	29.47	34.17
30% FA	21.20	23.10	25.67	25.90	28.53	37.80
40% FA	8.43	9.47	11.53	11.83	12.47	15.63

After 4 weeks the sample strength in sulfate solution became higher than water solution. At the later age (13 weeks) the value of compressive strength of PCC and 30% FA in sulfate solution was almost 40.65 and 39.03 MPa. So, the relationship represents that the strength is higher in contact of sulfate for OPC.

3.2. Development of Compressive strength of Concrete

The following plot represents the relationship between the compressive strength of concrete cylinder and the immersion time in sulfate solution. The time scale was plot in days. The

results showed that the compressive strength of the concrete increased when Fly Ash used in concrete by replacement of OPC. But at a time the compressive strength became decreased by using high percentage of Fly Ash.

Also for the curing type the compressive strength changed. When the cylinder was curing in normal water the compressive strength was high but the compressive strength was decreased by 5%-15% for curing by Na_2SO_4 water. For OPC cylinder specimen it has observed that the compressive strength decreased when using Na_2SO_4 water for curing. For PPC cylinder specimen it has observed that the compressive strength decreased when using Na_2SO_4 water for curing. For 20% FA (Fly ash) cylinder specimen it has observed that the compressive strength decreased when using Na_2SO_4 water for curing. For 30% FA (Fly ash) cylinder specimen it has observed that the compressive strength decreased when using Na_2SO_4 water for curing. For 40% FA (Fly ash) cylinder specimen it has observed that the compressive strength decreased when using Na_2SO_4 water for curing.

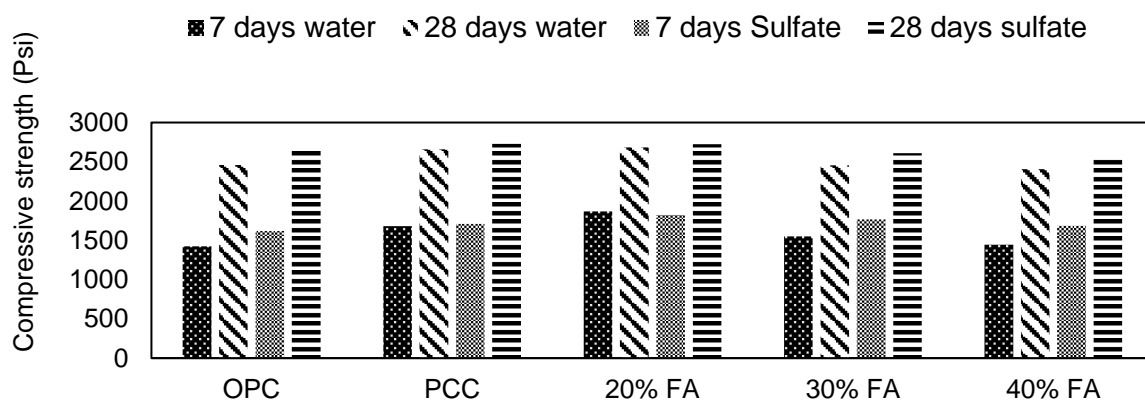


Figure 1: Comparison of compressive strength of concrete cylinder

Due to the externally and internally sulfate attack the loss of bond between the cement paste and aggregate were occurred. So every time the compressive strength of Na_2SO_4 water curing sample was 5%-15% less than normal water curing sample for sulfate attack. And for using higher percentage of fly ash the compressive strength gradually decreased because of the property of using extensive amount of fly ash the cement paste and aggregate bond become loss.

3.3. Resistance of Sulfate attack

From the graph of Expansion vs Time, it is seen that the highest length change of the mortar bars specimens of OPC is 0.078% and the lowest length change was PCC an 40% FA was about 0.013 % at 28 days.

The expansion rate at later age will become stable. The expansion after 8 weeks in sulfate solution of OPC, PCC and 30% FA sample was 0.280%, 0.032% and 0.166% in sulfate solution. The lowest length change of the mortar bars specimens is 0.001% at 28 days. In water, length change of mortar bar is lower than the length change of mortar bar in sulfate solution.

After 8 weeks the expansion of mortar bar became stable for PCC, 20% FA and 30% FA. Because in sulfate solution, ettringite is produced and as a result, cube specimens are expanded and its length change is increased with respect to time. After 8 weeks the expansion of mortar bar became stable for PCC, 20% FA and 30% FA. Because in sulfate

solution, ettringite is produced and as a result, cube specimens are expanded and its length change is increased with respect to time.

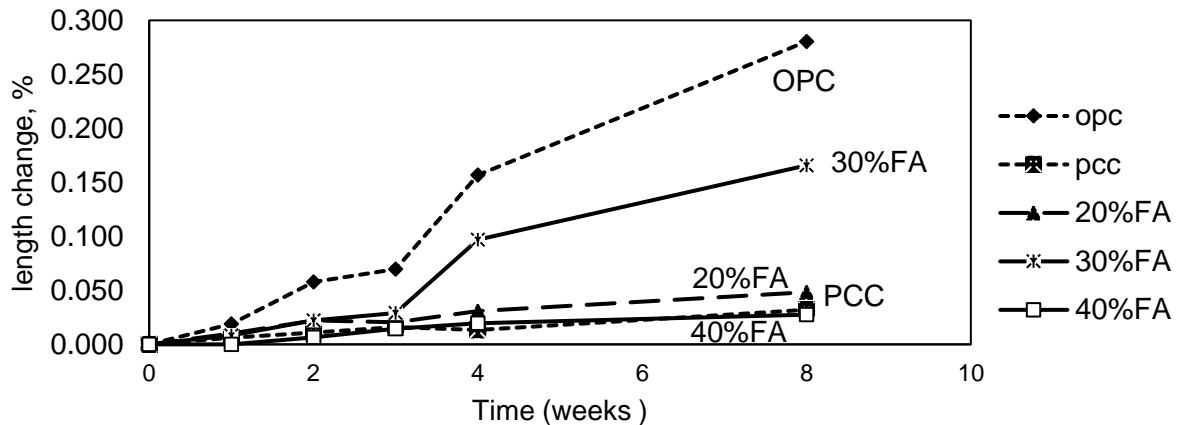


Figure 2: Comparison of length change with sulfate immersed time

The expansion rate in both water and sulfate was rapid at early age because the water absorption rate at early age increases while dry concrete was immersed for curing. When the sample immersed in sulfate solution, the sulfate is replaced by water molecule. The size of sulfate particle is larger than the water molecule, the expansion rate was initially high. After time passes the pore structure of the samples developed, the amount of water and sulfate in the pore space decreases with time.

3.4. Resistance to chloride ion penetration

The chloride ion penetration test was measured by the total charge (expressed in coulomb) passed through a slice of concrete cylinder in 6 h at age of 7, 14, 21 & 28 days. The relationship between the amount of passing charge through the concrete cylinder and time is represented in the following Figure-3. The passing charge through OPC, PCC, 20% FA, 30% FA & 40% FA was measured. The passing charge was generally very high for low percentage Fly ash sample at the age of 7 days. High charge passed 5070 coulomb in OPC sample at 7 days.

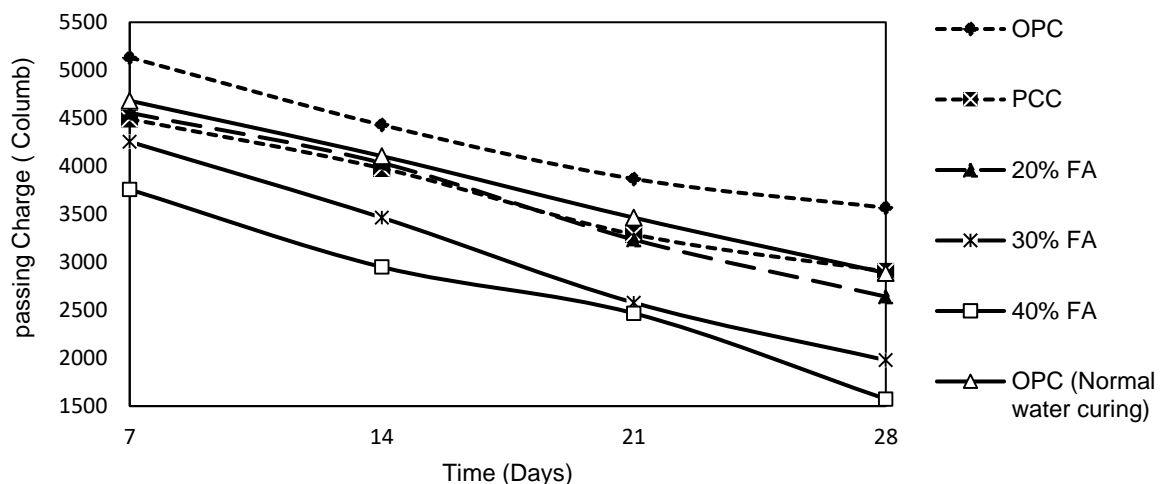


Figure 3: Comparison of chloride ion penetration with sulfate immersed

After 14 days the highest passing charge for OPC was still in high range. At the age of 21 & 28 days passed charge through OPC sample was still higher than other samples. The OPC sample in normal water curing the amount of charged was lower than OPC sample curing by

Na₂SO₄ water. The amount of charge in coulomb at 7, 14, 21 & 28 days of OPC sample (curing in Na₂SO₄ water) is 5133 C, 4430 C, 3868 C & 3567 C respectively. And the amount of charge in coulomb at 7, 14, 21 & 28 days of OPC(N) sample (curing in normal water) was 4682 C, 4105 C, 3512 C, & 2887 C respectively. So the Na₂SO₄ solution reduce the resistance of chloride ion penetration in concrete. Because the fly ash with blended cement reduces the pore of the concrete that resists more chloride ion passing through the concrete.

4. CONCLUSION

This study was carried out in three parts. First, measurement of the compressive strength of 2x2x2 in samples. Second, measurement of the length change of 250 ±2.5 mm cement mortar. Third, analysis the compressive strength by Φ4 in x 8 in cylindrical specimens. And finally chloride ion penetration test of the cylindrical specimens. All the sample casing was carried by same amount of mix proportion with different type of cement. The fly ash was replaced by the same amount of cement by weight. From this study, we all have concluded that the 30% FA sample showed the greater strength after 13 weeks and the length change of 30% FA was the largest compared to other composition of FA. Looking at the strength at 28 days the sample shows a higher expansion rate is reasonable. After long time the strength is developing and length change is dropping. Studying the concrete cylindrical specimen the PCC, OPC and 30% FA gives almost same amount of strength with a great variety of length change. The Chloride ion permeability of 30% FA is low in the scale ASTM standard category.

So Instead of OPC and PCC we can use 30% FA cement by replacing 30% cement by Fly ash for reducing environmental effect by using wastage.

ACKNOWLEDGEMENTS

We would like to express my deepest appreciation to Almighty Allah that this project has been finalizing within the limited time frame. We would also like to thanks all those who provided us the possibility to complete this report for their co-operation to complete this study.

REFERENCES

- ASTM, C. (2004). 1012, *Standard Test Method for Length Change of Hydraulic-Cement Mortars Exposed to a Sulfate Solution,* ASTM International, West Conshohocken, PA.
- ASTM, C. (2006). 157, *Standard Test Method for Length Change of Hardened Hydraulic-Cement Mortar and Concrete.*
- ASTM, C. (2006).1202, *Standard test method for electrical indication of concrete's ability to resist chloride ion penetration. Philadelphia, PA: Annual Book of ASTM Standards.*
- ASTM, C. (2007). 109, *Standard Test Method for Compressive Strength of Hydraulic Cement Mortars (Using 2-in. or [50-mm] Cube Specimens).*
- Bosunia, S. Z., & Chowdhury, J. R. (2001). Durability of concrete in coastal areas of Bangladesh. *Journal of Civil Engineering, IEB, 29(1), 41-53.*

DISPLACEMENT ANALYSIS OF SAC FRAMES UNDER DIFFERENT BRACING SYSTEMS & ISOLATORS

Tanjim Hossain¹, Shovona Khusru², Md. Abdullah-Al-Kafi³ and Nayeem Ahmed⁴

¹ Student, Ahsanullah University of Science and Technology, Bangladesh,
e-mail: dishatanjim@gmail.com

² Assistant Professor, Ahsanullah University of Science and Technology, Bangladesh,
e-mail: shovonakhusru@yahoo.com

³ Student, Ahsanullah University of Science and Technology, Bangladesh,
e-mail: akashkafi@gmail.com

⁴ Student, Ahsanullah University of Science and Technology, Bangladesh,
e-mail: vorerpakhi612@gmail.com

ABSTRACT

Earthquake causes the shaking of the Earth's surface, resulting from the sudden release of energy in the Earth's lithosphere that creates seismic waves. The objective of the study has been to observe the displacement behavior of a structure under different earthquake excitations and static loading. A 9 story SAC (joint venture between the Structural Engineers Association of California, the Applied Technology Council and the California Universities for Research in Earthquake Engineering) frame model is selected for this present study following LOS Angles method of FEMA-355C using the computer program SAP2000 v14. Different types of bracing systems namely: eccentric bracing and V bracing and also rubber base isolator have been incorporated into the structure accordingly. Excitations data from Fukushima and Corralit earthquake has been used as dynamic loading. A comparative study has been carried out amongst all the cases to observe different response under static and dynamic loading. Results showed that, the maximum displacement values are governed by the base isolated structure and the minimum displacement values are governed by the V braced structure for both static and dynamic loading. The maximum top displacement value of isolated structure is 1.7 inch & the minimum value is 0.003 inch for V braced structure. Again, maximum displacement value under static loading is 64.7 percent higher than that under Corralit earthquake. Finally, it can be said that, the structure has more displacement when it is subjected to static loading than being subjected to dynamic loading.

Keywords: Displacement, SAC frame, base isolator and different bracing systems, static loading, Fukushima and Corralit earthquake.

1. INTRODUCTION

The sac (joint venture between the structural engineers association of California, the applied technology council and the California universities for research in earthquake engineering) joint venture was formed in mid-1994 with the goal of developing reliable, practical and cost-effective guidelines and standards of practice for repairing or upgrading damaged steel moment frame buildings, the design of new steel buildings, and the identification and rehabilitation of at-risk steel buildings ("sap2000 v14"). In this study, the sac frame behaviour is noticed under static and dynamic loading. For dynamic analysis, two earthquake data is selected, namely Fukushima and Corralit earthquake. The same building model with this different earthquake data is also analyzed for different frame conditions such as base isolated, chevron (v) braced, eccentric and unbraced conditions.

Fukushima earthquake data ("Revolvy", n.d.) is gathered from the earthquake occurred on 11th April, 2011 in the Hamadori region of Fukushima, Japan. The earthquake was a potent intraplate aftershock of 6.6 mw magnitude. With a shallow focus of 13 km (8.1 mi), the earthquake was centred inland about 36 km (22 mi) west of Iwaki. Corralit

earthquake data is taken from the software package sap2000 v-14 which comprised the excitations of a sharp aftershock felt throughout the Santa Cruz mountains and the Pajaro river valley, in the central coast region of California on 19th September, 1923. The earthquake reached an intensity vi according to the Rossi-Forel scale.

Displacement profiles are observed and compared when the structure is subjected to static loading and earthquake excitations. Deformed shapes of the external corner column, external middle column and central column of the structure are considered. The result indicated the extent of effect of the static and dynamic loading as well as the isolation and bracing forms' effect on the structure.

Previous study on 'Effect of base isolation and different bracing system to improve building performance under earthquake excitations' for a 20 story sac frame was done by Ms. F.T. Zahura, Mr. S. A. Javed & Ms. R. Naznin from department of Civil Engineering, Ahsanullah University of Science and Technology, Dhaka, Bangladesh. This study illustrated that the displacement of a base isolator frame is higher than the e bracing (eccentric bracing) frame for the case of El Centro earthquake. In present study, the structure under base isolation condition also have showed more displacement under Fukushima and Corralit earthquake than its e braced (eccentric braced), chevron (v) braced and unbraced conditions.

2. METHODOLOGY

The structural responses which have been found from this present study can help to identify the load which has more effect in deforming the structure and also the form in which the structure is most weak under the loading systems. The observations will contribute further in selecting the appropriate dimensions and materials for the member sections of a structure for withstanding the possible acting loads on the structure.

2.1 Numerical Modelling and Load Assigning

Numerical modelling uses some sort of numerical time-stepping procedure to obtain the models behaviour over time. Computer software package SAP2000 V-14 is used following LOS Angles method of FEMA (Federal Emergency Management Agency)-355C for creating the model and accomplishing the result of this analysis. SAP2000 V-14 is a general purpose finite element program which performs the static or dynamic, linear or nonlinear analysis of structural systems. In this study, a 9 story SAC frame model is created ("SAP2000 V14.2.0"). Behaviour of the structure is analyzed under static loading & earthquake excitations. Base isolated, eccentric braced, chevron (V) braced and unbraced conditions of the structure are introduced in the analysis. Static loading is taken from BNBC requirements in which roofing, ceilings/flooring, mechanical/electrical, partitions and exterior wall loading along with live load, wind load and seismic load are included. Static loading consisted of 10 combinations of loads including live load, dead load, wind load and earthquake load. Envelope load is also included into static loading. Envelope load represents the possible worst condition of failing of the structure under loading. It is the summation of all of the 10 load combinations. Dynamic load is given by time history analysis.

2.1.1 Analysis

Creating model, assignment of bracing and installation of base isolator have been done before the analysis. Defining function, graph plotting and defining load case data are the steps of giving dynamic load on the structure. After applying the static and dynamic loading, the model has been run under these loadings using software package SAP2000 V-14. The analysis results have showed the structural behaviour in different bracing conditions and base isolation condition under static and dynamic loadings. This analysis results are illustrated by graphs.

3. ILLUSTRATIONS

3.1 Figures

A 9 story SAC frame model has been created by software package SAP2000 V-14. The plan view and 3D view of the model is given below.

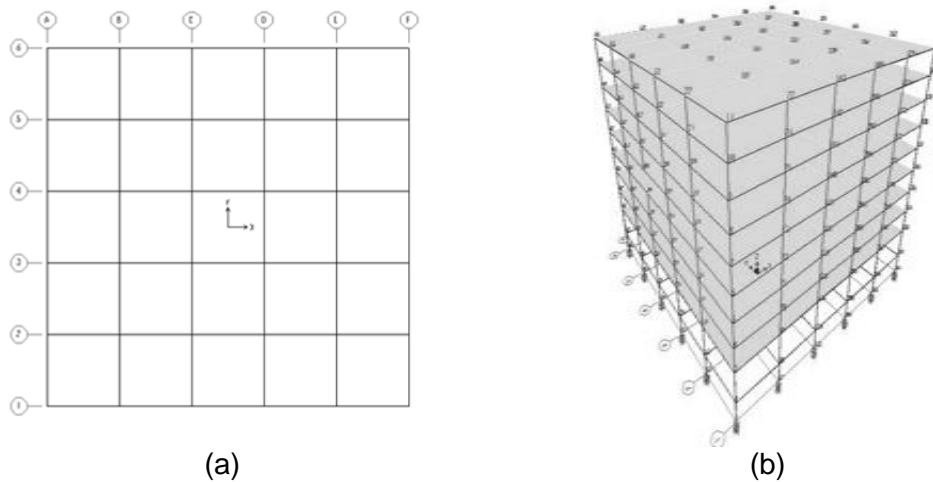


Figure 1: (a) Plan View of 9 Story SAC Frame & (b) 3D View of 9 Story SAC Frame

3.2 Tables

According to LOS Angles method of FEMA-355C, A99 steel is used for beams, girders and columns. The design yield strength of the beams and girders is given by 36 ksi and of the columns is 50 ksi. Material properties of the structural members are given in the table below:

Table 1: Material properties of the structural members

Members	Materials
Beams and Girders	A99Fy36
Columns	A99Fy50

According to LOS Angles method of FEMA-355C, the following section properties are used for the structural members:

Table 2: Section properties of the members

Story/Floor	Column		Doubler Plates (in)	Girder
	Exterior	Interior		
-1/1	W14x370	W14x500	0,0	W36X160
1 /2	W14x370	W14x500	0,0	W36X160
2/3	W14x370, W14x370	W14x500, W14x455	0,0	W36X160
3/4	W14x370	W14x455	0,0	W36X135
4/5	W14x370, W14x283	W14x455, W14x370	0,0	W36X135
5/6	W14x283	W14x370	0,0	W36X135

6/7	W14x283, W14x257	W14x370, W14x283	0,0	W36X135
7/8	W14x257	W14x283	0,0	W30X99
8/9	W14x257, W14x233	W14x283, W14x257	0,0	W27X84
9/Roof	W14x233	W14X257	0,0	W24X68

3.3 Graphs, Results and Discussion

Under static loading, displacement profiles of corner column, external middle column & central column are considered.

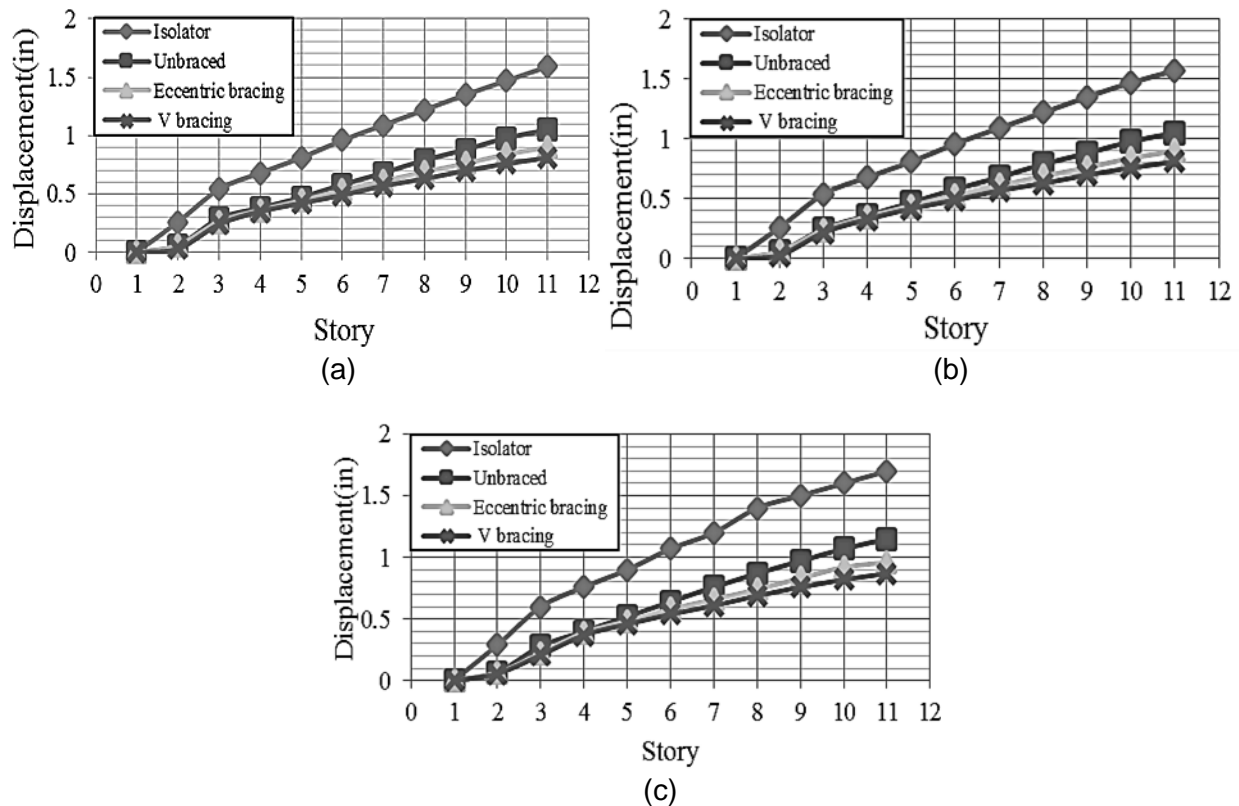


Figure 2: Displacement Profiles under static loading at (a) corner column (b) external middle column (c) central column.

All of the displacement profiles follow a same ascending pattern. For corner, external middle and central column, the structure has highest displacement when it is in base isolation condition than its unbraced, eccentric braced and chevron (V) braced condition. Chevron (V) braced condition gives the lowest displacements to the structure at all of these columns. At central column, the structure has the maximum displacements in base isolation condition in figure 3(c). In figure 3(a) and 3(b), the displacements are almost same at corner column and external middle column respectively.

Displacement profiles of corner column, external middle column & central column are observed under Fukushima earthquake.

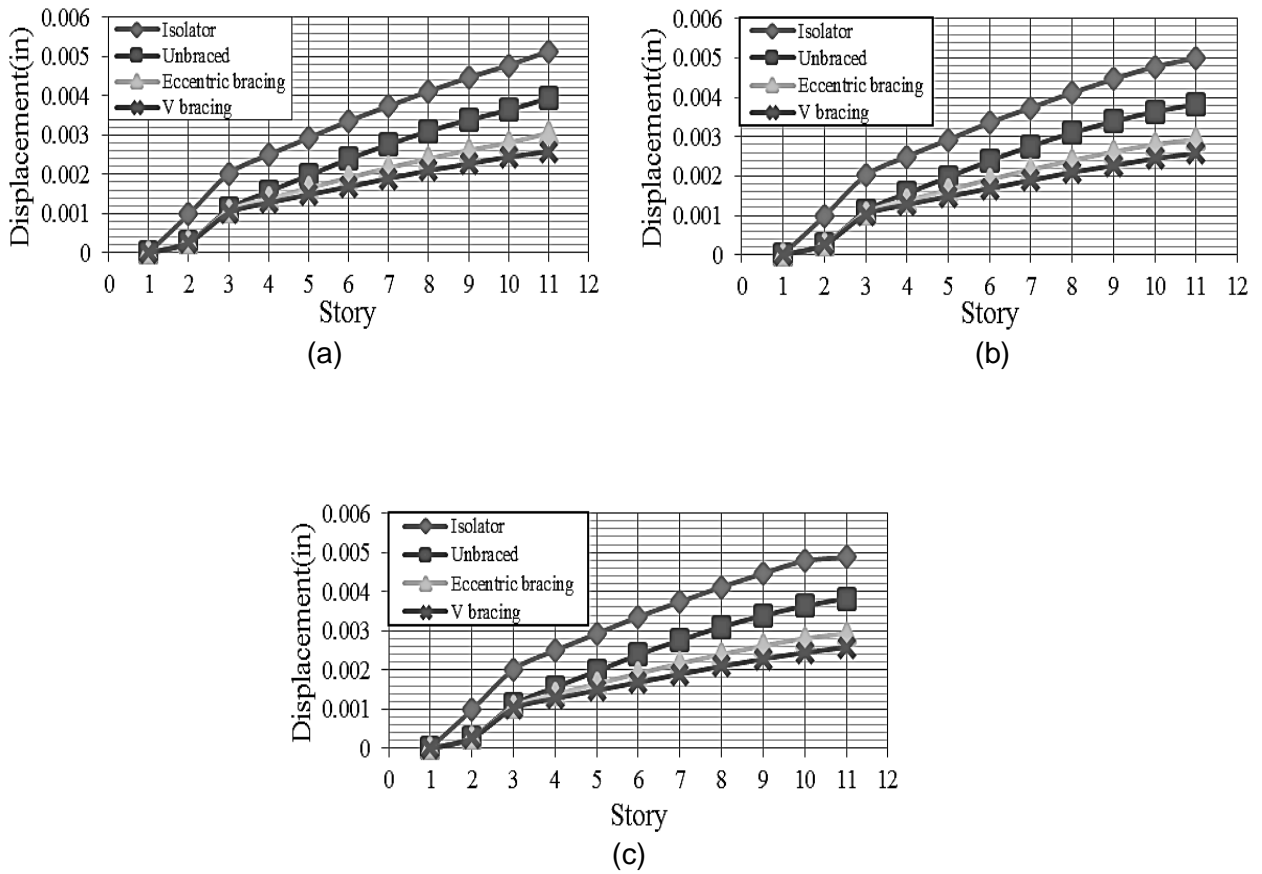
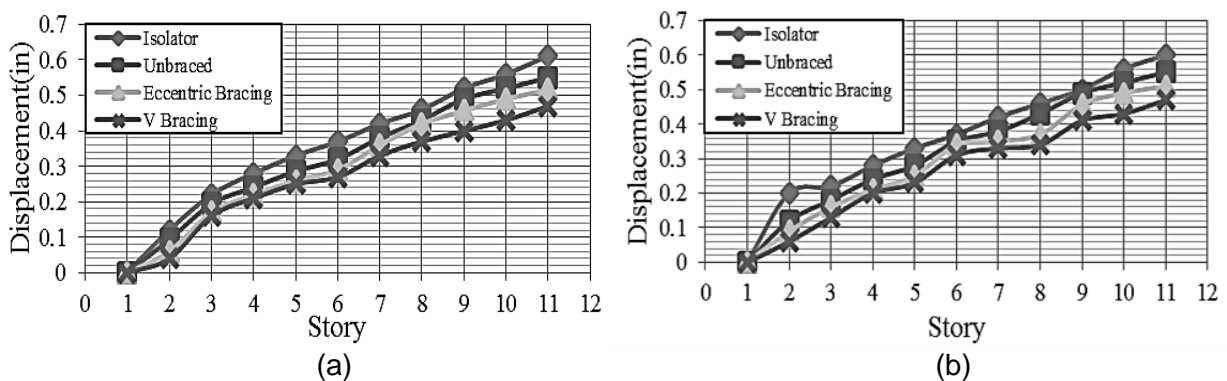
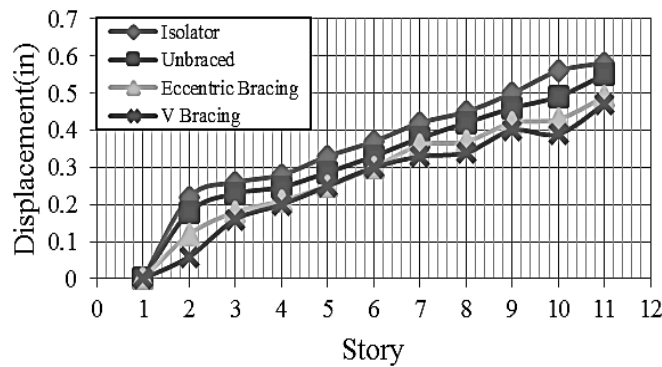


Figure 3: Displacement Profiles under Fukushima earthquake at (a) corner column (b) external middle column (c) central column.

All of the displacement profiles are in a rising pattern. When the structure is in base isolation condition, it carries the largest displacements at corner, external middle and central column than its unbraced, eccentric braced and chevron (V) braced condition. At all of these three columns, Chevron (V) braced condition gives the minimum displacements to the structure under Fukushima earthquake too. At corner column, the structure has the maximum displacements in base isolation condition in figure 4(a). In figure 4(b) and 4(c), the displacements are less than the corner column at external middle column and central column respectively.

At corner column, external middle column & central column, displacement profiles are noticed under Corralit earthquake.





(c)

Figure 4: Displacement Profiles under Corralit earthquake at (a) corner column (b) external middle column (c) central column.

The displacement profiles are in a developing form. The structure has showed the maximum displacements under the earthquake excitation in base isolation condition than its unbraced, eccentric braced and chevron (V) braced condition at corner, external middle and central column. Like under static loading and Fukushima earthquake, chevron (V) braced condition gives the minimum displacements to the structure under Corralit earthquake at these three columns. At corner column, the structure has the maximum displacements in base isolation condition in figure 5(a). In figure 5(b) and 5(c), the displacements are less than the corner column at external middle column and central column respectively.

Under both Fukushima and Corralit earthquake, the structure has behaved similarly. Displacement profiles have showed a rising shape for both of these dynamic loadings. Base isolation condition has carried the maximum displacement and Chevron(V) condition has showed the minimum displacement in the structure at corner, external middle and central column for dynamic loadings. Among the three types of columns, the corner column has suffered from the highest displacements under both earthquake excitations. Exterior middle column has carried slightly higher displacements than central column. Under these earthquakes, the unbraced and eccentric braced conditions of the structure have taken higher displacements respectively after base isolation condition.

After comparing the values of displacement profiles obtained under Fukushima and Corralit earthquake, it has been found that the displacement profiles have carried higher values when the structure has been under Corralit earthquake than under Fukushima earthquake at the corner column in base isolation condition. So, further comparison of the effect on structure has been made between Corralit earthquake and static loading.

Static loading agrees at some point with dynamic loadings. For both static and dynamic loadings, displacement profiles are following an increasing shape. Base isolation condition has underwent the largest displacements and the Chevron (V) braced condition has given the lowermost displacements to the structure under static and dynamic loadings. Unbraced and eccentric braced conditions of the structure have had higher displacements respectively after base isolation condition under static loading too. But the central column displacements are highest among the three types of columns under static loading while under dynamic loadings it is the corner column which has the highest displacements. The maximum top displacement value of 1.7 inch is found when the isolated structure has been under static loading. The value is found to be 0.003 inch for V braced structure under Fukushima earthquake. As the base isolation condition of the structure carries maximum displacement values under both static and dynamic loadings, so,

displacement values of the isolated structure is taken for further comparison between static and dynamic loading.

Comparison between static and dynamic loading on displacement:

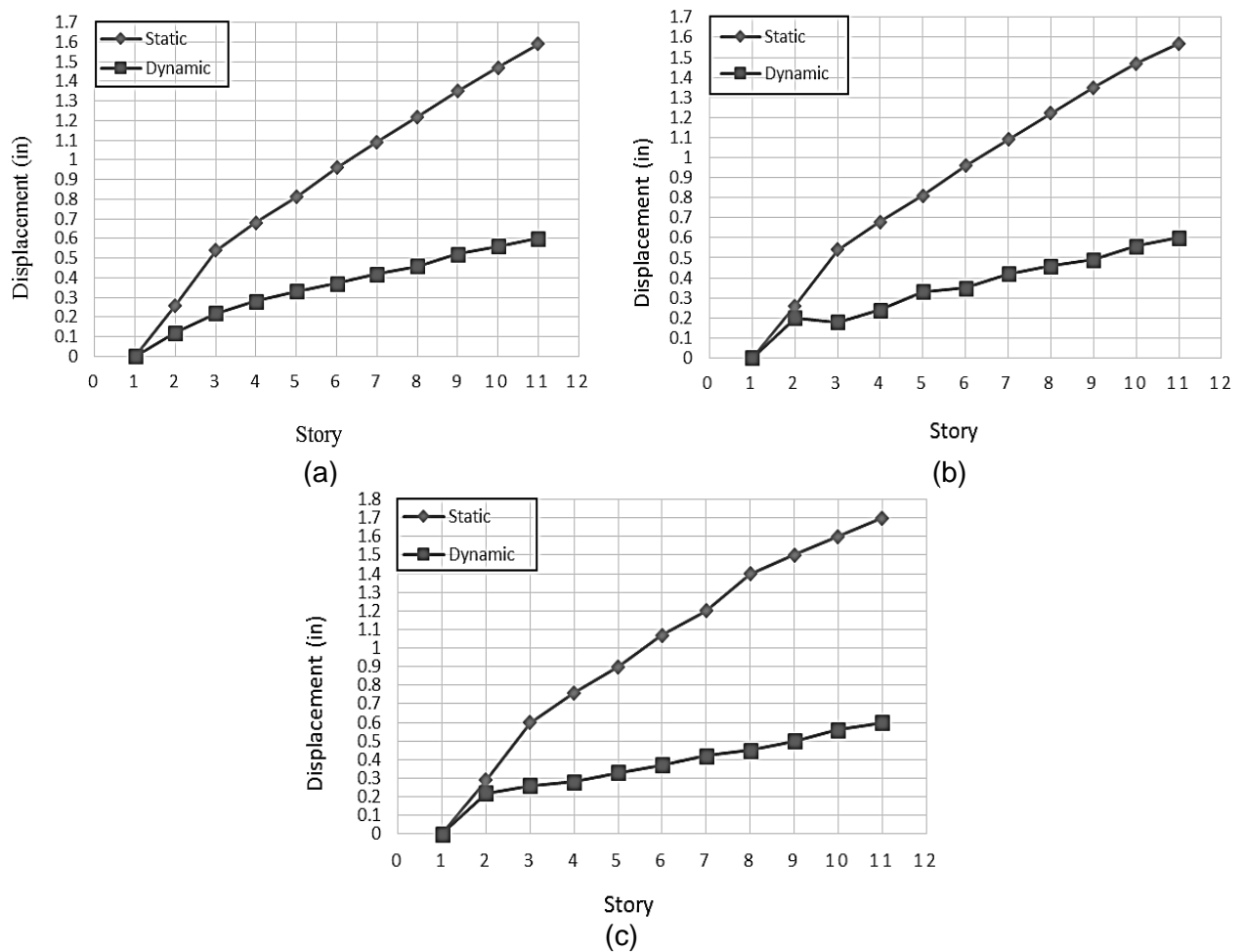


Figure 5: Comparison of displacement Profile under static and dynamic loading at (a) corner column (b) external middle column (c) central column.

After comparing among the displacement profiles of corner column, external middle column and central column in figure 6(a), (b) and (c), it is observed that static loading has more effect on these columns than dynamic loading. The maximum central column displacement is found to be 1.7 inch under static loading and maximum corner column displacement is 0.6 inch under Corralit earthquake. So, maximum displacement value under static loading is 64.7 percent higher than that under Corralit earthquake.

4. CONCLUSIONS

- After comparing the displacement profiles under static and dynamic loading, it is noticed that the structure goes through higher displacement when it is subjected to static loading than dynamic loading.
- The structure undergoes more displacement at its central column under static loading and under dynamic loading, corner column carries the higher displacement.
- Introducing base isolator into the structure provides higher displacements than Unbraced,

Eccentric braced and Chevron (V) braced structural conditions.

- Chevron (V) braced condition provides less valued displacement into the structure under loading.

REFERENCES

- BNBC (2006), Bangladesh National Building Code, Housing and Building Research Institute, Dhaka, Bangladesh, Second Edition, pp., 10655,1 0608, 10621.
- Fema-355c. 2000. State of the Art Report on Systems Performance of Steel Moment Frames Subjected to Earthquake Ground Shaking. Sac Joint Venture for the Federal Emergency Management Agency, Washington, Dc.
- Numerical Models. (n.d.). from <https://serc.carleton.edu/introgeo/mathstatmodels/Numerical.html>
- Revolvy. (n.d.),from <https://www.revolvy.com/main/show.php?cmd=list>
- SAC Steel Project: Project Description. (n.d.),from <http://www.sacsteel.org/project/>
- SAP2000 V14.2.0, Structural Analysis Programme, Integrated Software for Structural Analysis and Design; Computers and Structure Inc.,California, U.S.A.
- STRUCTURAL ANALYSIS WITH SAP2000. (n.d.), from http://www-ce.cny.cuny.edu/Courses/CE5754/SAP2000_Manual.htm
- The Structural Engineers Association of California (SEAOC), the Applied Technology Council (ATC) and the Consortium of Universities for Research in Earthquake Engineering (CUREE) The Structural Engineers Association of California (SEAOC), the A. T. C. (ATC) and the C. of U. for R. in E. E. (CUREE). (n.d.). NEES: SAC Steel Project Database. Retrieved from <https://datacenterhub.org/resources/262>

STRUCTURAL RESPONSE EVALUATION OF MULTI-STORIED FRAME USING OPTIMAL CONTROL SCHEME

Mohammad S. Miah

Assistant Professor, University of Asia Pacific, Bangladesh, e-mail: mshamim@uap-bd.edu

ABSTRACT

Vibration reduction and control of structures is a well-known problem in the area of structural engineering and mechanics. This is a branch of engineering which brings researcher from different major (i.e., mechanical, control, aerospace, and so on) in a single platform. And interestingly, all of the branches are trying to resolve the issue related to vibration mitigation and control in their respective area. In some areas such as electrical and control engineering it is quite common that they use observer such as Kalman filter for updating or predicting any missing information as they often deal with projection of trajectories. However, in order to control the vibration of any dynamical system, it is essential that the aforementioned filter is combined with a control algorithm as number of available sensors might be limited. To do this end, herein, a quite simple control algorithm so-called the viscous damping with negative stiffness (VDNS) is employed. Additionally, the VDNS scheme has been coupled with a nonlinear observer namely the unscented Kalman filter (UKF) in order to get the possibility of adding a nonlinear system. The performance of a 10-storied frame is evaluated numerically and it is observed that a significant reduction of vibration is possible via the investigated approach.

Keywords: Vibration mitigation and control; Unscented Kalman filter; Viscous damping with negative stiffness, Dynamical system.

1. INTRODUCTION

Dealing with dynamic loads are often a serious challenge in the area of structural vibration mitigation and control. This is a common problem in different areas of science and engineering such as aerospace engineering, mechanical engineering, physics, mechanics as well as in civil engineering. Even though several alternatives have been developed and used into the real structures still further improvement is necessary. There are various alternatives available to handle the aforementioned problem e.g. vibration mitigation. Active control (AC) is one of the best technologies among available alternatives. Typically, the implementation of the AC requires a control algorithm. Among many, the linear-quadratic regulator (LQR) is considered to be one of the best optimal control algorithm due to its simple form (Anderson and Moore 1989). However, the main drawback associated with the LQR control law is that it fully depends on full-state feedback meaning all of the floors information is necessary which is not possible due to cost effectiveness. Additionally, the selection of the weight parameters Q and R is a challenge as there is almost no proper guideline for selection of those parameters. Even though there are some guideline regarding initial starts but that doesn't help for a complicated problem reported by several researchers (Oral et al. 2010, Nekoui and Bozorgi 2011, Miah et al. 2013). Hence, it is essential to have an efficient alternative for optimal vibration mitigation. However, it needs to be mentioned that the performances may vary depending on the selection of the appropriate control law.

The use of linear Kalman filter (KF) is quite common where missing information are needed to be estimated. However, the KF is widely used for the linear system. The drawbacks of the aforementioned method are that it cannot deal with large amount of noise as well as nonlinear system (Miah 2015, Miah et al. 2017). Hence, herein a nonlinear filter is employed so-called the unscented Kalman filter (UKF). There are several advantages of using UKF such as it can handle nonlinear system quite efficiently as well as large amount of noise

(Chatzi et al. 2010, Miah 2015). Furthermore, it has the possibility to update the system states i.e., displacement and velocity and structural parameters such as stiffness (Miah et al. 2013).

There are several control laws available, broadly, they can be divided into two categories depending on their feedback; (i) full-state feedback, e.g. LQR (ii) partial feedback, e.g. viscous damping with negative stiffness (VDNS) (Dyke 1996, Preumont 2004, Miah 2015). The superior performances of VDNS control law has been verified by several researchers (Bhowmik 2011, Miah et al. 2014, Weber 2015). The aforementioned control laws have been used in different fields of science and engineering (Mobaieen et al. 2012), in particular, in the area of control, robotics, and mechanics. It needs to be mentioned that the control laws are essential not only for AC but also for semi-active control scheme as well. However, herein this study will focus on active control scheme in combination with VDNS. The efficacy of the AC has been verified by several researchers (Preumont 2004, Dyke 1996).

In this study, a 10-storied frame is considered and two dampers are assumed to be placed at the first-floor level and at top floor level. The responses are evaluated and compared with a benchmark namely uncontrolled model where no damper was used. The VDNS control law is employed and combined with UKF to get the advantage of nonlinear problems. Also, parameters of the system along with unknown displacement and velocity can be estimated simultaneously. And the active actuator actuation principle is employed.

2. METHODOLOGY

A benchmark model of a 10-storied frame is considered where no damper is used. And in the second model there are two dampers are considered to be placed at first and top floor. The VDNS is employed and the responses are evaluated and compared. For the simplicity, it is assumed that all of the floors are having the same mass. The 10-storied dynamical system can be described via the given equation of motion,

$$M\ddot{z}(t) + C\dot{z}(t) + Kz(t) = \beta p(t) \quad (1)$$

where M, C and K indicates the mass, damping and stiffness matrices (10×10) of the system $M = \begin{bmatrix} m_1 & \cdots & 0 \\ \vdots & \ddots & \vdots \\ 0 & \cdots & m_{10} \end{bmatrix}$, $K = \begin{bmatrix} k_1 + k_2 & -k_2 & \cdots \\ -k_2 & \ddots & \vdots \\ \vdots & \cdots & k_{10} \end{bmatrix}$, $C = \begin{bmatrix} c_1 + c_2 & -c_2 & \cdots \\ -c_2 & \ddots & \vdots \\ \vdots & \cdots & c_{10} \end{bmatrix}$, \ddot{z}, \dot{z} and z are the acceleration, velocity and displacement of the system, t is the time vector, β is a control vector that controls the input force, $p(t)$ is the input excitation.

In order to perform simulations, compact formulation is essential to make the overall simulation faster. Therefore, the state space formulation is adopted herein. There are two basic equations of state space formulation, (i) the process or system equation and (ii) measurement or observation equation. The process and observation equations are described by,

$$\begin{aligned} \dot{z}(t) &= Az(t) + Bu(t) + w(t) \\ y(t) &= Cz(t) + Du(t) + v(t) \end{aligned} \quad (2)$$

where A is the system matrix $A = \begin{bmatrix} 0_{10 \times 10} & I_{10 \times 10} \\ -(M^{-1}K)_{10 \times 10} & -(M^{-1}C)_{10 \times 10} \end{bmatrix}$ and B is the input matrix $B = \begin{bmatrix} 0 & 0 & 0 & 0 & -1 & -1 & -1 & -1 & -1 \\ -m_1^{-1} & 0 & 0 & 0 & 0 & 0 & 0 & 0 & -m_{10}^{-1} \end{bmatrix}^T$, z is the state vector that contain displacement and velocity vector, u indicates the input force $u = [x_g \quad f_{control}]^T$, x_g is the

input excitation and $f_{control}$ represents the control force, C is the output matrix, D means the feedthrough matrix, w and v are the process and observation noise respectively.

The performance of the LQR control law heavily depends on the weight factors and the control force is estimated from the full-state feedback. In order to avoid the aforementioned problem, the VDNS is employed as control law due to its simplicity and another advantage is that it only requires the collocated information. However, herein non-collocated (e.g. third floor) information is used to get the best performance in terms of vibration reduction. The control law is described via the equation below,

$$f_{control}^{vdns}(t) = -k^{vdns} \times x(t) + c^{vdns} \times \dot{x}(t) \quad (4)$$

where $f_{control}^{vdns}$ is the optimal control force estimated via VDNS control law, k^{vdns} and c^{vdns} indicates the stiffness and damping coefficients of the control law accordingly, x and \dot{x} are the displacement and velocity used to estimate the control force. The implemented closed-loop is depicted in Figure 1.

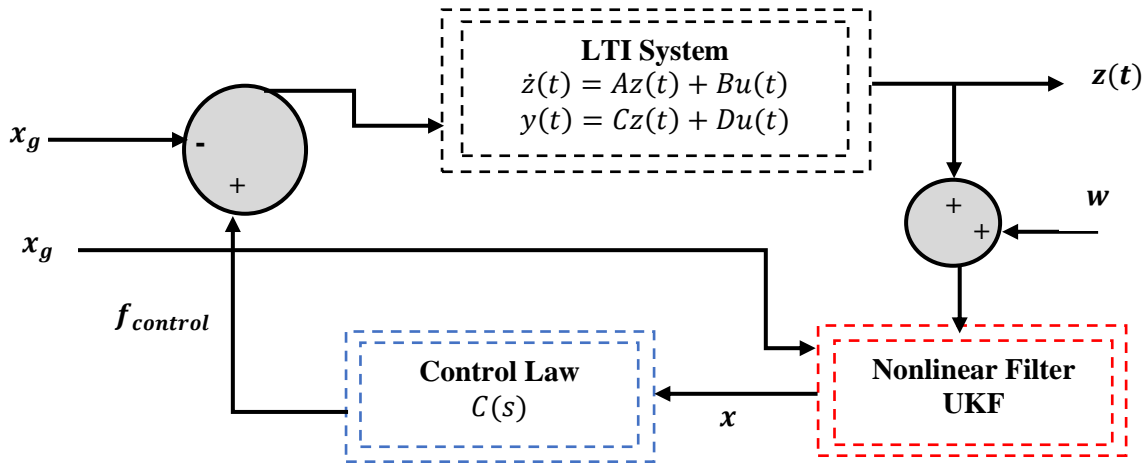


Figure 1: Closed-loop of the studied problem.

In order to perform simulations the above described closed-loop implementation is adopted. Where the *LTI System* block represents the linear time-invariant system/structure, *Nonlinear Filter UKF* block indicates the nonlinear observer and the *Control Law* block represents the implemented control scheme e.g. VDNS. It needs to be mentioned that only few floors (i.e., 1st, 5th and 10th) information e.g. accelerations are assumed to be measured.

3. NUMERICAL IMPLEMENTATIONS

The numerical simulations are done via MATLAB/SUMILINK[®]. The simulation is done for a sampling frequency of 500Hz and maximum time of 70sec and the load was turned off after ~46sec. A harmonic type dynamic load is employed; and the structure was excited at the first resonant frequency to observe the extreme level of vibration. The simulations are done in a nearly real-time platform so-called SIMULINK[®]. Firstly, a benchmark problem is evaluated to compare the responses with controlled case. The benchmark case has been named as “Uncontrolled” for simplicity. And the controlled case has been named as “Controlled-VDNS”, represents the case with VDNS control law is combined with UKF. The responses such as displacements, velocities and acceleration are observed and compared at different floor level of the structure.

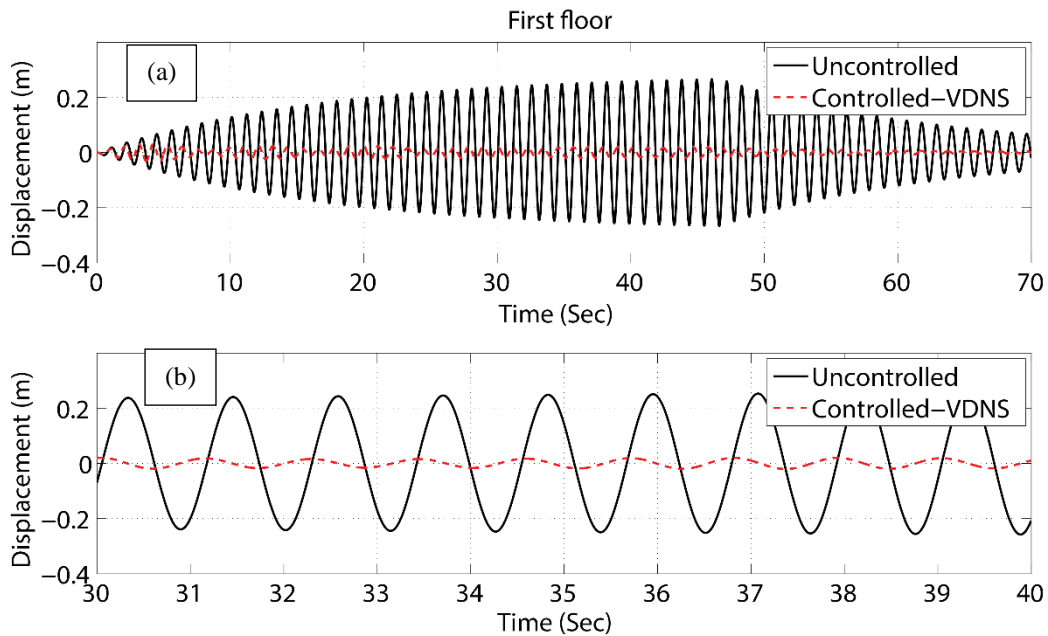


Figure 2: Comparison of the 1st floor displacement; (a) full-time history, (b) zoomed view.

In Figure 2, the comparison of the first floors' displacement trajectories are presented. In the aforementioned figure, the full time history 0-70 sec is depicted and a zoomed view from 30-40 sec is shown for the visualization purpose.

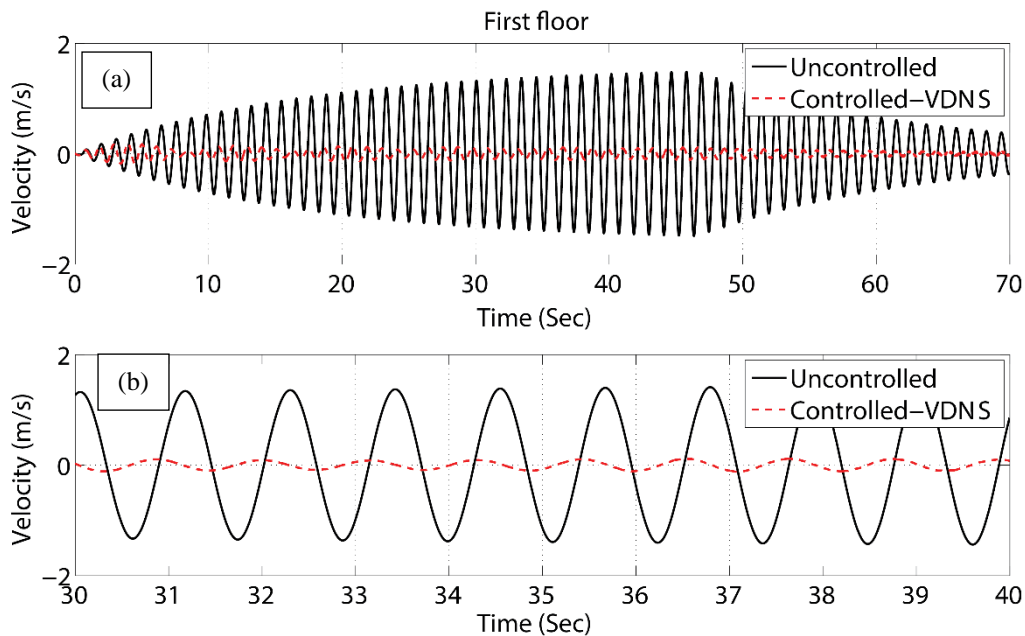


Figure 3: Comparison of the 1st floor velocity; (a) full-time history, (b) zoomed view.

The uncontrolled case is shown by black line, the dotted red line represents the VDNS control case. It can be summarized from Figure 2 that the vibration has been reduced significantly via the VDNS control approaches. It is happening due to the real-time update of the control force based on the current displacement and velocity.

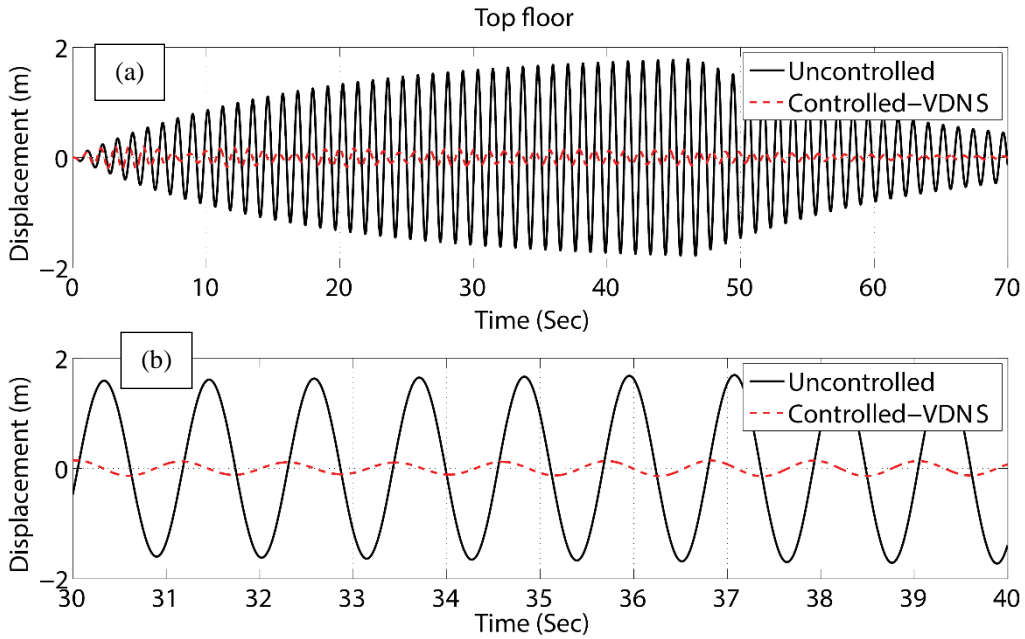


Figure 4: Comparison of the 10th floor displacement; (a) full-time history, (b) zoomed view.

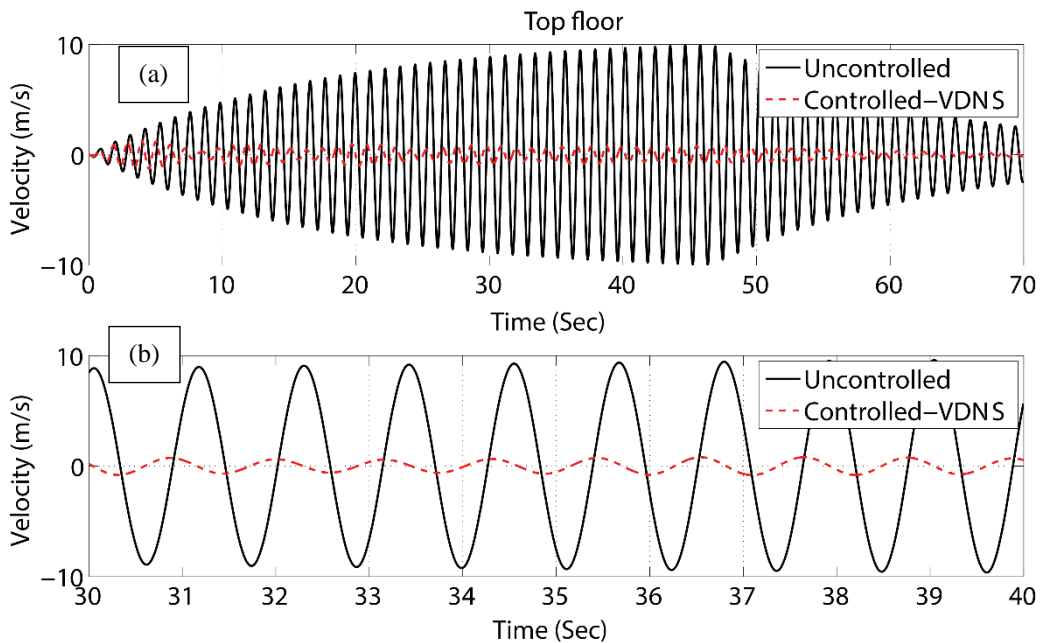


Figure 5: Comparison of the 10th floor velocity; (a) full-time history, (b) zoomed view.

Along with the aforementioned figure the velocity of the first floor is depicted in Figure 3 and quite similar results are obtained. In order to confirm the above statement, the top floor's (e.g. 10th floor) response is evaluated and presented in Figures 4-5. The color coding remain same as Figures 2 and 3. It is expected that the top floor will have more deflection which is visible in Figures 4-5. However, the reduction of the response is significant and the efficacy of the control investigated approach is observed. And most importantly, the used control scheme has the advantage over LQR as it does not require full-state feedback.

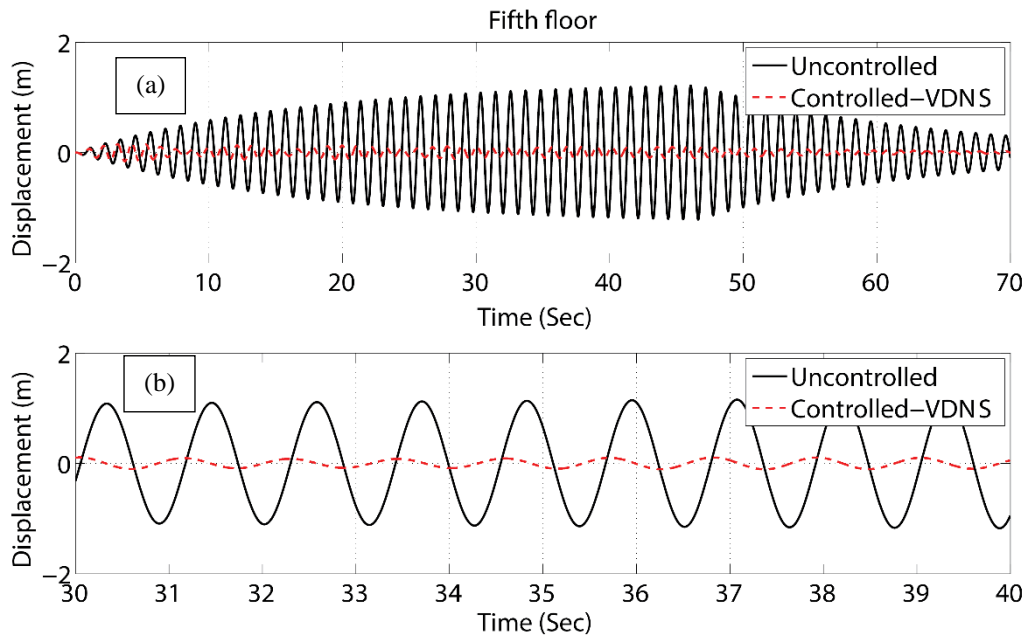


Figure 6: Comparison of the 5th floor displacement; (a) full-time history, (b) zoomed view.

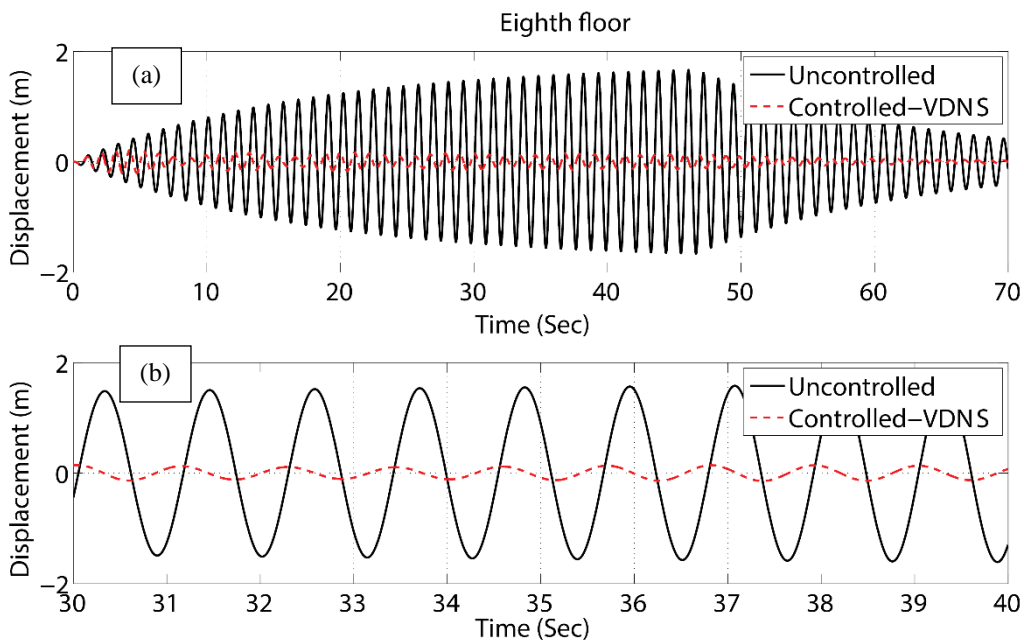


Figure 7: Comparison of the 8th floor velocity; (a) full-time history, (b) zoomed view.

Furthermore, fifth floor and eighth floors responses are evaluated and similar results are obtained. Hence the above indicated statement holds for all of the individual floor. Additionally, to observe the stability of the control closed-loop the displacement and velocity versus control force hysteresis is presented in Figures 8-9. And the results confirm that an optimal control force was implemented in real-time. The colour coding of Figures 2-7 remains same, means the black line indicates the uncontrolled displacement and the dotted red line represents the controlled one.

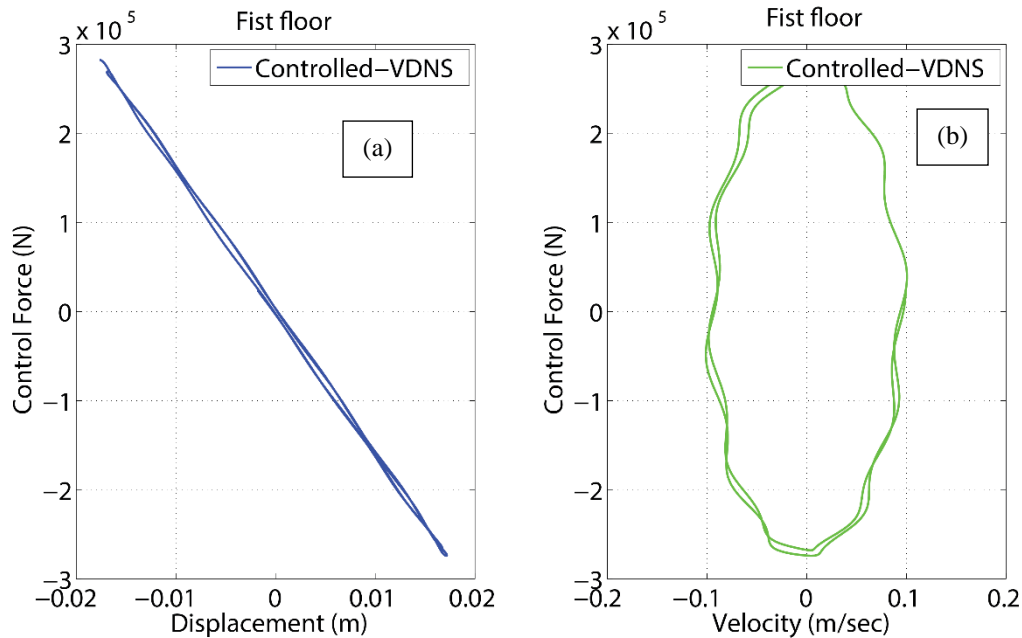


Figure 8: The 1st floor (a) displacement and (b) velocity versus control force hysteresis.

It needs to be mentioned that the stable control force was implemented based on the current displacement and velocity information. To do this end, the SIMULINK[®] was used to ensure nearly real-time implementations. And the estimated responses confirmed that the real-time information helps to reduce the vibration optimally. Also the effect of negative stiffness is visible in the displacement versus control force hysteresis. Further, the velocity versus control force confirms the active actuation was successfully implemented.

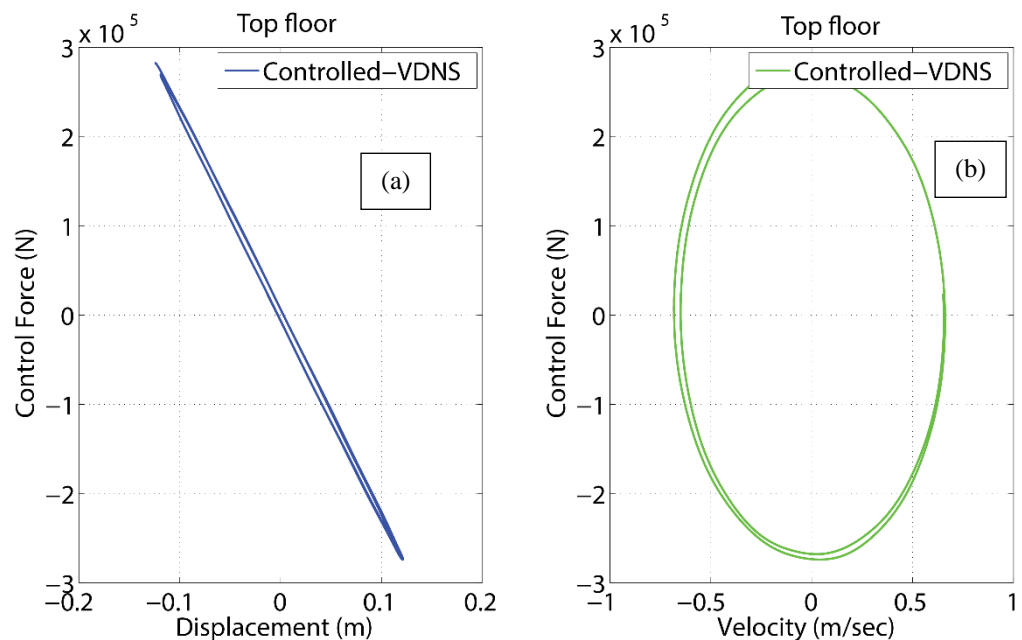


Figure 9: The 10th floor (a) displacement and (b) velocity versus control force hysteresis.

4. CONCLUSIONS

The possibilities of real-time vibration mitigation and control via a simplified control law e.g. VDNS is investigated by employing a 10-storied frame structure. The aforementioned control

law was combined with UKF. Two dampers are used, the first damper was placed at the first floor level and the second damper was placed at the top floor level. The simulations are performed via MATLAB/SUMILINK[®] by considering a nearly real-time implementation. The responses are evaluated and it is observed that the VDNS control law is capable of reducing significant level of vibration. In addition to the real-time vibration reduction the studied approach has the possibility to update model in real-time. Also the investigated approach has the potential to deal with nonlinear system. Hence, the VDNS control law is recommended for its simplest structure and overall efficiency over LQR. The proposed approach is going to assist the monitoring the overall structural performances in real-time.

ACKNOWLEDGEMENTS

The author acknowledges the assistance of the department of Civil Engineering, University of Asia Pacific (UAP), Dhaka, Bangladesh.

REFERENCES

- Preumont, A. 2004. *Vibration control of active structures: an introduction*, 2nd ed, Kluwer Academic Publishers, Dordrecht: Kluwer, The Netherlands.
- Oral, E., Çetin, L., and Uyar, E. 2010. A novel method on selection of Q and R matrices in the theory of optimal control, *Journal of Systems Control*, 1, 84–92.
- Miah M. S., Chatzi E. N., Dertimanis V. K., and Weber F. (2017) Real-time experimental validation of a novel semi-active control scheme for vibration mitigation, *Struct. Control Health Monit.*, 24: e1878. doi: 10.1002/stc.1878.
- Anderson, B.D.O. and Moore, J. B. 1989. *Optimal Control Linear Quadratic Methods*, Englewood Cliffs, Prentice-Hall, NJ: USA.
- Dyke, S. 1996. *Acceleration feedback control strategies for active and semi-active control systems: modeling, algorithm development, and experimental verification*. University of Notre Dame, Notre Dame, Indiana, USA.
- Mobaieen, S., Mohamady, B., Ghorbani, H., and Rabii, A. 2012. Optimal Control Design Using Evolutionary Algorithms with Application to an Aircraft Landing System, *Journal of Basic and Applied Scientific Research*, 2(2), 1876–1882.
- Miah, M. S., Chatzi, E. N. and Weber, F. 2013. Semi-active control of structural systems with uncertainties using an unscented Kalman filter, *Research and Applications in Structural Engineering, Mechanics and Computation*, Edited by Alphose Zingoni, CRC Press, 61-66, doi:10.1201/b15963- 13.
- Miah, M. S. 2015 *Semi-active control for magnetorheological dampers via coupling of system identification methods*. ETH-Zürich, Zurich, Switzerland, 22776. <http://dx.doi.org/10.3929/ethz-a-010532900>.
- Nekoui, M. A., and Bozorgi, H. H. J. 2011. Weighting Matrix Selection Method for LQR Design Based on a Multi-Objective Evolutionary Algorithm. *Advanced Materials Research*, 383–390, 1047–1054. <http://doi.org/10.4028/www.scientific.net/AMR.383-390.1047>.
- Weber, F. 2015. Robust force tracking control scheme for MR dampers. *Structural Control and Health Monitoring*. <http://doi.org/10.1002/stc.1750>.
- Miah, M. S., Chatzi, E. N. and Weber, F. 2014. MR Damper based Vibration Mitigation using a Bouc-Wen Model and a Nonlinear Observer. In J. Rodellar, A. Güemes, and F. Pozo (Eds.), Sixth World Conference on Structural Control and Monitoring, pp. 1185–1194. Barcelona, Spain.
- Bhowmik, S. 2011. *Modelling and Control of Magnetorheological Damper: Real-time implementation and experimental verification*, Technical University of Denmark, DCAMM Special Report No. S139, Lyngby, Denmark.
- Chatzi, E. N., Smyth, A. W. and Masri, S. F. 2010. Experimental application of on-line parametric identification for nonlinear hysteretic systems with model uncertainty. *Structural Safety*, 32(5), 326–337. <http://doi.org/10.1016/j.strusafe.2010.03.008>.

MODELING OF COVER CONCRETE CRACKING DUE TO UNIFORM CORRSION OF REINFORCEMENT

Sheikh Shakib¹, Abu Zakir Morshed²

¹ Lecturer, Khulna University of Engineering & Technology, Bangladesh,
e-mail: sheikhshakib10@gmail.com

² Professor, Khulna University of Engineering & Technology, Bangladesh,
e-mail: azmhappy@gmail.com

ABSTRACT

Cracking of cover concrete due to the corrosion of reinforcing steel is one of the main causes of deterioration in Reinforced Concrete (RC) structures. The level of oxidation depending on the supply of adequate oxygen, water and chloride ions, causes varying levels of expansion of reinforcement. Expansive stress is developed in concrete surrounding the reinforcing steels due to the expansive corrosion products of reinforcement leading to cracking of the concrete cover. Depending on the cracking characteristics, the service life of the structures would be affected. In this paper, the effect of geometrical and material parameters, i.e. concrete cover thickness, reinforcing bar diameter, and concrete tensile strength, on the required pressure for concrete cover cracking due to corrosion has been investigated through detailed numerical simulations. The accuracy of the numerical simulations is achieved by comparison of the numerical results with experimental data obtained from the literature. Finally the crack initiation and propagation has been simulated for different arrangements of reinforcements.

Keywords: Corrosion, Reinforced Concrete structures, cracking of the concrete cover, Crack initiation and propagation.

1. INTRODUCTION

A surface film of ferric oxide and Fe_2O_3 , known as layer of passivation, which is formed due to high alkalinity of the concrete pores solution, protect the steel from corrosion (Z. P. Bazant, 1979). Depassivation of this film can be happened by either Carbonation of the concrete cover or the presence of sufficient chloride ions on the steel bars surfaces (Z. P. Bazant, 1979). Corrosion of steel is a process of chemical reaction in which products are consists of various oxides, collectively known as rust (S. J. Pantazopoulou et al. 2001), which expands as much as it's six times its original volume (Liu and Weyers, 1998) depending on the level of oxidation. The corrosion products diffuse into capillary voids in concrete. If the total amount of corrosion products is less than the porous zone volume, free expansion occurs when there is no additional stress is developed in concrete. However when the products volume exceeds that of the porous zone, expansive stress is developed in concrete surrounding the reinforcing bars. Once the stress exceeds tensile strength of concrete, cracking initiates (K. Bhargava et al., 2006). Therefore, RC structures which are exposed to aggressive environments are prone to fail before reaching the end of their service lives.

A variety of analytical models dealing with corrosion-induced concrete cover cracking can be found in the literature (Pantazopoulou et al. 2001, Bhargava et al. 2006, Bazant 1979, Liu and Weyers 1998). Bazant (1979) proposed an analytical model to predict the time of the cover cracking caused by corrosion of embedded reinforcing steel. Another model was developed by Bhargava et al. (2006) to predict the time required for cover cracking and the weight loss of reinforcement.

Dagher and Kulendran (1992) simulated the corrosion-induced fracture of concrete via finite element analysis where smeared crack approach was employed for fracture analysis. The model considered only the radial expansive deformation around the reinforcing bar induced by corrosion while other loadings, such as dead and live loads, were not included. Du et al. (2006) presented a two-dimensional (2D) finite element (FE) model under a plane strain assumption to idealize three dimensional physical specimens, tested by the simulated method and investigated the development mechanism of the concrete cracking. The model was then employed to predict test results from reinforced concrete accelerated corrosion. Dimitri V. Val et al., 2009, considered crack initiation and propagation as a 2D problem—plain strain formulation. The model was mainly employed to predict the thickness of concrete porous zone and volume of corrosion product penetrating into the concrete pores before crack initiation.

The mechanical process of the corrosion product expansion due to corrosion is shown in Figure 1. The steel might be considered as a metal cylinder with an initial radius r , immersed in a semi-infinite concrete medium with a cover c , and undergoing corrosion. As corrosion progresses, the radius decreases by an amount x (corrosion penetration). However, corrosion products occupy a volume that is larger than the original metal. The final volume increase corresponds to an increase Δr , over the initial rebar radius, for a total value of, $r + \Delta r$. The surrounding concrete is stressed by this effective radial expansion and provokes the concrete-cover cracking and spalling. This work contributes to the study of the pressure needed to crack a certain cover and to confirm a predictive model for corrosion penetration taking into account specimen dimensions and fracture mechanic properties of the concrete.

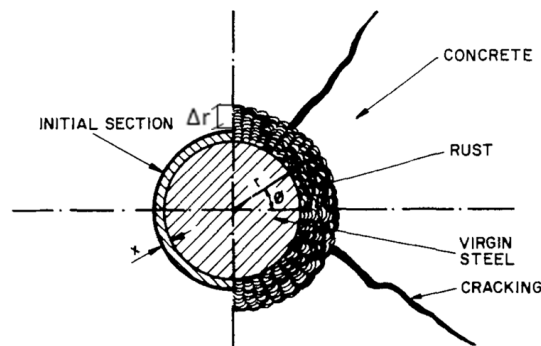


Figure 1: Representation of a cross-section of a corroded rebar with expansive oxides

2. DEVELOPING THE MATERIAL MODEL

2.1 Concrete Damaged Plasticity model (CDPM)

Commercial software ABAQUS, is employed as a modelling platform. The software is capable of simulating the damage using either of the three crack models for reinforced concrete elements: (1) Smeared crack concrete model, (2) Brittle crack concrete model, and (3) Concrete damaged plasticity model. Out of the three concrete crack models, the concrete damaged plasticity model is selected in the present study.

The concrete damaged plasticity model assumes that the two main failure mechanisms in concrete are the tensile cracking and the compressive crushing. In this model, the uniaxial tensile and compressive behaviour is characterized by damaged plasticity.

In general, the nonlinearity of concrete under compression can be modeled by approaches based on the concept of either damage or plasticity, or both (T. Yu et al., 2010) which is shown in Figure 2. T. Yu et al., 2010, defined Plasticity as the unrecoverable deformation after all loads have been removed and Damage as the reduction of elastic constants. In

order to present the inelastic behaviour of concrete, the CDPM uses concepts of isotropic damage in combination with isotropic tensile and compressive plasticity (T. Yu et al, 2010). The key aspects of this model are compressive and tensile behaviour of concrete, including the damage variable, the yield criterion, the hardening/softening rule, and the flow rule, which are summarized as follows.

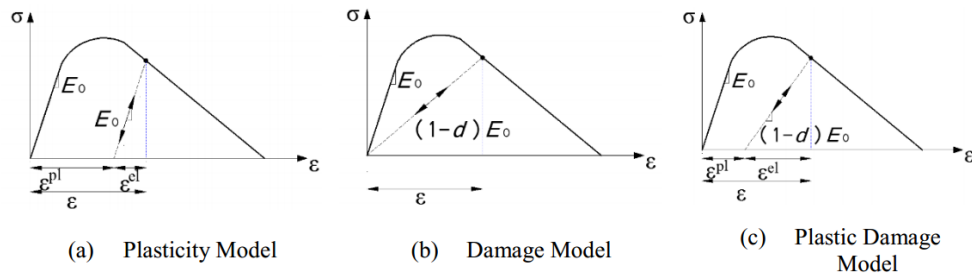


Figure 2: Representation of CPDM

2.1.1 Compressive and Tensile Behavior of Concrete

The uniaxial tensile and compressive response of concrete, characterized by damaged plasticity, is shown in Figure 3. Under uniaxial tension the stress-strain response follows a linear elastic relationship until the value of the failure stress, σ_{t0} , is reached. The failure stress corresponds to the onset of micro-cracking in the concrete material. Beyond the failure stress the formation of micro-cracks is represented macroscopically with a softening stress-strain response, which induces strain localization in the concrete structure. Under uniaxial compression the response is linear until the value of initial yield, σ_{c0} . In the plastic regime the response is typically characterized by stress hardening followed by strain softening beyond the ultimate stress, σ_{cu} .

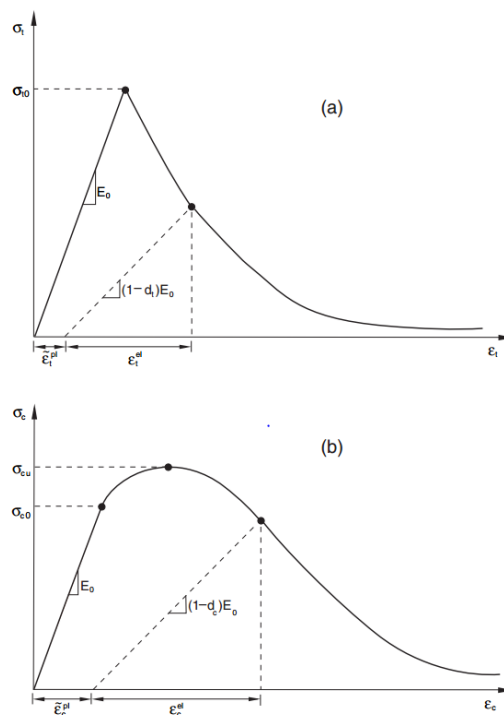


Figure 3: Response of concrete to uniaxial loading in tension (a) and compression (b).

2.1.2 Damage

As shown in Figure 3, when the concrete specimen is unloaded from any point on the strain softening branch of the stress-strain curves, the unloading response is weakened: the elastic stiffness of the material appears to be damaged (or degraded). The degradation of the

elastic stiffness is characterized by two damage variables, d_c and d_t , which are assumed to be functions of the plastic strains, temperature, and field variables:

$$d_t = d_t(\tilde{\varepsilon}_t^{pl}, \theta, f_i); \quad 0 \leq d_t \leq 1,$$

$$d_c = d_c(\tilde{\varepsilon}_c^{pl}, \theta, f_i); \quad 0 \leq d_c \leq 1.$$

The damage variables can take values from zero, representing the undamaged material, to one, which represents total loss of strength.

If E_0 is the initial (undamaged) elastic stiffness of the material, the stress-strain relations under uniaxial tension and compression loading are, respectively:

$$\sigma_t = (1 - d_t)E_0(\varepsilon_t - \tilde{\varepsilon}_t^{pl}),$$

$$\sigma_c = (1 - d_c)E_0(\varepsilon_c - \tilde{\varepsilon}_c^{pl}).$$

This model assumes that the main two failure mechanisms are tensile cracking and compressive crushing of the concrete material. The evolution of the yield (or failure) surface is controlled by two hardening variables, $\tilde{\varepsilon}_t^{pl}$ and $\tilde{\varepsilon}_c^{pl}$, linked to failure mechanisms under tension and compression loading, respectively. $\tilde{\varepsilon}_t^{pl}$ and $\tilde{\varepsilon}_c^{pl}$ are tensile and compressive equivalent plastic strains, respectively. Abaqus automatically converts the tensile cracking strain ($\tilde{\varepsilon}_t^{ck}$) and compressive inelastic strain ($\tilde{\varepsilon}_c^{in}$) values to plastic strain values using the relationships,

$$\tilde{\varepsilon}_t^{pl} = \tilde{\varepsilon}_t^{ck} - \frac{d_t}{(1 - d_t)} \frac{\sigma_t}{E_0}.$$

$$\tilde{\varepsilon}_c^{pl} = \tilde{\varepsilon}_c^{in} - \frac{d_c}{(1 - d_c)} \frac{\sigma_c}{E_0}.$$

The cracking strain is defined as the total strain minus the elastic strain corresponding to the undamaged material; that is $\tilde{\varepsilon}_t^{ck} = \varepsilon_t - \varepsilon_{0t}^{el}$, where, $\varepsilon_{0t}^{el} = \sigma_t/E_0$, the Elastic strain corresponding to the undamaged material, ε_t = total tensile strain which is shown in Figure 4(a). The compressive inelastic strain is defined as the total strain minus the elastic strain corresponding to the undamaged material, $\tilde{\varepsilon}_c^{in} = \varepsilon_c - \varepsilon_{0c}^{el}$, where, $\varepsilon_{0c}^{el} = \sigma_c/E_0$, Elastic strain corresponding to the undamaged material and ε_c = Total tensile strain as illustrated in Figure 4(b).

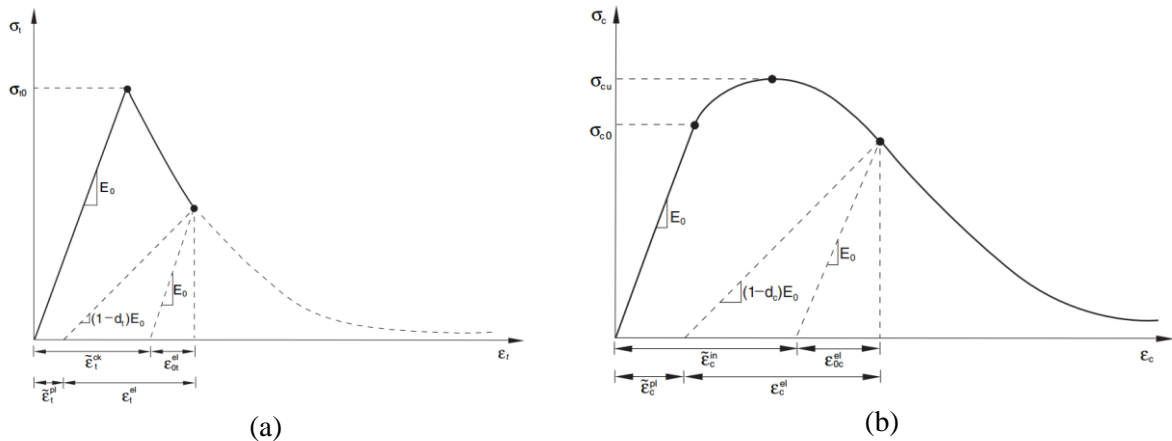


Figure 4: Illustration of the definition of the (a) cracking strain ($\tilde{\varepsilon}_t^{ck}$) and (b) inelastic strain ($\tilde{\varepsilon}_c^{in}$) used for the definition of tension stiffening and compression hardening data respectively.

2.1.3 Yield function

The model makes use of the yield function of Lubliner et. al. (1989), with the modifications proposed by Lee and Fenves (1998) to account for different evolution of strength under tension and compression. The evolution of the yield surface is controlled by the hardening variables, $\tilde{\varepsilon}_t^{pl}$ and $\tilde{\varepsilon}_c^{pl}$. In terms of effective stresses, the yield function takes the form

$$F = \frac{1}{1 - \alpha} (\bar{q} - 3\alpha\bar{p} + \beta(\tilde{\varepsilon}^{pl})(\hat{\sigma}_{\max}) - \gamma(-\hat{\sigma}_{\max})) - \bar{\sigma}_c(\tilde{\varepsilon}_c^{pl}) = 0,$$

With

$$\alpha = \frac{(\sigma_{b0}/\sigma_{c0}) - 1}{2(\sigma_{b0}/\sigma_{c0}) - 1}; 0 \leq \alpha \leq 0.5,$$

$$\beta = \frac{\bar{\sigma}_c(\tilde{\varepsilon}_c^{pl})}{\bar{\sigma}_t(\tilde{\varepsilon}_t^{pl})}(1 - \alpha) - (1 + \alpha),$$

$$\gamma = \frac{3(1 - K_c)}{2K_c - 1}.$$

Where, $\hat{\sigma}_{\max}$ is the maximum principal effective stress; σ_{b0}/σ_{c0} is the ratio of initial equibiaxial compressive yield stress to initial uniaxial compressive yield stress (the default value is 1.16); K_c is the ratio of the second stress invariant on the tensile meridian, $q_{(TM)}$, to that on the compressive meridian $q_{(CM)}$. It must satisfy the condition $0 < K_c \leq 1$ (the default value is 2/3); $\bar{\sigma}_t(\tilde{\varepsilon}_t^{pl})$, $\bar{\sigma}_c(\tilde{\varepsilon}_c^{pl})$ are the effective tensile and compressive cohesion stress respectively. Typical yield surfaces in the deviatoric plane are shown in Figure 5 for different values of K_c .

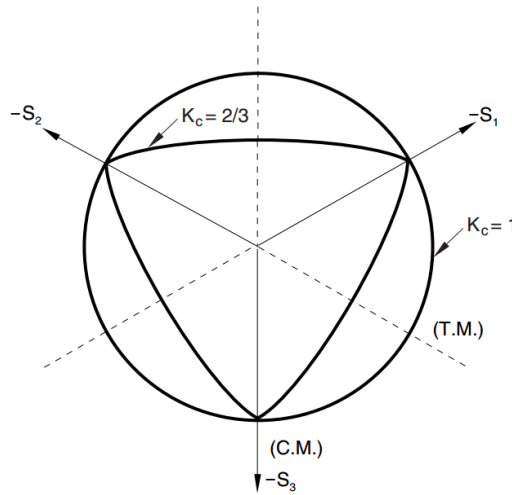


Figure 5: Yield surfaces in the deviatoric plane, corresponding to different values of K_c

2.1.4 Flow rule

The concrete damaged plasticity model assumes nonassociated potential plastic flow. The flow potential G used for this model is the Drucker-Prager hyperbolic function:

$$G = \sqrt{(\epsilon\sigma_{t0} \tan \psi)^2 + \bar{q}^2} - \bar{p} \tan \psi,$$

Where, ψ , is the dilation angle measured in the p - q plane at high confining pressure; σ_{t0} , is the uniaxial tensile stress at failure; ϵ , is a parameter, referred to as the eccentricity, that defines the rate at which the function approaches the asymptote (the flow potential tends to a straight line as the eccentricity tends to zero). The default value is 0.1.

2.2 Numerical Model of Concrete

The CDPM requires concrete compressive and tensile constitutive relationship, cracking and crushing damage parameters and special parameters such as dilation angle, eccentricity, biaxial loading ratio, the coefficient K_c and viscosity parameter. These parameters can be assigned to their commonly used values in the literature (Table 1). A low viscosity parameter helps to improve the convergence rate in the softening regime of concrete stress-strain curve.

Table 1: Parameters for CPDM

ψ	ϵ	σ_{b0}/σ_{c0}	K_c	Viscosity Parameter
30^0	0.1	1.16	2/3	0.0001

Uniaxial compressive strength can be easily obtained through laboratory experiments of standard sized specimens. Similarly, the uniaxial tension strength can be determined by splitting cylinder tests. The tensile strength of concrete is usually estimated to be 10 to 15 percent of compressive strength. When experimental data is not available, the tensile strength can be calculated from the equation (Oluokun et al., 1991)

$$f_{ctsp} = 1.38(f_c)^{0.69} \text{ psi}$$

Elasticity modulus and Poisson's ratio of concrete are more difficult to obtain by laboratory tests. The elasticity modulus estimation based on compressive strength was given by, ACI 318-02., 2002,

$$E_c = 57000\sqrt{f_c} \text{ psi}$$

Poisson's ratio of concrete is usually taken between 0.15 and 0.20. In the present study Poisson's ratio is chosen as 0.20.

In the literature there are numerous analytical constitutive models suggested for concrete material. In this study, the unconfined stress-strain relationship model for concrete which was first proposed by Popovics, 1973. According to this model, the relation between compressive strain (ϵ_c) and stress (f_c) is given by

$$\frac{f_c}{f'_c} = \frac{n \left(\frac{\epsilon_c}{\epsilon_{co}} \right)}{(n-1) + \left(\frac{\epsilon_c}{\epsilon_{co}} \right)^n}$$

where f'_c , ϵ_{co} are the compressive strength and strain corresponding to the maximum stress, respectively. The 'n' is defined by,

$$n = 0.4 \times 10^{-3} f'_c (\text{psi}) + 1.0$$

Tensile stress strain (σ - ϵ) relationship was assumed to be linear up to the uniaxial tensile strength and then determined using the exponential function (Thorenfeldt et al.. 1987)

$$\sigma = f_t \left(\frac{\epsilon_t}{\epsilon} \right)^{(0.7+1000\epsilon)}, \quad \epsilon_t = \frac{f_t}{E_c}$$

3. FINITE ELEMENT MODELLING AND VERIFICATION

In this study crack initiation and propagation are considered as a 2D problem—plain strain formulation. Since this study concentrates on the analysis of RC beams subject to accelerated corrosion tests, in which uniformity of corrosion along the beam length is ensured, the 2D simplification is suitable. For modeling natural corrosion, which may be strongly nonuniform along the length of RC elements, the use of a 3D formulation can be more appropriate. The model is implemented in ABAQUS—a commercial software package for nonlinear FE analysis. 3-node linear plane strain triangle is used to represent concrete.

The two-dimensional (2D) finite element model is verified through comparison of numerical results with respective experimental data reported by Williamson and Clark (2000). The test specimens were cubes with edge length 150 mm and a cylindrical hole located at one corner with diameter of 8 mm, as seen in Figure 6. The ratios of concrete cover thicknesses to the hole diameter, i.e. C/d , were 0.5, 1.0, and 2.0. A uniform and gradually increasing outward internal strain is applied into the holes to simulate the expansion induced by corrosion of steel bars.

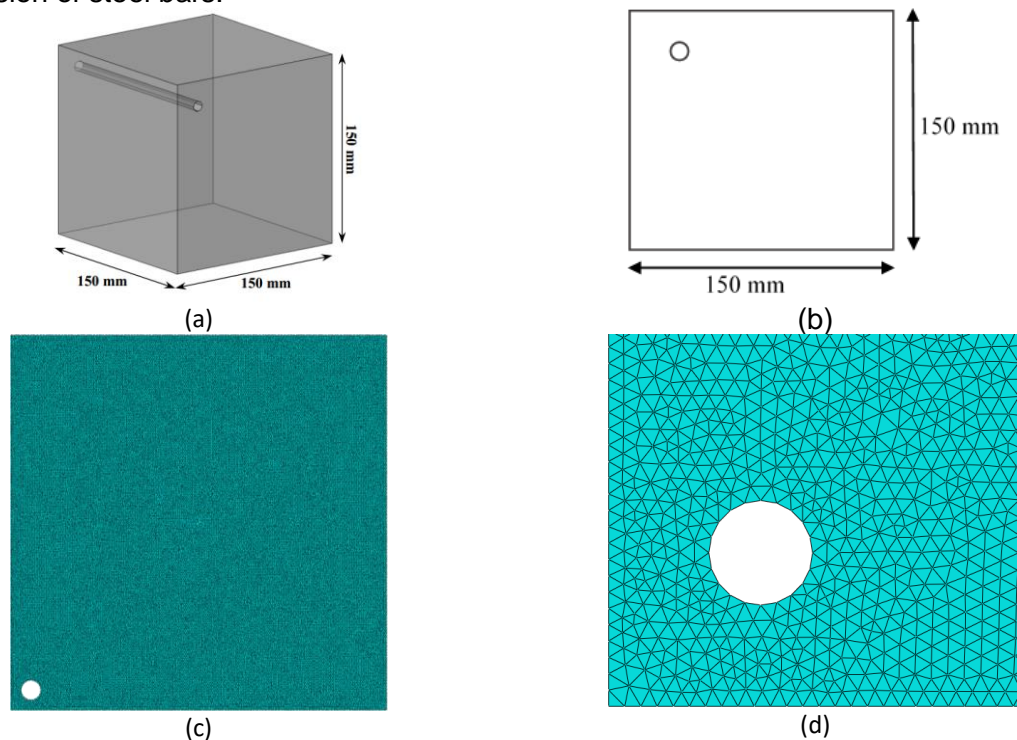


Figure 6: Specimens' dimensions tested by Williamson and Clark (2000) (a) 3D specimen (b) 2D formulation (c) Meshing & (d) magnified view of meshing

In order to validate the model it is necessary to compare it with experimental results. However, a quantitative comparison with actual corrosion tests is difficult. Corrosion-induced cracking occurs because corrosion products have a larger volume than the original steel of a corroding reinforcing bar. Thus, as corrosion progresses the volume occupied by the reinforcing bar and the corrosion products accumulating around it increases. This creates ever increasing pressure on the surrounding concrete, which eventually leads to the concrete cracking. Williamson and Clark (2000), investigated cracking of the concrete cover due to pressure applied within holes made in concrete specimens. Parameters varied in the tests included the diameter of the holes, d , the thickness of the concrete cover, c , and the tensile strength of concrete. Results of the comparison of pressure needed to cause crack initiation are shown in Figure 7 and Table 2. As can be seen, there is a good agreement between the test and analytical results for $d=8$ mm (Figure 7 and Table 2).

Table 2: The required pressure for concrete cover cracking

c/d	P _{max/numerical} (MPa)	P _{max/exp} (MPa)	ΔP (%)
0.5	2.70	2.65	1.9
1.0	4.72	4.08	15.7
2.0	6.00	7.71	22.2

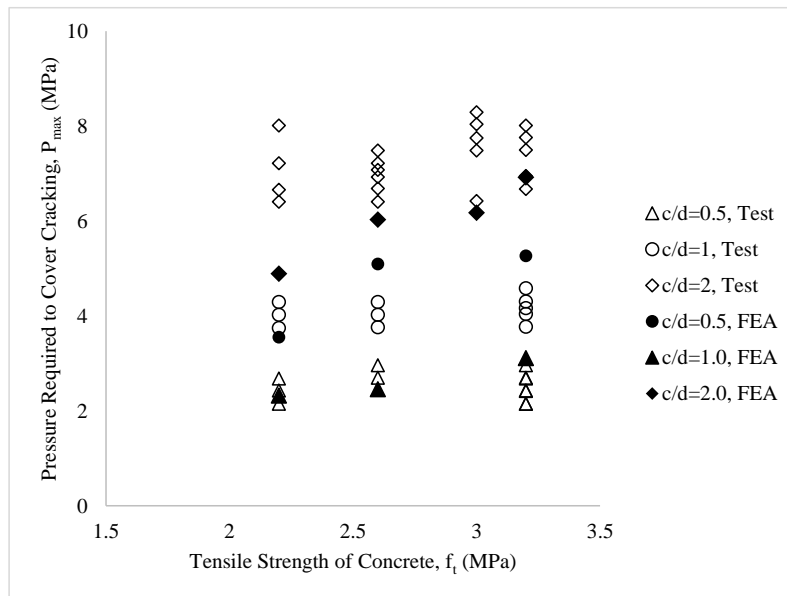


Figure 7: Comparison of results of finite-element analysis with test results from Williamson and Clark (2000): for $d=8$ mm;

4. RESULTS

4.1 1 Relation of Concrete cracking pressure with concrete cover

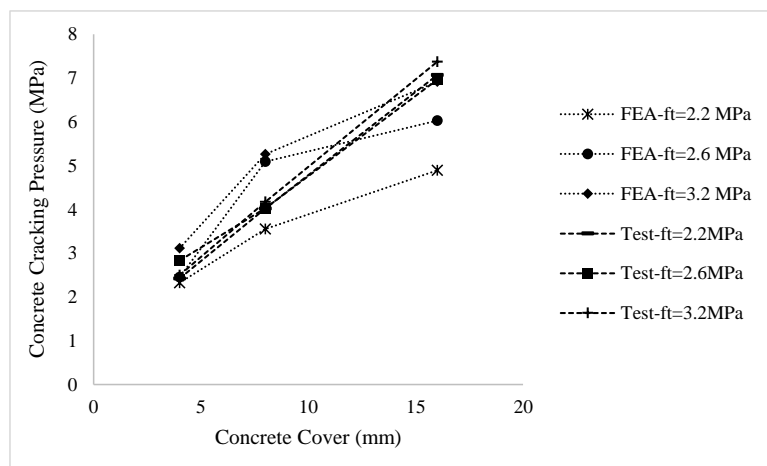


Figure 8: Effect of concrete cover thickness on the required pressure and comparison with the results of Williamson and Clark, 2000

The effect of the cover thickness variation on the required expansive pressure are provided in Figure 8. As can be seen, by increasing the cover thickness, the required pressure is

increased, i.e. the thicker the cover, the higher the pressure. As can be seen that the model predict the pressure required to cover cracking similar to that of test for cover thickness 4mm. On the other hand, for cover thickness 8mm, the model overestimates for higher tensile strengths ($f_t = 2.6, 3.0, 3.2$ MPa) but underestimate for tensile strength 2.2 MPa. For cover thickness 16mm model underestimate the pressures irrespective of the tensile strengths.

4.2 Relation of Concrete cracking pressure with hole diameter

Five finite element models are developed with varying hole diameters (d), from 10 mm to 25 mm, where all other geometrical and material properties are kept constant ($C = 37.5$ mm, $f_t = 3.4$ MPa). The pressure required for cracking of the concrete cover for each model is shown in Figure 9. As seen in the figure, the expansive pressure decreases as the hole diameter increases. By increasing of the hole diameter, the lateral surface of the hole increases which results in higher outward force and consequently lower required pressure for the cracking.

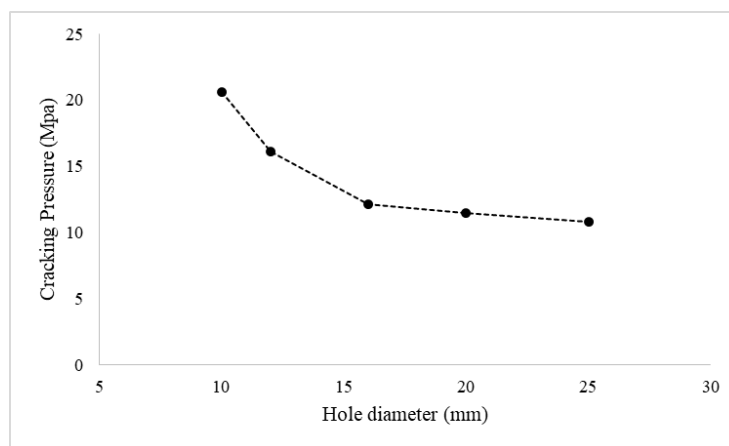


Figure 9: Effect of hole diameter on the required pressure for cracking

4.3 Relation of Concrete cracking pressure with modulus of elasticity

The variation of concrete cracking pressure with respect to modulus of elasticity of concrete has shown in figure 10. Williamson and Clark, 2000 didn't report the effect of modulus of elasticity of concrete on corrosion pressure. As shown in figure the higher the value of E_c the pressure required to cover crack.

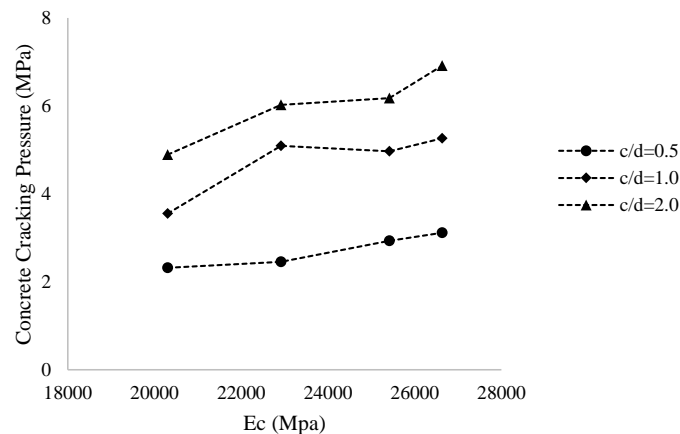


Figure 10: Effect of concrete Modulus of elasticity on the required pressure

4.4 Crack patterns of concrete cover for single reinforcement

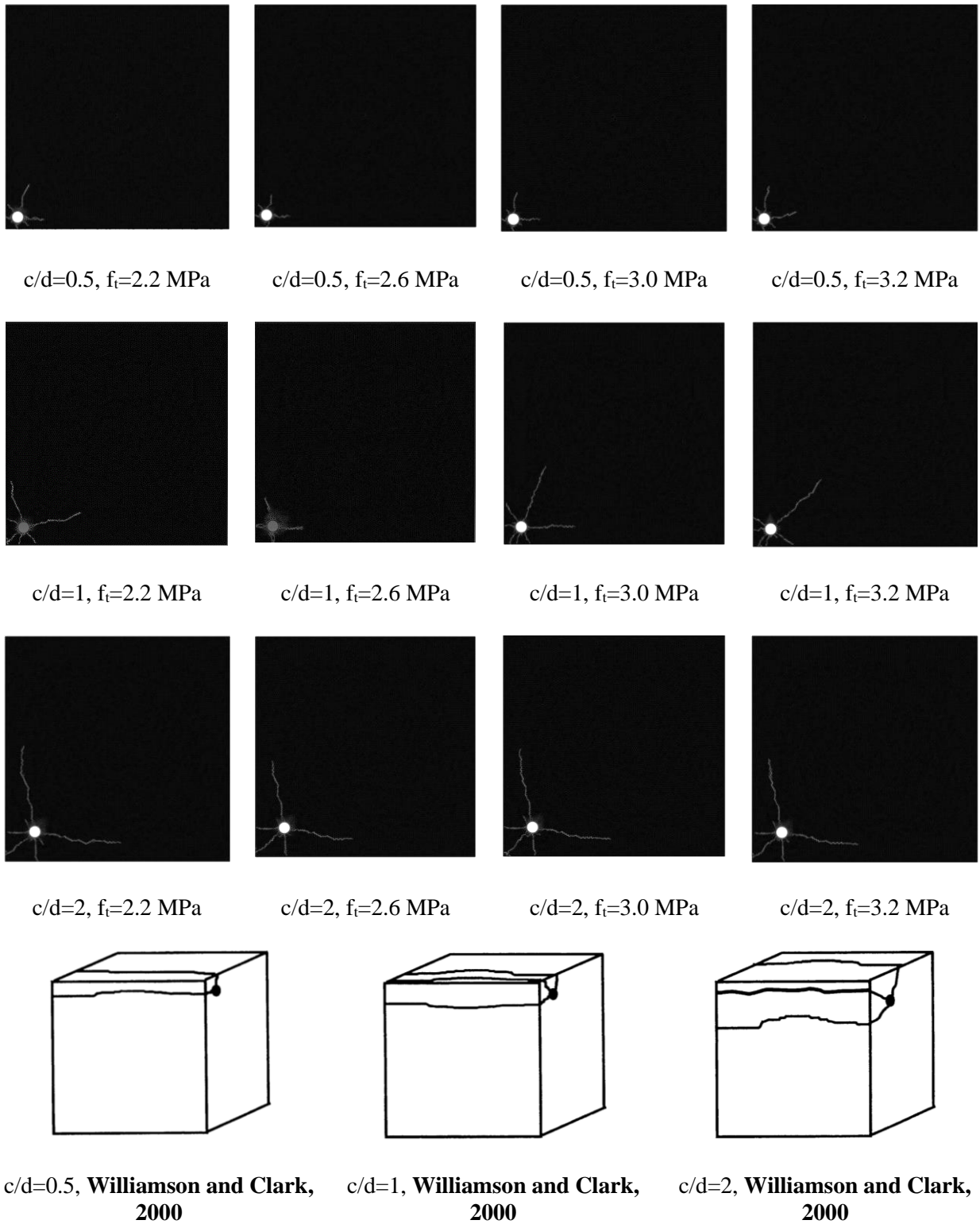


Figure 11: Final stage of cover cracking

5. INITIATION AND PROPAGATION OF CRACKS FOR ARRANGEMENTS OF BARS

Reinforcement bars were arranged in different configuration for a section with dimensions (W × H) of 250 × 250 mm, cover thickness (C) of 37.5 mm. Cracking initiation and propagation pattern of four different configurations with 2, 3, 4 & 8-12 mm diameter plain bar are shown in Figure 12.

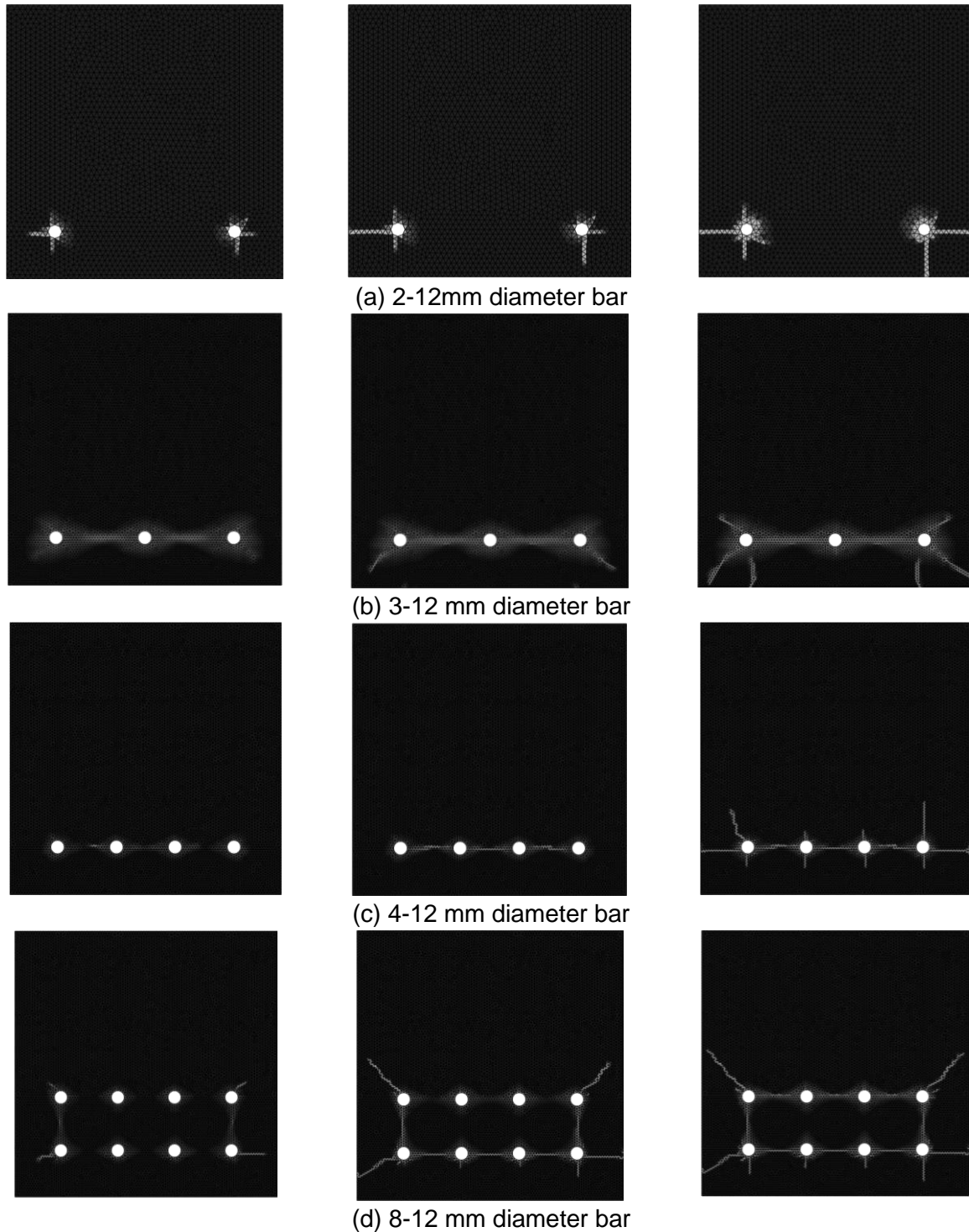


Figure 12: Crack initiation and propagation for reinforcement arrangements of a section

6. CONCLUSIONS

This paper presents a generic 2D FEM model to simulate the concrete cover cracking due to internal expansive pressure induced by steel reinforcing bars corrosion. The following conclusions can be drawn:

- Increase in cover thickness or concrete tensile strength raises the required pressure for cover cracking, however, in bar diameter decreases the pressure.
- The 2D model can be employed to determine sections configurations in order to achieve desirable cracking initiation and propagation due to internal expansive pressure induced by corrosion of reinforcing steel.

ACKNOWLEDGEMENTS

I am most grateful for the support and fine cooperation with Prof. Dr. Md. Rokonzaman from the Department of Civil Engineering, KUET, with whom I have had an excellent cooperation regarding the constitutive modelling of concrete.

REFERENCES

- ACI 318-02., 2002 Building Code Requirements for Structural Concrete (ACI 318-02) and Commentary (ACI 318R-02). Farmington Hills, MI: ACI
- Bazant, Z. P., (1979b). "Physical Model for Steel Corrosion in Concrete Sea Structures—Theory," Journal of the Structural Division, V. 105, No. ST6, pp. 1137-1153.
- Bhargava, K., Ghosh, A.K., Mori, Y. and Ramanujam S. (2006), "Model for cover cracking due to rebar corrosion in RC structures", Eng. Struct., 28(8), 1093-1109.
- Dagher, H.J. and Kulendran, S. (1992), "Finite element modeling of corrosion damage in concrete structures", ACI Struct. J., 89(6), 699-708.
- Dimitri V. Val, Leonid Chernin and Mark G. Stewart, 2009, "Experimental and Numerical Investigation of Corrosion-Induced Cover Cracking in Reinforced Concrete Structures", Journal of Structural Engineering, Vol. 135, No. 4, April 1, 2009, ASCE
- Du, Y.G., Chan, A.H.C. and Clark, L.A. (2006), "Finite element analysis of the effects of radial expansion of corroded reinforcement", Comput. Struct., 84(13-14), 917-929.
- E. Thorenfeldt, A. Tomaszewicz, and J. J. Jensen, , 1987 "Mechanical properties of high-strength concrete and application in design," in Proc. Symposium on Utilization of High-Strength Concrete, Tapir, Trondheim, Norway, pp. 149-159.
- F. A. Oluokun, E. G. Burdette, and J. H. Deatherage, 1991. "Splitting tensile strength and compressive strength relationships at early ages," ACI Materials Journal, vol. 88, no. 2, pp. 115-121
- Lee J, Fenves GL, 1998, "Plastic-damage model for cyclic loading of concrete structures". J Eng Mech, ASCE 1998; 124(8):892-900.
- Liu, Y., and Weyers, R. E. (1998). "Modeling the time-to-corrosion cracking in chloride contaminated reinforced concrete structures." ACI Mater. J., 95(6), 675–681.
- Lubliner J, Oliver J, Oller S, Onate E, 1989, "A plastic-damage model for concrete." Int J Solid Struct 1989; 25:299-329.
- Pantazopoulou, S. J., and Papoulia, K. D., 2001. "Modeling cover cracking due to reinforcement corrosion in RC structures." J. Eng. Mech., 127(4), 342–351.
- S. Popovics, 1973 "A numerical approach to the complete stress-strain curves of concrete," Cement and Concrete Research, vol. 3, no. 5, pp. 583-599,
- T. Yu, J.G. Teng, Y.L. Wong, S.L. Dong, 2010, "Finite element modeling of confined concrete-II: Plastic-damage model" Engineering Structures 32 (2010) 680-691.
- Williamson, S. J., and Clark, L. A., 2000. "Pressure required to cause cover cracking of concrete due to reinforcement corrosion." Mag. Concrete Res., 52(6), 455–467.